Aerodynamics and Acoustics of the Virginia Tech Stability Tunnel Anechoic System

Erin Dawne Crede

Thesis submitted to the faculty of Virginia Polytechnic Institute and State University in partial fulfillment of the requirements for the degree of

Master of Science
In
Aerospace Engineering

William J. Devenport
Ricardo A. Burdisso
Roger L. Simpson

June 11, 2008
Blacksburg, Virginia

Keywords: anechoic, wind tunnel, acoustics, wind turbines

Aerodynamics and Acoustics of the Virginia Tech Stability Tunnel Anechoic System

Erin D. Crede

ABSTRACT

The acoustic treatment and calibration of a new anechoic system for the Virginia Tech Stability Wind Tunnel has been performed. This novel design utilizes Kevlar cloth to provide a stable flow boundary, which eliminates the need for a free jet and jet catcher. To test this concept a series of measurements were performed both to validate the reduction in overall test section noise levels and to ascertain the effect of these modifications on the test section aerodynamics.

An extensive program of experiments has been conducted to examine the performance of this new hardware under a range of conditions. These include baseline experiments that reveal the aerodynamic and aeroacoustic performance of the tunnel in its original configuration, treatment of the tunnel circuit with validation of in-flow noise reduction, wind tunnel tests to examine the effect of the test section acoustic treatment, and measurements of the aerodynamic and aeroacoustic characteristics of a NACA 0012 airfoil model over a range of angles of attack and Reynolds numbers.

These measurements show that acoustically treating the walls of the circuit both upstream and downstream of the test section, as well as the fan, result in an overall reduction of 5 dB depending on frequency, of the in-flow noise level. These measurements also show that the complete system provides a reduction of between 15 to 20dB depending on frequency, in the in-flow background noise level. Measurements taken both within the test section and in the adjacent chambers also show that large Kevlar windows can be used to quietly and stably contain the flow, eliminating the need for an open-jet and jet catcher system, as well as overall noise levels competitive with many other facilities. Measurements on several airfoils at various angles of attack and Reynolds number show that the interference correction for the fully anechoic configuration is approximately -22% for model with a chord length equal to half the test section height.

Aerodynamic measurements with the NACA 0012 airfoil show its lift, drag and boundary layer characteristics at high Reynolds numbers are consistent with theoretical expectations. Measurements of the window deflection as well as examination of flow transpiration through the Kevlar windows were accomplished, both with and without the NACA 0012 model. These measurements, along with the interference correction data, confirm that the Kevlar windows are a stable flow boundary.

ACKNOWLEDGEMENTS

The author would like to acknowledge the financial support of the Office of Naval Research, under grants N00014-05-1-0464 and N00014-04-1-0493, and its technical monitor Dr. Ronald Joslin, and the National Renewable Energy Laboratory, in particular Drs. Pat Moriarty and Paul Migliore, through grant ZAM-4-33226-0. The support and guidance of Dr. William Devenport, Dr. Roger Simpson and Dr. Ricardo Burdisso is also gratefully acknowledged. Special thanks go to Amanda Chou, Matt Rasnick, and Philip van Seeters, for their support in running this test. In addition, the author would like to thank Bill Oetjens for all of his help and advice during the tunnel modification process and Bruce Stanger, James Lambert and Mark Montgomery for their expertise in fabricating hardware used in the test. Without the help of these individuals, the results in this thesis could not have been obtained. Finally, the author would like to thank everyone in the ATFRG and everyone in VAL who volunteered their time to help.

All photographs presented in this thesis were taken by the author.

TABLE OF CONTENTS

LIST OF SYMBOLS, TABLES AND FIGURES

List of Symbols

α	angle of attack (degrees)
c	model chord length
C_α	angles of attack that best matched the theoretical comparison
$Cp\|_{static}$	static pressure coefficient
$Cp\|_{total}$	total pressure coefficient
$Cp\|_{rail}$	static pressure coefficient measured on the aluminum rail
$Cp\|_{strut}$	static pressure coefficient measured using the hard wall strut
ΔC_p	change in static pressure coefficient
δ	boundary layer thickness
δ^*	boundary layer displacement thickness
f	correction factor relating contraction probe to test section probe
θ	boundary layer momentum thickness
μ	dynamic viscosity
v_i	flow rate through a surface at low Reynolds number
I	lift interference correction
P	static pressure
P_o	total pressure
q	Tunnel dynamic pressure (inH_20)
R	ratio of the effective to geometric angle of attack
R_p	inverse of a resistance coefficient
U_e	edge velocity
u	measured velocity (X component)
w	test section width
X,Y,Z	Cartesian coordinates

List of Tables

List of Figures

Chapter 2

Chapter 3

Chapter 4

1. INTRODUCTION

Early research in aero-acoustics has been almost exclusively conducted in open-jet wind tunnels. These facilities generally allow noise measurements to be carried out in the far field and in an environment with low background noise levels that are free from acoustic reflections. Open-jet wind tunnels, however, have two disadvantages, both of which are a result of the free jet boundary. First, large eddies that entrain air from around the wind tunnel may form at the jet shear layer boundary. This leads to a source of instability and noise at the point where the jet re-enters the tunnel, both because of the impact of the eddies and because the extra mass flow they contain cannot be reabsorbed into the wind tunnel circuit. Designing a quiet jet catcher may alleviate some of these problems; its design is not a trivial one. The second disadvantage is that open-jet test sections are quite sensitive to lift interference. Lift interference can be a complicating factor in studies of acoustic emissions from aerodynamic surfaces under load.

The advent of microphone phased arrays in the early 1990s has rendered possible, and even common, the ability to collect acoustic data in hard-walled wind tunnels and several solid wall facilities have been acoustically modified to allow for aero acoustic measurements. Solid wall facilities have the advantage of a relatively low lift interference, which provides dramatically better aerodynamic results. These facilities however, have much higher background noise levels, and can be highly reverberant. Additionally, the size of the test section may prohibit measurements in the far field.

The design of a facility that can be used to gather good acoustic data as well as perform well aerodynamically is a primary concern. There are several key research areas that need to be addressed to have a solid understanding of the problem at hand. The first of these is the role of the interference correction in various tunnel configurations; these include solid wall, open jet and porous walled tunnels. Additionally the design of porous wall tunnels and their application was considered. Finally data was collected on a selection of tunnels that use a conventional aeroacoustic tunnel design.

The determination of the lift interference correction for a wind tunnel has been a research topic for over 70 years and a general theory for calculating the wind tunnel wall interference correction was proposed by in Theodorsen (1931). This paper considers two

primary types of tunnels; a closed and open section. He proposes that there are boundary solutions for the prediction of the lift interference, one for each type of wall. In the case of the closed section, the velocity normal to the boundary must be zero. Likewise for the open section there must be an unaltered, or constant, flow velocity over the range of interest. Several iterations of the two primary types of tunnels are considered; complete solid wall, completely open test section, horizontal boundaries only, vertical boundaries only, and finally a single lower boundary. The comparison of the interference correction for these cases shows that the most promising tunnel choice for the lowest interference correction would be an free jet with a lower boundary; this type having an interference correction 5-8 times lower than a free jet alone.

Another technical paper was submitted by the National Advisory Committee for Aeronautics concerning wall interference in wind tunnels with slotted and porous boundaries. Barrett *et al* (1954) attempted to determine the lift interference of several wall configurations: solid, porous, slotted and free jet. In the case of the porous boundary, the average boundary condition was derived by assuming that the velocity normal to the wall is proportional to the to the pressure drop through the wall. This is a linearized approximation for viscous flow through a porous medium, where the pressure drop outside the wall is equal to the free stream pressure. This assumption implies a porosity parameter*, R,* which is equal to the free stream density multiplied by the free stream velocity and then divided by the pressure difference. This means that porosity relation, *R,* can be determined experimentally by measuring the mass flow and pressure drop across the porous wall as a function of velocity.

L.C Woods authored a paper on the theory of two dimensional wind tunnels with porous walls; see Woods, L.C. (1955). In this paper two interference "effects" were considered; that due to the solid blockage (result of the airfoil thickness) and wake blockage. He sought to reduce the interference correction from these two effects by designing a finite length porous wall that was solid at the ends with a sealed jacket over the porous section to control the pressure over the porous region. The addition of the jacket covering the outside of the porous region built on the research mentioned in Barrett *et al* (1954). Through moving the solid panels to control the length of the porous section for various model positions, the contribution of the two interference effects could be

controlled, and thus the total interference correction reduced. An important assumption was made regarding the porous walls, namely that the velocity normal to the porous wall was proportional to the pressure loss across that part of the wall. This would imply a constant of proportionality that was inherent to the type of porous surface chosen.

Several other papers were published throughout the following decades concerning the use for slotted and porous walled tunnels; for example a paper published by M. Mokry (1990) dealt with the residual interference in wind tunnel wall adaptation, while Botin *et al* (1997) published an article on the calibration and first test runs of the T'3 tunnel at the von Karman Institute. The primary use of these facilities came with the advent of transonic wind tunnels, however model trends in subsonic wind tunnel testing are driving ratio of model size to test section area upward to better simulate flight Reynolds numbers. Larger model sizes introduce stronger coupling with the walls so in several methods have been considered to reduce the interference effects in subsonic wind tunnels through adaptive wall technology and ventilated wall techniques. These methods were presented in Crites (1995), and are discussed briefly here.

The basic principle behind adaptive wall technology is to reduce the interference effects by modifying the wall so that the stream tube containing the model would not change if the walls were removed. One of the ways to accomplish this would be to streamline the walls, or to control the cross flow through ventilated walls. Reducing the interference correction is only a small portion of the difficulties in aero acoustic testing. The problem still remains that for aero acoustic testing, where the ability to measure the noise levels on the model is of paramount importance, most of the tunnels that are currently in operation consist of a free jet and jet catcher. However over the last two decades, advances have been made to modify existing solid wall facilities to make them suitable for acoustic testing. The NASA Lewis wind tunnel was modified in 1977 to achieve lower background noise levels in the test section (Dietrich *et al*.). These modifications include acoustic treatment on the test section walls floor and ceiling, as well as a remote drive muffler, acoustic muffler between the compressor and the test section and finally acoustic treatment on the first turn upstream and downstream of the test section. With these features the background noise levels (1/3 octave band) in the test section are 83 dB at 1000 Hz for a 40 m/s flow velocity.

Another anechoic chamber that was designed in 2002 is the Anechoic Test facility at the University of Florida (Jansen *et al*.). This facility was designed to enable scaled aerodynamic testing of various types of models. This tunnel measures 5.5 x 5.3 x 2.3 m and consists of fiberglass wedges with cloth covers. The wedges are designed to achieve a low frequency cut-off of 100 Hz. The tunnel contains a free jet with variable acoustically treated flow restrictor panels to entrain the flow, and a variable speed fan assists in pulling the flow through the chambers. The dual screw compressor can continuously feed a 2.54 cm diameter Mach 2 jet. With these features the background noise levels (1/3 octave band) in the test section are approximately 60 dB at 1000 Hz for a 0.3 Mach flow.

This facility was updated in 2005 to upgrade the previously calibrated ISO3745 anechoic chamber into an anechoic wind tunnel facility capable of measuring airframe noise (Mathew *et al*.). This facility features a rectangular test section measuring 0.74 m x 1.12 m x 1.83 m with a maximum test section velocity of 76 m/s (Reynolds number based on chord of about 3 million). This is an open jet configuration as well, with the overall sound pressure level (SPL) from 100 Hz – 20 kHz of about 50 dB at 17 m/s. The interference correction was not reported for this facility.

While these solid wall modifications have greatly improved the aerodynamic quality of the data, they are still below the free jet facilities in acoustic quality, and the current anechoic free jet facilities are still limited in aerodynamic capabilities. Is needed is a facility that has the aerodynamic performance characteristics of a solid wall tunnel, with the low background noise levels inherent in the free jet design.

Researchers at Virginia Tech have attempted to overcome these difficulties through the design of a Kevlar walled test section and pair of anechoic chambers that will function aerodynamically as a solid wall test section, but will be acoustically open. Jaeger *et al* investigated different means of shielding a microphone phased array embedded in a wall of a test section and found that tensioned thin weave Kevlar 120® (7.9 grams/cm2) transmitted sound with very little attenuation up to at least 25 kHz, and to be much more durable than metal weave or fiberglass. They then compared measurements made with their phased array system recessed behind a Kevlar sheet and flush with the wind tunnel wall, demonstrating much greater signal-to-noise ratio in the

former case. Tests with this material at Virginia Tech have produced similar results (Ravetta, *et al.*).

Over the past 3 years several modifications have been made to the Virginia Tech stability wind tunnel to modify the facility to function as both an aerodynamic solid wall test section (original configuration) and as an aeroacoustic tunnel. This has been accomplished in several stages. In 2005, a prototype section was designed and tested (Smith *et al* and Camargo *et al*) to validate the concept. The existing stability tunnel solid wall test section was modified to incorporate prototype acoustic treatment, two large Kevlar side-walls and surrounding acoustic enclosures. In-flow microphone measurements over the whole speed range of the facility showed that the acoustic treatment was effective in reducing noise levels by 8 to 15 dB. A NACA0012 airfoil model was placed inside the modified test section to perform aerodynamic and aeroacoustic measurements for proof-of concept. Tests with and without an airfoil model showed the Kevlar side-walls can quietly and stably contain the flow. Furthermore, they were shown to significantly reduce lift interference. Complete prototype facility diagrams and details on the measurements performed can be seen in the previously cited publications: Smith *et al* (2005) and Camargo *et al* (2005).

Following the successful proof on concept data gathered from the 2005 prototype installation. an iterative sequence of calibration measurements and improvements were then performed; the results were a facility that combines low background noise and high aerodynamic quality. The novel anechoic test section design utilizes Kevlar cloth to provide a stable flow boundary, which eliminates the need for a free jet and jet catcher and greatly reduces aerodynamic interference corrections. An extensive program of experiments has been conducted to examine the performance of this new hardware under a range of conditions. This thesis serves as the conclusion of a developmental research program with the following goals:

1. To acoustically treat the wind tunnel circuit to provide further reductions in background noise levels.
2. To perform a calibration of both the aerodynamic and acoustic properties of the anechoic facility in preparation for future commercial use.

3. To determine the interference correction for the anechoic facility and to prove its accuracy through testing with other commercial models and validation through a modified panel method.

This thesis will cover the second and third phases of this program in which the prototype facility (phase one) that was designed and tested in 2005 has been completed and installed as a part of the Virginia Tech Stability Wind Tunnel. Chapter 2 contains a detailed description of the Virginia Tech Stability Wind Tunnel in the current solid wall configuration, the newly designed removable anechoic facility, and the various apparatus and instrumentation that were designed to complete the range of calibration measurements. Chapter 3 will contain the details on phase 2, in which the initial full scale anechoic facility was constructed and tested during the summer of 2006. Phase 3 (2007), which details the modifications made after the intermediate calibration and conversion of the facility into its current state, will be covered in chapter 4.

2. APPARATUS AND INSTRUMENTATION

2.1 Stability Wind Tunnel

All experiments were performed in the Virginia Tech Stability Wind Tunnel. In the hard wall configuration, this facility is a continuous, single return, subsonic wind tunnel with a 7.3 m long removable solid walled rectangular (1.83 m square) test section. The general layout is shown in figure 2-1.

The tunnel has a maximum speed in the test section of about 80m/s with a Reynolds number per meter up to about 5,300,000. The fan (figure 2-2) has 8 Clark Y section blades measuring 4.27 m in diameter. Power is generated by a 0.45 MW variable speed DC motor driving the propeller at up to 600 revolutions per minute (rpm). During testing the tunnel rpm limit has been exceeded several times during testing, and a more accurate limit of the motors capability is a current limit of 900 Amps. The model catcher that is shown in figure 2-2 has been removed and replaced by a newer and more acoustically friendly apparatus, which will be discussed in detail in a later section. While this tunnel forms a closed loop, there is a section open to the atmosphere in the air exchange tower located downstream of the fan.

The flow leaving the fan travels downstream into a 5.5 m square settling chamber which contains 7 turbulence reduction screens, featuring a 60% open air ratio. The flow exits this chamber into a 9:1 contraction nozzle which accelerates the flow entering the test section. After the flow travels the length of the 7.3 m test section, it passes into a 3 degree diffuser which contains 16 vortex generators spaced at 0.39 m around the floor, walls, and ceiling (figure 2-3). The four corners in the flow path (refer to figure 2-1), are equipped with a diagonal arrays of shaped turning vanes. Spacing between the vanes is 30 cm except in the corner immediately ahead of the settling chamber where the spacing is reduced to 7.6 cm. These vanes were a suspected noise source during the initial prototyping, and several experiments were preformed to examine the possibility of reducing the overall noise of the circuit through treatment of these turning vanes, as well as several of the larger wall areas along the flow path. This will be discussed in more detail later in section 2.2.4.

Flow through the empty hard wall test section is both closely uniform and of low turbulence intensity. Choi and Simpson (1987) measured the lateral integral scales of the stream wise velocity in both the horizontal L_z and vertical L_y directions. They found L_z=56mm for 15m/s and 28mm for 37.5m/s and L_y=122mm for 15m/s and 25mm for 37.5m/s. Table 2-1 shows recent measurements made in 2006 (courtesy of Staubs and Borgoltz) detailing the flow uniformity and stream wise turbulence intensity as functions of flow speed. Turbulence levels for the two primary testing speeds were as low as 0.024% and 0.031% at 30 and 57 m/s respectively.

The test section itself is located in a hermetically sealed steel building, and the pressure inside this control room is equalized through a small opening in the diffuser side wall. Subsequent testing has shown that this door can be removed and covered with a Kevlar cloth to further reduce noise levels in the tunnel. The sealant surrounding the main personnel entrance to the tunnel was also replaced to reduce potential air leakage.

2.2.1 Hard Wall Test Section

In its original configuration, the Stability Wind Tunnel has a 7.3 m long and 1.83 m square hard walled test section. The test section is built around a steel beam structure with the primary structural members defining a series of rectangular frames. These frames are filled in with panels of various materials, ranging from steel plate to Plexiglas. The nominal dimensions for each frame are 1.83 x 0.91 m or 1.83 x 0.76 m depending upon the panel location. Each of these panels is attached to the test section frame using a series of countersunk screws, and the panels can be removed and replaced to accommodate various testing situations. Over the last few years more of the steel panels have been replaced with Plexiglas to allow for greater visibility into the test section. At the upstream and downstream edges of the test section there is a shallow rectangular cavity. This cavity provides the clearance necessary for the interchangeable test section system to be removed and installed. This configuration will be referred to as “hard walled” throughout the remainder of this thesis.

In order to characterize the flow entering the test section, a series of measurements were taken at eight stream wise positions along the length of the test section. A 1/8th in diameter bent Pitot static probe was attached to the steel airfoil strut

used for the single microphone noise measurements (described in detail in section 2.5). This apparatus was attached to the floor of the test section using four of the Neodymium rare earth magnets and positioned at eight stream wise positions (0, 123.19, 175.26, 241.3, 365.76, 393.7, 510.54, and 581.66 m) and a vertical distance of 1.003 m above the floor and 0.1 m from the port side wall. This required making eight individual measurements because the bent Pitot static probe mount had to be re positioned by hand which required running the tunnel up and back down for each of the eight measurements for each speed. This procedure introduces a marginal amount of uncertainty into the measurement, but special care was taken to maintain the tunnel flow speed to within 0.5 m/s. With the bent Pitot static probe measurements, the pressure field along the hard wall test section could be determined. The static pressure measured along the Port side test section wall is given in figure 2-4. . These measurements were made 0.1 m inside the wall and midway between the test section floor and ceiling. Stream wise position refers to distance from the test section entrance. C_p is the static pressure coefficient and is referenced to conditions to the test section entrance center. Figure 2-4 shows that there is a slight gradient along the hard wall test section that reaches a maximum at the exit of about negative 0.03. This negative pressure gradient is a result of the boundary layer growing along the walls and reducing the effective area at the test section exit, increasing the local flow velocity and reducing the pressure. Similar trends were observed for 30 and 50 m/s flow speeds.

2.2 Acoustic Treatment

A major focus of this study was to examine the effectiveness of various acoustic treatments that could be applied to areas within the tunnel circuit to reduce the background noise levels in the flow. Additionally this thesis serves to analyze the effectiveness of the anechoic system that was installed after analysis of the prototype configurations was completed in 2005 (Camargo *et al*).

Conversion of the original hard wall configuration of the stability tunnel into an acoustic facility required designing three sections; a replacement test section, and two anechoic chambers. Figures 2-5 and 2-6 show the overall layout of the redesigned

facility. The following sections describe the redesigned test section and anechoic chambers in detail.

2.2.1 Test Section

Figure 2-7 is a detailed view of the anechoic facility test section. The top diagram is a view of the suction side of the test section from the exterior, while the bottom diagram is drawn from inside of the suction side of the test section. This diagram represents the view from both inside and outside of the test section across sectional line B-B in figure 2-6. A photograph with some dimensions and other features is shown in figure 2-8. This photograph shows the test section exterior without the acoustic window installed, as dimensioned in figure 2-7. The interior of this test section has the same interior dimensions as the original hard wall test section. This allows the anechoic test section to replace the hard wall section with few modifications to the facility.

The new test section has a 1.85 m square cross section, with an interior Kevlar window length of 5.13 m in the stream wise direction (see figure 2-7). The remaining 2.13 m of the test section length are steel panels that lead into the contraction and diffuser on each end of the test section. Diagrams of the floor and ceiling of the anechoic test section are given in figure 2-9. The ceiling of the test section consists of six stream wise panels that are 1.168 m in length and span the width of the test section. These panels are 1.83 m wide and measure 1.219 m in the stream wise direction although some panels vary in length as shown in figure 2-9. Each panel is 0.32 cm thick steel perforate with 2.5 cm diameter holes for structural rigidity and covered in tensioned Kevlar cloth. Above and below these panels are 0.46 m tall acoustic wedges arranged in alternating directions. These wedges were sized with a low frequency limit of approximately 185 Hz. The third panel downstream from the contraction was modified to contain a mount for aerodynamic models (figure 2-9). Several of the 0.46 m acoustic wedges were removed from the ceiling panels and a steel beam 1.85 m long and 0.15 m wide was mounted above the steel perforate panel's perpendicular to the flow direction to support a model (refer to figure 2-8 and 2-9). A 0.15 m square aluminum block with an 88.9 mm diameter circular cut out was mounted to the steel beam to hold the spar of the airfoil

models (figure 2-10). The circular opening in the floor of the ceiling panels (0.216 m in diameter) was covered with an aluminum tape when the test section was empty.

The floor of the test section was designed in much the same way as the ceiling. There are two Kevlar covered steel perforate panels that form the exit from the contraction (figure 2-19), that are lined with 0.46 m acoustic wedges and two of the same panels that lead into the diffuser. The center floor panels exactly replicated the ceiling configuration; with one center panel that could be removed to access the wedges and the model mount underneath.

Each wall of the test section comprised of an aluminum tensioning frame which held a tensioned Kevlar cloth window. The tensioning frame, shown in the upper diagram of figure 2-7, is a Roller Chase Frame manufactured by ENCO, and modified by the Aerospace Engineering Machine Shop personnel to fit the test section. The exterior dimensions of the tensioning frame are 4.95 x 2.48 m. The four aluminum sections that form the walls of the frame are 0.15 m wide and 0.0508 m thick, and contain Nylon tensioning rods 4.75 ± 0.15 mm in diameter. There are 18 aluminum angles 51 mm on end that secure the tensioning frame to the sides of the test section.

On the exterior of the test section is a seal consisting of 19 mm of rubber. When the chambers are placed adjacent to the test section, the open end of each chamber presses against the steel frame of the test section with the rubber providing an insulating seal.

2.2.2 Acoustic Chambers

Two anechoic chambers were designed to enclose the modified test section. The chamber, shown in detail in figure 2-11, consists of a steel and MDF wall structure enclosing an arrangement of acoustic wedges. Each chamber is assembled in two parts, with the upper section detached during the installation and removal process. The lower section of the acoustic chambers is 2.92 m tall, 5.52 m wide and 2.75 m deep. The upper sections of the acoustic chambers measure an additional 1.17 m in height. Additionally they were mounted onto a platform to each the test section, the base of which sits approximately 3.05 m off of the floor. As seen in figure 2-4, the full width and height of the assembled facility measure 8.255 m and 6.096 m respectively. A single door

measuring 1.016 m wide and 2.235 m tall is located on one side of each chamber. These doors have 3 clamps on the exterior of the chamber that seal the doors from the outside. This requires any mass flow passing through the windows to remain inside the chambers. When the system is completely installed the port side chamber door is on the downstream end of the chamber and the starboard chamber door is on the upstream end of the starboard side chamber. A side view of the port side chamber is shown in figure 2-12.

Arrays of acoustic wedges line each of the 5 solid walls of each chamber. The 0.610-m high acoustic foam wedges are glued to 19-mm thick MDF boards using standard urethane adhesive. These wedges, measuring 0.31×0.62m at the base, were arranged in a checkerboard pattern (figure 2-13) with a few modifications around the door and open side of the chamber. Nine acoustic foam cubes span the length of the open side of the anechoic chamber floor and ceiling, each measuring 0.610 m tall, 0.603 m wide and 0.432 m deep. The wedges that line the sides of each chamber that meets the test section are quarter ellipses, these transition pieces are 0.601 m in length, with a base of 0.203 m by 0.610 m (figure 2-14). Once the chambers have been placed against the test section, modified quarter elliptical acoustic wedges (figure 2-15) are placed atop the cube wedges that line the floor and ceiling edges of the acoustic chamber. The ceiling transition wedges are attached with 6 in wide industrial strength Velcro, so they can be removed during assembly and removal. Figure 2-16 shows a view into the test section from the chamber with a section of the window removed on the starboard side. This figure also shows the wedges that were used to create a smooth transition between the edges of the chamber and the test section floor.

2.2.3 Kevlar Windows

Many of the anechoic facilities that are currently in operation or in the design phases utilize an open test section, namely a free jet and jet catcher system. This results in a flow that is both acoustically and aerodynamically open. A different approach was designed and tested in 2005 (Smith *et al*) in the Virginia Tech Stability Wind Tunnel.

The current configuration of the anechoic facility that has been described in the previous sections utilizes a tensioned Kevlar cloth to form the test section flow surface. The Kevlar is transparent to sound but at the same time largely contains the flow. It thus

offers the potential to produce an acoustically open test section without the need for a jet catcher and while eliminating at least a fraction of the lift interference effect. The use of tensioned Kevlar cloth as an acoustic window was pioneered by Jaeger *et al.* (2000). While Jaeger *et al.* (2000) demonstrated the usefulness of Kevlar cloth as a covering for a wall-mounted phased array system; the goal was to use the Kevlar cloth as a replacement for the free-jet boundary that is conventionally used in acoustic wind tunnels.

Details of the small prototype frames that were used during initial testing are discussed in Camargo *et al* (2005). This technology was then scaled up to cover the entire length of the test section. There is currently no commercially available Kevlar cloth that fits the dimensions needed for this facility; so in order to cover the test section completely, the Kevlar had to be sewn at two locations to generate the full 1.854 m of test section height. In order to minimize possible failure locations, two seams visible to the flow ran the length of the test section at approximately 0.216 m from the test section floor and ceiling (see figure 2-7). This 25 mm seam was covered with super glue as an added support measure. Figure 2-17 shows a photograph of the window before installation.

To mount and tension the material an ENCO Large Roller Chase frame was used. The cloth is tensioned using 4 rollers (figure 2-18) one on each side of the frame – a system that can apply tensions as large as 1 tonne per linear meter of the frame length. This type of frame also holds the cloth slightly above of the rest of the frame, allowing one side of the cloth to be used as the flow surface, without any part of the frame projecting into the test section. Plain weave Kevlar 120® cloth was mounted in the frame and tensioned and the frame mounted to the test section wall. The Kevlar provided a smooth and subjectively rigid flow surface.

2.3 Discussion of Absolute Coordinate Systems

In order to simplify several of the measurements that will be discussed over the next several sections, all of the data will be referenced to a main coordinate system. Individual measurements will have coordinate systems unique to the measurement, but all final data will be reported using the following system shown in figure 2-19. The X coordinate is positive in the stream wise direction, and the Z coordinate is positive up, which by right hand rule yields a Y coordinate to the right looking upstream. The

absolute origin was located on the port side of the test section at the upstream edge (figure 2-19). For the measurements that utilized an airfoil, positive angle of attack was defined with the trailing edge towards the left looking upstream (figure 2-20). This would imply that the pressure side of the model was on the port window, and the suction side of the model was towards the starboard window. For the purposes of this report, port and starboard are used almost exclusively, but some of the details regarding the model are referenced to the pressure-side and suction-side. Additionally the anechoic chambers were named port and starboard chamber for their corresponding test section window.

2.4 Airfoil Models

Throughout the calibration process (spanning 2006 and 2007) several models were installed in the anechoic and hard wall test section to determine various characteristics of the system. The following sections cover the details (where available) of all of the models that were used for the calibration of the anechoic facility.

2.4.1 NACA 0012

The primary aerodynamic measurements used to calibrate the tunnel were performed on an NACA 0012 airfoil model, figure 2-21. The model, constructed by Novakinetics LLC, was designed to span the complete vertical height of the test section, with a 181.6 cm span, 91.4 cm chord and 11.0 cm maximum thickness. A steel tube measuring 8.89 cm in diameter forms the main spar centered on the quarter chord location. The steel tube projects 16.6 cm from each end of the airfoil and was used for mounting. The model has a fiberglass composite skin and a fill of fiberboard and polyurethane foam.

The model was instrumented with a total of 82 pressure taps of 0.5mm internal diameter located near the mid span, locations of these taps are listed in table 2-2. The shape of the model was measured in the AOE Machine shop in 2004 by comparing the model section at the ¼, ½ and ¾ span locations with a measured reference thickness distribution. Deviations from this profile were found to be less than ±0.13mm at all locations, except over the hatch at mid span where the deviations were less than ±0.3mm. The reference profile itself shows the airfoil to be slightly thicker than the intended shape

by about 0.15% chord at most stations. Details on the measured profiles and comparison with actual port locations can be found in Camargo *et al*.

During the 2006 initial entry, the NACA 0012 model was mounted vertically in the test section, as shown in figure 2-22, with its leading edge (at zero angle of attack) 3.315 m downstream of the test section entrance ($X = 3.315$). In this configuration there was still approximately a half inch on the top and bottom of the airfoil that had to be sealed before any acoustic measurements were taken. This proved time consuming during periods of multiple angle of attack changes, and a system redesign was considered for future entries.

The zero angle of attack of the model was determined using the measured pressure distribution, and the computed interference correction, discussed in detail in chapter 4. During the 2006 entry, the angle of attack was computed using the distance the trialing edge had moved away from the pressure window. The general uncertainty in this system was estimated to be ± 0.3 degrees.

2.4.2 Model DU96

Like the NACA 0012 model discussed in Section 2.4.1, the DU96 model (figure 2-23) was also constructed by Novakinetics Inc. This airfoil section has a maximum thickness of 15% and a chord length of 0.9144 m. The model was instrumented with a total of 82 pressure taps of 0.5mm internal diameter located near the mid span, locations of these taps are listed in table 2-3. The mounting configuration for this model (and the rest of the models presented) was the same as the NACA 0012. This model was only installed during the 2007 entry and was used primarily for a corporate test. The pressure distributions acquired for this model were used to confirm the lift interference correction for the facility. These distributions are presented in chapter 4.

2.4.3 Model DU97-W300

The DU97-W300 model (figure 2-24) was constructed by Novakinetics Inc., and has a maximum thickness of 30% and a chord length of 0.9144 m. Unlike some of the models previously discussed, this section shape has a thick (25 mm) trailing edge. The model was instrumented with a total of 82 pressure taps of 0.5mm internal diameter

located near the mid span, locations of these taps are listed in table 2-4. The mounting configuration for this model was the same as the NACA 0012; vertically between the two Kevlar windows with the center of rotation 3.54 m from the entrance of the test section. This model was only installed during the 2007 entry and was used primarily for a corporate test. The pressure distributions acquired for this model were used to confirm the lift interference correction for the facility. These distributions are presented in chapter 4.

2.4.4 Other Models

Several other models were used to confirm the lift interference correction. Additionally these models were used to examine the correlation between the lift interference correction and the wall deflection compared to a modified panel method prediction. Three other airfoil sections will be mentioned at various times throughout this thesis. The first is a RISO airfoil section. This is a proprietary model, so airfoils section shape and pressure tap locations cannot be reported. The model was constructed in the same fashion as the DU97-W300 and the DU96, and featured 82 pressure ports arrange around the mid span, and featured a chord length of 0.914 m. The maximum thickness of the model was 11% thick. Pressure distributions for this model will be presented in chapter 4 to confirm the interference correction.

Another model that was chosen for this calibration was a 0.6096 m chord NACA 0015 airfoil section. This model was used concurrently with some other testing during the 2006 preliminary calibration, and the majority of the results obtained on this model are presented in Chapter 3. During the recent 2007 calibration, some wall deflection and surface pressure data was gathered to compare with that of the NACA 0012 and to use in the modified panel method developed in Chapter 4.

The final model used for comparison with the interference correction was a 0.203 m chord NACA 0012. This model was chosen to examine both the lift interference correction results as well as the performance of the Kevlar windows under varying model conditions. The majority of the results for all of the models in sections 2.4.1 through 2.4.4 are presented along with determining the lift interference correction both experimentally and with the panel method prediction in Chapter 4.

2.5 Aerodynamic Instrumentation

During all measurements various flow conditions were monitored. Throughout the various experiments several different systems were used, some designed locally and others that were purchased or part of the original tunnel configuration. The following sections detail the various apparatus that contributed to this experiment. All dimensions were measured using a Master Mechanics 15 m tape measure, with an uncertainty of 3.mm unless otherwise noted.

2.5.1 General Instrumentation

The test section flow speed was monitored using an 8-mm diameter Pitot static probe located just upstream of the test section in the contraction. The mouth of the Pitot probe was located 0.41 m upstream of the test section entrance, 1.22 m from the floor and 0.20 m from the port side wall. A calibration of the pressure difference from the contraction to the desired reference location near the center of the test section entrance was accomplished by performing a sequence of measurements using a second Pitot probe positioned here (figure 2-25). This second probe, a single 1/8th inch Pitot static probe, was mounted on a magnetic stand 0.152 m downstream of the inlet and placed at the 0.914 m form the port wall and 1.003 m above the test section floor. We may define a pressure coefficient in terms of the conditions at the contraction probe as:

$$C_{p_{raw}} = \frac{P - P_c}{P_{o\infty} - P_c} \quad \textbf{(1)}$$

Alternatively, we may define a coefficient in terms of the conditions at the reference probe as:

$$C_p = \frac{P - P_\infty}{P_{o\infty} - P_\infty} \quad \textbf{(2)}$$

Here, P is the measured pressure, P_c is the static pressure at the contraction Pitot static probe, $P_{o\infty}$ is the reference total pressure, and P_∞ is the reference static pressure. The total pressure at the contraction Pitot static probe and the reference Pitot static probe

will be equal since both probes are outside of the boundary layer region. Combining equation 1 and 2, an equation for the static pressure coefficient C_p can be written in terms of C_{praw} as:

$$C_p = C_{p_{raw}}\left(\frac{P_{o\infty} - P_c}{P_{o\infty} - P_\infty}\right) + \frac{P_c - P_\infty}{P_{o\infty} - P_\infty}$$

$$= C_{p_{raw}}\left(\frac{P_{o\infty} - P_c + P_\infty - P_c}{P_{o\infty} - P_\infty}\right) + \frac{P_c - P_\infty}{P_{o\infty} - P_\infty}$$

$$= C_{p_{raw}}\left(1 + \frac{P_\infty - P_c}{P_{o\infty} - P_\infty}\right) + \frac{P_c - P_\infty}{P_{o\infty} - P_\infty}$$

This equation could be rewritten as:

$$C_p = C_{p_{raw}}\left(1 - C_p\Big|_c\right) + C_p\Big|_c \qquad \textbf{(3)}$$

Where the correction factor $C_p\Big|_c$ is given by:

$$C_p\Big|_c = \frac{P_c - P_\infty}{P_{o\infty} - P_\infty} \qquad \textbf{(4)}$$

The static pressure coefficient measured in terms of conditions at the contraction mounted probe can therefore be corrected to reference conditions by experimentally determining the correction factor. Using the previously discussed Pitot static probes, the value for $C_p\Big|_c$ was evaluated over various flow speeds, and the average was experimentally determined to be 0.01. This correction was applied to the data at the conclusion of testing.

Pressure differences at the contraction Pitot static probe were sensed using a Setra 239 pressure transducer with a range of 0-15" H_20. Temperature in the test section was monitored using an Omega 19 Thermistor type 44004 (accuracy ±0.2°C) and the ambient absolute pressure was determined using a Validyne DB-99 Digital Barometer (resolution 0.01" Hg). A series of Setra model 239 pressure transducers (with ranges of ±7.5" H2O,

±15" H2O and ±2.5 p.s.i.) were used to measure static pressures on the airfoil surface. During the 2006 entry these transducers were zeroed and calibrated against the wind tunnel transducer to minimize errors associated with difference in offset and sensitivity. Pressures from the 82 pressure taps on the airfoil model surface were directed through a Scanivalve system for measurement. Using a sampling frequency of 1000 Hz, 3 seconds of data were recorded to form time average values. During the 2007 entry a different Setra 239 pressure transducer with the same range was used as the reference transducer. Pressures from the 82 pressure taps on the airfoil model surface were directed through a modified Scanivalve system for measurement. The pressure from each tap, converted to voltage by the transducer, was measured simultaneously with the reference dynamic pressure using an HPVee Agilent Pro data acquisition system and manually stepped through the pressure ports. Using a sampling frequency of 1000 Hz, 1 second of data was recorded to form time average values.

The two-axis wind tunnel traverse shown in figure 2-26 was used to position probes in the test section. The traverse, which is capable of positioning a probe to within about 0.025mm (Zsoldos, 1992) mounts inside the test section or inside the diffuser depending on the measurement location. The traverse produces an overall solid blockage of about 10% so probes are supported upstream to avoid accelerations associated with this. Additionally a traverse restraint system was designed to prevent the traverse from moving when it was placed in the diffuser for test section exit boundary layer measurements. This system consisted of two aluminum beams 1.524 m in length and 10 mm in cross section that were attached to the wooden supports at the base of the traverse, and positioned against the vortex generators.

2.5.2 Intermediate Calibration Instrumentation

During the 2006 intermediate calibration, the empty test section boundary layer and the Kevlar window pressure distribution measurements were accomplished with a single Pitot static probe mounted on a moveable stand that could be magnetically attached to the test section floor. This set up (shown in figure 2-27) allowed measurement of discrete static and total pressure measurements at predetermined stream wise positions along the Kevlar windows. Static and total pressures were measured at the

test section inlet and exit to determine the boundary layer thickness on the windows. Additionally this mount could be magnetically attached to the side walls of the inlet and exit (figure 2-28) to determine the boundary layer thickness at the floor and ceiling. Static pressures were recorded along the length of the window to compute the velocity of the flow through the windows as well as the total mass flow across the surface. All static and total pressure measurements were taken using a Dwyer Mark III digital hand manometer with a resolution of 0.01" H20. While these systems gave good preliminary results, the limited value of data that could be acquired required that new systems be designed for the 2007 calibration to reduce the measurement and statistical uncertainty.

2.5.3 Wall Pressure Mounting Rail and Transducers

The desire to make more measurements in a smaller time frame along with a larger test matrix was the driving factor behind the design of the aluminum rail window pressure measurement system. The aluminum rail system shown in figure 2-29 was used to measure the static pressure along the interior of the Kevlar windows in the test section. Five Dwyer straight Pitot static probes with a 1.6 mm diameter and measuring 0.432 m in length were used to obtain static pressure measurements. The probes were mounted on a 7.62 m section of 51 mm x 25 mm aluminum extrusion beam manufactured by 80/20 Inc. The rail was secured to the contraction and diffuser with two diagonally offset screws on each end, and mounted with the 51 mm dimension in the *Z* direction to reduce the potential "droop" at the centermost stream wise position. Aluminum standoffs (0.305 m) were used to separate the probe tip from the influence of the beam, and were attached to the rail with free moving sliders that could be fixed in place using wing nuts (figure 2-30). When the beam was mounted the maximum deflection of the beam was approximately 76 mm ± 9 mm depending on where the sliders were located. With the probes mounted to the sliders there was a clearance of 0.273 m between the top of the beam and the probe tips. The probes were positioned 102 mm ± 12 mm away from the window to prevent contact between the Kevlar and the probe tips. The Pitot static probes as well as the transducer system used in this test were the same described in the previous section. The sampling scheme used for all wall pressure measurements was 30000 samples at 3200 Hz for a total sampling time of about 10 seconds.

As a baseline for measurements made in the anechoic test section, static pressure measurements were made to determine the difference in the static pressure sensed by a straight Pitot static probe compared with a standard Pitot static probe. In standard bent Pitot probe design, the static ports are placed at a location to exactly cancel out a pressure gradient developing along the probe stem with that induced by the bend in the Pitot probe. For a straight Pitot static probe, there is no "bend" to cancel out the pressure gradient that grows along the probe stem. In order to determine a correction that could be applied to the data acquired using the straight Pitot static probes the aluminum rail was mounted in the tunnel with the probe tips 0.343 m above the floor adjacent to the port window side of the test section. The eight Pitot static probes were mounted at various stream wise distances (0, 123.19, 175.26, 241.3, 365.76, 393.7, 510.54, and 581.66 m) along the length of the test section. A series of data points were taken at nominal speeds of 30 and 50 m/s Figure 2-31 and 2-32 show the plots of the measured pressure coefficients for the two probes at 30 and 50 m/s. The pressure coefficients measured using the straight probe are consistently 0.005 and 0.007 above those measured with the standard probe at 30 and 50m/s respectively. For all subsequent pressure measurements using the straight Pitot static probes, static pressure coefficients have been adjusted to account for these straight probe corrections.

2.5.4 Probe Rake and Transducers

Several of the measurements that were planned for the 2007 calibration required the development of a Pitot static probe rake system (figure 2-33). In the rake configuration, this system was used to measure the boundary layer profiles at the four walls of the entrance and exit of the test section. The rake consisted of five Dwyer straight Pitot static probes with a 1.6 mm diameter and measuring 0.432 m in length. These probes were mounted 25 mm apart using an aluminum mounting block (T6061 aluminum measuring 254 mm x 51 mm x 9.5 mm) and secured with five set screws to prevent rotation. A thin (6 mm) Nylon block was used to maintain the probe spacing along the length of the probes. Figure 2-34 is a photograph of the probe holder for the rake system. The aluminum mount was attached to a 38 mm diameter piece of conduit, 2 m in length with a 60 degree bend 1 m downstream from the aluminum mount to

minimize an interference effects. With the probes mounted on the conduit, this entire system was clamped to the two axis wind tunnel traverse (figure 2-26) using a clamp design shown in figure 2-35. There were two clamps placed approximately 356 ± 25 mm apart in the stream wise direction. This system allowed the conduit to be rotated to any angle (full 360 degree rotation) to reach the four walls of the entrance and exit of the test section. Mounting the conduit in this fashion placed the aluminum block 1.568 m upstream of the plane of the traverse and the static pressure ports and additional 0.318 m upstream. This gave a final total pressure port location of 1.911 m upstream of the traverse. The rake could also be used vertically to measure the wake behind the various airfoil sections at five simultaneous positions, allowing an average value to be determined. Each of the five probes was connected to two Setra 239 transducers, via 3 mm Tygon tubing, to measure total and static pressure against the tunnel reference pitot static system previously described. These 10 measurement transducers were set with a range of ±7.5" H2O. The sampling scheme used for all boundary layer measurements was 30000 samples at 3200 Hz for a total sampling time of about 10 seconds. For all pressure measurements using the straight Pitot static probes, static pressure coefficients have been adjusted to account for the straight probe correction in the same manor as discussed in section 2.5.3.

2.5.5 Wall Deflection Measurement Equipment

The wall deflection measurement apparatus shown in figure 2-36 was used to determine the absolute displacement of the Kevlar windows during tunnel operation. The top and bottom wedges were removed from each chamber to insert this 25 mm x 25 mm aluminum extrusion (manufactured by 80/20 Inc.). A special slider (51 mm x 102 mm) was attached to the rail and could be traversed up and down the beam and secured by a hand break. A steel metric ruler was then placed just touching the window and the distance was recorded. A zero flow profile was determined by recording the distance where the magnets attached to the test section at the top and bottom of the window (forced zero deflection) and a linear slop was used to fill in the points throughout the window. Measurement of the deflection was accomplished from inside the chamber while the tunnel was running. Several conditions were measured including the empty

tunnel at nominal 30 and 50 m/s, as well as with the NACA 0012 model at 0 and 8 degrees effective angle of attack at 30 m/s.

2.6 Microphones

Measurements of in flow noise levels in the test section out of flow noise levels within the chambers were made using Brüel & Kjær (B&K) microphones and related equipment. The flowing sections give details on each of the measurement set-ups.

2.6.1 In Flow Microphones

To measure the background noise levels within the test section a $1/8^{th}$ diameter condenser microphone, model 4138 was used. This microphone was fitted with a model UA 0355 nose cone and mounted to a model 2670 preamplifier (using a model UA 0160 adapter). The microphone was aligned with the free stream and supported, using the airfoil strut shown in figure 2-37, some 756mm above the center of the test section floor. This strut measures 76 mm at the base and 35 mm at the top with an upper surface thickness of approximately 8.4 mm. The microphone cable was allowed to hang loose and secured to the floor after previous testing determined that taping the cable to the trailing edge of the model strut promoted vortex shedding, producing a measurable narrow band sound (Camargo *et al, 2005*). The microphone was operated using a B&K NEXUS 2690 conditioning amplifier, and signals were recorded using the Agilent digitizer at a sampling rate of 51.2 kHz with anti-alias filtering above 20 kHz. The acoustic spectra were formed by averaging 250 records of 8192 samples, resulting in a frequency resolution of 6.25 Hz. The microphone was calibrated prior to each set of measurements using a pistonphone so sensitivities could be determined for each measurement. The sensitivity, reported for each measurement in the subsequent chapters, was approximately 0.55mV/Pa, with slight variation depending on the daily conditions.

2.6.2 Out of Flow Microphones

To measure the background noise levels within the test section a 0.5 in diameter condenser microphone was used. This microphone was fitted with a model B&K nose cone and mounted to a B&K preamplifier. The microphone was aligned perpendicular to

the test section window (figure 2-38) to measure the suspected contribution of the 1/8th inch microphone mount to the background noise levels in the test section. Out of flow measurements confirmed the interference of the microphone strut over a range of frequencies, (details in the chapter 4). The microphone was operated using a B&K NEXUS 2690 conditioning amplifier, and signals were recorded using the Agilent digitizer at a sampling rate of 51.2 kHz with anti-alias filtering above 20 kHz. The acoustic spectra were formed by averaging 250 records of 8192 samples. The microphone was calibrated prior to each set of measurements using a pistonphone so sensitivities could be determined for each measurement. Several other measurements were taken using this microphone set up, details of which are given in Staubs (2008).

Freestream Velocity	RMS Streamwise Fluctuations
V [m/s]	u'/V
12	0.016%
21	0.021%
30	0.024%
48	0.029%
57	0.031%

Table 2-1 Flow Quality in the Virginia Tech Stability Wind Tunnel

Hatch Side		Opposite Side	
x/c	z/c	x/c	z/c
0	0.1032	0	0.2302
0.0025	0.1038	0.0025	0.2296
0.005	0.1043	0.005	0.229
0.0075	0.1049	0.0075	0.2284
0.01	0.1055	0.01	0.2278
0.0125	0.1061	0.0125	0.2273
0.015	0.1066	0.015	0.2267
0.0175	0.1072	0.0175	0.2261
0.02	0.1078	0.02	0.2255
0.025	0.1089	0.025	0.2244
0.05	0.1147	0.05	0.2186
0.075	0.1205	0.075	0.2128
0.1	0.1263	0.1	0.2071
0.125	0.132	0.125	0.2013
0.15	0.1378	0.15	0.1955
0.175	0.1436	0.175	0.1898
0.2	0.1494	0.2	0.184
0.225	0.1551	0.225	0.1782
0.25	0.1609	0.25	0.1724
0.275	0.1667	0.275	0.1667
0.3	0.1724	0.3	0.1609
0.325	0.1782	0.325	0.1551
0.35	0.184	0.35	0.1494
0.375	0.1898	0.375	0.1436
0.4	0.1955	0.4	0.1378
0.425	0.2013	0.425	0.132
0.45	0.2071	0.45	0.1263
0.475	0.2128	0.475	0.1205
0.5	0.2186	0.5	0.1147
0.55	0.2302	0.55	0.1032
0.6	0.2186	0.6	0.1147
0.65	0.2071	0.65	0.1263
0.7	0.1955	0.7	0.1378
0.75	0.184	0.75	0.1494
0.8	0.1724	0.8	0.1609
0.85	0.1609	0.85	0.1724
0.9	0.1494	0.9	0.184
0.92	0.1447	0.92	0.1886
0.94	0.1401	0.94	0.1932
0.96	0.1355	0.96	0.1978
0.98	0.1309	0.98	0.2025

Table 2-2. Pressure tap locations on the NACA 0012 airfoil model

Suction Side		
x/c	x (in)	y (in)
0.0000	0.00	3.7144
0.0025	0.09	3.7352
0.0050	0.18	3.7560
0.0075	0.27	3.7767
0.0100	0.36	3.7975
0.0125	0.45	3.8183
0.0150	0.54	3.8391
0.0175	0.63	3.8598
0.0200	0.72	3.8806
0.0250	0.90	3.9222
0.0500	1.80	4.1300
0.0750	2.70	4.3377
0.1000	3.60	4.5455
0.1250	4.50	4.7533
0.1500	5.40	4.9611
0.1750	6.30	5.1689
0.2000	7.20	5.3767
0.2250	8.10	5.5844
0.2500	9.00	5.7922
0.2750	9.90	6.0000
0.3000	10.80	6.2078
0.3250	11.70	6.4156
0.3500	12.60	6.6233
0.3750	13.50	6.8311
0.4000	14.40	7.0389
0.4250	15.30	7.2467
0.4500	16.20	7.4545
0.4750	17.10	7.6622
0.5000	18.00	7.8700
0.5500	19.80	8.2856
0.6000	21.60	7.8700
0.6500	23.40	7.4545
0.7000	25.20	7.0389
0.7500	27.00	6.6233
0.8000	28.80	6.2078
0.8500	30.60	5.7922
0.9000	32.40	5.3767
0.9200	33.12	5.2104
0.9400	33.84	5.0442
0.9600	34.56	4.8780
0.9800	35.28	4.7118
1.0000	36.00	4.5455

Pressure Side		
x/c	x (in)	y (in)
0.0000	0.00	8.2856
0.0025	0.09	8.2648
0.0050	0.18	8.2440
0.0075	0.27	8.2233
0.0100	0.36	8.2025
0.0125	0.45	8.1817
0.0150	0.54	8.1609
0.0175	0.63	8.1401
0.0200	0.72	8.1194
0.0250	0.90	8.0778
0.0500	1.80	7.8700
0.0750	2.70	7.6622
0.1000	3.60	7.4545
0.1250	4.50	7.2467
0.1500	5.40	7.0389
0.1750	6.30	6.8311
0.2000	7.20	6.6233
0.2250	8.10	6.4156
0.2500	9.00	6.2078
0.2750	9.90	6.0000
0.3000	10.80	5.7922
0.3250	11.70	5.5844
0.3500	12.60	5.3767
0.3750	13.50	5.1689
0.4000	14.40	4.9611
0.4250	15.30	4.7533
0.4500	16.20	4.5455
0.4750	17.10	4.3377
0.5000	18.00	4.1300
0.5500	19.80	3.7144
0.6000	21.60	4.1300
0.6500	23.40	4.5455
0.7000	25.20	4.9611
0.7500	27.00	5.3767
0.8000	28.80	5.7922
0.8500	30.60	6.2078
0.9000	32.40	6.6233
0.9200	33.12	6.7896
0.9400	33.84	6.9558
0.9600	34.56	7.1220
0.9800	35.28	7.2882
1.0000	36.00	7.4545

*** Reference NREL Subcontract AAM-4-44831-01**

Table 2-3. Pressure tap locations for the DU96 airfoil model.

Suction Side				Pressure Side			
x/c	x (in)	y (in)cl6	y(in)cl 12	x/c	x (in)	y (in) cl6	y(in)cl 12
0.0000	0.00	3.7144	-2.2856	0.0000	0.00	8.2856	2.2856
0.0025	0.09	3.7352	-2.2648	0.0025	0.09	8.2648	2.2648
0.0050	0.18	3.7560	-2.2440	0.0050	0.18	8.2440	2.2440
0.0075	0.27	3.7767	-2.2233	0.0075	0.27	8.2233	2.2233
0.0100	0.36	3.7975	-2.2025	0.0100	0.36	8.2025	2.2025
0.0125	0.45	3.8183	-2.1817	0.0125	0.45	8.1817	2.1817
0.0150	0.54	3.8391	-2.1609	0.0150	0.54	8.1609	2.1609
0.0175	0.63	3.8598	-2.1402	0.0175	0.63	8.1401	2.1401
0.0200	0.72	3.8806	-2.1194	0.0200	0.72	8.1194	2.1194
0.0250	0.90	3.9222	-2.0778	0.0250	0.90	8.0778	2.0778
0.0500	1.80	4.1300	-1.8700	0.0500	1.80	7.8700	1.8700
0.0750	2.70	4.3377	-1.6623	0.0750	2.70	7.6622	1.6622
0.1000	3.60	4.5455	-1.4545	0.1000	3.60	7.4545	1.4545
0.1250	4.50	4.7533	-1.2467	0.1250	4.50	7.2467	1.2467
0.1500	5.40	4.9611	-1.0389	0.1500	5.40	7.0389	1.0389
0.1750	6.30	5.1689	-0.8311	0.1750	6.30	6.8311	0.8311
0.2000	7.20	5.3767	-0.6233	0.2000	7.20	6.6233	0.6233
0.2250	8.10	5.5844	-0.4156	0.2250	8.10	6.4156	0.4156
0.2500	9.00	5.7922	-0.2078	0.2500	9.00	6.2078	0.2078
0.2750	9.90	6.0000	0.0000	0.2750	9.90	6.0000	0.0000
0.3000	10.80	6.2078	0.2078	0.3000	10.80	5.7922	-0.2078
0.3250	11.70	6.4156	0.4156	0.3250	11.70	5.5844	-0.4156
0.3500	12.60	6.6233	0.6233	0.3500	12.60	5.3767	-0.6233
0.3750	13.50	6.8311	0.8311	0.3750	13.50	5.1689	-0.8311
0.4000	14.40	7.0389	1.0389	0.4000	14.40	4.9611	-1.0389
0.4250	15.30	7.2467	1.2467	0.4250	15.30	4.7533	-1.2467
0.4500	16.20	7.4545	1.4545	0.4500	16.20	4.5455	-1.4545
0.4750	17.10	7.6622	1.6622	0.4750	17.10	4.3377	-1.6623
0.5000	18.00	7.8700	1.8700	0.5000	18.00	4.1300	-1.8700
0.5500	19.80	8.2856	2.2856	0.5500	19.80	3.7144	-2.2856
0.6000	21.60	7.8700	1.8700	0.6000	21.60	4.1300	-1.8700
0.6500	23.40	7.4545	1.4545	0.6500	23.40	4.5455	-1.4545
0.7000	25.20	7.0389	1.0389	0.7000	25.20	4.9611	-1.0389
0.7500	27.00	6.6233	0.6233	0.7500	27.00	5.3767	-0.6233
0.8000	28.80	6.2078	0.2078	0.8000	28.80	5.7922	-0.2078
0.8500	30.60	5.7922	-0.2078	0.8500	30.60	6.2078	0.2078
0.9000	32.40	5.3767	-0.6233	0.9000	32.40	6.6233	0.6233
0.9200	33.12	5.2104	-0.7896	0.9200	33.12	6.7896	0.7896
0.9400	33.84	5.0442	-0.9558	0.9400	33.84	6.9558	0.9558
0.9600	34.56	4.8780	-1.1220	0.9600	34.56	7.1220	1.1220
0.9800	35.28	4.7118	-1.2882	0.9800	35.28	7.2882	1.2882
1.0000	36.00	4.5455	-1.4545	1.0000	36.00	7.4545	1.4545

Table 2-4. Pressure Tap locations for the DU97-W300 Model.

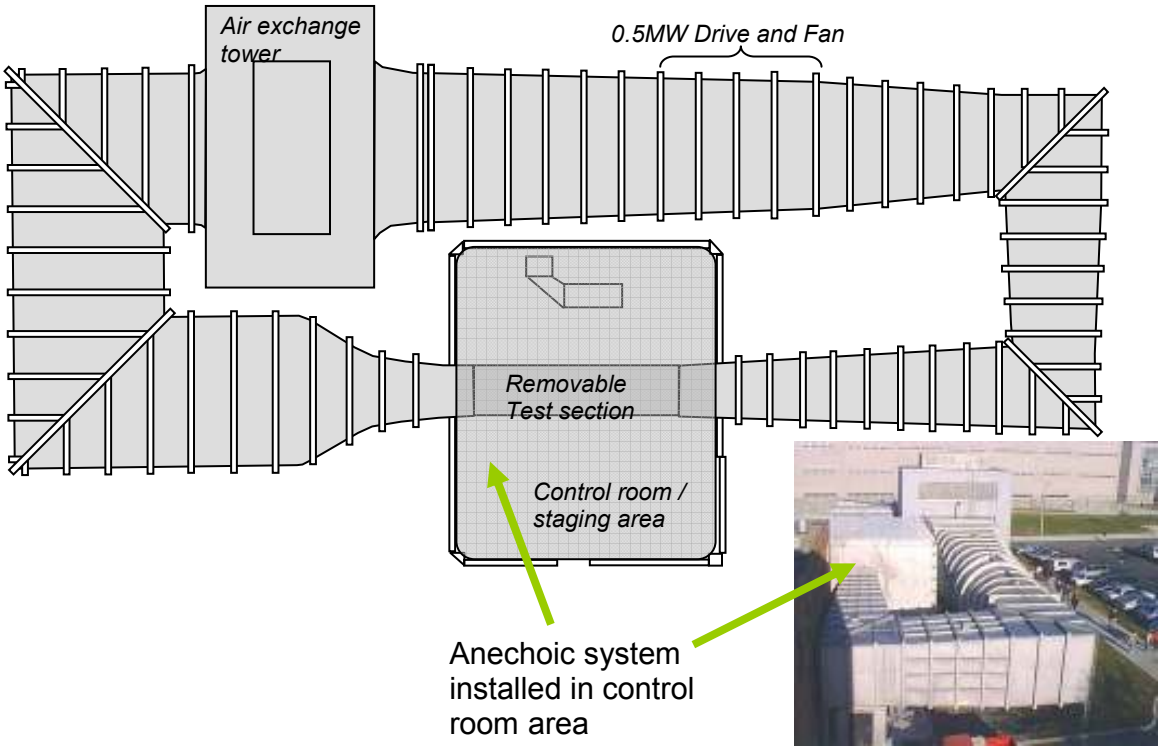

Figure 2-1 Plan view (top) and photograph (bottom right) of the Virginia Tech Stability Wind Tunnel. The photo shows the pressure sealed steel control room which contains the operating console as well as the test section (courtesy AOE department).

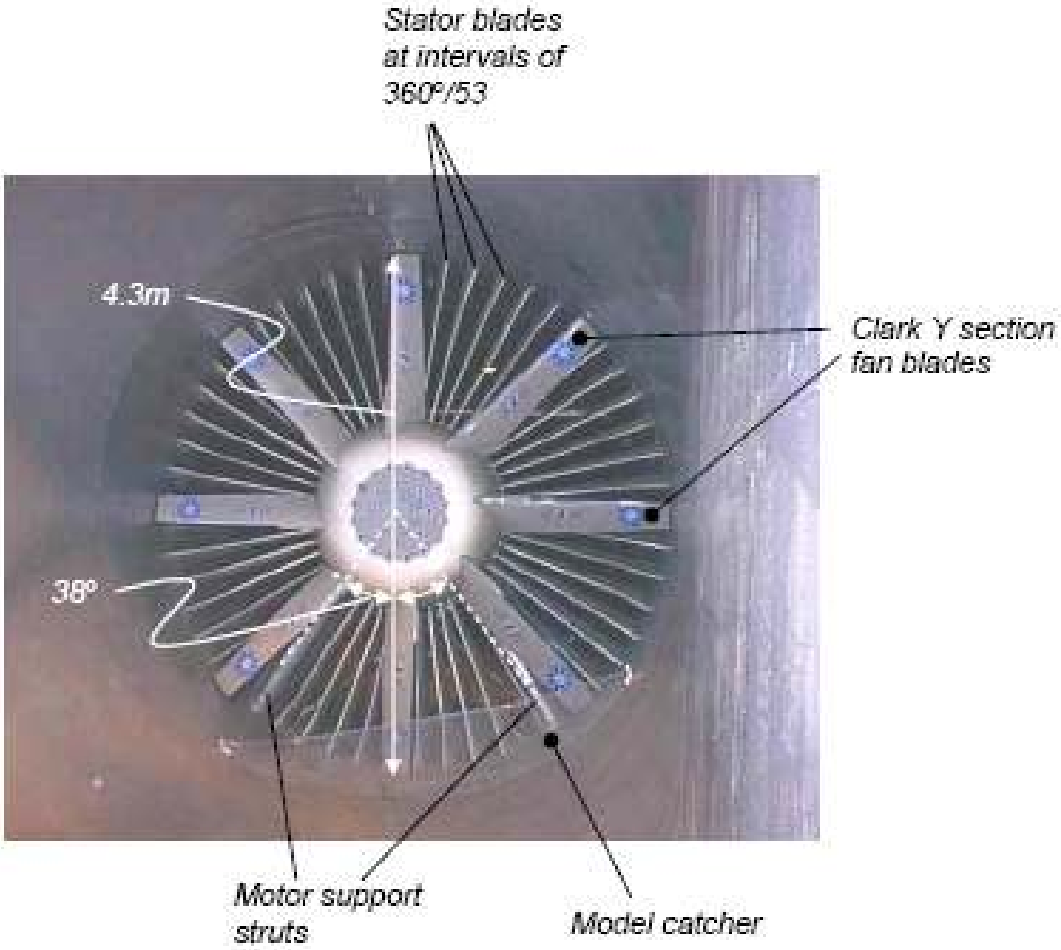

Figure 2-2. Photograph showing the wind tunnel fan and old model catcher. Diagram adopted from Camargo *et al (2005)*.

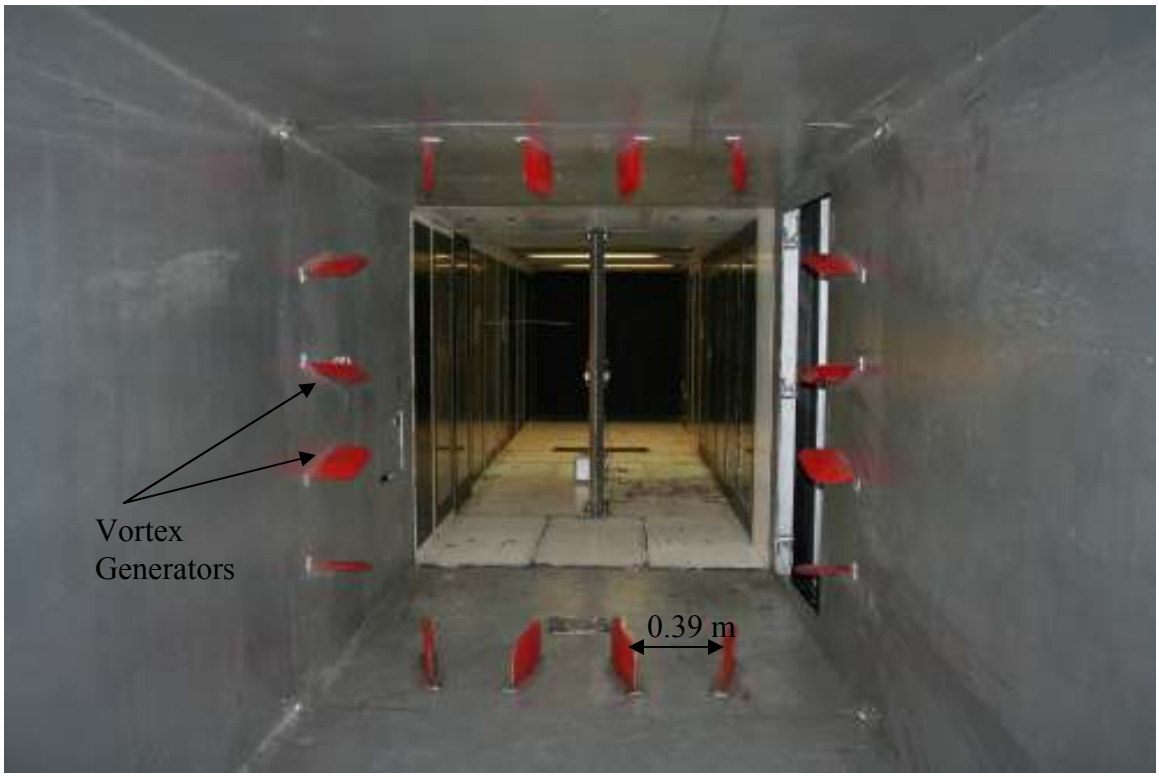

Figure 2-3. Photograph looking upstream showing the vortex generators in the diffuser of the wind tunnel

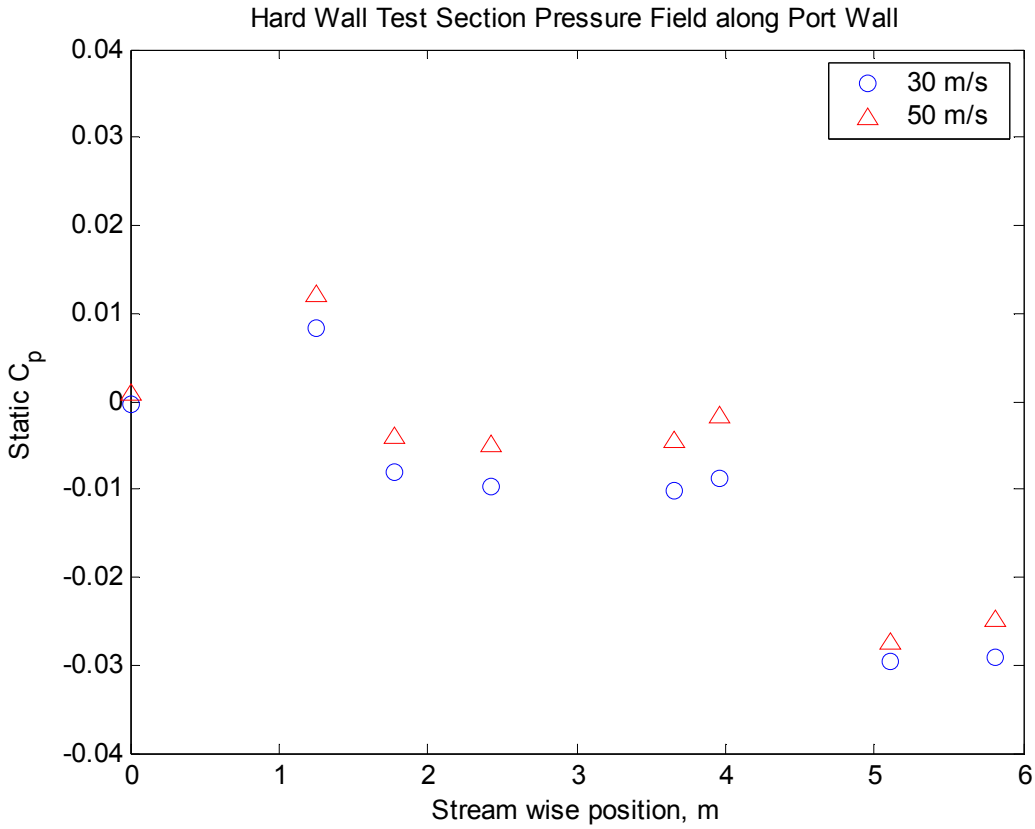

Figure 2-4. Static Pressure Coefficient variation along the Port Wall in the Hard Wall test section.

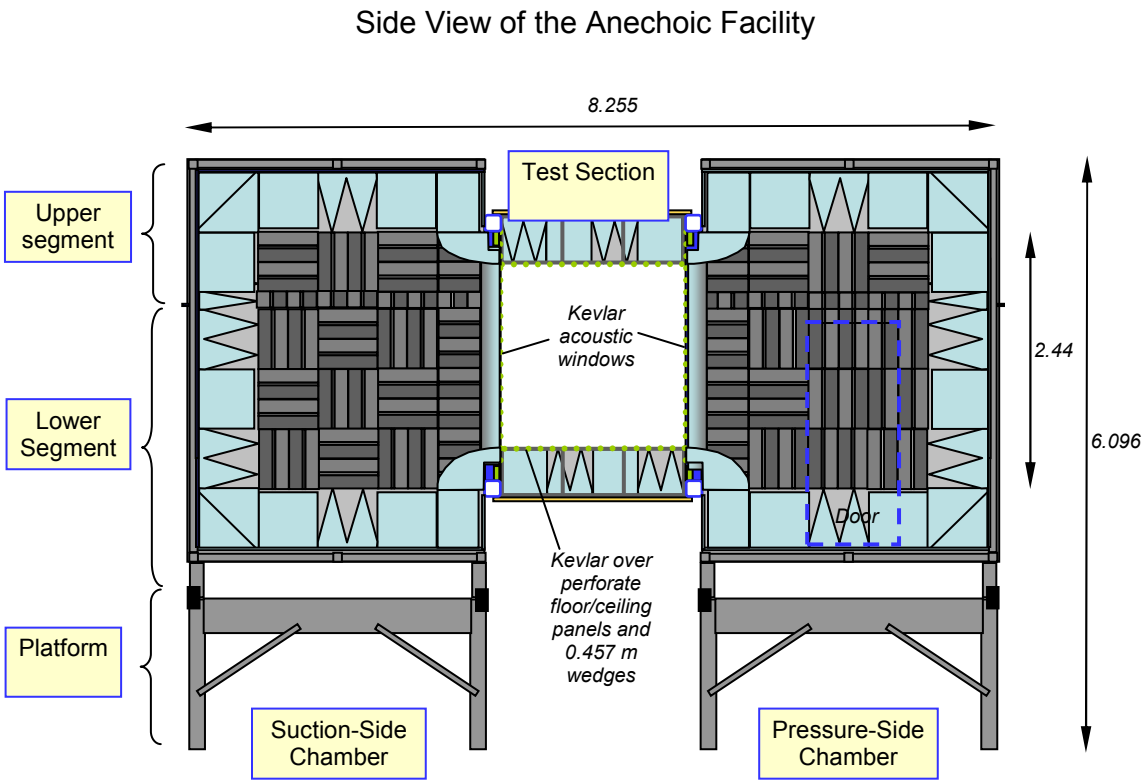

Figure 2-5. Side View of the Virginia Tech Anechoic Facility looking downstream. All dimensions in meters

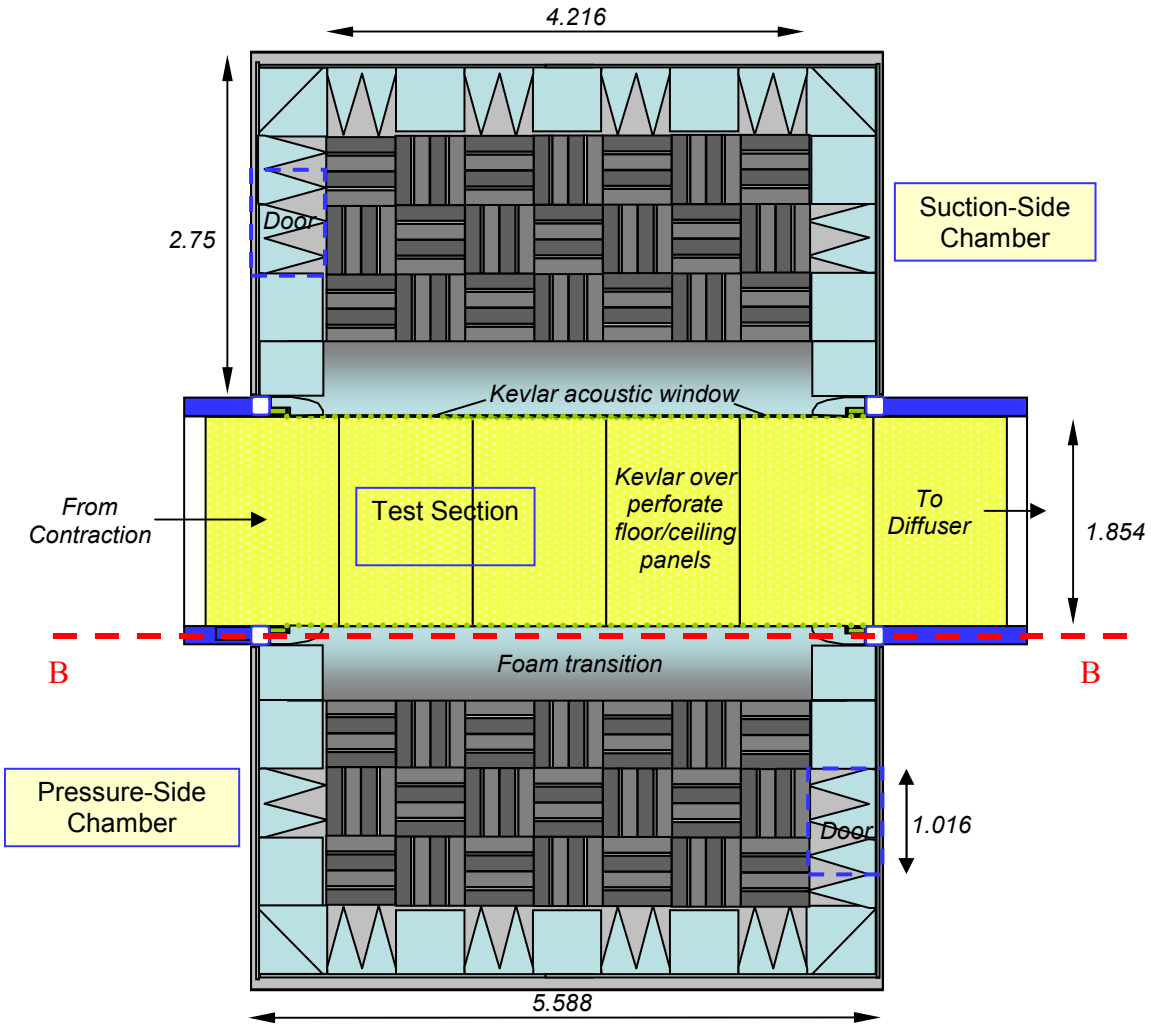

Figure 2-6. Top View of the Virginia Tech Anechoic Facility. All dimensions in meters

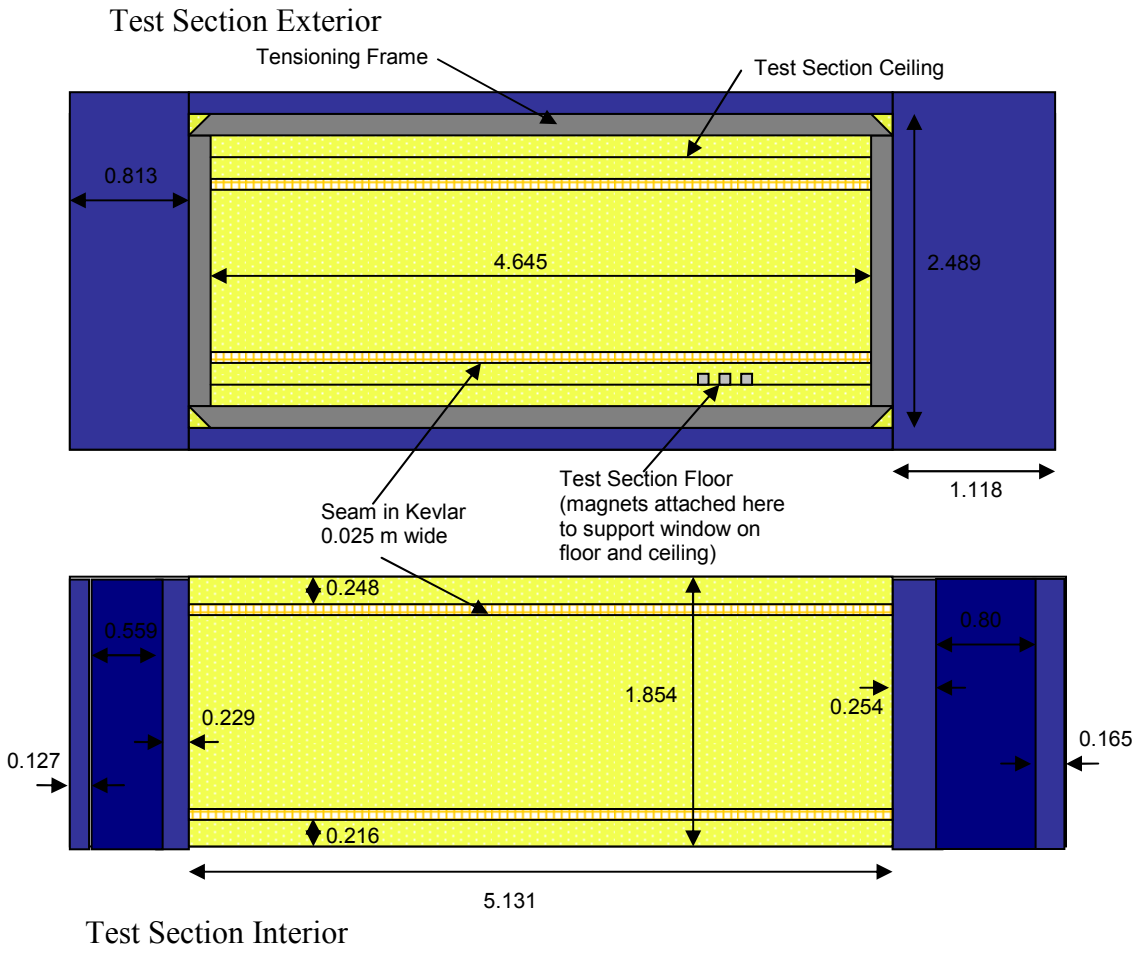

Figure 2-7. Diagram of the exterior of the test section (top) and interior (bottom). All dimensions are in meters.

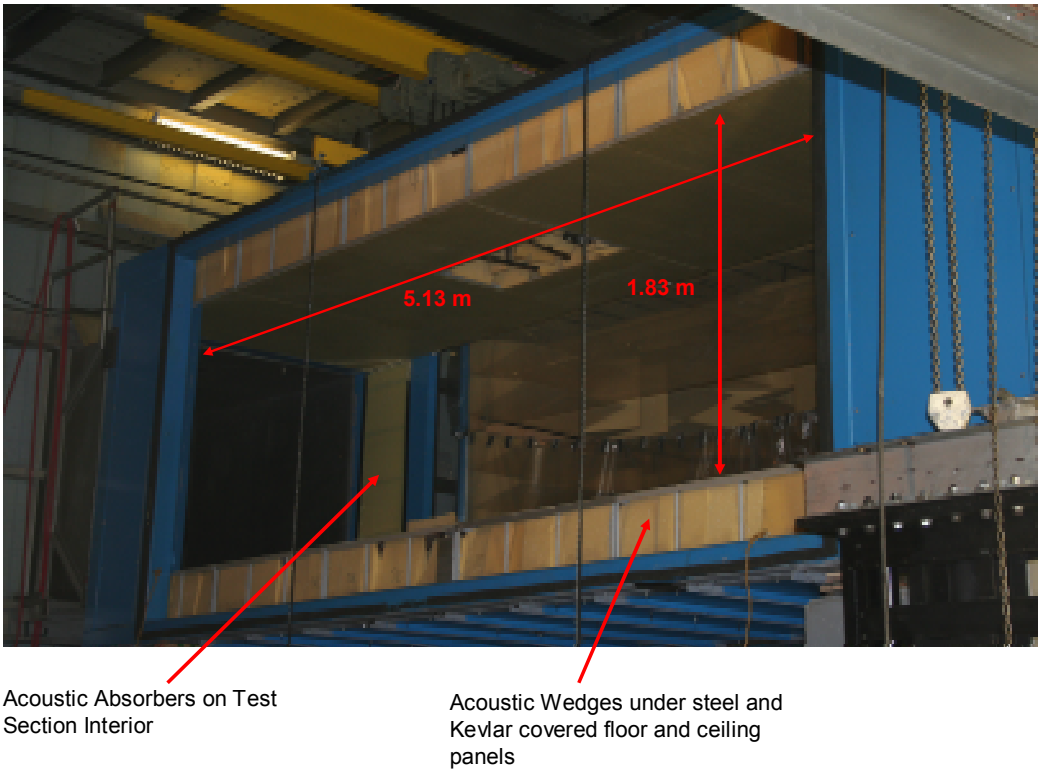

Figure 2-8. Diagram of the exterior of the test section with some of the important features. Kevlar windows have not been mounted and flow is moving from left to right.

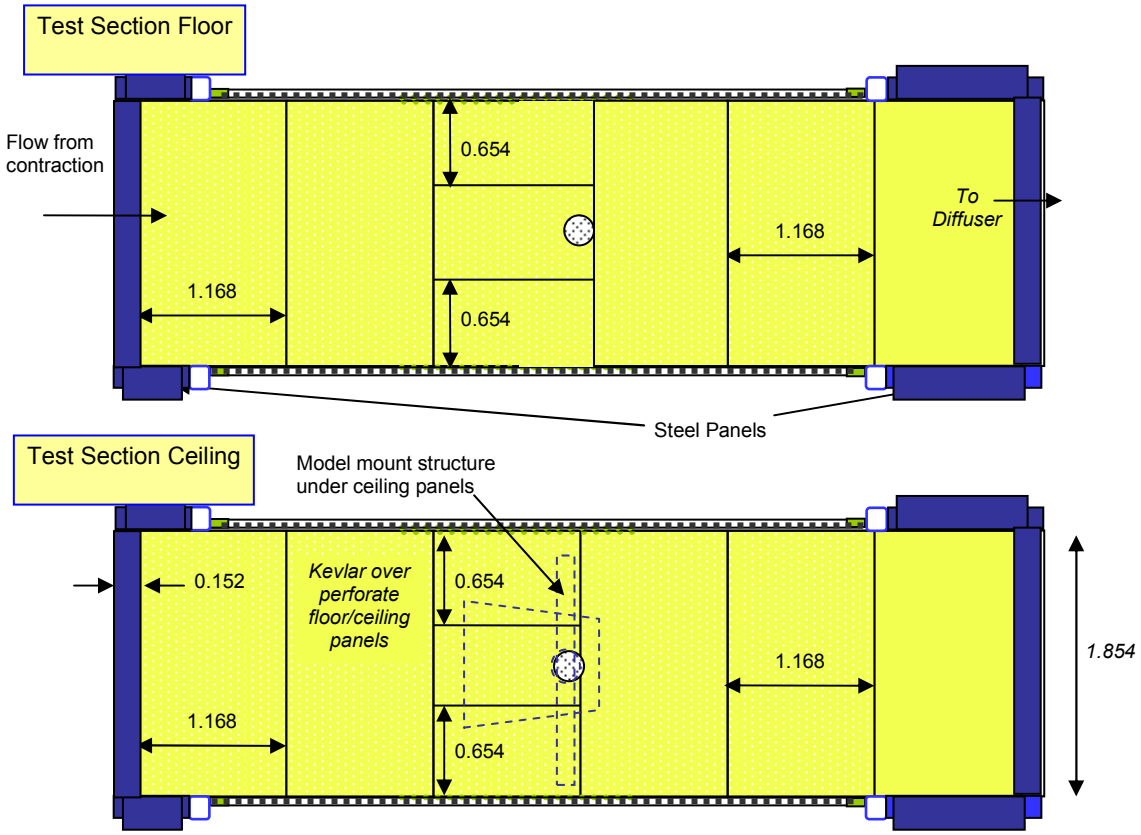

Figure 2-9. Diagram of the floor of the test section (top) and the ceiling (bottom). All dimensions are in meters.

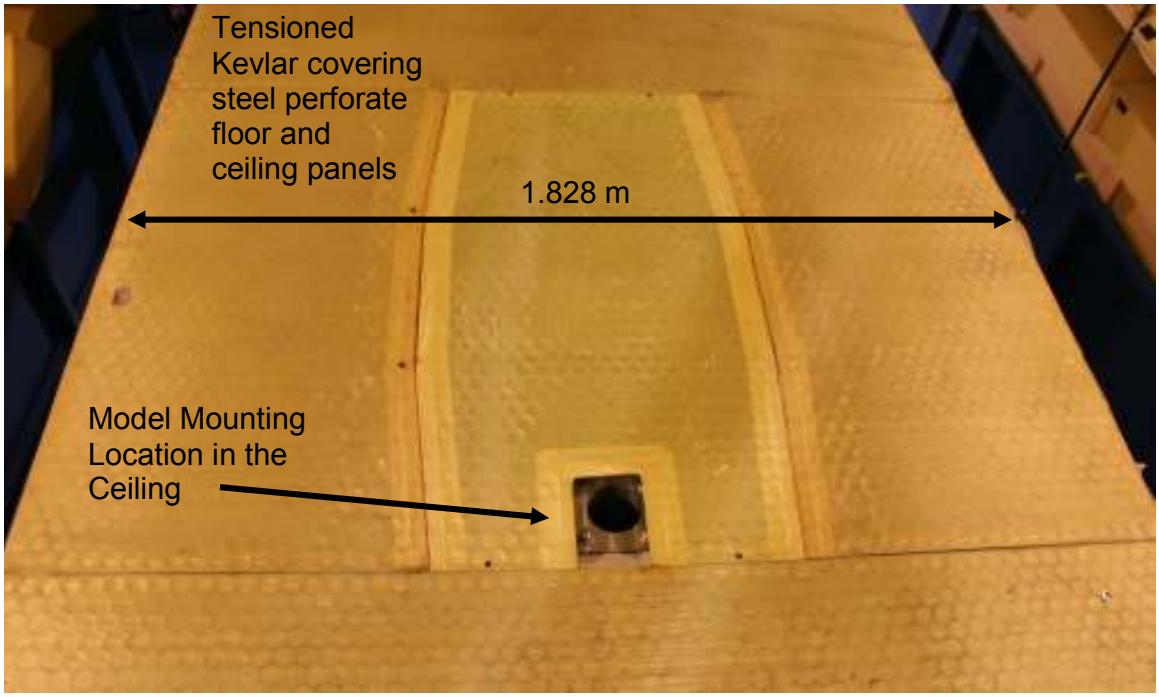

Figure 2-10. Diagram of the test section ceiling and floor with the relevant features. All dimensions in meters.

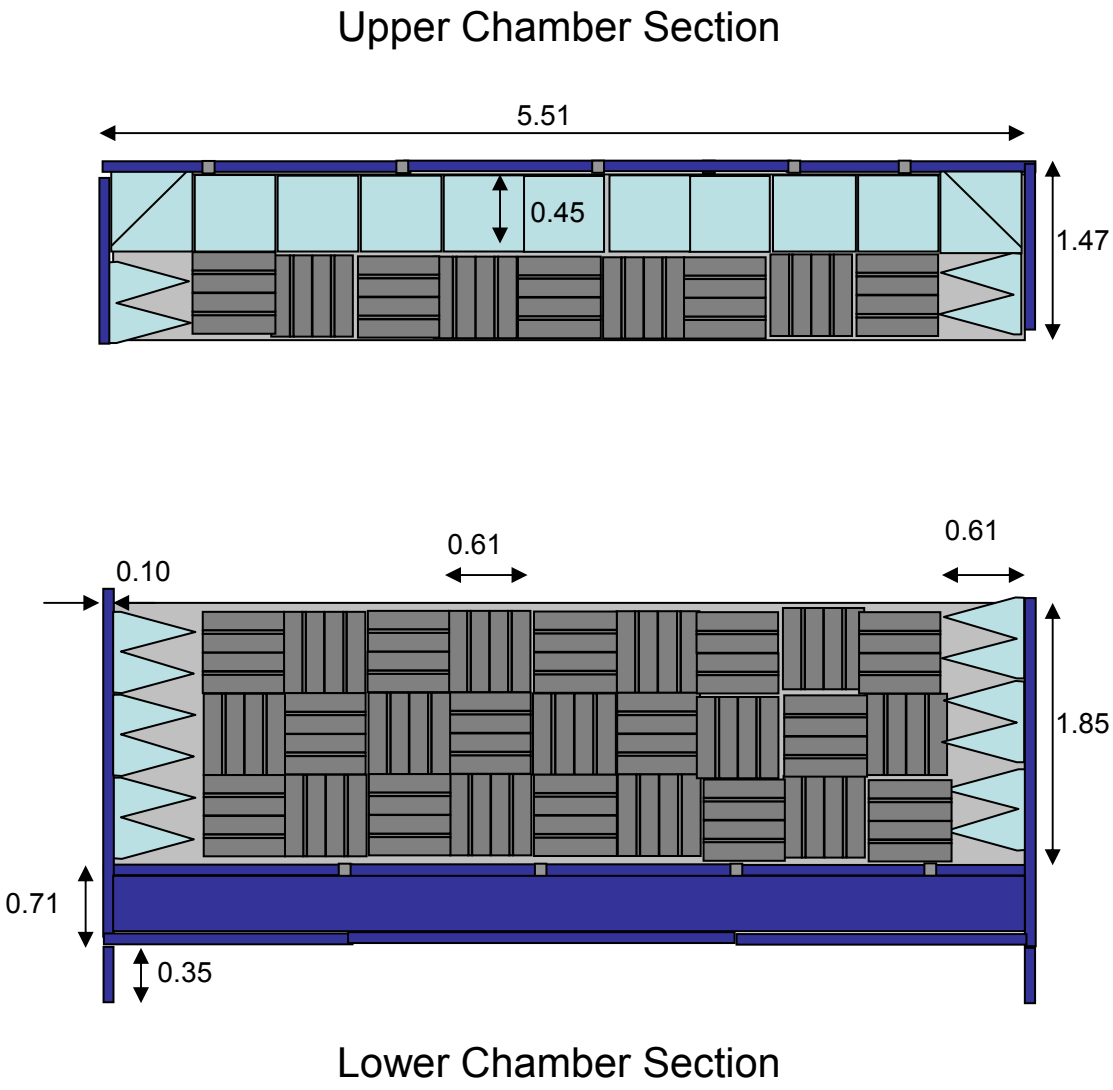

Figure 2-11. Diagram of the interior of each anechoic chamber. All dimensions in meters.

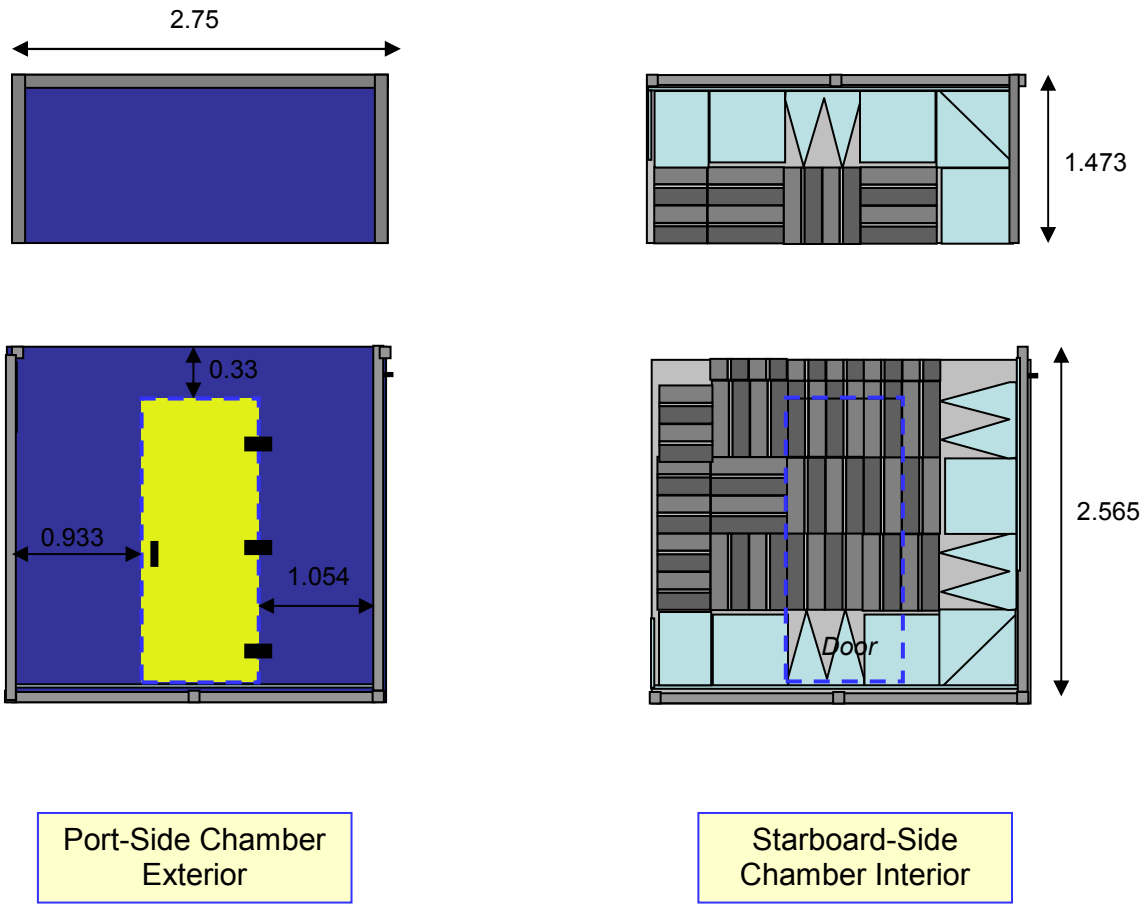

Figure 2-12. Side view of the interior and exterior of the anechoic chambers. All dimensions in meters.

Figure 2-13. Photograph showing the foam wedges that form the 3 walls, floor and ceiling of the anechoic chambers.

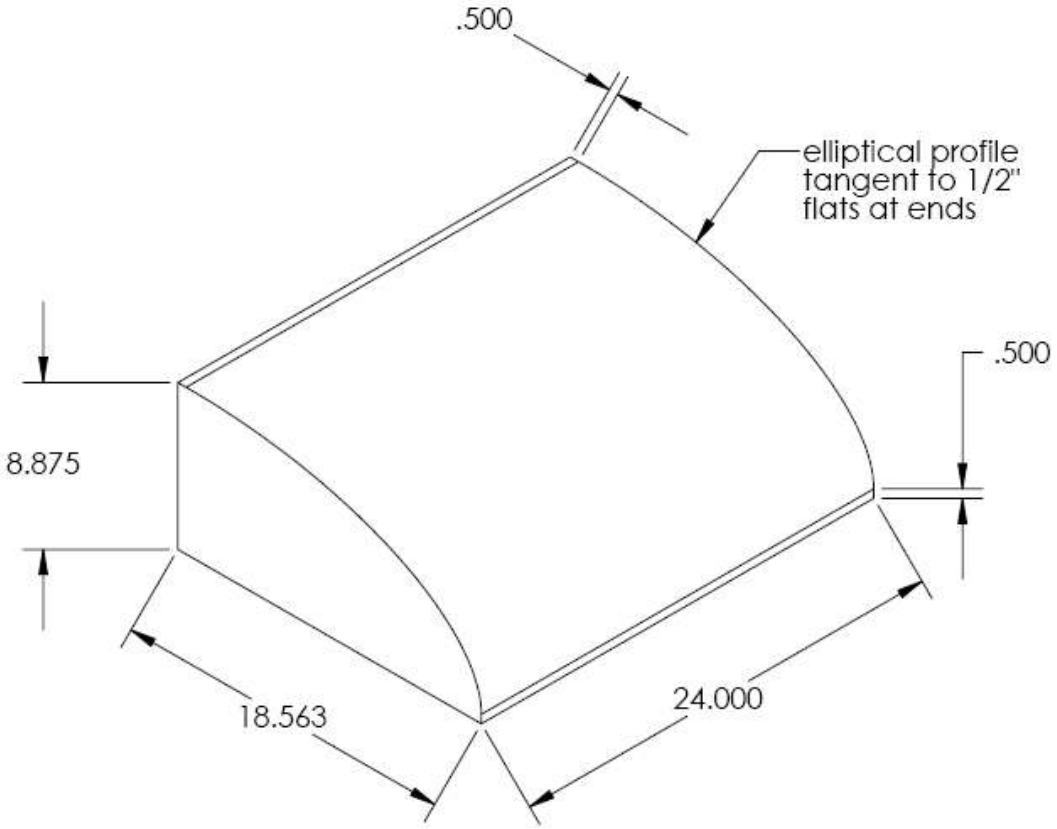

Figure 2-14. Transition wedges that line the open side walls of each chamber. All dimensions in inches.

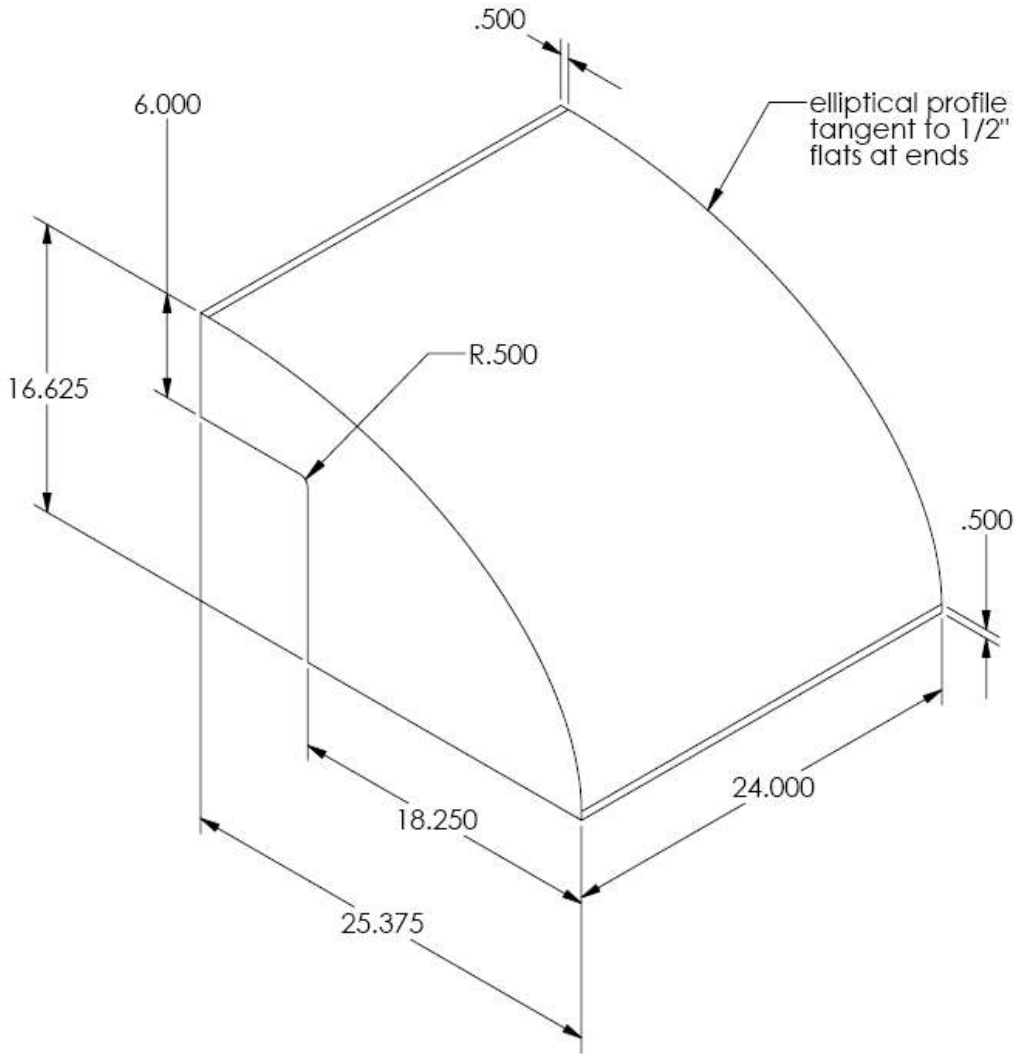

Figure 2-15. Transition wedges that line the open floor and ceiling of each anechoic chamber. All dimensions in inches.

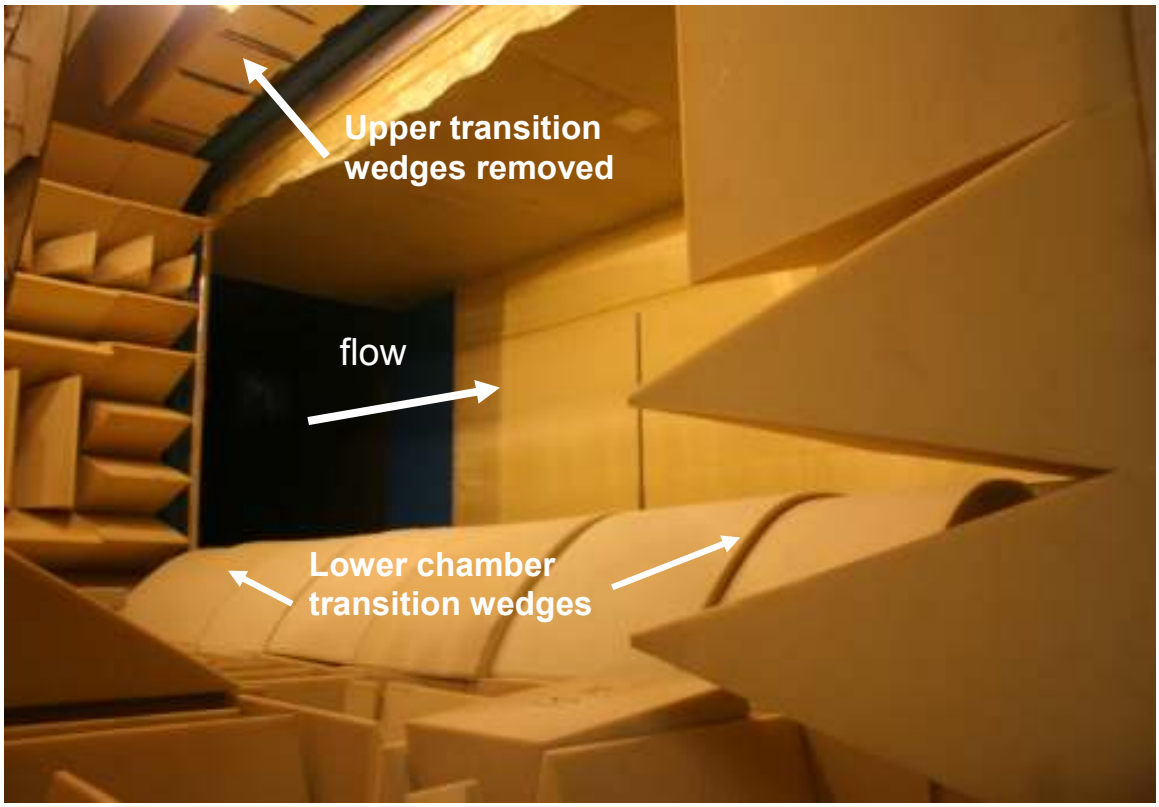

Figure 2-16. View into the test section from the pressure chamber with a section of the window removed. This figure also shows the wedges that were used to create a smooth transition between the edges of the chamber and the test section floor

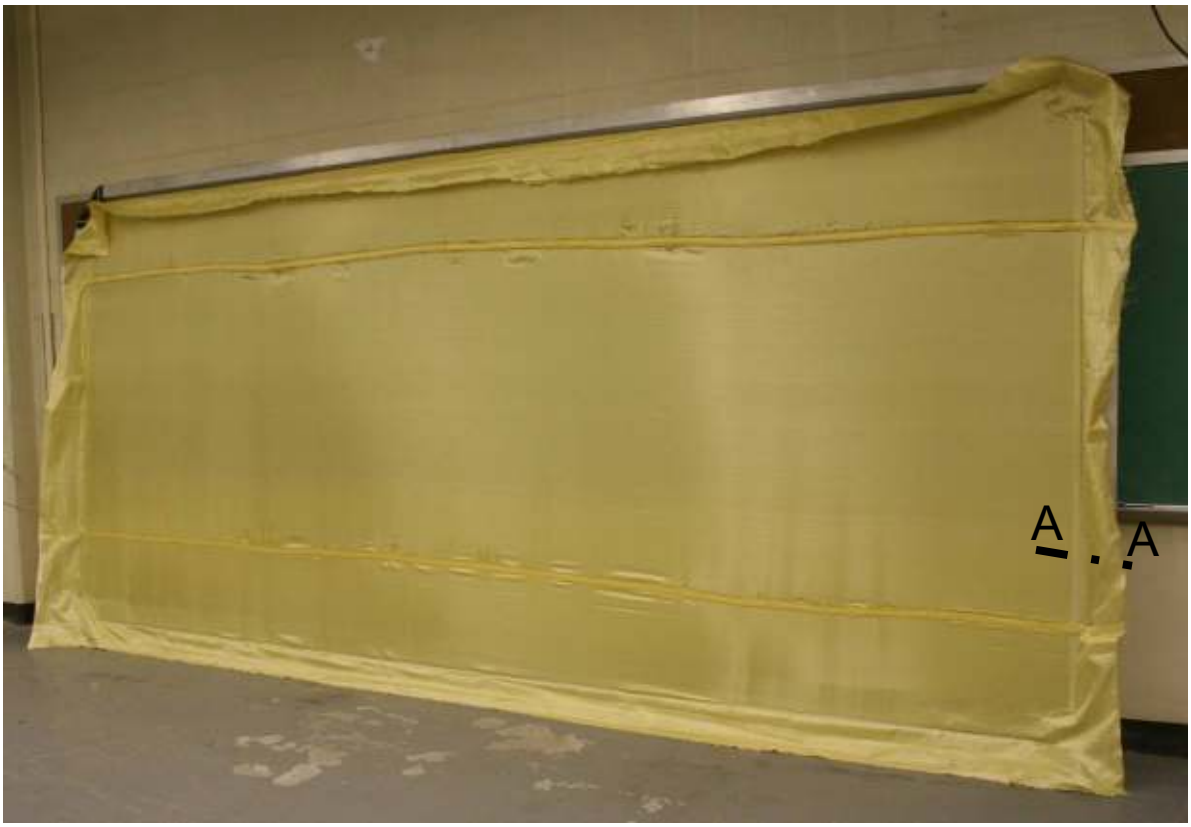

Figure 2-17. Kevlar Window installed in tensioning frame just prior to installation. The tensioning frames are attached to the chamber sections so that pure Kevlar covered surfaces form the interior walls, and thus the flow surfaces, of the test section.

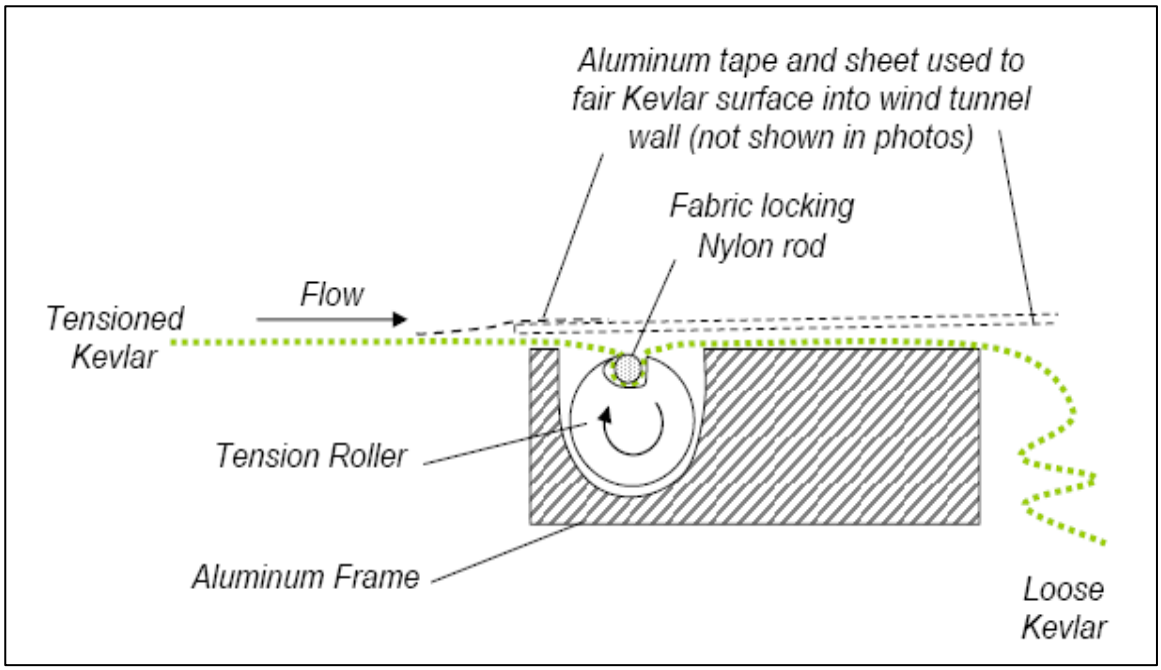

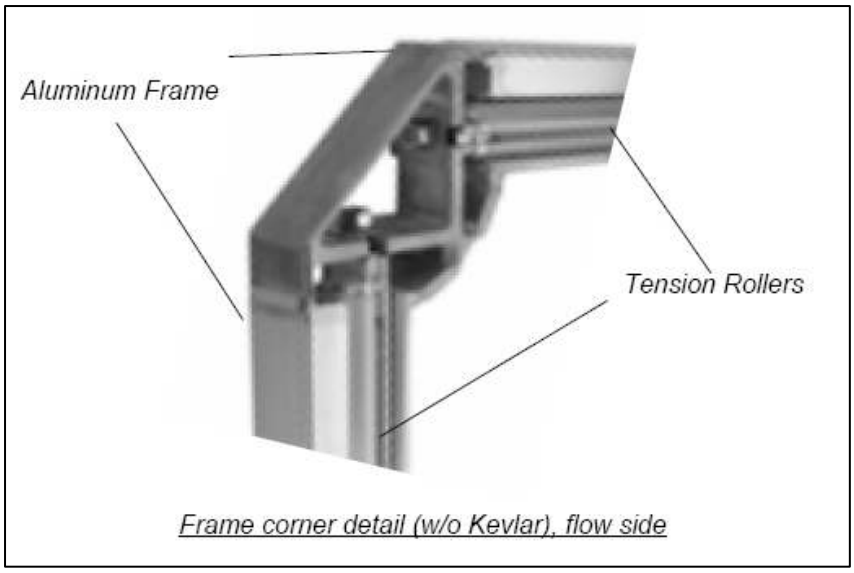

Figure 2-18. Section A-A from Figure 2-4 (Top) showing the Kevlar mounting arrangement and Roller Chase Frame configuration (Bottom). Figure adopted Camargo *et al (2005)*

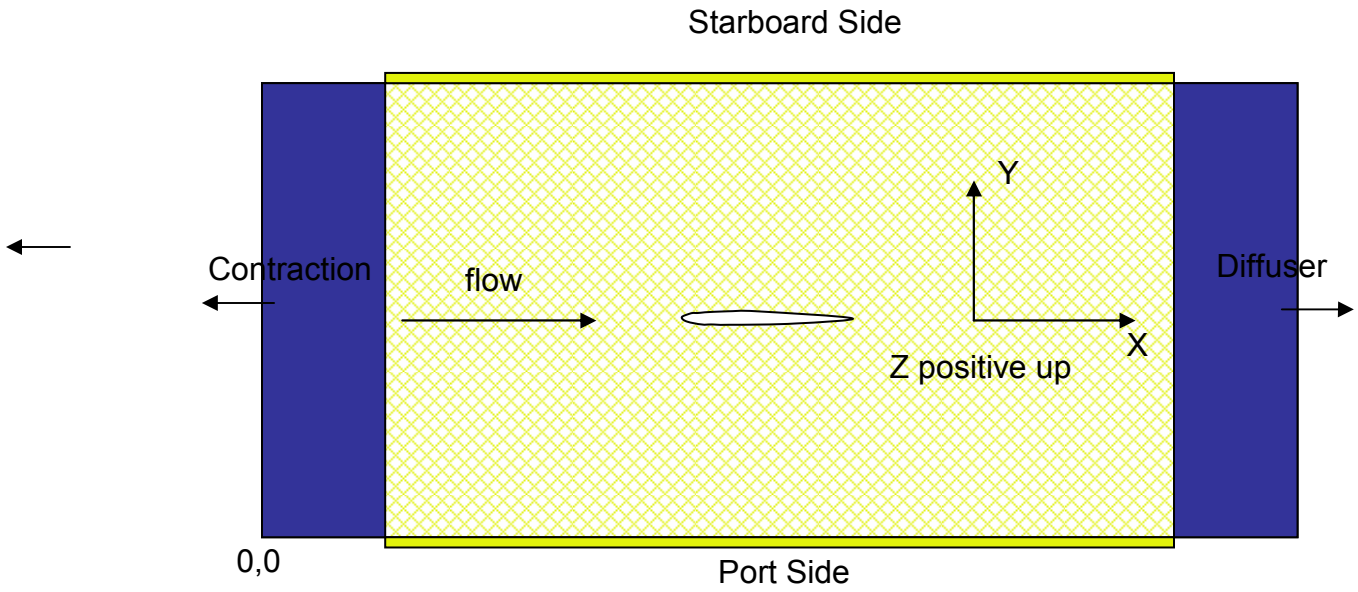

Figure 2-19. Diagram showing the coordinate system used to present final data.

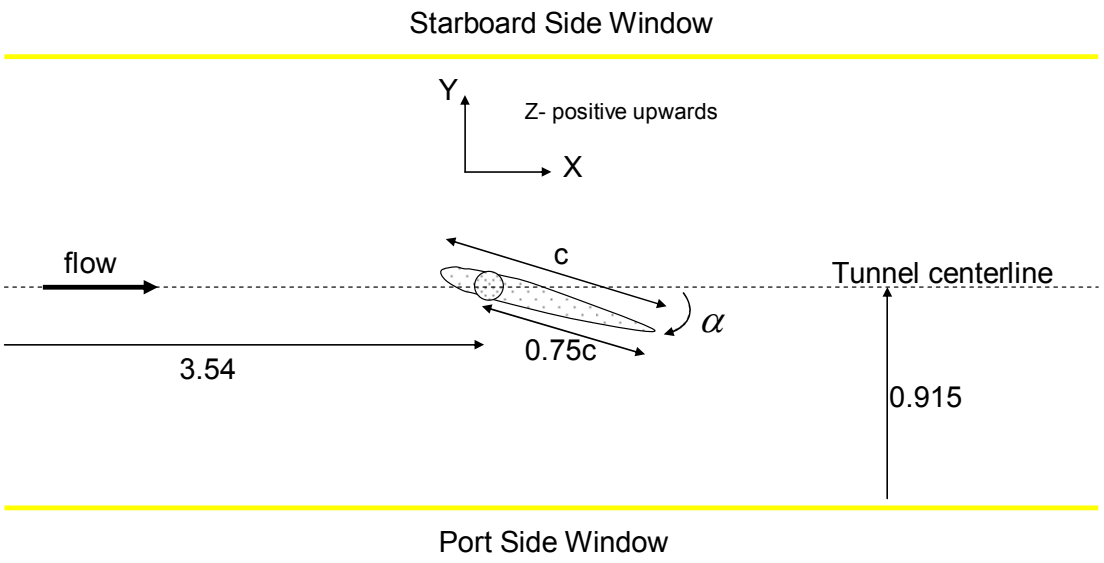

Figure 2-20. Final coordinate system used to determine the model angle of attack.

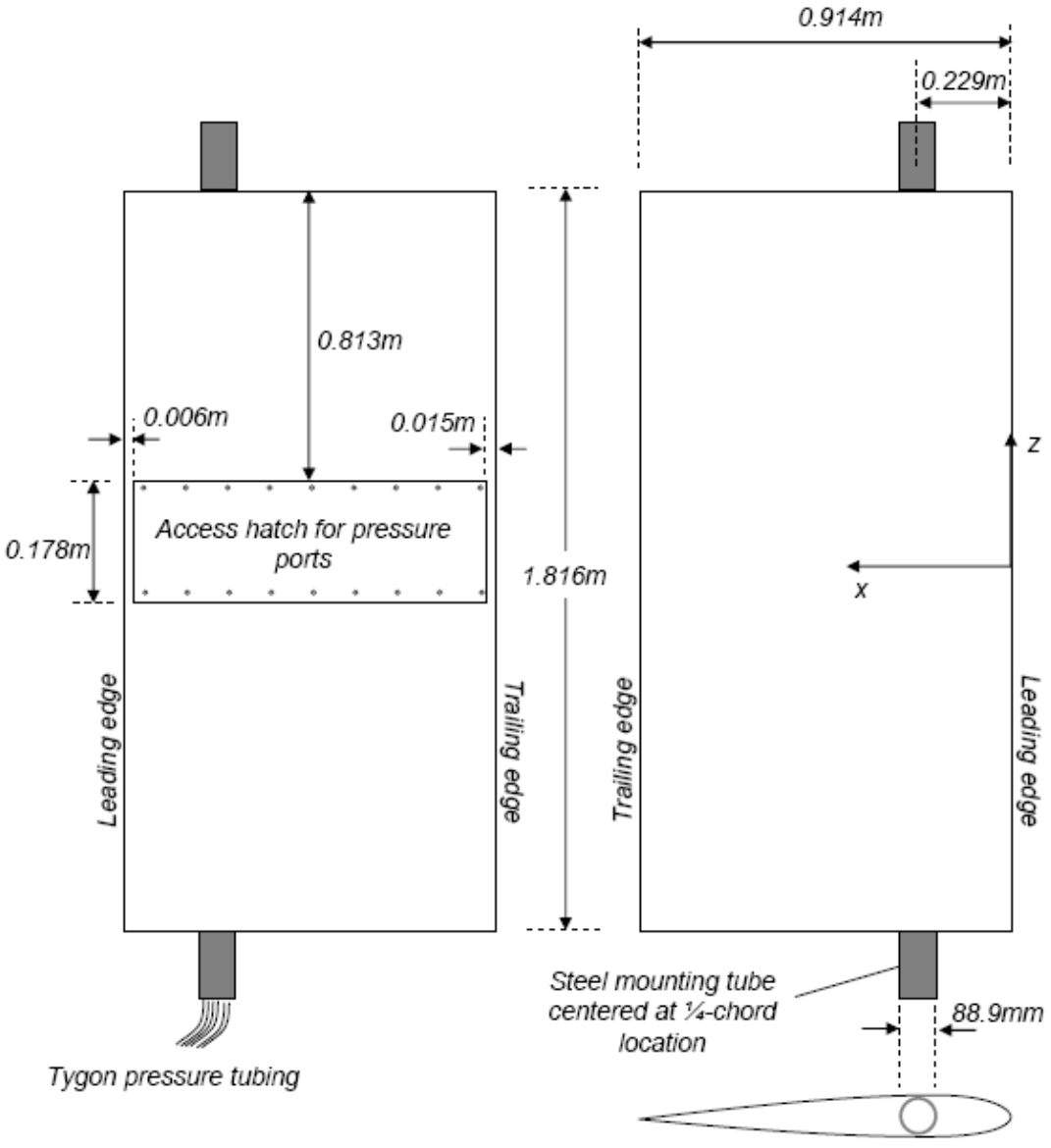

Figure 2-21. Diagram for the NACA 0012 Model. Figure adopted from *Camargo et al (2005)*.

Figure 2-22. NACA 0012 Model mounted in the test section during the 2006 intermediate calibration.

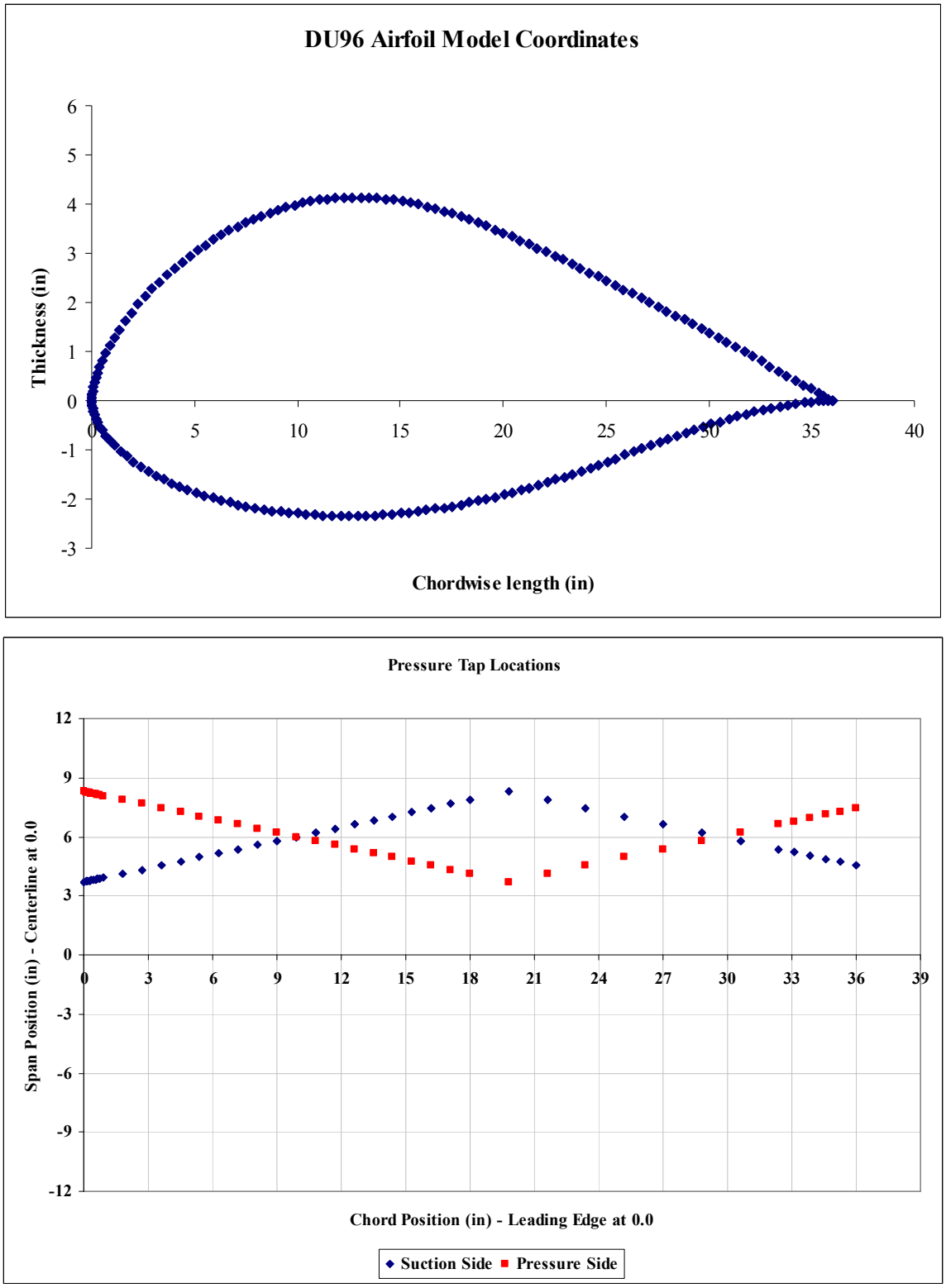

Figure 2-23. Model section shape and pressure tap locations for the DU96.

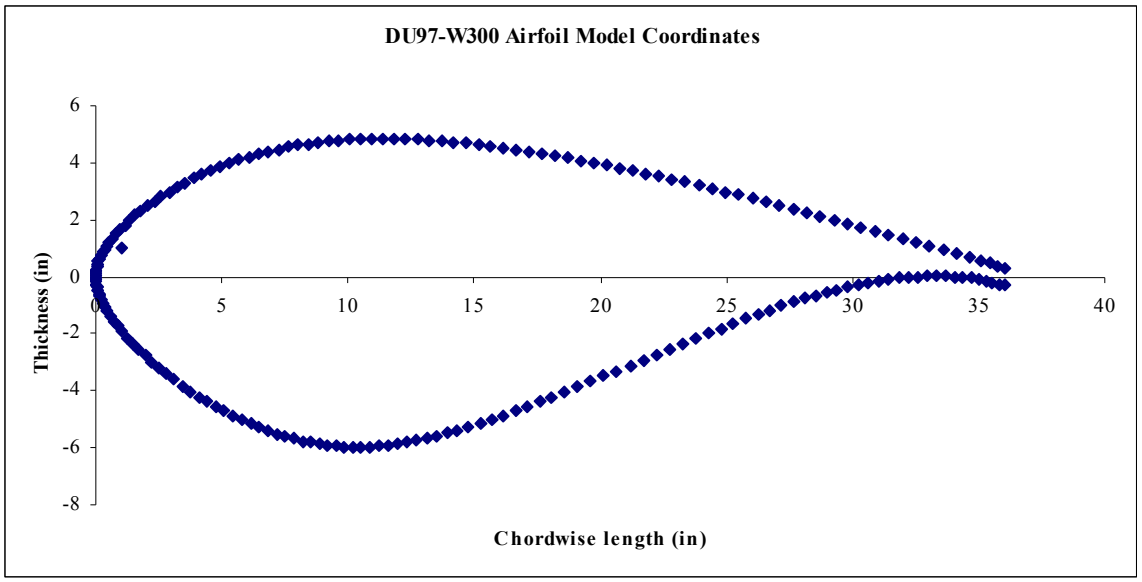

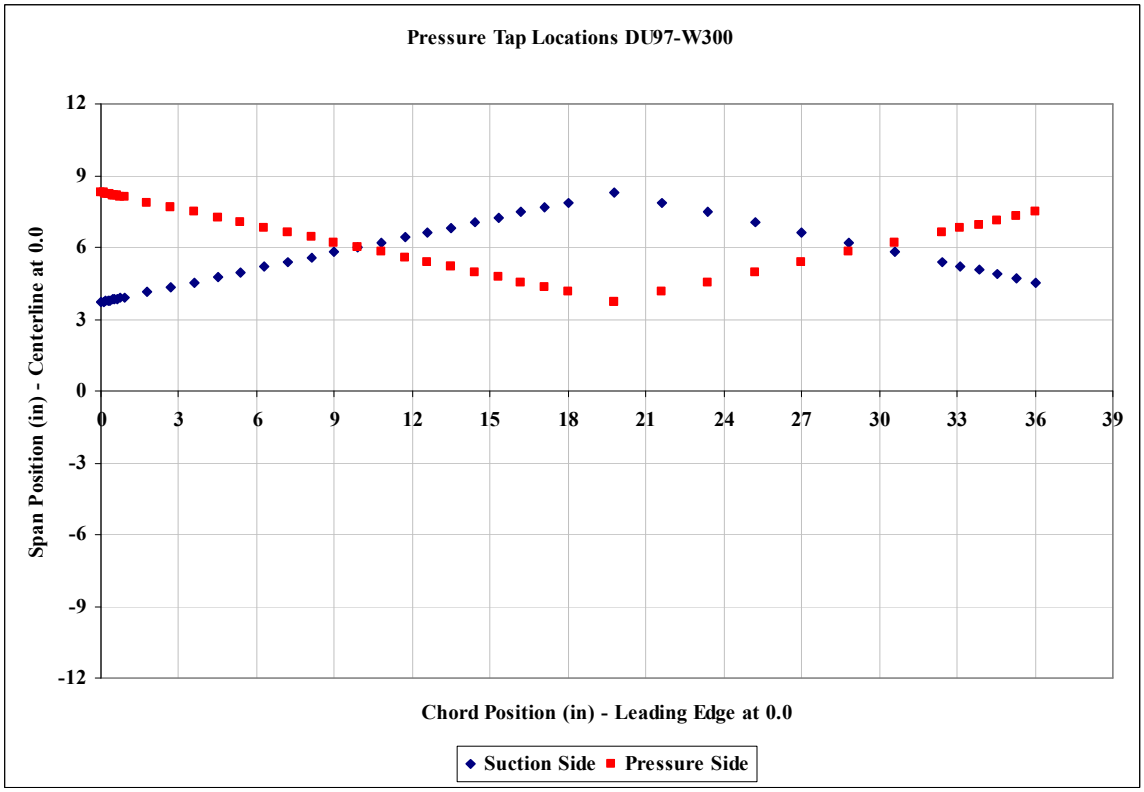

Figure 2-24. Section Airfoil shape and pressure tap locations of the DU97-W300.

Figure 2-25. Diagram of the se up for the calibration of the tunnel pitot static probe. All dimensions in meters

Figure 2-26. Photograph of the stability tunnel traverse. Aluminum angles (T6061 3” x 4” x ¼”) were lined with a neoprene rubber matting and placed under the feet of the traverse to protect the Kevlar and to distribute the traverse load evenly. Wood blocks (2x4 in) were used to adjust the height at the floor.

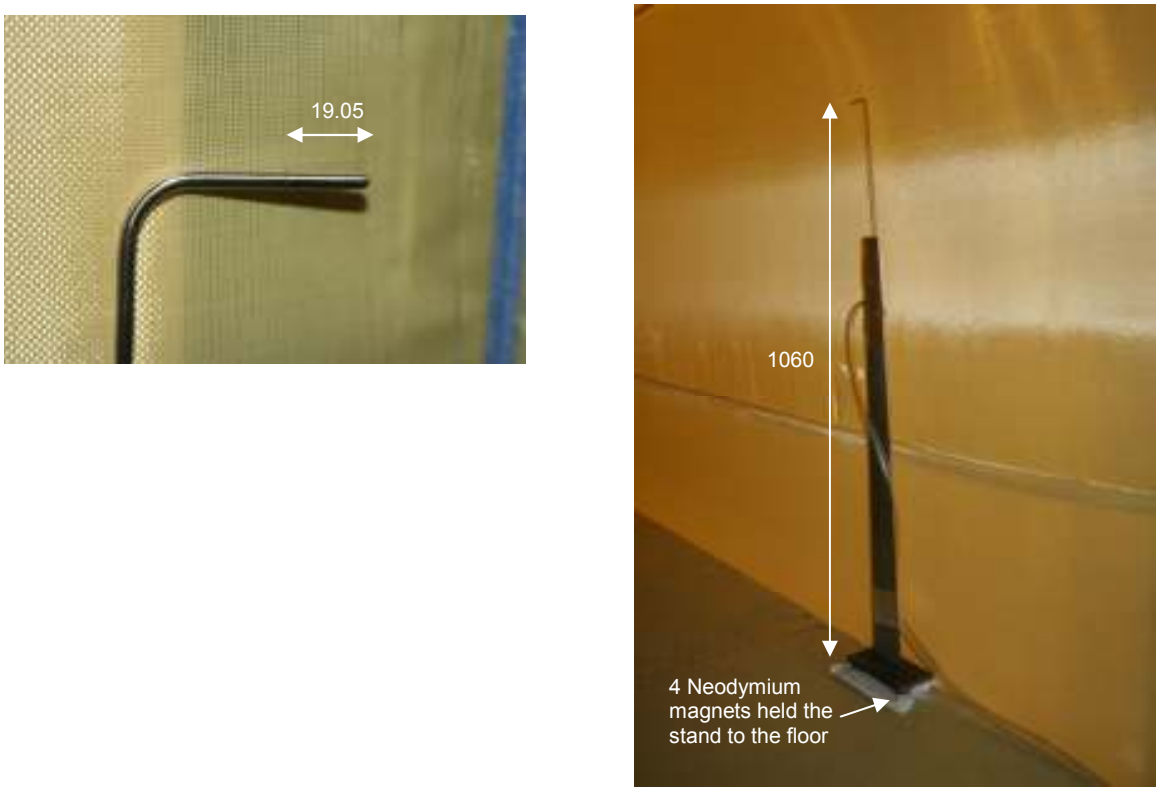

Figure 2-27. Window pressure measurement system used during the 2006 intermediate calibration. Note this strut was used for multiple measurements. All dimensions in mm.

Figure 2-28. Boundary layer measurement system used during the 2006 intermediate calibration. Note this strut was used for multiple measurements.

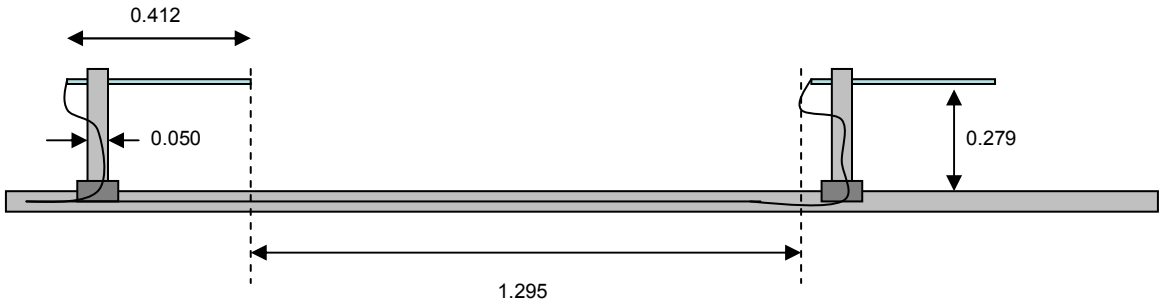

Figure 2-29. Diagram showing the general dimensions and spacing of 2 of the rail probes and mounts (top). Aluminum rail spanning the length of the test section used to measure the pressure difference across the Kevlar window. A series of 4 probes were traversed the length of the window to make the pressure measurements.

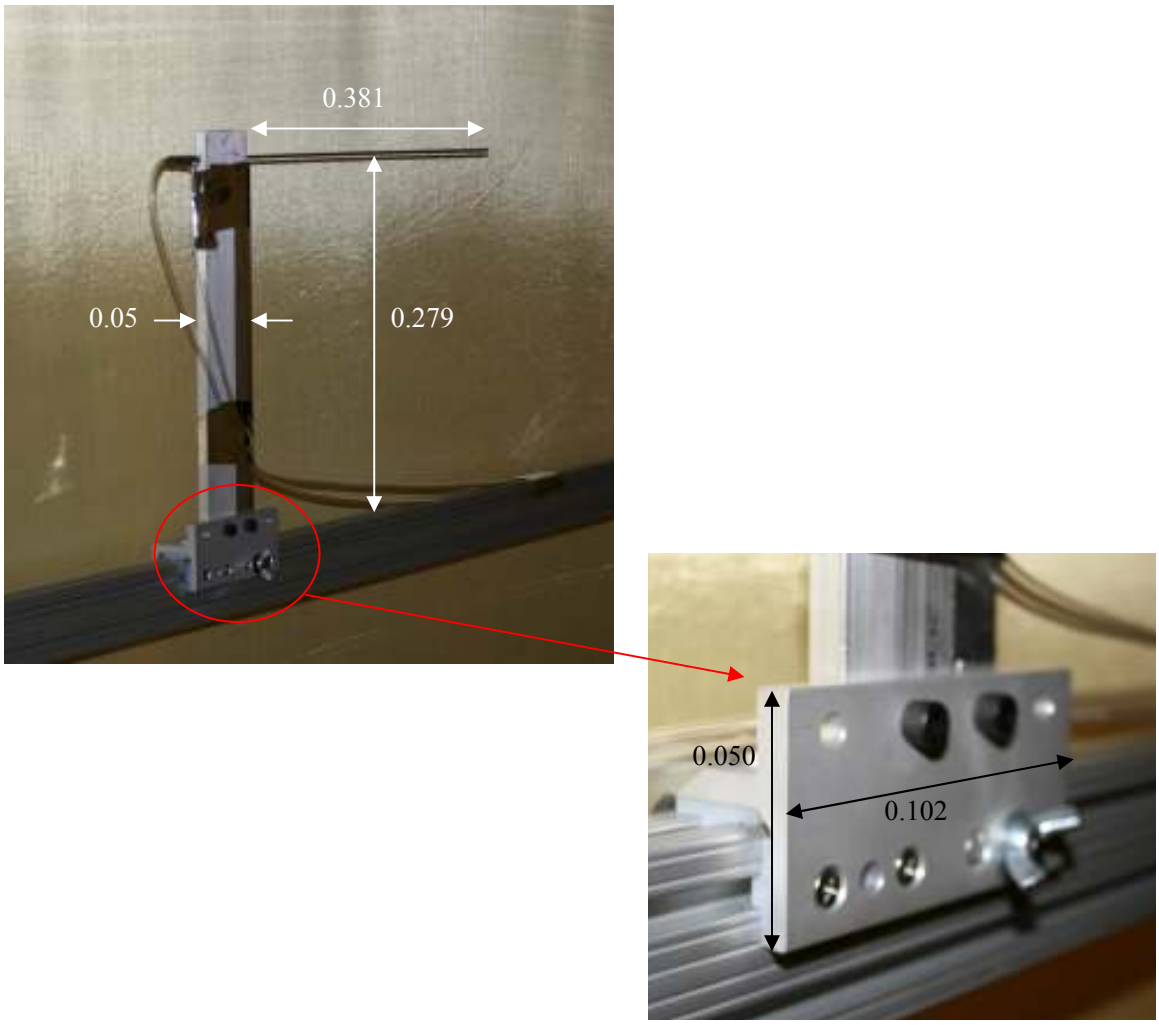

Figure 2-30. Detailed photograph of the slider system used to move the probes for the window transpiration measurements. Aluminum standoffs (12 inches) were used to separate the probe tip from the influence of the beam. Each slider was held in place during tunnel operation by the wing but beak shown in the lower photograph.

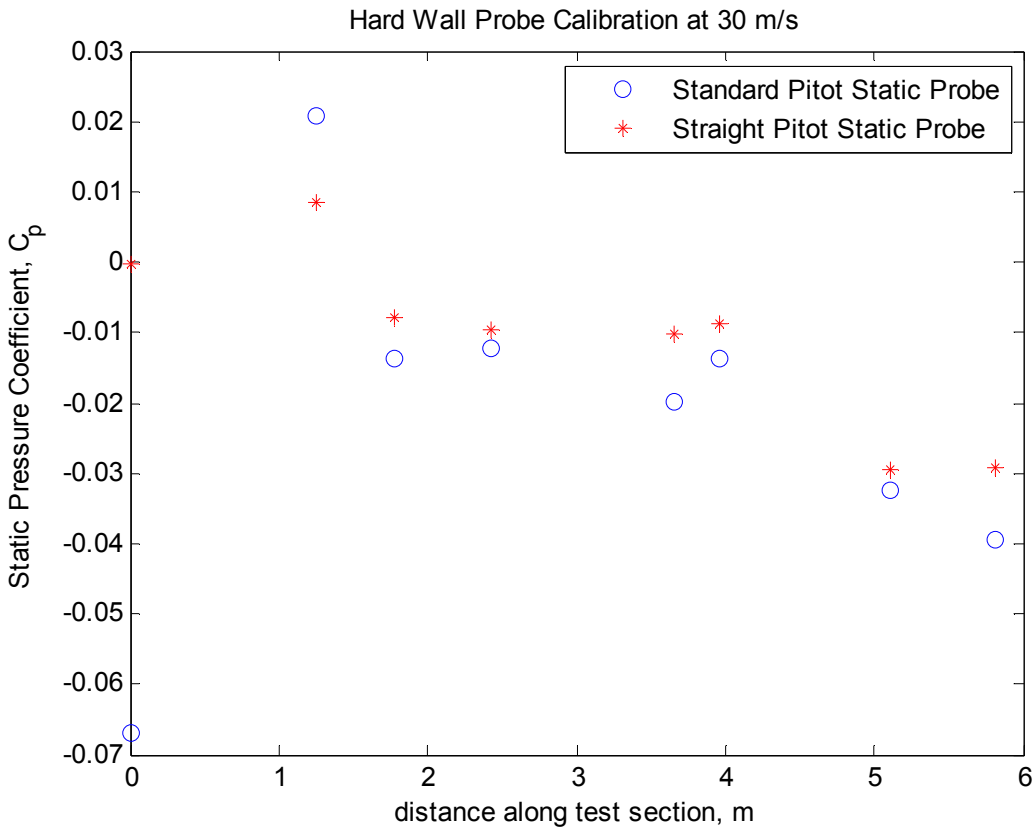

Figure 2-31. Pressure coefficient measurements using the two Pitot-static probe geometries in the hard-wall test section at 30 m/s

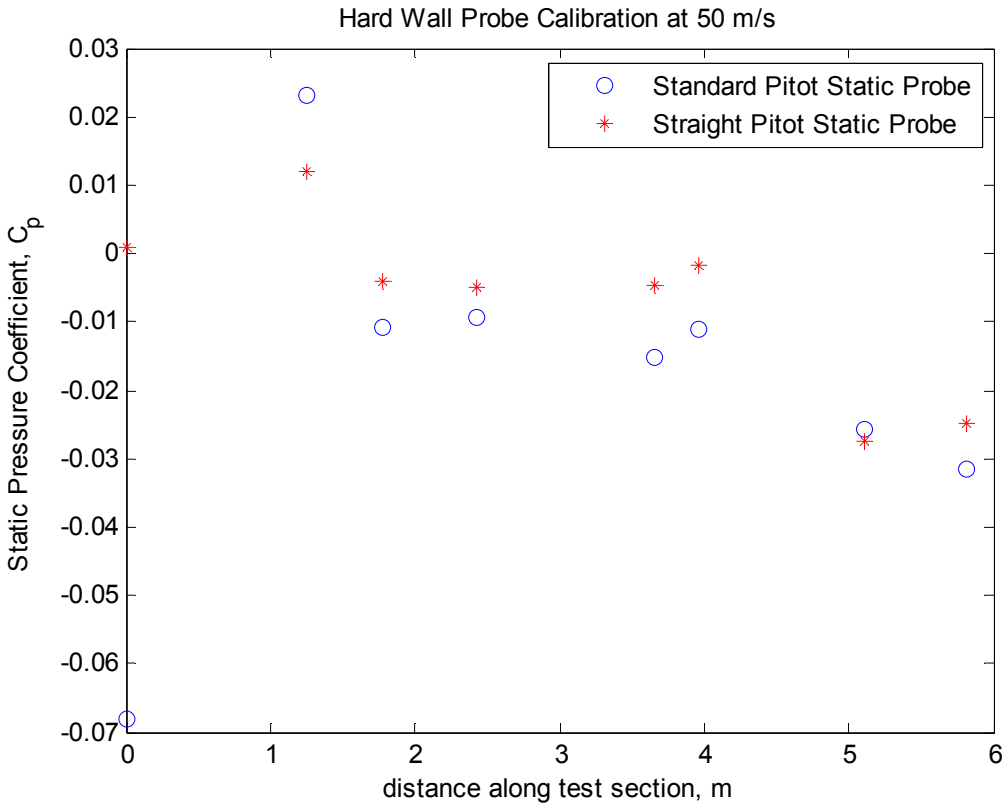

Figure 2-32. Pressure coefficient measurements using the two Pitot-static probe geometries in the hard-wall test section at 50 m/s

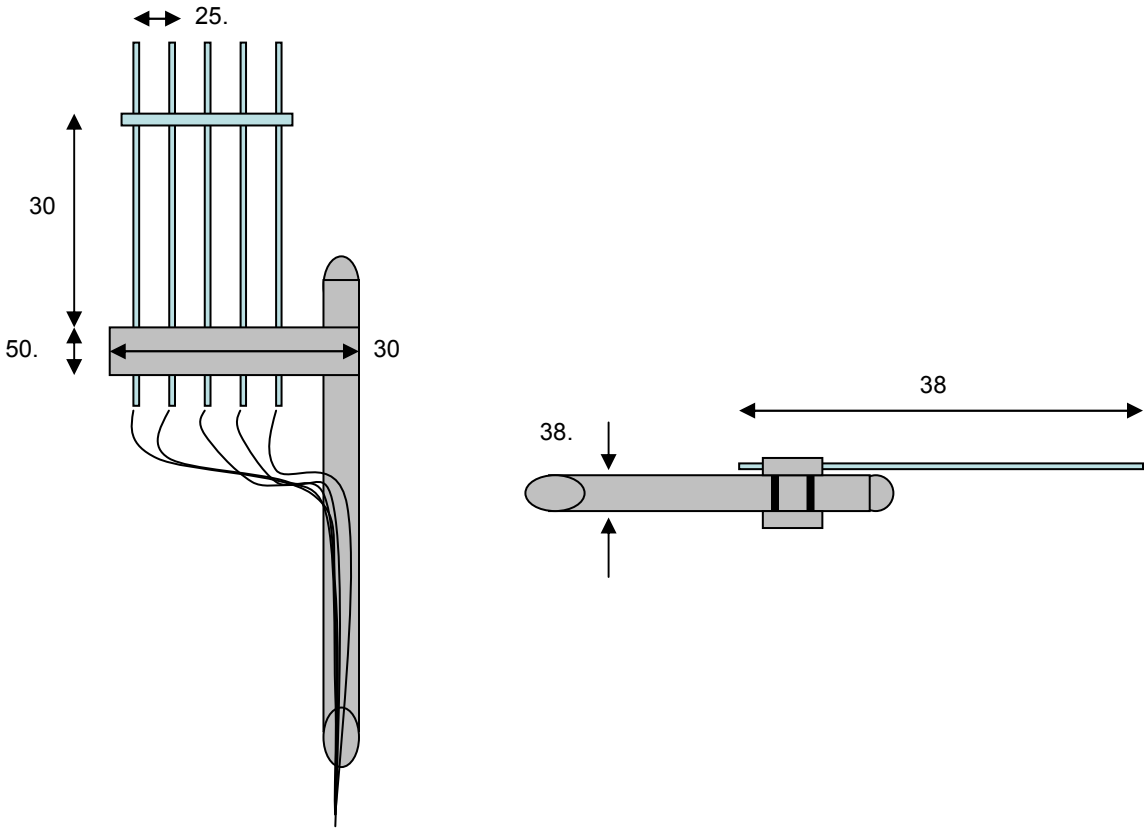

Figure 2-33. Probe Rake diagram top view (right) and side view (left). All dimensions in mm.

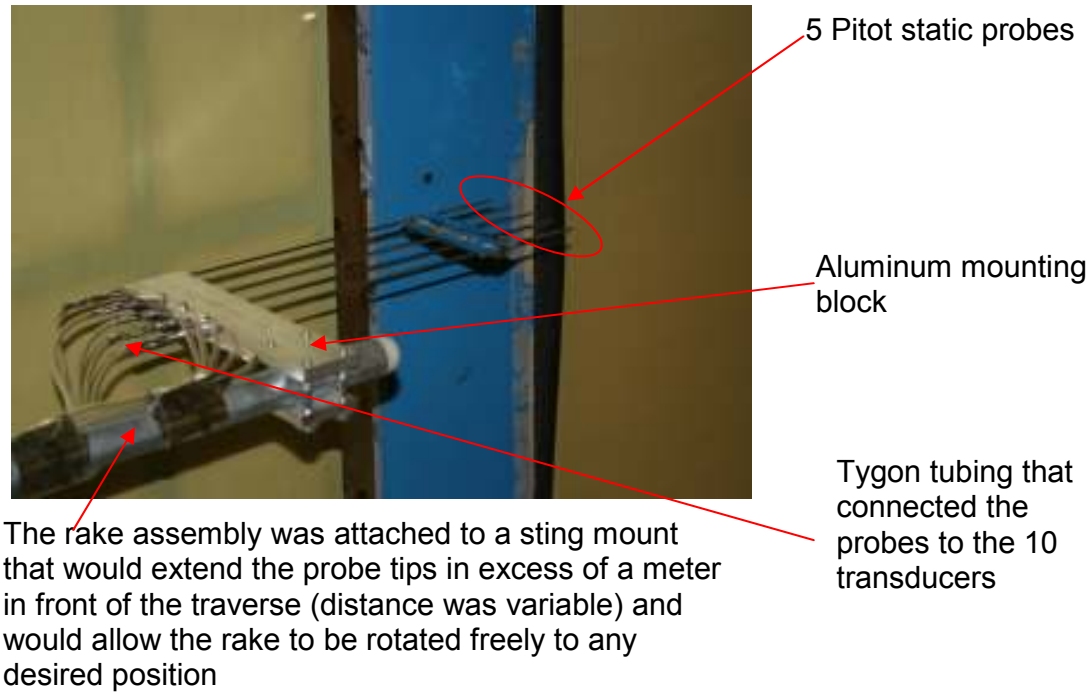

Figure 2-34. Probe Rake shown mounted in the horizontal orientation used to obtain boundary layer profiles on the Kevlar windows

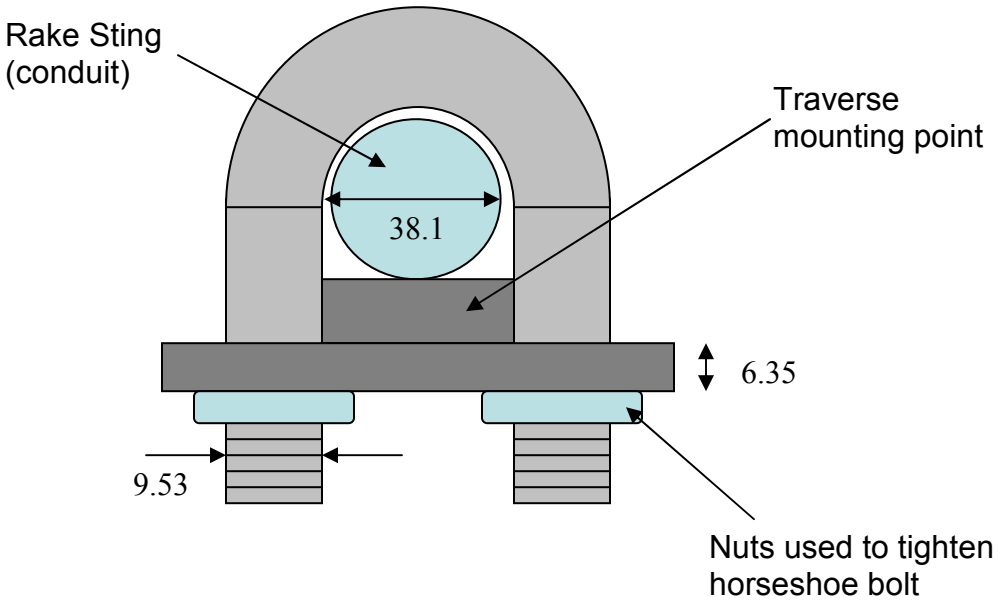

Figure 2-35. Horseshoe mounting bolt used to secure conduit sting to the wind tunnel traverse. All dimensions in mm.

Figure 2-36. Wall deflection measurement equipment.

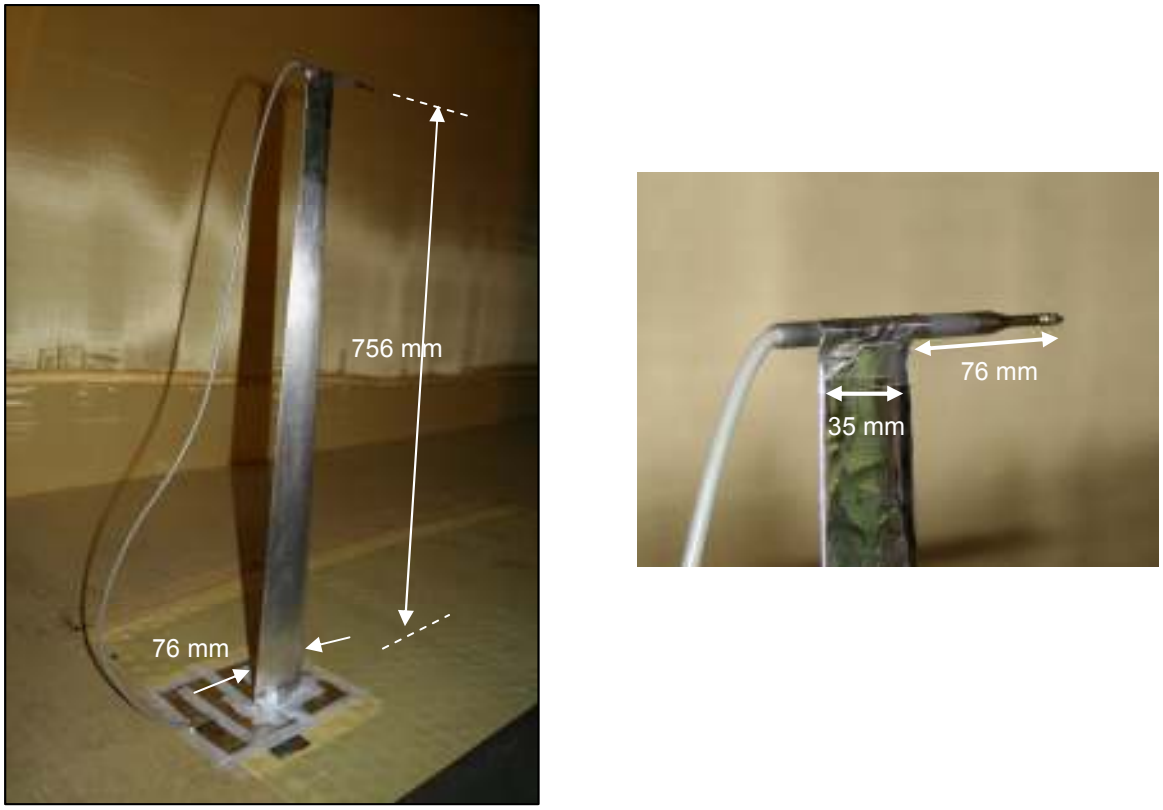

Figure 2-37. In Flow microphone stand and B and K 1/8th inch microphone. Conditioning amp (not shown) was located outside of the test section. Microphone was placed on stand in center of test section, at the same location that the models are mounted.

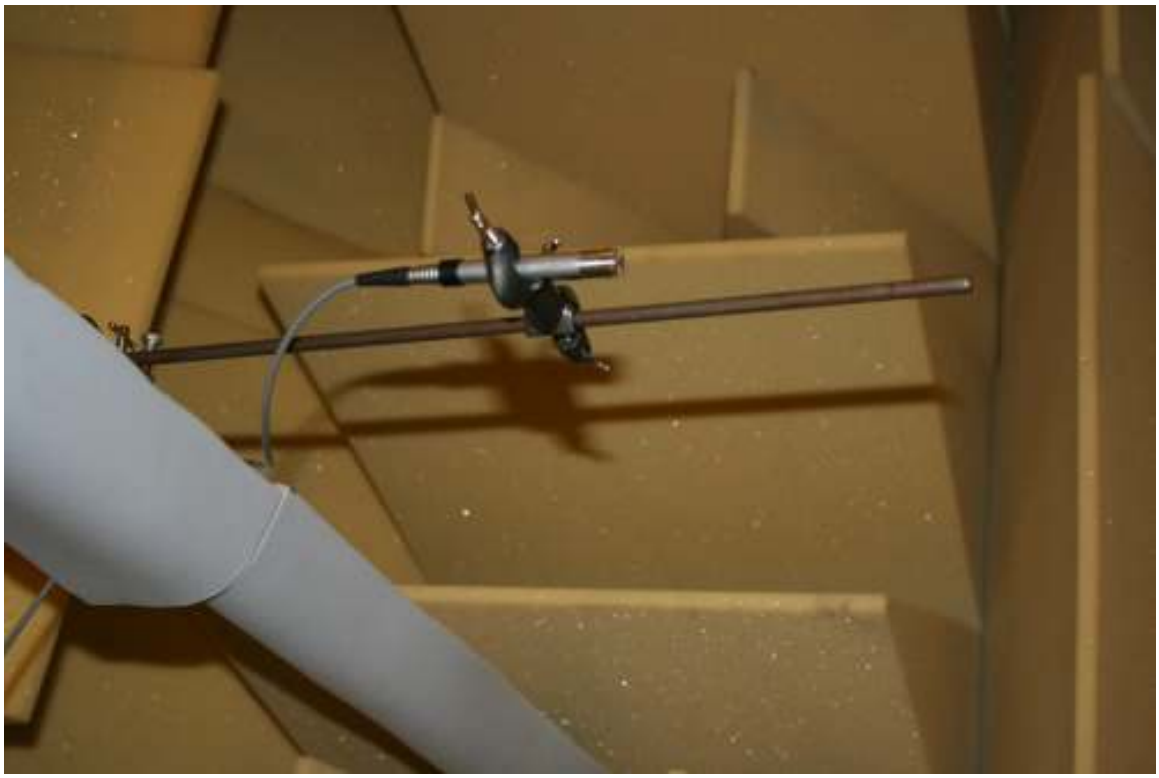

Figure 2-38. Out of Flow microphone stand and the B&K 0.5 inch microphone. Conditioning amp (not shown) was located inside chamber as well.

3. RESULTS OF 2006 INTERMEDIATE CALIBRATION

Upon completion of testing of the prototype anechoic configuration in 2005, construction began on a full scale facility. This chapter describes the results of these preliminary measurements taken in 2006. Considering the overall dimensions, weight and complexity of the anechoic system, the installation of the two acoustic chambers, anechoic test section, and associated apparatus went quite smoothly. However, the system was not without its problems. Mechanical interference in the test section support system caused a gap between the test section and the anechoic chambers. This did not allow the chambers to be pushed completely adjacent to the test section, and prevented an air tight seal between the anechoic chambers and the test section windows. Additionally the seaming technique used to create Kevlar panels large enough to cover the test section width was not strong enough to take full tensioning in the frames. Overtime the Kevlar window seams would fatigue and ultimately fail, under high levels of tension. This required that the tension in the windows be reduced to approximately 75-80% of its capability. These issues, in addition to other facility problems, contributed to higher background noise levels, and a lift interference correction that exceeded prototype predictions.

Work performed during the summer and fall of 2006 includes measurements of the in flow noise levels, boundary layer thickness values at the upstream and downstream edges of the acoustic windows, and examination of the fan performance (to determine if there was an increase in system workload). Additionally measurements were taken to assess the capability and performance characteristics of the Kevlar windows. Initial measurements also included data taken using a NACA 0015 airfoil section with a 0.610 m chord that spanned the full height of the test section (full model details in chapter 2). These measurements consisted of studies of the lift interference correction, and the influence of the model on the boundary layer thickness and Kevlar window performance.

3.1 Background Noise Levels

During the summer of 2006 several acoustic tests were completed to measure the background noise levels in the new facility, and these were compared to the sound

pressure levels measured in the prototype by Camargo *et al.* (2005). As described in chapter 1, the prototype configuration used the hard wall test section with acoustic absorbers and much shorter (??m) Kevlar acoustic windows.

Single microphone measurements were acquired using the B&K 1/8th inch microphone and airfoil strut described in chapter 2. This assembly was located 3.54 m downstream of the inlet and 0.927 m off the port wall, and data was taken for tunnel speeds ranging from 10-60 m/s in increments of 10 m/s. Figure 3-1 shows the acoustic spectra as a function of flow speed. Comparison of these measurements with those of Camargo *et al.* (2005) (figure 3-2) shows levels some 4-5 dB above those with the prototype acoustic treatment.

3.2 Wind Tunnel Fan Performance

There were several hypotheses on what could have caused the increase in the background noise levels. First was the possibility that the drag on the system was larger than initially anticipated, increasing the workload on the fan and consequently increasing the overall noise levels. Higher drag would result in a lower flow speed in the test section compared to the fan RPM needed to drive the flow. To test this hypothesis the ratio of test section flow speed to fan RPM, as a function of flow speed was measured, and compared with data from the prototype test. Measurements are plotted in figure 3-3. There is some scatter in the prototype data but, at least above 30m/s, the ratio of flow-speed to fan speed was higher with the anechoic system implying lower drag and thus refuting the hypothesis. This data shows that the fan RPM as a function of flow speed is comparable to the prototype for the anechoic configuration, except at low flow speeds. In order to further characterize this relationship, measurements of the boundary layer profiles at key locations at the inlet and exit of the test section would be measured. Measurement and analysis of these profiles is discussed in the next section.

3.3 Boundary Layer Growth

To determine the approximate boundary layer thickness a Pitot Static probe was used to measure stagnation and static pressure coefficient values at several locations along the test section wall for a flow speed of 30 m/s. This probe was secured to the steel

airfoil mount (see chapter 2 for details) that was attached to the test section floor using 4 industrial strength magnets. This set-up allowed the probe to be manually placed at any location within the test section so that pressure measurements could be obtained. Pressure measurements were desired at approximately mid span of the window which placed the probe at a distance of 0.986 m above the floor. The mount set up could then be moved manually to any desired position outwards (towards the center of the test section) to approximate the boundary layer thickness on the side walls, or placed horizontally at the rear of the test section to approximate boundary layer thicknesses on the floor or ceiling. At each location the probe was positioned an initial distance away from the wall and this distance was recorded.

The boundary layer thickness was determined when the stagnation pressure coefficient reaches a value of 0.95 (97.5% of the free stream velocity). The criterion that Cp_{total} be equal to 0.95 was chosen (instead of the traditional value of $U = 99\%\ U_e$) because of the limited number of data points that could be acquired at a given measurement location. Moving the measurement apparatus by hand also introduced levels of uncertainty that would make determining where the velocity was 99% of the free stream very difficult, so this constraint was relaxed. This process was repeated at varying distances away from the wall until the distance where Cp was 0.95 was located. These Cp values were plotted against the distance away from the wall for various locations. The boundary layer thickness could be determined through examination of these plots.

These measurements included several measurements along the Kevlar windows on both the pressure and suction sides at the mid height, and on all four sides of the aft location of the test section. Measurement locations and conditions with respect to tunnel dimensions can be seen in table 3-1. Figure 3-4 shows a qualitative set up of the locations that were measured for the boundary layer thickness. Measurements were made at the entrance and exit locations of the test section on both the port and starboard windows. Two additional locations were chosen on the port-side window to examine possible sources of boundary layer growth due to the condition of the Kevlar. A summary of the boundary layer thicknesses can be seen in table 3-1. A sample boundary layer profile for the inlet starboard window is given in figure 3-5.

The boundary layer thickness values measured on the 4 walls downstream of the Kevlar windows range from 92 mm on the floor of the test section to 117 mm on the suction side of the test section. These values are comparable with previous testing on a prototype test section using Kevlar as an acoustic treatment (boundary layer thickness of 110 mm). These thicknesses are shown graphically in figure 3-6. There was only slight variation for the values at all four locations around the test section. This lends well to the idea that the Kevlar windows function much in the same way as a hard wall as far as general growth of the boundary layer for this specific flow.

Computed thickness distributions were compared to previous testing on several test section configurations. Comparison of the boundary layer growth for the hard wall, prototype with acoustic window treatment, and full Kevlar window configuration can be seen in figure 3-7 for the empty test section only. Also drawn in this figure is the relevant test section geometry. The blue sections are the steel panels at the upstream and downstream ends of the test section and the yellow line symbolizes the extent of the Kevlar window. Hard wall boundary layer thickness data was collected at two nominal free stream velocities of 20 and 40 m/s and the boundary layer thickness was determined at 99% of the free stream value (Camargo *et al*.). The boundary layer thickness for the acoustic treatment of the prototype test section and for the full Kevlar window configuration were computed at a nominal free stream velocity of 30 m/s, with the boundary layer thickness being determined at greater than 95% of the total pressure coefficient. The thickness distribution for all configurations follows a similar trend with the values for the full Kevlar configuration only slightly higher than the original hard wall case. Uncertainty in measuring the distance the probe was away from the wall could account for some of the variation. Mounting the probe to the floor required extreme caution not to displace the floor while measuring the distance away from the window, as any weight placed too closely to the base of the mount could shift the probe into or away from the window. The overall uncertainty in the boundary layer data was approximated as $1/20^{th}$ of the measured boundary layer thickness. The difference in the magnitude of the boundary layer thickness could also be attributed to the deformation of the Kevlar window during tunnel operation, or flow possibly being circulated between the chambers

and the test section. All of theses hypothesis would be tested in the subsequent 2007 entry.

Qualitative notes were also taken during the boundary layer measurements to potentially explain some of the measured data. Viewing the window from inside the chamber during a test run showed that the window was indeed displaced at some points along the window. A quantitative shape of the window would be necessary to better understand the flow patterns that were evident from the boundary layer data. A series of measurements were designed to examine the performance of the Kevlar windows both with and without a model installed which are discussed in section 3.6.

3.4 Lift Interference Correction for a NACA 0015 Airfoil

In addition to characterizing the empty test section, the performance characteristics were also examined with a model installed. A 0.610 m chord NACA model (see section 2.4.1 for model specifications) was installed with the quarter chord at the midpoint of the port and starboard windows and 3.54 m downstream of the test section inlet. This model spanned near the full height of the test section, with a gap of approximately 51 mm gaps at the ceiling. This gap was covered with a custom cut aluminum shim and foil tape.

With the model installed in the tunnel, the trailing edge was placed at the midpoint between the port and starboard windows (geometric angle of attack equal to approximately zero) and a pressure distribution was taken using the Scanivalve system discussed in chapter 2. All test runs were completed at a nominal velocity of 30 m/s. This pressure distribution was then compared to a two dimensional vortex panel method solution to determine the effective angle of attack that best matched the measured pressure distribution. This same procedure was repeated for another known geometric angle of attack, and the ratio of the difference in effective angle of attack to the difference in the geometric angles of attack would determine the lift interference correction for the tunnel. Examination of the measured pressure distributions compared to two dimensional predictions gave a lift interference correction for the 2006 anechoic tunnel of -33%. Figures 3-8 and 3-9 show examples of two pressure distributions corresponding to 8 and 12 degrees effective angle of attack with a lift interference correction of -33%. For each

figure the negative static pressure coefficient is plotted as a function of *x/c*. The blue lines are the theoretical two dimensional vortex panel method solutions, and the circles are the actual data measured on the model. Both pressure distributions show good agreement over the entire chord length with the exception that the location of minimum pressure is over estimated by the panel method and there are no pressure ports at the trailing edge. Figures 3-8 and 3-9 correspond to geometric angles of attack of 11.95 and 17.9 degrees, which confirms the lift interference correction determined previously.

While the lift interference correction was repeatable for the NACA 0015 model at various angles of attack, the value was higher than expected following the prototype testing in 2005. A likely cause of this discrepancy was the reduced tension in the acoustic windows.

3.5 Boundary Layer Growth with the NACA 0015

All boundary layer profiles with the model installed were measured at a nominal velocity of 30 m/s with the NACA 0015 (refer to section 2.4.1 for model details) mounted with the quarter chord in the center of the acoustic windows 3.54 m downstream of the test section inlet. The airfoil was mounted at an 8 degree effective angle of attack, with positive angles of attack measured with the trailing edge towards the port wall.

The boundary layer thickness values measured at the mid height of the port and starboard windows for the model mounted at an 8 degree effective angle of attack are given in figure 3-10. The boundary layers show a somewhat steady growth to 135 mm at the aft location of the starboard window. The pressure window has an entrance boundary layer thickness of 51 mm and a corresponding exit thickness of approximately 147 mm. While these values are higher than the starboard side, the growth in thickness follows a similar trend to that of the other window. In order to attempt to explain this phenomenon, two other profiles were measured at 1.45 m and 2.07 m downstream on the port window, as well as a qualitative assessment of the window shape during testing. Profiles at these locations yielded approximate thicknesses of 60mm and 63 mm respectively. The foam wedges on the inside of the chamber restrained the movement of the Kevlar window at a location 1.45 m downstream on the port side window. This restraint created a corner like surface as well as a bulge in the Kevlar material. This sharp edge may have caused the

boundary layer to become thicker immediately following location 2 and may have resulted in the boundary layer thickness being lower at location 3. The exact reason for the decrease in boundary layer thickness is not immediately apparent, but may be a result of an error in accurately measuring the position of the strut from the port window. Additionally, flow around the airfoil caused the window to displace into the test section in some areas, and into the chamber in others.

3.6 Acoustic Window Performance

The performance of the Kevlar windows was examined over a range of flow speeds and angles of attack with the NACA 0015 model. Measurements of the window deflection as a function of angle of attack, pressure distribution over the Kevlar windows, and flow speed versus fan speed (an indicator of drag) were made.

3.6.1 Window Deflection

A quantitative depiction of the shape of the Kevlar windows was desired to better understand both the possibility of flow through the windows and the effect this variable shape would have on the interference correction for angle of attack. To determine the overall shape of the window, several measurements were taken from inside the anechoic chambers to assess the change in the window location along its length with the NACA 0015 model at different angles of attack. The measurement system used during the 2006 testing was a rudimentary version of what was later constructed for the 2007 test, both of which are described in Chapter 2. For each window, a series of data points were taken along the mid-height of the window with no flow. This data set would serve as a baseline to account for any variation in the window shape that occurred during the tensioning process. Initially a baseline shape was taken with no airflow (figure 3-11). The variation in the window in the no flow condition is also used to estimate the uncertainty in the measured data. The relatively smooth curve in the zero flow data appears to shows that there were some difficulties maintaining even forces during the window tensioning process. This is a variation of as much as 8 mm across the window length on the starboard window and about 4 mm on the port window. This was removed from all subsequent deflection measurements to yield the net deflection of the window. Then the

tunnel speed was increased to a nominal speed of 30 m/s and both window shapes were measured for an angle of attack of 0 and 8 degrees effective. These were adjusted for the no flow condition and then plotted as a function of distance along the test section. Figures 3-12 and 3-13 are the net deflection in each window shown separately with the relevant test section geometry: notably the yellow line depicting nominal zero window deflection, the location of the edge of the hard wall, and placement of foam wedges from the chamber that restrict some movement of the window. The starboard window shows similar deflection patterns for both the 0 and 8 degrees effective angle of attack, with larger magnitudes for the higher angles of attack. At the inlet the window is displaced approximately 2 cm into the starboard chamber. Just upstream of the model leading edge, the window begins to displace into the test section. At 0 degrees angle of attack the effect is almost imperceptible, but at the 8 degree angle of attack case the maximum deflection reaches near 6 cm.

On the inlet side of the port window the displacement is into the test section for both angles of attack and quickly moves into the port chamber upstream of the model leading edge. At the test section exit the window displaces back into the test section. Again a similar pattern is observed for both angles of attack and deflection magnitudes are on the order of 4 cm in both directions for the 8 degree angle of attack.

3.6.2 Pressure Distribution on Acoustic Windows

Along with the potential deflection of the Kevlar windows, the possibility of flow moving between the windows and the acoustic chambers was of principal interest. As a means to quantify any transpiration that may have occurred with the Kevlar windows, several pressure measurements were taken both inside the chambers and along the length of the window bordering the test section. These measurements were taken using the same apparatus discussed earlier for the boundary layer profiles, namely a probe positioned on a vertical mount that was attached to the floor using industrial strength magnets. Pressure measurements were taken approximately every half meter down the length of the test section on both the pressure and suction side of the Kevlar windows. This pressure data was converted into a static pressure coefficient.

Values of the static pressure coefficient along the test sections walls were compared to the deflection of the windows in figure 3-14. The data appears consistent with theory that the decreasing static pressure coefficient is actually exerting a pressure on the Kevlar and forcing the window into the test section in some locations. Likewise where the static pressure coefficient has a positive value, the Kevlar is forced into the chamber.

The desired result of this test was to determine the amount of flow through the windows that was generated by the static pressure gradient along the length of the test section. The only data available relating the porosity of the Kevlar was determined by Josh Demoss in 2006, a courtesy copy of the plot is presented in figure 3-15. Using a hot wire calibration tunnel, air was forced through a stretched Kevlar panel to determine the relationship between the free stream velocity and the velocity of the air that passes through the material. During the full scale facility testing in 2006, the pressure differences measured were far too small to be related to figure 3-16, so only the pressure coefficient (and not the velocity) was plotted. A parabolic curve fit through figure 3-15 was used to attempt to compute the velocities at each location. For all cases considered, velocities through the Kevlar were estimated to be less than 0.3 m/s and in many cases were far lower. The lack of available data on the porosity of the Kevlar windows was of great concern, and a panel method was developed for the 2007 entry as a comparison for the static pressure difference across the window. This panel method, along with window static pressure differences, boundary layer growth and the deflection of the Kevlar will be presented and discussed in detail in Chapter 4.

Location Number	Port	Starboard	Condition	Thickness
1	0.9144		Airfoil	0.051
2	1.4494		Airfoil	0.061
3	2.0694		Airfoil	0.063
9	5.7044		Airfoil	0.147
1		0.9394	Airfoil	0.024
10		6.0594	Airfoil	0.135
Top		1.025	Empty	0.108
Bottom		1.025	Empty	0.092
10	6.0444		Empty	0.112
10		6.0594	Empty	0.117

Table 3-1. Comprehensive list of all of the boundary layer profiles that were gathered for the 2006 test. Location numbers and corresponding distance along the Kevlar Window. All dimensions are given in meters and are measured from entrance of the test section on the port side. Top and Bottom locations are measured into center of test section from Starboard wall.

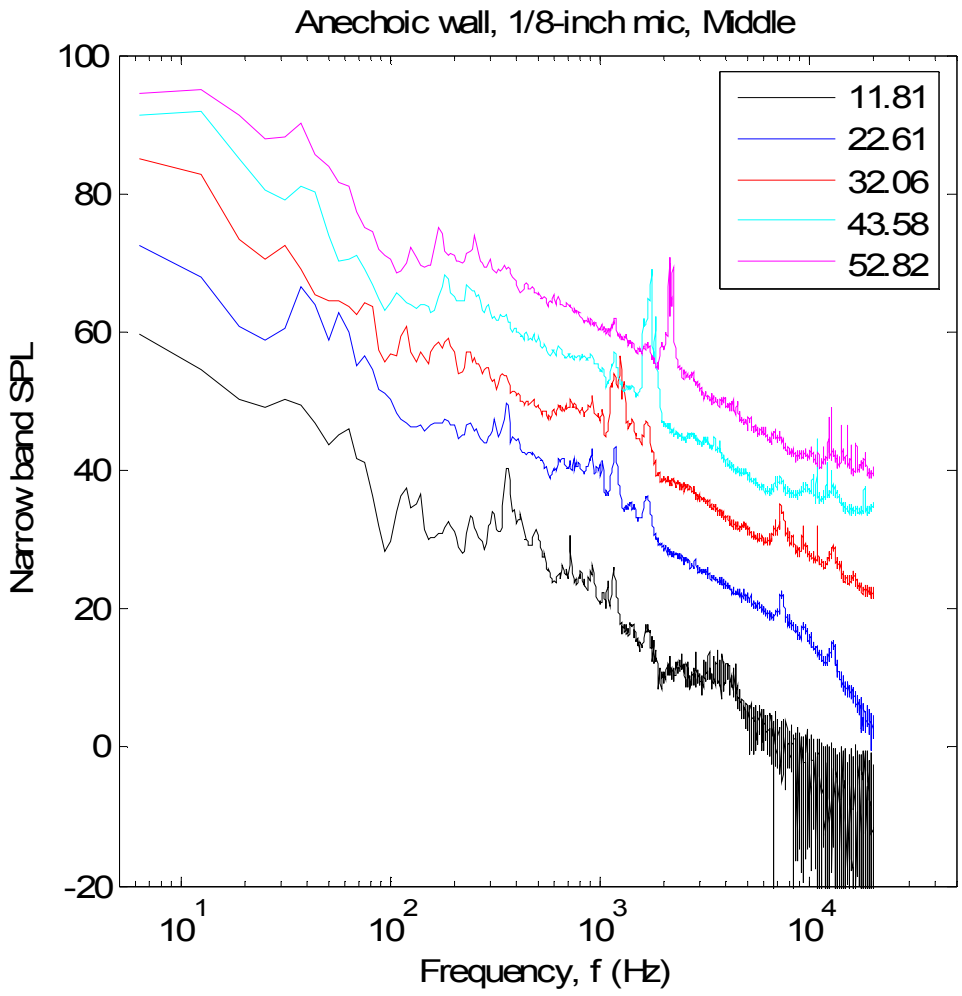

Figure 3-1. Background Noise Levels for the initial installation of the anechoic facility in 2006.

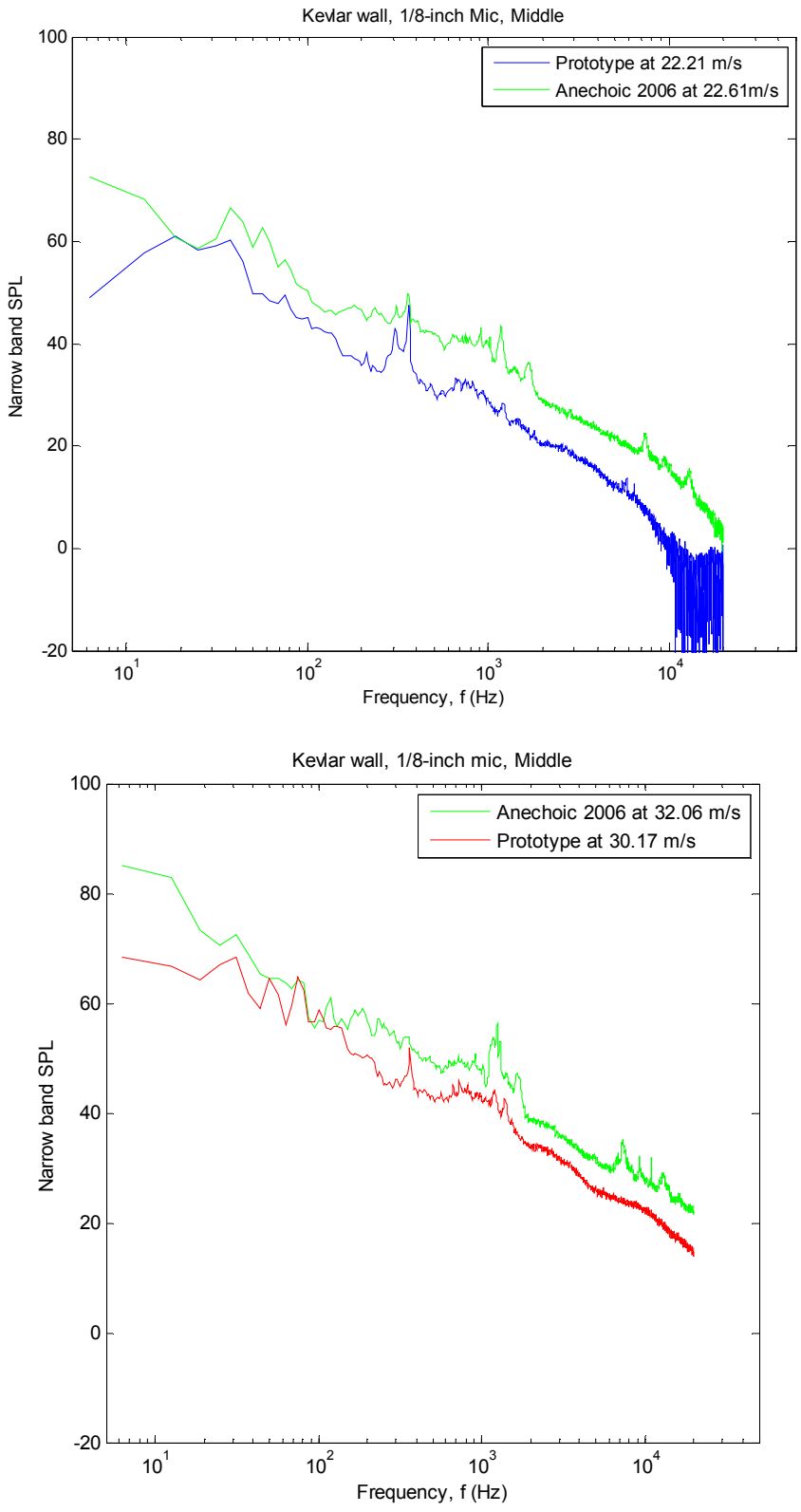

Figure 3-2. Background Noise Levels in the 2006 anechoic facility compared to the predicted prototype values at nominal 20 m/s (top) and 30 m/s (bottom)

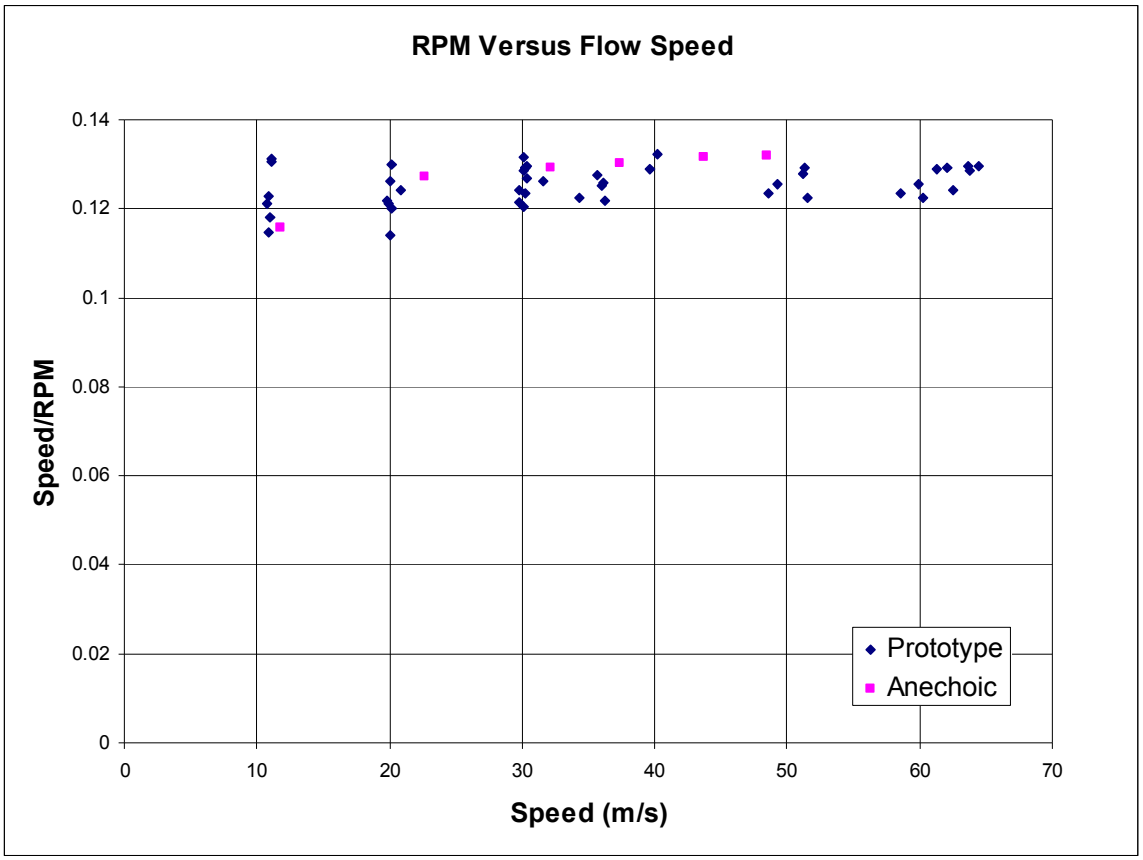

Figure 3-3. Comparison of fan r.p.m as a function of flow speed for several hard wall conditions as well as the 2006 anechoic facility.

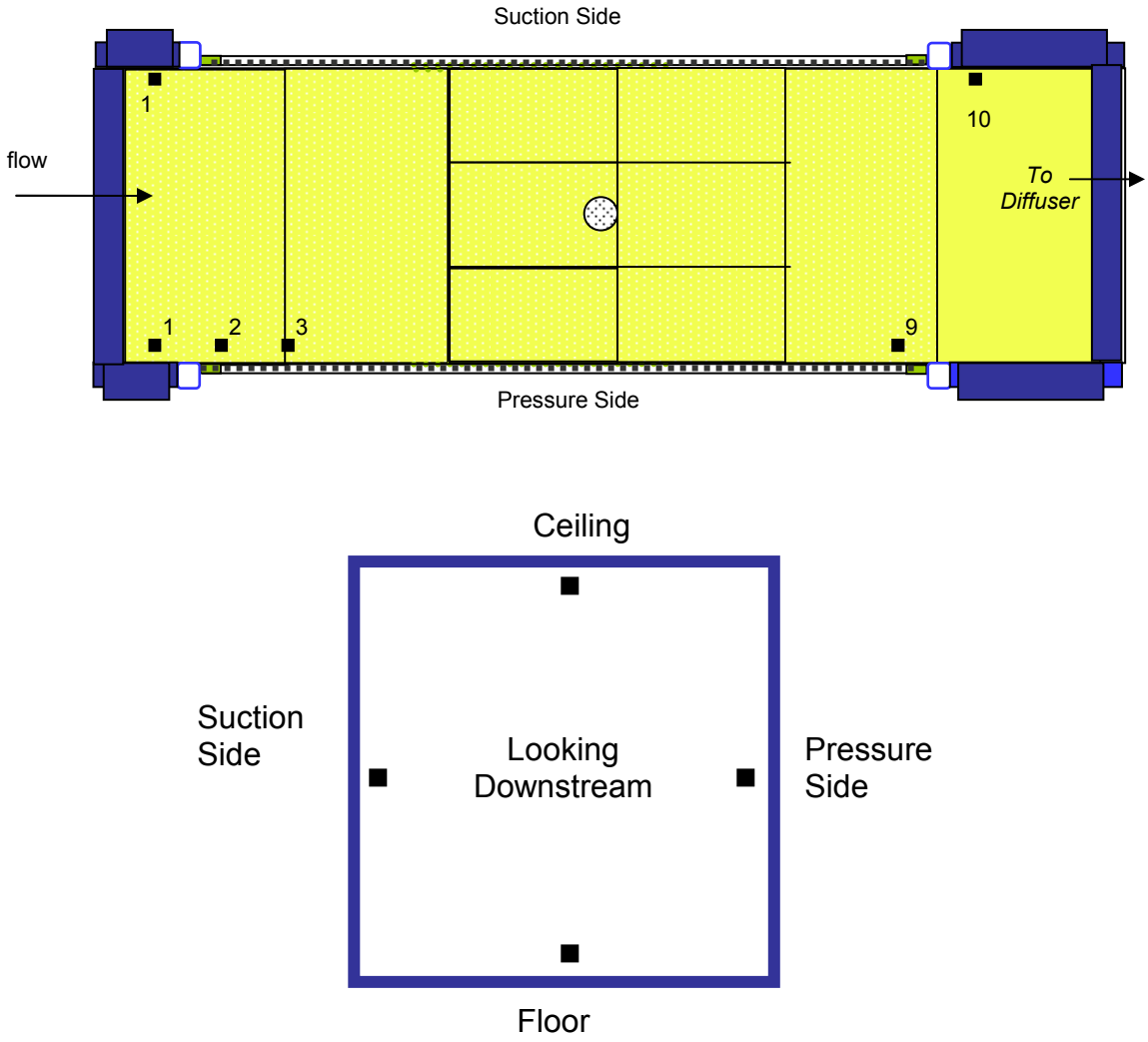

Figure 3-4. Boundary Layer measurement locations along the stream wise length of the test section (top) and locations at the exit of the test section (bottom)

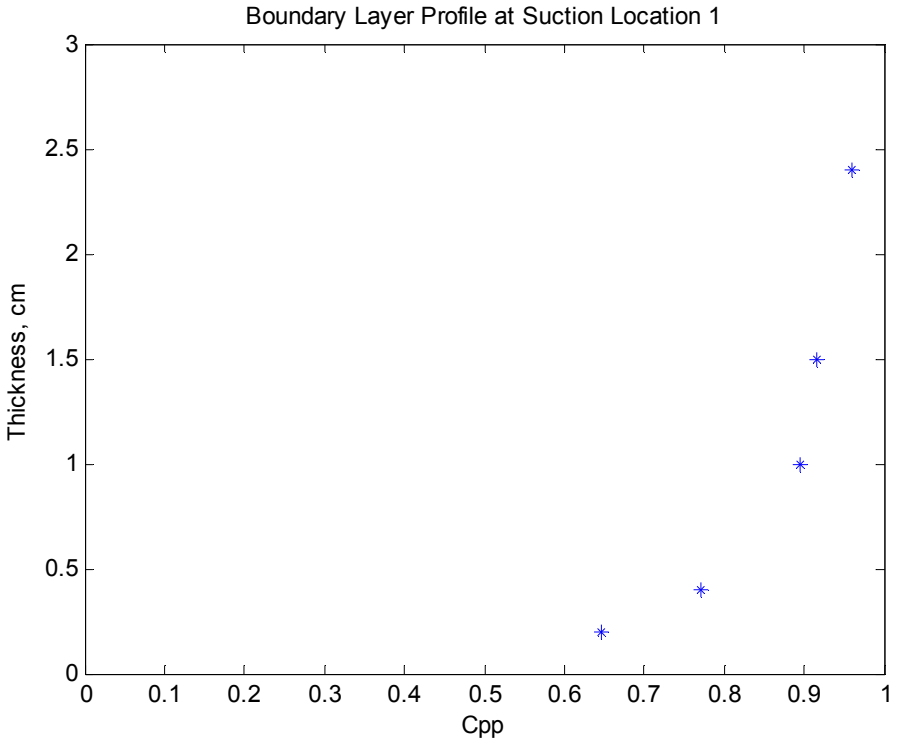

Figure 3-5. Boundary Layer Profile at the inlet of the Suction window at 30 m/s nominal velocity.

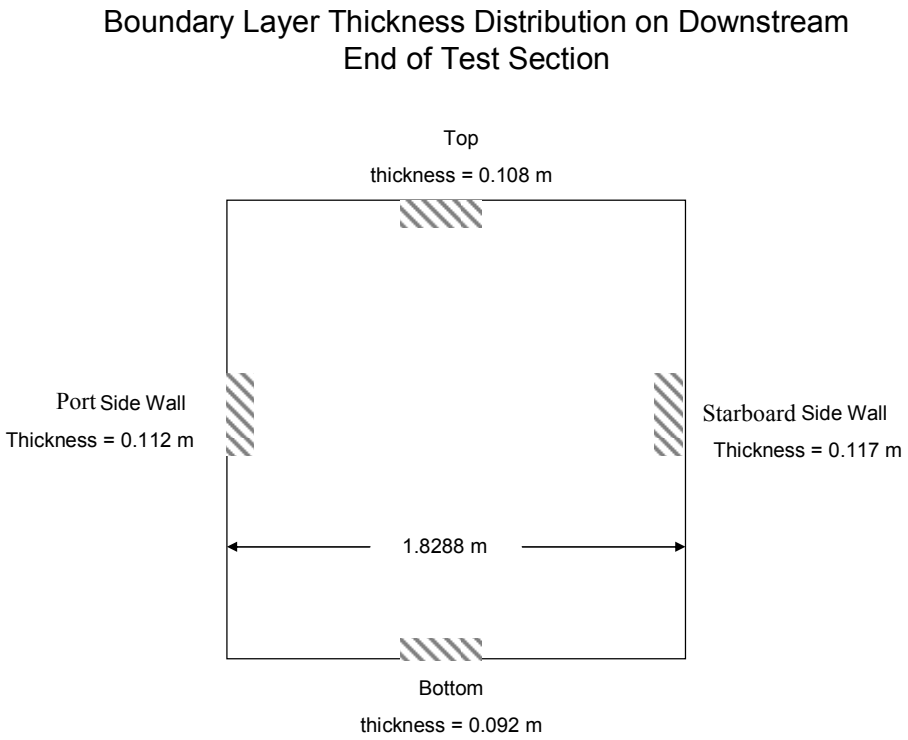

Figure 3-6. Graphical presentation of the boundary layer thickness at the walls and ceiling at the edge of the Kevlar windows. Above drawing has thicknesses scaled to the dimensions of the test section.

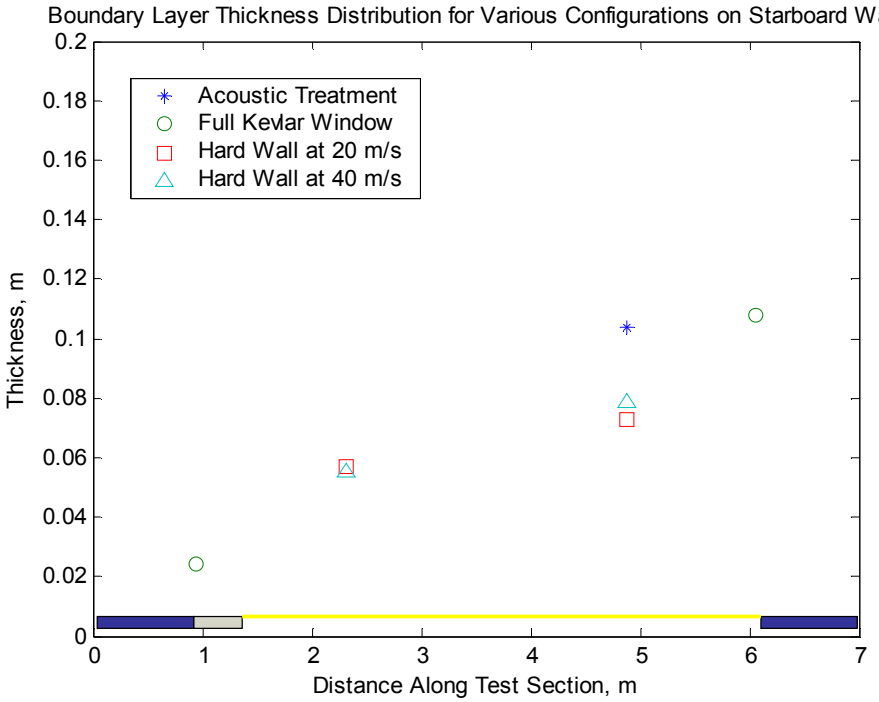

Figure 3-7. Comparison of Boundary Layer Thickness Distribution along the Suction side wall for various configurations. Geometry shown here is for the current testing configuration, with the hard wall, location of foam and window drawn in.

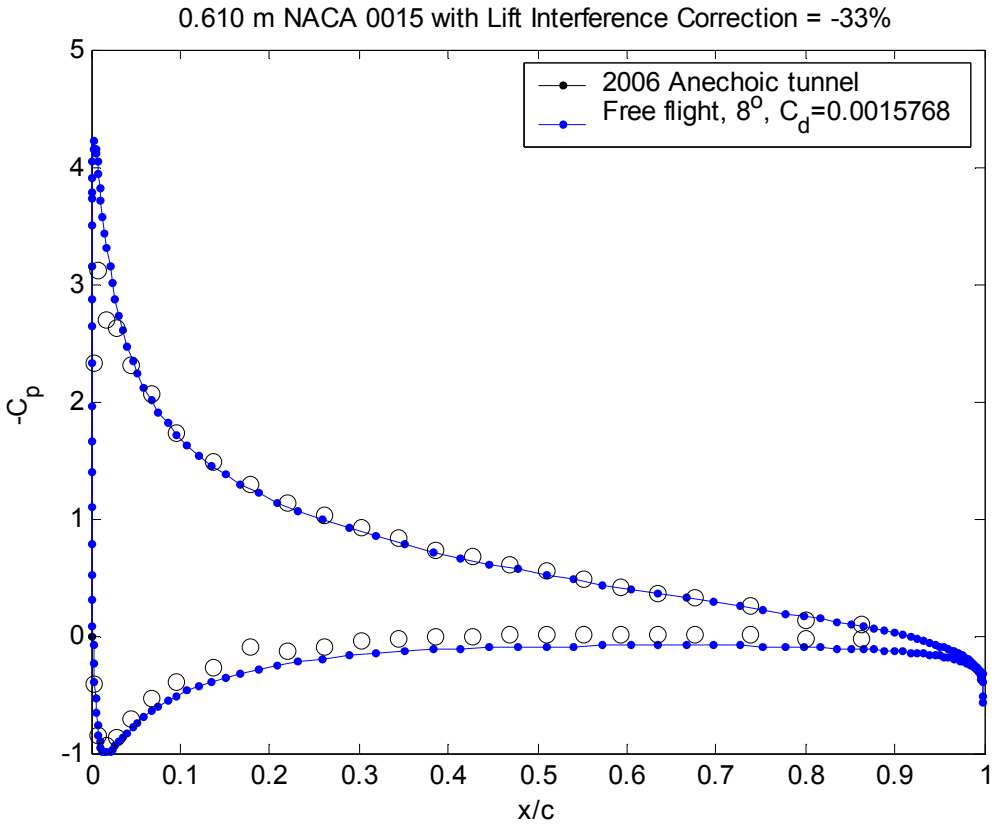

Figure 3-8. Comparison of the measured and theoretical pressure distributions for the NACA 0015 model mounted at 8 degrees effective angle of attack (geometric = 11.94) in the 2006 Anechoic tunnel (Lift Interference = -33%).

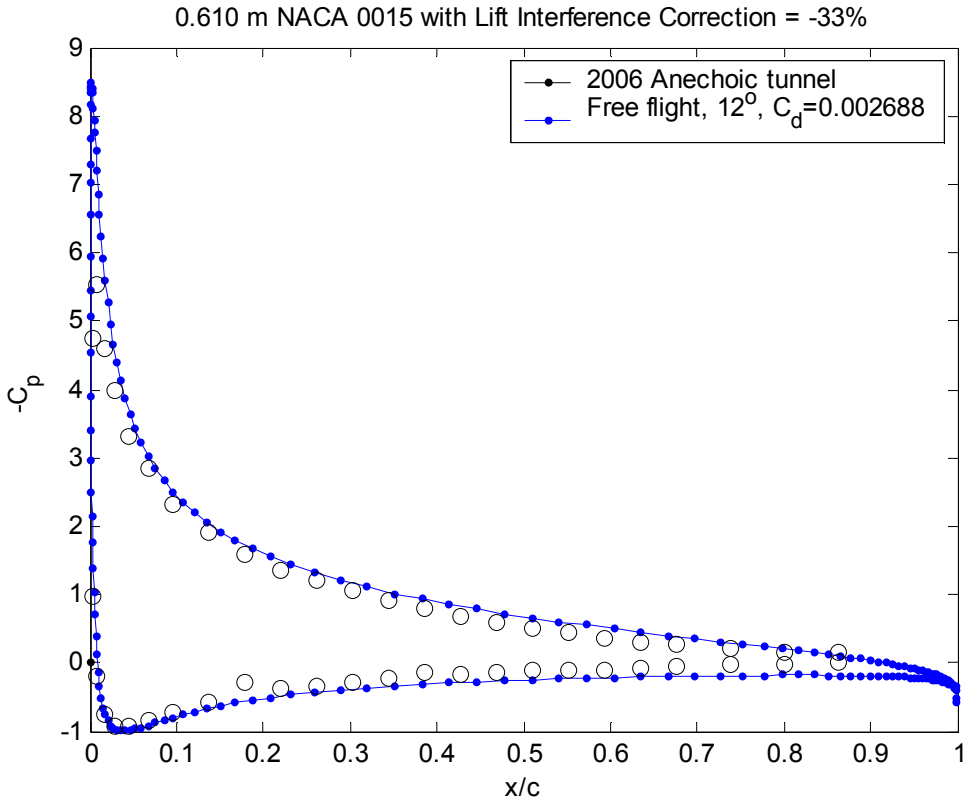

Figure 3-9. Comparison of the measured and theoretical pressure distributions for the NACA 0015 model mounted at 12 degrees effective angle of attack (geometric = 17.91) in the 2006 Anechoic tunnel (Lift Interference = -33%)

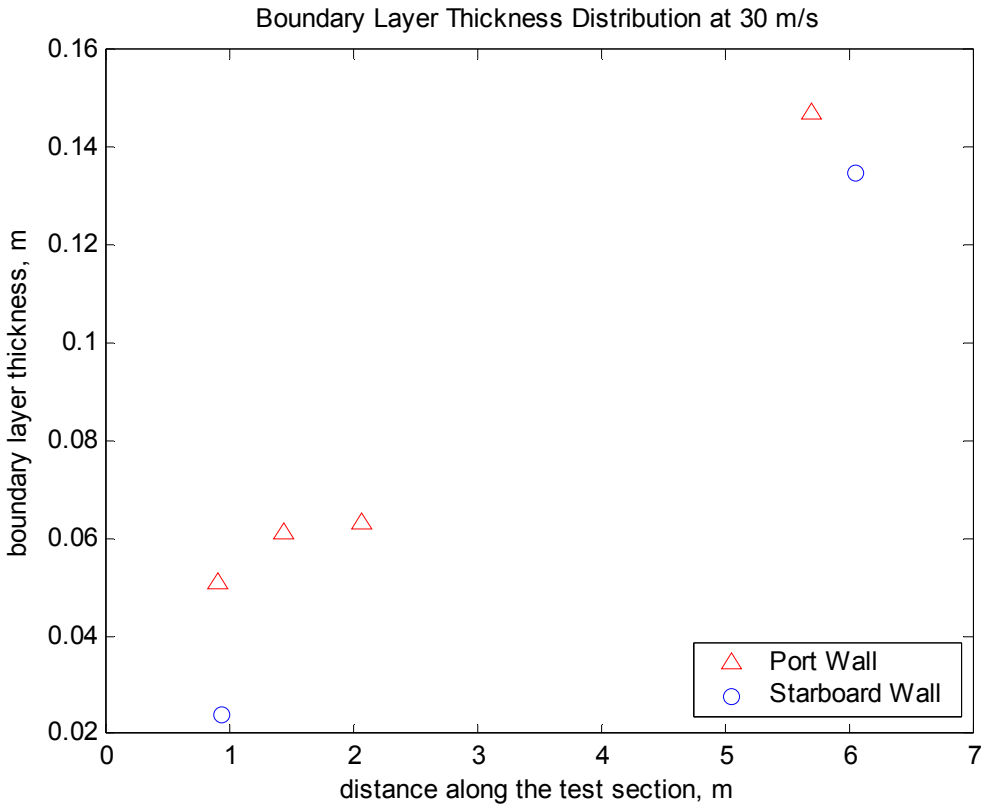

Figure 3-10. Boundary Layer growth with the NACA 0015 model mounted at an 8 deg effective angle of attack

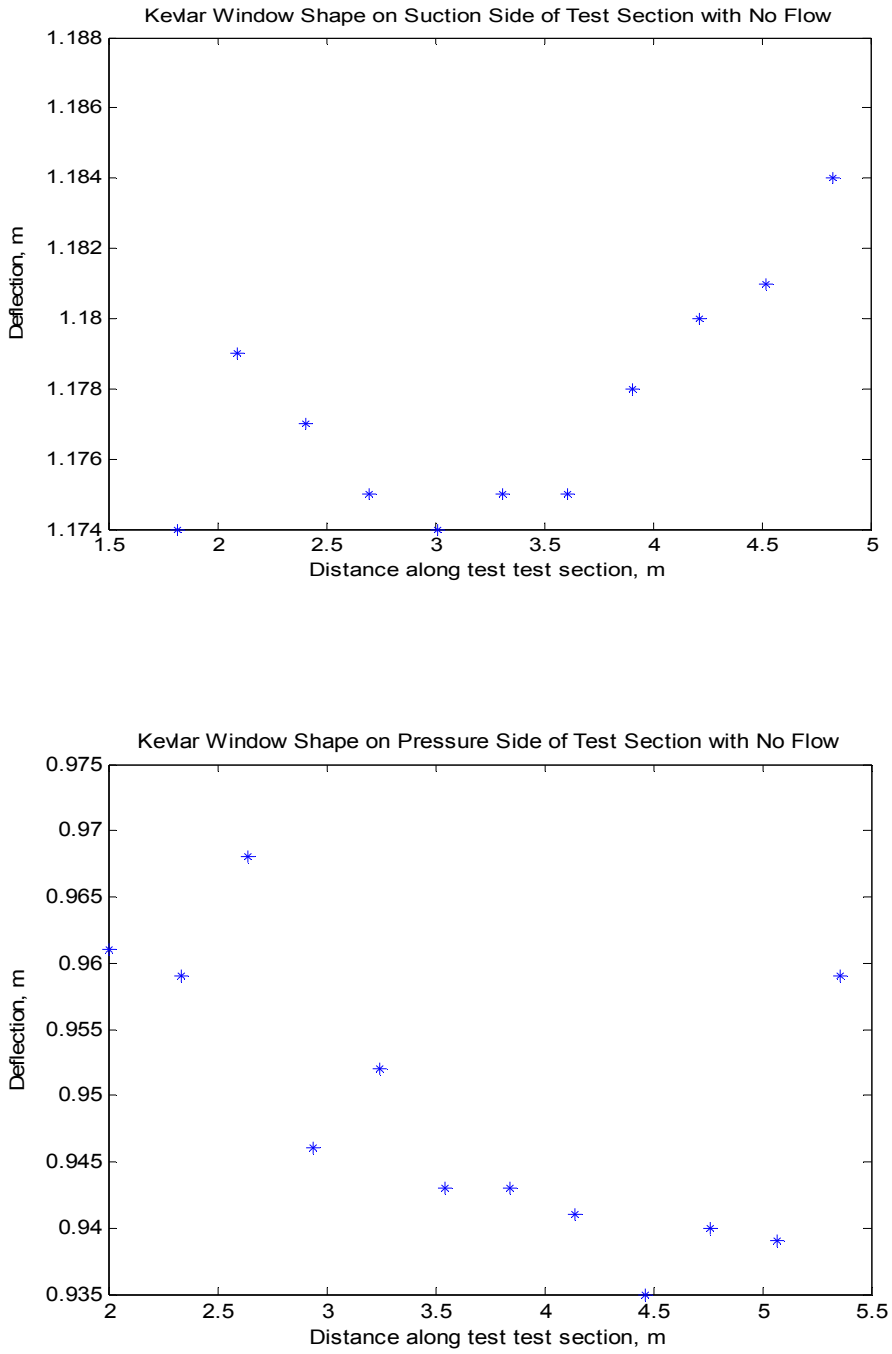

Figure 3-11. Initial Window shape of the Starboard side window (top) and Port-side window (bottom) taken with no airflow and with the airfoil at 0 degrees angle of attack. This was subtracted off future measurements to determine net deflection.

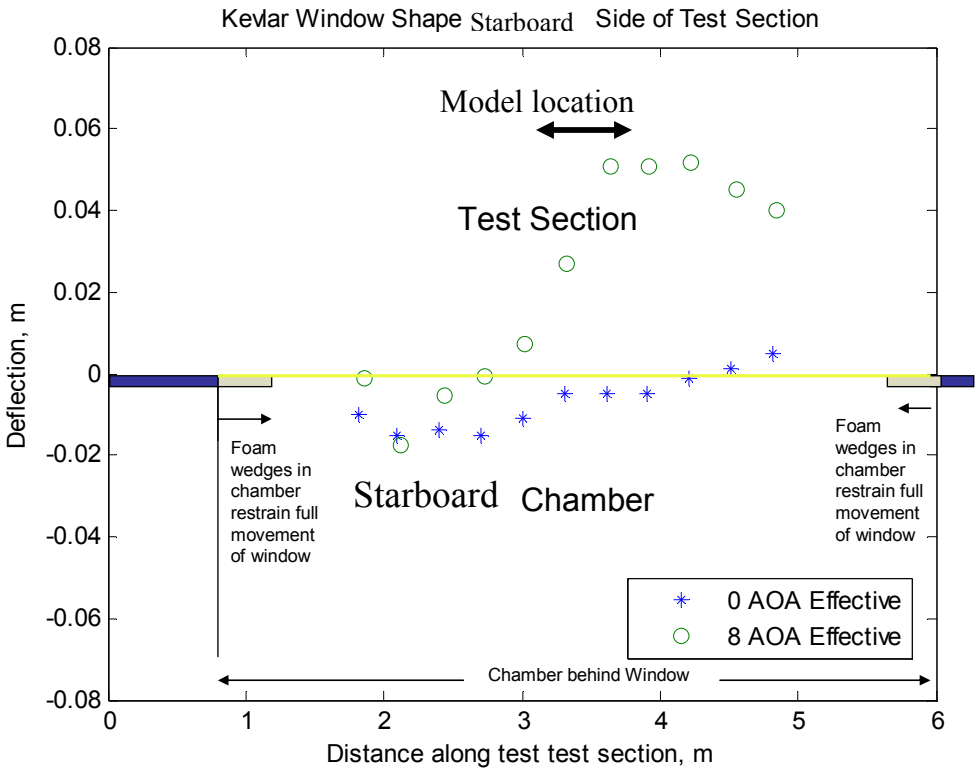

Figure 3-12. Deflection of starboard-side window with relevant test section geometry for both 0 and 8 degrees effective angle of attack.

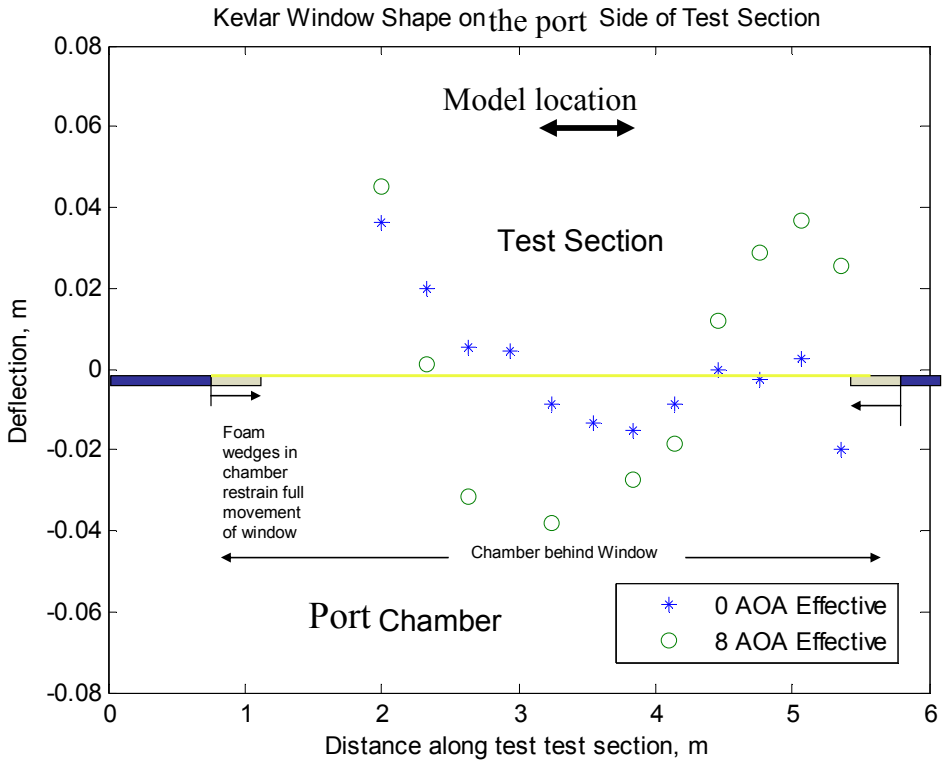

Figure 3-13. Deflection of the port-side window with relevant test section geometry for both 0 and 8 degrees effective angle of attack.

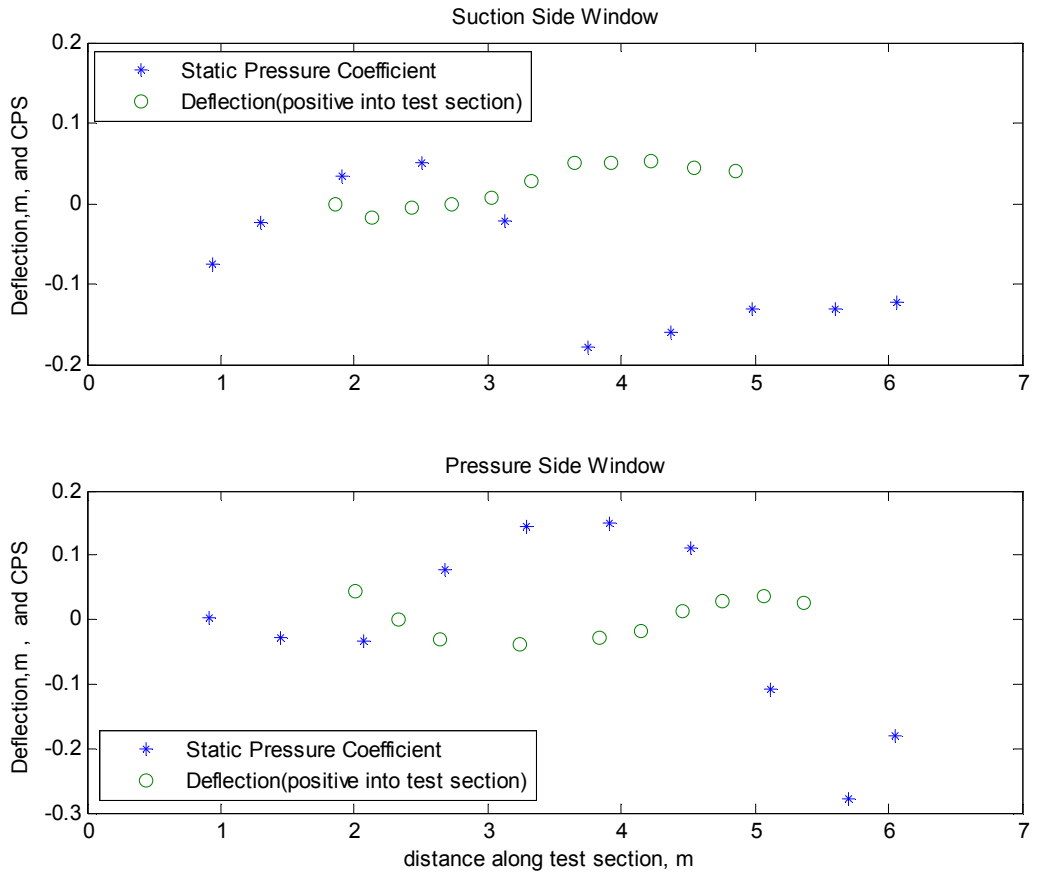

Figure 3-14. Comparison of the deflection of both Port and Starboard Side windows of the test section with the static pressure coefficient along the window.

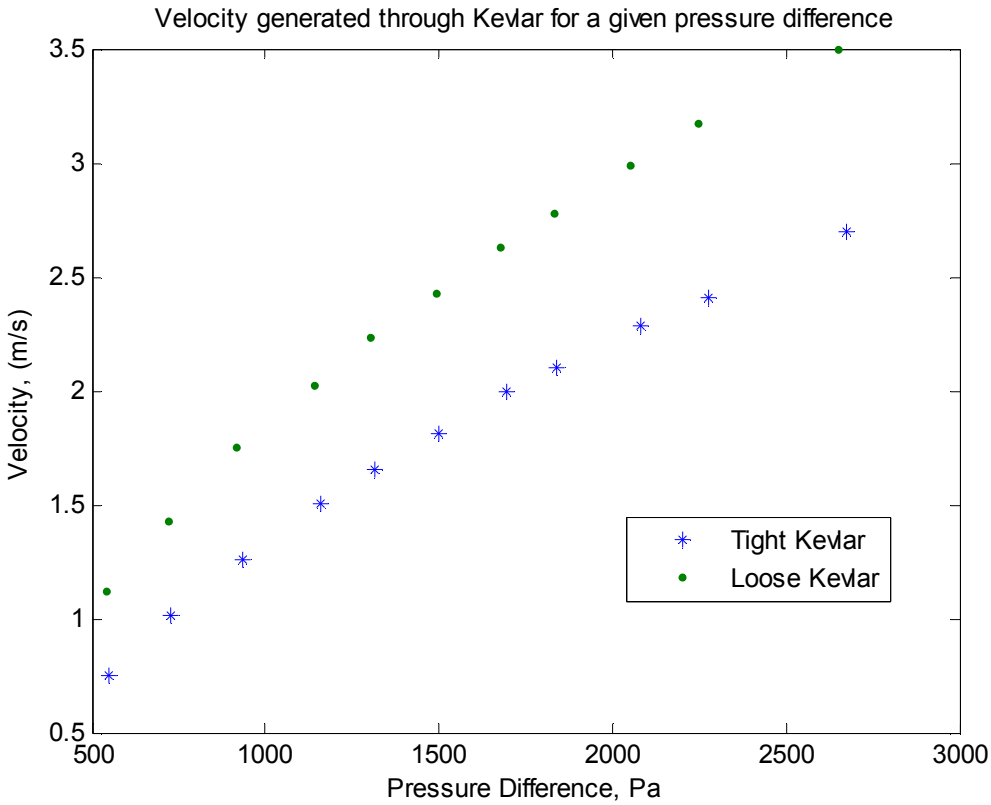

Figure 3-15. Experimental determination of the pressure drop across tensioned Kevlar cloth (courtesy Josh Demoss)

4. RESULTS OF 2007 FINAL CALIBRATION

During the months following the preliminary calibration in 2006, a detailed analysis of the data was performed. These results showed background noise levels that were larger than those predicted during the prototype test, and aerodynamic characteristics that fell short of expectations. It became clear that another set of calibration measurements would be needed following the acoustic treatment of the circuit and other facility modifications made during the spring of 2007. The following sections contain details on these tunnel modifications, calibration measurements and give final specifications for the completed Virginia Tech Anechoic Wind Tunnel.

4.1 Treatment of the Tunnel Circuit

During the months preceding the 2007 anechoic facility installation, steps were taken to further reduce the background noise levels by covering the circuit walls and lining the area around the fan blades with various acoustic foam treatments. At each stage of the treatment, in-flow noise levels were measured in the empty hard wall test section to judge the relative effects of the treatment. Measurements were made in approximately 10 m/s increments to a final low velocity of 70 m/s with the microphone (refer to chapter 2 for details) located 3.54 m downstream of the inlet, midway between the port and starboard windows, and 0.756 m above the floor. This location, referred to as mid-section, is close to halfway down the length of the test section. The first treatment application began in January of 2007 where approximately 28 square meters of 51 mm thick self adhesive melamine foam was installed on the port side diffuser wall (figure 4-1). Styrofoam transitions with a 16.67 % grade were added to the front of the foam to prevent aerodynamic blockage that would result in an increase in drag and thus fan rpm required to maintain speed. A small section of the starboard side diffuser wall was also covered to maintain symmetry. Following this treatment noise measurements were taken to determine a baseline for the remaining tunnel modifications and acoustic treatments (figure 4-2). Each additional measurement will be presented in a similar fashion, with 1Hz bandwidth sound pressure level (SPL) as a function of Frequency. Spectra were

measured approximately every 10 m/s using the 1/8th inch B&K microphone, and only frequencies less than 20 kHz were considered.

During March of 2007, after the diffuser was completed, custom cut variable thickness melamine foam was used to line the circular section of the circuit that housed the fan. This melamine foam was approximately 0.762 m wide and covered the complete circumference of the fan housing (figure 4-3). This treatment effectively reduced the fan tip gap, from around 15-25 mm to 3-5 mm. Concurrent with the fan treatment, the walls in the settling chamber (approximately 56 square meters) were treated with 51 mm self adhesive Urethane foam. Urethane foam has an advantage over Melamine in terms of longevity and resistance to damage from elements such as water and humidity. Additionally Urethane foam can be purchased at a lower cost than the Melamine foam, which makes it's a more suitable treatment for the larger areas of the tunnel circuit. In-flow noise levels were measured at the end of this stage of the treatment (figure 4-4). A more detailed comparison of noise levels with the baseline measurements is shown in figure 4-5 for nominal speeds of 20 m/s and 30 m/s. These figures indicate a reduction of 3-4 dB for frequencies less than 10 kHz.

After completing the settling chamber walls and the fan treatment, both walls of the north end of the circuit, between the northeast vane set and the settling chamber, were treated. This section added another 74 square meters of treated wall area within the circuit. As the treatment of the north end walls was concluding, Amanda Chou (undergraduate research assistant) performed work on treating the northeast turning vane set. Treatment of the turning vanes required modeling the vane and designing custom foam inserts that would not hinder the flow (figure 4-6). These inserts were created using 25 mm thick Melamine foam that was cut to a predetermined shape and glued to the concave side of each vane. The foam inserts were then trimmed with aluminum foil tape to create smooth edges, and prevent the foam from pulling away from the vanes.

The in-flow noise levels after the treatment of the wall area between the 3rd and 4th vane sets are shown in figure 4-7 and compared to the baseline in figure 4-8 for 20 and 30 m/s respectively. These plots show a reduction of another 1 dB from the previous treatment, for a total reduction of 3-5 dB. During the late spring of 2007 the floor of the north end section of the circuit was covered in 51 mm thick Urethane foam. This

treatment was in addition to the walls of the north end that had already been treated, and added another 37 square meters to the treated area. The last section of the circuit that was treated was the south end walls (just downstream of the diffuser); this was accomplished in the summer of 2007, during the second installation of the anechoic facility, with another 28 square meters of Urethane foam.

Throughout the year that the treatment was being accomplished, over 223 square meters of tunnel circuit surface area was acoustically treated, in addition to the fan liner and the northeast turning vane set. A diagram showing the extent of the tunnel treatment is shown in figure 4-9. After the rest of the treatment changes shown in figure 4-9 were accomplished, a final microphone measurement was taken. Figures 4-10 to 4-16 show the single flow speed comparison for the initial untreated circuit against the completed treatment of the circuit. Subsequent analysis of anechoic data out of flow microphone has shown that the frequency range between 1-3 kHz is partly influenced by the microphone stand. Further analysis of the in-flow acoustic data (discussed below) will take the contribution of the microphone stand into account.

4.2 Test Section and Model Catcher Modifications

The following sections contain details on the modifications that were made to the anechoic test section; a new Kevlar window seaming technique, the addition of acoustic absorbers and rare earth magnets, and a redesigned model mount. Additionally a new quieter model catcher was designed to replace the steel apparatus currently installed. Figure 4-17 shows a diagram of the test section with the major modifications and the following sections give specifics on these changes made prior to the 2007 calibration.

4.2.1 Anechoic Test Section

The first change made to the acoustic test section included a new seaming technique for the Kevlar windows developed along with C&C Sailmakers of Houston, Texas. This featured seam that was double the thickness and was approximately 1-1 ½ inches wide. This new stitching pattern greatly increased the load that the seam could hold, which allowed the windows to be tensioned to a much larger value. Along with the new stitching technique, the seam itself was covered in industrial strength super glue

prior to the tensioning process. While superglue was used during the 2006 iteration, it was added after the tensioning had been completed. Coating the seam prior to tensioning had the added effect of increasing the tensioning capability further, bringing the overall tension levels much closer to the maximum allowable for the Kevlar material. Along with the increased window tension, Neodymium rare earth magnets were added to the area where the Kevlar bordered the test section edge, to increase the overall loading that the window could handle. Over 200 Neodymium magnets (figure 4-18) measuring 25 x 25 x 6 mm were placed so as to hold the Kevlar to the side-edges of the test section walls and ceiling. Magnets were positioned at approximately 76 mm intervals along the Kevlar window floor and ceiling edges meet the Kevlar. These magnets served to transfer some of the aerodynamic load from the window to the frame. These magnets also functioned as an early warning system for excessive window load; they would start falling off the test section edge when the aerodynamic load became too high. These new measures allowed the tension on the Kevlar to be greatly increased, to about 5000 Newton's per meter.

For the 2007 entry, the entire floor model mount was replaced, which required modifying the floor panels further, to allow a larger portion of the floor to me removed. The main differences in the floor of the test section are the modified center panels. The center section of the test section was cut into 9 sections, with the centermost 3 being removed to install a model. The three centermost sections were constructed with 19 mm thick medium density fiberboard (MDF) and were mounted in the test section on aluminum extrusions mounted underneath the floor panels. The model rotation system was attached to the model before raising it through the floor of the test section, and rested on two steel beams (1.85 m long and 0.15 m wide) mounted to the main steel test section structure under the perforate panels. A system containing aluminum endplates (figure 4-19) that would fill the gap at the floor and ceiling as well as rotate with the model was devised for the 2007 entry. This rotation system, shown in figure 4-20, allowed the model to be rotated in just a few minutes with two personnel, one inside the tunnel to adjust the model, and one outside to loosen and tighten the gear holding the model in position. Additionally these plates could be used with any of the airfoil models tested. The endplates were 64 mm thick ellipses measuring 0.610 m in width and 1.524 m in

length, and lined around the circumference with thin strips of urethane foam to prevent damage to the Kevlar floor and ceiling during rotation. The plates were attached to the models at the spar (quarter chord). During the 2007 entry angles relative to zero were computed using a ruler attached to the gear at the base of the model from which distances could be converted to angles and vice versa. This system, shown in figure 4-21, allowed the model to be set with relative precision and reduced the uncertainty in repositioning the model to repeated angles of attack

The final major additions to the test section were the modified acoustic absorbers in the test section. These absorbers were created by removing sections of the steel panels upstream and downstream of the test section entrance and exit, and filling the area behind these panels with a combination of 5 cm thick Melamine foam and Fiberglass insulation and then covered in tensioned Kevlar. Figure 4-22 shows two views of the panel, one with the Kevlar covering and one with the Melamine liner showing. Not shown in these figure is the fiberglass insulation that is behind the Melamine foam. All four panels span the full height of the test section, and while the width of the upstream and downstream panel varies, the port and starboard panels are nominally identical at each location. The upstream panel measures 0.92 m on the test section interior, with 0.56 m of the panel removed and filled with the Kevlar covered acoustic insulation, as shown in figure 4-22. At the downstream end of the test section, the panel is a bit longer at 1.22 m with a Kevlar covered acoustic treatment measuring 0.80 m wide. These panels had two functions; firstly to remove excess hard wall area that would reflect any circuit noise sources, and the second to add more acoustically treated area closer to the primary measurement locations. As an extension of the acoustic absorbers, special transitions were made for the gap at the seam where the steel edge of the acoustic absorbers met the Kevlar window edge. This small (approximately 6 mm) gap was thought to be a possible source of sound radiation as well as a step that could incur some aerodynamic losses. As a solution to this problem, special poly-urethane tubing was cut to form a transition (figure 4-23) that could be inserted into the gap, and would provide a smooth transition for the flow from the steel plate to the window. These were placed at the two inlet and two exit acoustic absorbers.

This list is not inclusive, but includes the major test section modifications; additional care was taken in other areas during assembly to remove any additional noise sources. A complete list of the 2007 facility characteristics is given in table 4-1.

4.2.2 Model Catcher

There were a few other modifications made to the test section and circuit areas. First among these was the design of a new model catcher (figure 4-24) to replace the existing metal one. The new model catcher was constructed with barrier netting 7.62 m long and 1.219 m high. The net spans the entire width of the tunnel circuit along the second set of turning vanes immediately upstream of the fan. A 90% open air ratio was desired to minimize blockage, so 25 mm x 25 mm diagonal grid with single strand burst strength of 150 lbs was chosen. The net was attached to the sides of the tunnel with 6 "C" bolt closures and to the floor with 12 "P" clamps. This design was selected for its ease in removal and installation as well as beneficial acoustic properties (compared to the previous steel model). It could be removed for empty test section acoustic experiments, as well as large model tests, and the reinstalled in less than a half hour for smaller model, or non acoustic testing.

Additionally, the various conditions of each test, including flow speed through the test section and fan RPM were compared. Plotting these two parameters against each other, as has been done in figure 4-25, provides some insight into the effects of the acoustic treatments on overall tunnel operation and thus some useful background to the noise results. This plot shows, not surprisingly, a very close relationship between fan RPM and flow speed. Note that the anechoic measurements are closer to each other than they are to the hard wall regardless of the time accomplished. Additionally the anechoic configuration should have slightly increased the fan workload, and this increase does appear more distinctly at higher speeds. However, the fully anechoic facility data fall completely within the prototype band for all flow speeds.

Installing the acoustic treatment with Kevlar flow surfaces into the test section has a slight effect on the overall RPM/speed relationship, suggesting that the acoustic treatment added some drag to the test section. While the treatment increased the fan

RPM, and thus the overall drag on the system, these changes were small compared to the reduction in background noise levels.

4.3 Background Noise Levels

With the acoustic treatment of the wind tunnel circuit in place background noise levels could be measured at various conditions to examine the results of both the treatment and the acoustic modifications on the overall anechoic background noise levels. The 1/8th and ½-inch microphones discussed in chapter 2 were used for this purpose. The measurements discussed in this section include the in flow noise levels associated with the background noise levels in the completed anechoic configuration, and out of flow noise levels measured from the anechoic chambers.

4.3.1 In Flow Noise Levels

After the modifications to the tunnel circuit had been completed, the anechoic facility was installed and several background noise level measurements were taken. A list of the entire in flow microphone measurement test matrix associated with the final calibration is given in table 4.2. In this table the nomenclature "Test Point" was used to assign a run number to individual test runs at various speeds for comparison. The 1/8th inch B&K microphone used for the hard wall noise measurements was mounted 3.54 m downstream of the test section inlet with the microphone tip 0.756 m above the center of the test section floor and 0.927 m from the port side window. This "middle" position served as the airfoil model mounting (center of rotation) location as well. Spectra were taken every 10 m/s for flow speeds from 0-60 m/s.

Figure 4-26 shows the overall in-flow noise levels for the 2007 anechoic configuration. Each additional measurement will be presented in a similar fashion, with Narrow Band Sound Pressure Level (SPL) as a function of frequency. Only frequencies less than 20 kHz were considered. This plot shows background noise levels that are significantly lower than those for both the original tunnel configuration and for the 2006 preliminary anechoic test section as well. This overall decrease is attributed to the treatment of the circuit as well as the additional acoustic modifications made to the test section. Overall reductions for a nominal flow speed of 52 m/s range from 10 dB below

the 2006 data to 15-20 dB below the original hard wall data (figure 4-27). The background noise levels for several hard wall treatment configurations as well as both the 2006 and 2007 anechoic data are given in figures 4-28 and 4-29 for a nominal flow speed of 31 m/s and 51 m/s respectively. The treatment conditions in both of these figures correspond to the tunnel treatment stages previously discussed (hard wall baseline, completion of the fan liner and settling chamber, and the northeast wall and turning vane set) as well as both the anechoic tunnel configurations in 2006 and after the treatment and facility modifications in 2007. These plots show the hard wall baseline having the largest contribution to the background noise levels with the 2006 anechoic data showing only slightly lower levels. Following the treatment stages the overall noise levels continue to decrease, with the final 2007 anechoic tunnel (with treated circuit) having the lowest background noise levels. The area highlighted between 1-3 kHz appears to have a localized distortion that was later determined during the out of flow data measurements (section 4.3.2) to be a function of the microphone measurement stand, and indeed all of the previous measurements are suspected to contain this noise contribution. At the reduced background noise levels in the anechoic configuration the noise generated by the airfoil microphone strut is large relative to the ambient noise. This will be discussed and adjusted for in the next section.

Additionally the scaling of the noise spectra measured at the middle of the test section for the 2007 anechoic configurations was examined. Figure 4-30 shows these spectra plotted against frequency normalized on the fan rotation rate f_f = RPM/60. Signals at harmonics of the blade passing frequencies of the fan should be around 8ff. For the latest anechoic data set the spectra show low frequency peaks close to this frequency, at values of 7.75 f_f which is consistent with the 8 fan blades. They also show peaks that scale with the fan speed at frequencies of around 22 f_f. While these are most likely fan related they are not exactly harmonics of the blade passing frequency. All the spectra also show peaks between 250 to 350 times f_f (specifically 331 f_f) which is possibly a stator rotor interaction frequency.

Overall, scaling the frequency on fan rotation rate lines up some of the spectral features, with the exception of the very low-frequency modes. Figures 4-31 and 4-32 show attempts to scale the spectral level on the 4th and 5th powers of the flow velocity.

These plots exclude the 10 m/s spectra since the additional noise in this low speed data obscure the other spectra when they are scaled in this way.

4.3.2 Contribution of the Microphone Stand

Several acoustics measurements were taken from within the anechoic chambers to gather data on out of flow background noise levels. A detailed description of all of the acquired data can be found in Staubs (2008). During this collection process it was noted that there was a significant noise contribution from the microphone stand in frequencies between 800 Hz and 3 kHz. A comparison of the inflow noise levels compared to the out of flow noise levels for the empty test section is given in figure 4-33.

The measurements of the out-of-flow noise levels were measured using two B&K microphones located 1.8-m from the center of the test section (0.87-m from the Kevlar window) and 2.42-m from the upstream wall of the starboard side anechoic chamber. These microphones were spaced 15.2-cm apart and were located at the mid-height of the chamber. In this figure the out of flow noise levels are shown with and without the microphone stand for the blue and red spectra respectively. Both noise levels are equal over broad band sections of the frequency range, with the exception of the region between approximately 800 Hz and 3 kHz. Using this knowledge, figure 4-33 shows an approximation (dashed lines) of the spectra with the microphone stand removed compared to the original anechoic data. The significance of the microphone stand contribution was approximated using the dashed line approximation in figure 4-34. This approximation was developed by inferring a straight line between two frequencies on either edge of the area in question. From this plot the area under the measured spectra could be computed by converting the SPL values back into pressures and taking the area difference between the measured data and the straight line approximation. This difference in area for each flow speed could then be subtracted off of the pressure spectra, and converted back into narrow band sound pressure levels. From these adjusted levels the A-weighted SPL as a function of flow speed could be determined (figure 4-35). Removal of the microphone stand significantly decreases the overall A-weighted sound pressure levels, suggesting that at the reduced back ground noise levels in the test section, the contribution of the microphone stand is a considerable factor. While the

approximation used for this analysis potentially overestimates the noise levels for the microphone stand, data acquired by J. Staubs undoubtedly show the interference of the stand. Future detailed analysis of these spectra will undoubtedly result in lower background noise levels similar to those shown in the previous figures.

4.4 Determination of the Lift Interference Correction

One of the most important values attributed to an aerodynamic wind tunnel is the lift interference correction for a model of a given size and geometry. With model size increasing to match full scale flight Reynolds numbers, reducing the interference effects has become increasingly more important. The determination of this value has been the study of numerous papers spanning a period in excess of the past 50 years. Several methodologies have been considered during this time for numerically determining this value for many different tunnel configurations; among these are the open jet tunnels, hard wall wind tunnels or some combination of the two such as slotted wall tunnels (Baldwin *et. al* (1954)) or the porous wall tunnel (Woods (1955)). Additional research has been conducted to attempt to reduce the wall interference using various methods (Crites and Steinle Jr. (1995)) for subsonic tunnels; however most of the existing research is geared towards prediction methods for supersonic tunnels and using variable wall shape to reduce the wall interference.

The following two sections present the lift interference correction for a series of airfoil models mounted in this facility, both experimentally and using a modified panel code prediction method. For the experimental determination of the correction, several airfoil models were used; models with a 0.9144 m chord and 1.823 m vertical span with thickness values ranging from 11% to almost 30% and of varying degrees of camber. For the panel method prediction a combination of modified vortex and source panel codes were used to simulate a porous wall boundary condition and to account for the midline deflection of the Kevlar walls. Additionally pressure distributions were compared using the panel method approximation for 3 models; a 0.2032 m chord NACA 0012, a 0.9144 m chord NACA 0012 and a 0.6096 m chord NACA 0015. These results show that with some information regarding the airfoil, this code could be used to predict the interference correction for a given set of conditions.

4.4.1 Experimental Approach

During the calibration measurements acquired during the summer and fall of 2007, several airfoil models were being tested for the National Renewable Energy Laboratory (NREL) and Sandia National Labs. In order to run these airfoils in the tunnel an interference correction had to be determined for each model so that effective angles of attack could be set for the various acoustic and aerodynamic measurements. Aerodynamic measurements were performed on three airfoil models with DU96, DU97 W 300 and RISO sectional shapes. The models, constructed by Novakinetics LLC, were designed to span the complete vertical height of the test section and have a 0.9144 m chord. Since the RISO model was used for industrial testing (proprietary section shape), the coordinates of the RISO airfoil section shape are omitted, but the pressure distributions are presented as proof of the consistency of the experimental approach. These airfoils were chosen for their differing profile characteristics, with varying degrees of camber and thickness values. The DU96 is comparable to the NACA 0012 in thickness, has a slight amount of camber, and a sharp trailing edge. The DU97-W300 has a much larger maximum thickness (close to 30%) and a thicker trailing edge (2.78%).

The origin of the geometric angle of attack of a model was determined using the measured pressure distribution. Using the modified HPVee acquisition discussed in Chapter 2, several pressure distributions were measured and compared to the theoretical two dimensional panel method results to determine the effective angle of attack. In most cases the airfoil was set at two predetermined geometric angles of attack (0 and 5 degrees) and these two comparative pressures distributions and the difference in the geometric angle were used to determine the relationship between the effective and the geometric angle of attack. The ratio of effective to geometric angle of attack, R used to determine this relationship was computed as follows:

$$R = \frac{C_{\alpha 5} - C_{\alpha 0}}{5 - 0} \quad \textbf{(5)}$$

where $C\alpha_5$ and $C\alpha_0$ were the angles of attack that best matched the theoretical pressure distribution at a geometric angle of attack of 0 and 5 degrees. Once this ratio was determined, the interference correction and geometric angle of attack that would

produce the desired effective angle of attack could be calculated. The interference correction was found by,

$$I = 1 - R \tag{6}$$

and the required geometric angle of attack for a given effective angle was determined using:

$$AOA_{geometric} = \frac{AOA_{effective}}{R} \tag{7}$$

Angles relative to zero were set by using a lever arm and scale arrangement, attached to the bearing below the test section. The accuracy of changes in angle of attack was estimated to be ±0.2 degrees relative.

During the 2007 measurements, 0.9144 m chord NACA 0012, DU96, DU97-W300 and RISO airfoils (see details in chapter 2.4) were used to examine the aerodynamic performance of the facility. For all of the measurements that utilized the NACA 0012, the nominal angles of attack were 0 and 8 degrees effective and the target Reynolds numbers were 1.6 million and 3.2 million. The Reynolds numbers were chosen to mirror some earlier and future testing objectives and as a point of comparison for the determination of the interference correction. The other model pressure distributions are at various angles of attack, but maintain the similar Reynolds number targets for consistency.

Using the Scanivalve system discussed in Chapter 2, several pressure distributions were measured and compared to the theoretical two dimensional panel method results to determine the effective angle of attack. In most cases the airfoil was set at two predetermined geometric angles of attack (0 and 5 degrees were chosen for simplicity) and these two comparative pressures distributions and the difference in the geometric angle were used to determine the relationship between the effective and the geometric angle of attack. The preliminary results for the NACA 0012 airfoil model gave an interference correction of -22%, and this was used for remaining NACA 0012 plots.

Figure 4-36 and 4-37 show the measured pressure distribution for the NACA 0012 at a nominal speed of 28 m/s and 0 degrees effective (and geometric) angle of attack. This test point corresponds to a Reynolds number of about 1.45 million. Both

plots have the chord wise distance along the horizontal axis and the negative pressure coefficient on the vertical. Due to the large number of ports on each model this test was run at two separate times, one immediately following the other (tunnel remained running), so there are two curves, one for each side of the airfoil. Pressure side data is plotted with a clear circle, suction side data in the darker circle, and the theoretical two dimensional comparisons with a dashed line. For this particular model there were a few clogged ports that were unable to be cleared, and this data is removed from the plot to avoid distortion.

Figure 4-38 and 4-39 are the pressure distributions for a 0 degree effective angle of attack at a Reynolds number of 3.1 million. Like the lower Reynolds number case in figure 4-37, there is good correlation along the leading edge and through about 80% of the chord. Towards the trailing edge (80-100% chord) there is some deviation from the theoretical two dimensional data, namely that the pressure distribution does not recover to a pressure coefficient of unity. This is due to viscous effects not modeled by the panel method. The overall trend of the data correlates well to the theoretical prediction, for both the low and high Reynolds number cases, with the exception of a slight deviation at the trailing edge.

The final pressure distribution set that was gathered for this airfoil was an 8 degree effective (10.4 geometric) angle of attack at a Reynolds number of 1.53 million. This is equivalent to a -22% correction. This pressure distribution serves to provide a complete data set for the acoustic-window deflection and pressure measurements. Figure 4-40 and 4-41 give the two views previously described for the 0 degree angle of attack cases. An 8 degree angle of attack is well below the anticipated stall angle, and was chosen as a good representation of the mid range for this airfoil. Looking at the distributions there is good agreement with the two dimensional theoretical prediction at the leading edge and throughout adverse pressure gradient. The location of minimum pressure was accurately measured, with a value that was only slightly lower than predicted. While this distribution, like the previous two at 0 degrees, does not return to unity at the trailing edge, both the pressure and suction sides of the airfoil have smooth curves that close at the trailing edge.

Using this wall interference correction, and corresponding effective to geometric ratio, pressure distributions were measured for the other 3 models and presented in figures 4-42 through 4-45. Figure 4-42, shows the pressure distribution in three views for the DU96 at a 3 degree effective angle of attack (geometric 3.8 degrees) and a Reynolds number of 1.58 million. This is equivalent to a wall interference correction of -21.05% and with an uncertainty in angle of attack of ±0.2 degrees; this is well within tolerance for the NACA 0012 interference correction of -22%. Figure 4-43 is the pressure distributions for the DU97-W300, which has a max thickness considerably larger than the NACA 0012, and a blunt trailing edge (2.7% thick). The DU97-W300 is mounted at an 8 degree effective angle of attack (geometric 10.3 degrees) at a Reynolds number of 3.13 million. This is equivalent to a wall interference correction of -22.3%, very close to that measured for the NACA 0012 despite the sizeable difference in camber and thickness. Finally the pressure distribution for the RISO is presented in figure 4-44 and 4-45. This model was mounted at an effective angle of attack of 2.7 degrees (3.5 degrees geometric) at a Reynolds number of 2.94 million (figure 4-44), and at and 11 degrees effective angle of attack (14.2 geometric and Re = 3.11 million) in figure 4-45. This is equivalent to a wall interference correction of -22.8% and -22.5% respectively. The two views presented in both figures show quite good agreement over the entire length of the chord, implying again that the correction determined experimentally is accurate, and works for models of various camber and thickness of the same chord length. It also shoed that there do not appear to be any significant effects based on angle of attack.

Several other models of the same chord length were measured with the same resulting interference correction. Additionally these models were initially tested in the summer of 2007, removed and reinstalled in the fall of 2007, and the interference correction was measured again with the same conclusion, proving the results are not only accurate, but repeatable.

4.5 Boundary Layer Growth

Reviewing the boundary layer thickness data from the 2006 entry showed promising results; mainly that the overall thickness at the downstream end of the test section had boundary layer thickness values that were comparable to the hard wall tunnel.

This confirmed that the Kevlar was functioning as a stable flow boundary. In order to confirm the previous year's results, a new measurement system was designed to obtain full profiles with enough data to more accurately determine the boundary layer thickness and to calculate the displacement and momentum thickness as well. The following sections have the measurement details on both the empty test section, and with the NACA 0012 model installed.

4.5.1 Empty Test Section

Boundary layer data was measured on all four walls both at the test section inlet and exit to compare with the 2006 anechoic set-up and the hard wall configuration. The large Stability tunnel traverse described in chapter 2 was used to make the following measurements. The Pitot static probe rake system described in chapter 2 was used to gather the pressure data on the mid section of both pressure and suction walls, and then the floor and the ceiling. Boundary layer thickness, displacement thickness and momentum thickness were computed for a nominal speed of 30 m/s at the upstream location (0.889 m from inlet) and nominal 30 and 50 m/s at the downstream position (6.198 m from inlet). Table 4-3 lists all of the boundary layer measurements that were made during the 2007 calibration along with the measured thickness, displacement thickness and momentum thickness. Boundary layer thickness was considered to be where the measured velocity was 99.5% of the free stream velocity. Displacement and momentum thickness were determined using the equations below.

$$\delta^* \equiv \int_0^{\delta} \left(1 - \frac{u}{U_e}\right) dy \tag{8}$$

$$\theta \equiv \int_0^{\delta} \left(1 - \frac{u}{U_e}\right) \frac{u}{U_e} dy \tag{9}$$

Where δ* is the displacement thickness, θ is the momentum thickness, u is the measured velocity and U_e is the edge velocity. These integrals were evaluated using a summation of the measured quantity over the change in position between the wall and the final boundary layer thickness. The velocity at the wall was assumed to be zero.

An example of the velocity profile is plotted in figure 4-46. This profile shows the velocity ratio, u/U_e, plotted against the distance off the surface for the downstream pressure window at 30 m/s. The same plot for the inlet pressure window is given in figures 4-47. The final boundary layer thickness values for the downstream location (two window, floor and ceiling) are shown pictorially in figure 4-48 for a nominal velocity of 30 m/s and in figure 4-49 for a nominal velocity of 50 m/s. These values were compared to the boundary layer data acquired during the evaluation of the prototype in 2005, during the intermediate calibration in 2006, and for the original hard wall configuration. A comparison of these thickness values is given in figure 4-50. The boundary layer thicknesses measured on the pressure- and suction-side walls are compared with similar measurements made in 2005 in the hard-walled test section, and in 2006 during the initial anechoic test section installation, for which the Kevlar windows could not be fully tensioned. The hard-wall data was taken at a nominal flow speed of 20 m/s, which is considerably lower than for the other cases, and is shown only as a reference. Boundary layer thickness values at the inlet, upstream of the acoustic windows, vary by 3 mm or less between the different configurations, and are consistent with the hard-wall values referenced in 4-50. The blue sections in the lower portion of the plot indicate the edge of the steel panels at the upstream and downstream ends of the test section. The yellow line connecting the two represents the test section length covered by the Kevlar windows. The boundary layer thickness is about 30% greater at the back of the test section in anechoic configuration. This additional boundary layer growth would be expected to produce an additional acceleration of the free stream of between 0.5 and 1% over the length of the test section. Boundary layer thicknesses at the exit of the test section are the same for the initial and final acoustic test section configurations, but the rate of growth is faster than that seen with the hard wall, presumably because of the porosity of the Kevlar windows

4.5.2 NACA 0012 Model

With the NACA 0012 model installed boundary layer data was measured on the suction side window at 0 and 8 degrees effective angle of attack. The traverse and five Pitot static probe system described in chapter 2 were used to make the following measurements. Boundary layer thickness, displacement thickness and momentum

thickness were computed for a nominal speed of 30 m/s at the downstream position (6.198 m from inlet).

The data for these measurements were analyzed and processed in the same manor as for the empty test section, and equations 8 and 9 were used to compute the displacement and momentum thickness parameters. Figure 4-51 is the plot for the airfoil at 0 degrees angle of attack on the port window side at the downstream location. For the 0 degree angle of attack the boundary layer thickness (99.5% of the free stream velocity) was determined to be 130.2 mm and the displacement and momentum thickness values were 23.55 mm and 14.53 mm respectively.

Figure 4-52 contains the pressure side wall boundary layer profiles for the model at an 8 degree angle of attack. For the 8 degree angle of attack the boundary layer thickness was determined to be 210.8 mm and the displacement and momentum thickness values were 21.28 mm and 13.58 mm respectively. The model blockage and the pressure gradient created by the growth of the boundary layer result in a velocity acceleration of about 3% at 8 degrees effective angle of attack at the test section exit.

Boundary layer profiles were unobtainable for the centers of the floor and ceiling due to of the end-wall flows produced by the model. While the airfoil was designed to have two dimensional characteristics along the majority of the span, there were still some three dimensional effects near the floor and ceiling downstream of the model. While some of the flow around the floor and ceiling is exaggerated by the porosity of the Kevlar, three dimensional effects at the floor and ceiling are difficult to completely avoid. While this was not a factor in the measurements on the model, it affected the pressure measurements downstream of the model. For this reason only the profiles that have no residual interference are presented.

4.6 Kevlar Window Performance Characteristics

Tentative data was obtained for the window deflection as well as the pressure difference across the window during the 2006 preliminary calibration. For the 2007 entry, a more detailed approach was desired, with more data points that would cover a larger (two dimensional) area of each window. Deflection data was collected for both a grid pattern over each window at 2 speeds, and pressure measurements were made in a

similar grid for the pressure side window at two speeds. Both deflection and pressure difference measurements were taken in the empty test section and with the NACA 0012 model installed.

4.6.1 Window Deflection

In order to gain a better understanding of the potential influence of the window in the interference correction of the facility, several measurements were made to evaluate the three dimensional deflection of the window under aerodynamic load. Using the ruler and slider rail equipment discussed in chapter 2, window deflection measurements were made from inside the anechoic chambers. The steel edges of the test section on the upper and lower sections of the window were restrained by the neodymium magnets, and the sections along the upstream and downstream edges of the test section restrained by tensioning frame, were used as fixed points to determine overall deflection of the window. Using these points as the edge of the grid, 28 discrete points were added to fill out the window. A linear fit was used to determine the zero flow shape (baseline deflection) of the window from the upper edge of the window to the lower one, to account for any manufacturing defects in the frame or irregularities encountered during the window tensioning process. This zero flow baseline could be subtracted out of the subsequent data to generate the net deflection of the window.

Deflection profiles were taken at nominal speeds of 30 m/s and 50 m/s for both the pressure and suction windows. After the zero flow baseline was removed from the measured data, contour plots were generated to show pictorially the absolute deflection of the window. These plots utilize a cubic spline interpolation method, with approximately 20 points across the data set. This was determined through trial and error to determine the most realistic presentation of the data. Figures 4-53 and 4-54 show the window deflection for both pressure and suction windows in the empty tests section at 30 and 50 m/s respectively. The vertical lines before and after the measurement area (0.91m and 5.85 m) depict where the acoustic absorbers start and end. These are solid surfaces so no deflection is possible in these regions. Note that a positive window deflection is into the test section, while negative is into the corresponding chamber.

For the empty test section the maximum deflection does not exceed 2 cm into either chamber at the upstream test section region, and remains within approximately 1 cm at the downstream test section area. At no point during any of the testing runs were instabilities in the window or flapping observed, and there were no noticeable vibrations. This deflection profile is consistent with the air forcing the walls slightly outward at the inlet when the flow encounters the porosity difference of the new material, and a flow velocity that may still be accelerating (not at full test section speed) out of the contraction. In contrast at the downstream end of the test section, the windows are pulled in toward the test section as the airflow that exited the upstream section must come back in for mass to be conserved, and the continued growth of the boundary layer has increased the local flow velocity. Using the displacement thickness values that were determined during the boundary layer measurements for the inlet and exit of the test section the effective test section area was calculated for the nominal flow speed of 30 ms/s. At the inlet the effective area is 3.394 square meters while at the exit the area is reduced to 3.345 square meters. This gives an area ratio of 1.0145, and a corresponding velocity gradient of 1.45% along the length of the empty test section. This increase in the flow speed at the exit is the most likely cause for the window deflection into the empty test section.

The amount of window deflection with the NACA 0012 model installed was determined in the same manner as previously discussed for the empty test section. Deflection profiles were taken at nominal speeds of 30 m/s for both the pressure and suction windows. After the zero flow baseline was removed from the measured data, contour plots were generated to show pictorially the absolute deflection of the window. These plots utilize a cubic spline interpolation method, with approximately 20 points across the data set.

Figure 4-55 shows the deflection profile for the model at a 0 degree angle of attack at a nominal speed of 30 m/s. The deflection contour is similar in appearance to that of the empty test section. At the upstream end of the model, the window displaces outward into the chambers as the pressure in the test section is higher than that in the chambers. This increase in pressure could be a result of blockage in the test section due to the presence of the model increasing the fan requirements. As the airflow moves

around the model it must accelerate slightly, creating a lower pressure region, thus the window displaces into the test section. Since the NACA 0012 is a symmetric airfoil, at 0 degrees angle of attack, both the pressure and suction side windows are experiencing similar pressure differences. These values are larger than for the empty test section due to small pressure variation generated by the airfoil blockage in the test section.

Looking at the case of the 8 degree angle of attack (figure 4-56), the pressure and suction sides of the window continues to displace into their respective chambers at the farthest location upstream from the model. As the flow approaches the airfoil on the pressure side window, the deflection of the window is the largest upstream and over the leading edge of the model. The region immediately adjacent to the leading edge, where the majority of the lift is being generated, has deflection values on the pressure window of approximately 4 cm, which is still quite small relative to the almost 500 cm length of the window. The flow then begins to increase in velocity around the trailing edge of the model due to some blockage effects resulting from the angle of attack. This increase in velocity reduces the pressure and actually reduces the windows displacement into the pressure chamber to about 3 cm, eventually returning to zero deflection at the test section exit.

On the suction side of the window, much the opposite occurs. The flow displaces into the test section as the flow increases velocity around the leading edge, and the suction window displacement increases to a maximum of 4 cm into the test section at the trailing edge of the model. Additional data was compiled for the midline of the window, at a distance 0.927 m above the test section floor. Here 15 discrete points were measured to attempt to explain the behavior of the two dimensional plots above. Figure 4-57 shows the displacement for each window along the midline for the airfoil at 8 degrees effective angle of attack. In this figure, the blue lines correspond to the edges of the test section solid walls, and the yellow line depicts a nominal zero line for the Kevlar window. An approximate placement of the model is also given. Data above the zero line for the suction window and below the zero line for the pressure window is displacement into the anechoic chambers. Another concern regarding the window performance was the effect of the chamber seal on the overall system. To test this concept, a window deflection measurement was taken with the chamber doors wide open, to compare to the previous

measurement. Figure 4-58 has a comparison of the window deflection data for the NACA 0012 model at an 8 degree effective angle of attack. Two data sets were compiled for this plot; red triangles signify the chamber doors were left ajar, and blue circles signify that the system was completely sealed. The variation in the magnitude of the deflection is on the order of 1 cm. Figure 4-59, is a scaled version of the same data showing the model at the 10.4 degree geometric angle of attack, necessary to obtain an effective angle of attack of 8 degrees. Additionally included with this figure is some of the relevant test section geometry. On this large scale the doors appear to make no difference to the overall deflection of the window. This plot also shows the deflection at the leading edge towards the model on the suction window and away from the model on the pressure window. This is consistent with theoretical predictions for a symmetric model at angle of attack. When the flow reaches the ¾ chord location on the pressure side of the model, the effect of the model blockage becomes evident, and the window displaces back into the test section. On the suction side of the airfoil, the flow begins to decelerate and the suction window displacement levels off.

Additional measurements with models of varying thickness and camber could be examined in future testing to further characterize this blockage effect. For both sides of the test section there is an increase in the magnitude of the deflection as the angle of attack is increased, but the overall deflection for both windows is minimal compared to the scale of the tunnel. Generally, the Kevlar performed well over a large range of test conditions and model configurations. There was slight deflection at the inlet and exit sections of the window, but this appeared consistent with mass conservation within the chambers. Deflection of the windows with the model installed was consistent with pressure distributions measured over the model surface. Negligible vibration of the window was observed except with the model at very high angles of attack, and then the amplitude was less than a 10^{th} of the mean deflection.

4.6.2 Pressure Distribution on Acoustic Windows

A slider rail with five Pitot static probes (described in chapter 2) was designed to aid in the collection of pressure data along the length of the interior test section window. This system was designed to enable measurement of the static pressure coefficient at

various positions along the inside of the Kevlar window. These static pressure coefficients, combined with the pressures that were measured in each of the anechoic chambers for a given run, were used to compute the pressure difference across the window. Static pressure coefficients were measured in each chamber using $1/8^{th}$ inch Tygon tubing that extended through a small hole cut into the sides of each chamber. Two pressure differences were measured in each chamber for each test point; the chamber pressure – atmospheric pressure, and the chamber pressure – reference static pressure. These pressure differences and the reference dynamic pressure in the test section could be used to determine a static pressure coefficient for each chamber. The difference in the static pressure coefficient measured on the inside of the test section (rail measurement corrected for the straight probe effect) and the static pressure coefficient in the chamber was used as the pressure difference across the window.

$$\Delta C_p\Big|_{window} = C_p\Big|_{window} - C_p\Big|_{chamber} \qquad \textbf{(10)}$$

Static pressure coefficients were measured at eight stream wise positions along the window, and at three window heights (0.343 m, 0.953 m, and 1.359 m above test section floor) for nominal tunnel speeds of 30 and 50m/s. The probes were positioned approximately 0.1 ± 0.01 m off of the window to prevent any possible vibrations of the probes from damaging the Kevlar. The distance of the probe tip from the window would vary by about 0.01 m along the length of the window. This was attributed to the approximately 0.03 m deflection of the beam at the midpoint where the two aluminum extrusions met. No vibration of the beam was observed at any time during testing. Using the same interpolation method as the deflection measurements, contour plots of the pressure difference along the window were created for the empty test section and shown in figures 4-60 and 4-61 for 30 m/s and 50 m/s respectively. These plots show static pressure coefficient variations over the window to be small for the empty test section. There is some pressure variation along the length of the window that is most likely a result of the boundary layer growth, and/or interaction of the flow with the leading and trailing edge regions of the window (see calibration discussion chapter 2). The slightly

positive static pressure coefficient at the inlet is consistent with the deflection pattern seen in the previous section. The locally higher pressures in the test section cause the flow to move outward into the chambers, which is shown as a slight bowing outward of the windows. Flow patterns along the majority of the test section show the increase in the flow velocity generates a lower pressure along the inside of the window, which returns very near to zero at the test section exit. Had window pressure measurements been taken for the suction side window, a similar pattern would have been observed confirming the deflection profiles and that mass is conserved within the system. Overall the variation in the static pressure coefficient difference across the window is ± 0.05 at the extreme.

With the NACA 0012 model installed the same pressure side window measurements were repeated with the airfoil at 0 and 8 degrees effective angles of attack. Using the same interpolation method as the deflection measurements, contour plots of the pressure difference along the window were created and shown in figures 4-62 and 4-63 at a nominal speed of 30 m/s for effective angles of attack of 0 and 8 degrees effective.

With the model mounted at 0 degrees angle of attack, there is very little pressure variation along the length of the test section, which is consistent with the small pressure window displacement measured. The slightly negative value of the static pressure coefficient is most likely due to the slight velocity acceleration around the airfoil. There will also be some boundary layer growth that will reduce the effective area at the test section exit. This will generate a velocity gradient along the length of the test section, which will lower the pressure along the interior of the windows. Overall the static pressure coefficient was less -0.05 along the length of the window.

With the NACA 0012 model mounted at an 8 degrees effective angle of attack (figure 4-63) the largest static pressure coefficient was just downstream of the airfoil trailing edge. This value was measured on the wall to be approximately -0.19. For a model at this angle of attack the blockage in the tunnel will be larger (compared with a 0 degree angle of attack) and consequently the growth of the boundary layer will be greater as well. Comparison of the displacement thickness along the pressure and suction window with the model at 8 degrees shows a pressure window displacement thickness that is a little more than three times smaller than that of the suction window (table 4-4).

Therefore the majority of the flow acceleration due to boundary layer growth is occurring on the suction side of the airfoil, which is reflected in the positive pressure coefficient along the suction window, until the downstream edge of the test section. The relative magnitudes and window areas covered by both positive and negative pressure coefficients present a good indication that mass is conserved. Both the 0 and 8 degree angle of attack contours show relatively little variation in the vertical direction, which would confirm the belief that the flow is mostly uniform along the height of the test section, and that the assumption of two dimensional flows over the airfoil is appropriate.

At the conclusion of the experimental measurement of the pressure variation across the windows along the length of the test section, a panel method was developed to both compare the model pressure distributions to a two dimensional theoretical profile (similar to the comparison used for determining the interference correction) and to examine the effect of the window deflection on the model pressure distributions, and the pressure variation along the window for various sized models. This comparison will be presented in section 4.7

4.7 Comparison with the Panel Method

With the ability to experimentally establish a repeatable lift interference correction for multiple airfoils of varying profiles, it was desirable to determine a prediction method for modeling the airfoil in a porous wall tunnel. This prediction code would allow the user to view the pressure distributions along the length of the window, and predict what effect other models might have on the interference correction. The following subsections present the details on the modified panel method, and the results of test cases run on several airfoil sections.

4.7.1 Modified Panel Method

The panel method designed to examine the effects of the interference correction and the wall deflection originated from a combination of a linear source panel code and linear vortex panel code written for a graduate Aerospace Engineering course (AOE 5104 Advanced Aero and Hydrodynamics). Many iterations of this code have been used successfully in other cases to model various other flow phenomena (see Glegg *et.al*

(2006) for one example) and the individual versions of each code were used extensively in the graduate course. The challenge in developing a code for this study was determining an appropriate way to model the walls of the wind tunnel; these walls are not only porous, but flexible, with their shape varying with the type and angle of attack of the model. This code was developed by W. Devenport for use as an early indicator of the possible interference correction range for the anechoic tunnel.

The original porous wall tunnel code developed by W. Devenport used linearly varying source panels to define the walls of the tunnel. The porous wall condition was determined using a low Reynolds number model (G.I Taylor) which gives the flow rate through a surface at low Reynolds number as:

$$v_i = \frac{R_p \left(P_i - P_a \right)}{\mu} \tag{11}$$

where R_p is the inverse of a resistance coefficient, μ is the viscosity, and P_i and P_a are the pressures at the panel on the window interior, and the ambient respectively. The advantage of this formulation is that the velocity is linear in the pressure coefficient and, since the pressure coefficient can be linearized this entire boundary condition can be linearized and solved as part of the matrix solution of the panel method, with no need for iteration. Note that this type of approach is also used by Ulbrich (2000) and Keller (1972). This flow rate was incorporated into the source panel code as a boundary condition, and tested using a cylinder model placed in the center of the test section. The value of R_p will later be optimized to confirm the experimentally determined interference correction for the NACA 0012 model at an 8 degree effective angle of attack.

The method as presented so far does not incorporate the requirement that there be no net mass flow into the test section. This can be accomplished by adding the pressure outside the porous surface as an unknown and adding a column to the coefficient matrix representing the condition that that pressure be set so that the net mass flux is zero. The code was then modified to generalize this method for porous walls on either side and on both sides. In this latter case the option of balancing the mass flow on both sides together (i.e. the sides are linked by a flow outside the test section) and separately (sides are backed by separately sealed chambers. The ability to restrict the mass flow

conservation to the system as a whole, or to within each chamber separately will allow for direct comparison to the experimental wall pressure data.

The next step was to combine the current porous wall code with an incompressible ideal flow linear vortex panel method that could model an airfoil, specifically the NACA 0012. In such a method the airfoil surface may be considered to be wrapped in a vortex sheet of continuously varying strength. In the present implementation the vortex sheet is approximated by a series of straight panels each of linearly varying strength. The paneling, developed using a NACA 0012 section, consists of 200 panels that decrease linearly with edge length as the trailing and leading edges are approached. Paneling schemes for other thickness airfoils were generated simply by scaling the y coordinates for the NACA 0012. For steady flow calculations, panel strengths are determined by enforcing the non penetration condition (at control points at the center of each panel) and the Kutta condition (requiring that the vortex sheet strength at the trailing edge be zero).

The most fundamental change required in the merger of the two pieces of code was the simultaneous use of constant source panels for the tunnel walls, and linear vortex panels for the airfoil. This results in two different equations to calculated influence coefficients for the tunnel wall and airfoil parts of the paneling. With W. Devenport's prediction method working well to predict the pressure distribution both on an airfoil mounted in the tunnel and along the porous Kevlar windows, other modifications were considered.

The most fundamental difference between the panel method prediction programmed by W. Devenport, and what was observed during actual testing was the deflection of the Kevlar windows under load. As discussed in section 4.6.1, the deflection of the window was small and relatively evenly distributed under empty tunnel loading conditions, but took on a noticeable pattern with the model installed at angle of attack. Deflection measurements were taken at the mid height of the window at approximately 15 points along the stream wise length of the test section. These data points were then used to modify the current wall shape of the prediction code. The major coding change resulted in source panels along the wall that have defined endpoints (fixed length based on the measured data) instead of a 3/2 power rule to determine their

locations. While the power rule placed more panels of shorter length near the leading edge of the model, the deflection based source panels were defined based on the location where the data was measured. This modification results in less panels used to define the wall shape, but a far more accurate depiction of the actual pressure field along the tunnel walls.

The following section contains the experimental approach used to determine the interference correction on several airfoils, and the application of the modified panel method developed by W. Devenport, with wall deflection modified by E. Crede to compare both the interference correction that was determined experimentally to that predicted by the code. In addition to the interference correction, an accurate model of the value for R_p was determined by comparing model pressure distributions for both measured and the two dimensional vortex panel method pressure distributions. For the NACA 0012 at 8 degrees angle of attack, the measured pressure differences along the window were compared to those predicted by the panel code with modified wall shape.

4.7.2 Panel Method Results

The panel method described in the previous section was used to compare the measured pressure distribution along the window, to that predicted by the modified porous source panel walls. Measured data was acquired using the Pitot static probe rail system described in chapter 2, with the static pressure coefficients measured at eight stream wise positions along the window, and at three window heights (0.343 m, 0.953 m, and 1.359 m above test section floor). The probe tips were 0.1 m off the port side Kevlar window and data was taken for nominal tunnel speeds of 30 and 50m/s. Details on the window pressure distributions were given in section 4.6.2. The first comparison (figures 4-64 to 4-66) does not have the deflection of the windows included. Figure 4-64 and figure 4-65 show the port side wall pressure distribution with the 0.9144 m NACA 0012 model installed in the modified wall tunnel at 0 and 8 degrees angle of attack and a nominal flow speed of 30 m/s. Measured pressure distributions for the model at these configurations are given in section 4.4.1. For these test runs the wall interference correction was assumed to be that determined experimentally (-22%), and the porosity of the Kevlar windows has been calibrated based on a fixed porous boundary to be R_p =

1.24. These experimental window pressures have only been corrected for the straight Pitot static probe offset and all three window heights have been plotted against the panel method results. Note also that the "*x*" location plotted centered on the quarter chord, where negative values are upstream and positive downstream from the model. Figure 4-64 shows experimental static pressure coefficient values that follow a similar trend, but are lower along the length of the test section that those predicted by the panel method. This more negative pressure difference is presumably the result of the deflection of the windows upstream of the model, and the growth of the boundary layer along the length of the test section. Both of these aerodynamic phenomena will affect the velocity gradient that exists along the window walls, which the panel method doesn't yet account for.

Figure 4-65 is the port side wall pressure distribution for the model at the 8 degree effective angle of attack condition. The panel method shows fairly good agreement in the regions along the length of the model chord, but again is far greater in magnitude in areas upstream and downstream of the model. Similarly to the 0 degree angle of attack case, the deflection of the windows upstream and downstream of the model will influence the velocity gradient along the test section length (and consequently the static pressure coefficient). Finally figure 4-66 shows the panel method predicted stream line pattern for the NACA 0012 model at 8 degrees angle of attack and the fixed porous wall boundary condition.

The general trend in the static pressure coefficient is correctly predicted by the panel method for both of these cases. However there are some slight variations in the magnitude of the pressure gradient in the experimental data compared to the panel method results. The regions of the windows that are directly adjacent to the model show good agreement, suggesting that the general inputs in the panel method (porosity approximation) and boundary conditions are adequate. The areas upstream of the model, near the inlet, have pressures that are lower than those predicted by the panel method. This is suspected to be a result of the window deforming upstream of the model, a phenomenon that the panel method does not currently account for. The region of the window that is downstream of the model has flow speeds that are faster (lower pressures) than those predicted by the panel method as well. Wall deflection may also be a factor here, but additional boundary layer growth associated with the pressure gradients

imposed by the airfoil may also be to blame. The displacement thickness values measured with the airfoil suggest an additional acceleration of about 3% produced by this blockage which would result in a fall in the static pressure coefficient of about -0.06.

In order to determine the effects of the window deformation for the panel method comparison, midline window deflection data was taken for 3 models of varying size and thickness to compare with the results of the prediction code. One NACA 0015 and two NACA 0012 models were chosen; the 0.9144 m chord model that was used extensively for the other testing, a 0.2032 m chord NACA 0012, and a 0.6096 m chord NACA 0015. Wall deflection measurements were taken at mid height of the window at approximately 15 stream wise locations along the interior of each anechoic chamber with the model at an 8 degree effective angle of attack and a nominal flow speed of 30 m/s. This window deflection data, along with the measured pressure distribution for the 8 degree effective angle of attack (using the experimentally determined interference correction) was used in the modified panel method to compare the experimental and the predicted results. This data was taken in addition to the three dimensional window deflection characterization test points previously presented for the larger NACA 0012 for the overall deflection patterns of the Kevlar windows. The data that was used for the smaller (0.203 m chord) NACA 0012 and for the 0.610 m chord NACA 0015 is given in figure 4-67 and 4-68. Also shown in this figure is the relevant test section geometry. The blue lines represent the edges of the solid wall acoustic absorbers (no deflection possible here) and the yellow line simulates the undisturbed Kevlar window position. Note that the deflection for the 0.203 m chord NACA 0012 is less than 1 cm at 8 degrees effective angle of attack, while the NACA 0015 has significantly larger deflections at approximately 3 to 6 cm. The larger deflection of the NACA 0015 window is presumably do to reduced tensioning of the windows towards the end of the testing period.

For the 0.9144 m chord NACA 0012 model, the window deflection pattern for an 8 deg angle of attack was modeled in the prediction code, and the porosity coefficient (R_p) was adjusted until the measured pressure distribution matched the two dimensional theoretical pressure distribution. The porosity coefficient was confirmed using the measured NACA 0012 pressure distribution to be 1.24, and was assumed constant for the remaining test conditions. The streamline pattern, along with the pressure distribution

comparison, is shown in figure 4-69. This pressure distribution was generated using a 10.39 degree angle of attack for the theoretical comparison and with the model mounted at an 10.39 geometric angle of attack (corresponding to 8 degrees effective with the -22% correction). The predicted static pressure coefficient along the pressure side window is compared to the measured values for the three window heights in figure 4-70. Comparing this plot with figure 4-64, the predicted values are much closer to those that were with the correction of the porosity coefficient and the addition of the wall deformation. Additionally the predicted data shows a trend that more accurately depicts the measured window pressures. The measured static pressure coefficients at the test section exit are lower, presumably due to the growth of the boundary layer, and the resulting increase in local flow speeds. The prediction method does not currently account for the boundary layer growth along the length of the test section, but the code could be modified at a later date to allow for those effects. The region upstream of the predicted data has lower static pressure coefficients as well, and this could be a function of some residual acceleration from the contraction, or slight non uniformities in the flow. The variation in the static pressure coefficients for the three window positions at the most upstream location indicates that latter is correct. Finally using a cumulative trapezoidal rule, the cumulative mass flux as a function of test section flow is given in figure 4-71.

Next a similar set of plots was generated for the smaller chord NACA 0012 (0.2032 m chord). Using the measured wall deflection profile for the model at 8 degrees effective angle of attack, and the same porosity coefficient that was determined for the larger NACA 0012 the theoretical pressure distribution is compared to that measured (figure 4-72). In this figure the model was installed at an 10.39 geometric angle of attack (corresponding to 8 effective with a -22% correction) but the panel method shows the best fit for angle of attack is 8.4 degrees. This gives a panel method prediction of the lift interference correction of -4.5%. The model has very little effect on the facility, which is consistent with the smaller chord and significantly lower window deflection magnitude. The cause of the discrepancy between the panel method and measured interference correction is believed at this stage to be the result of uncertainty in the setting of the angle of attack. The pressure coefficient predicted by the panel method on the pressure wall is shown in figure 4-73. This predicted data follows closely to that predicted (and

measured) for the 0.9144 m chord NACA 0012, with the exception that the magnitude of the static pressure coefficient is lower, which is consistent with a model of smaller size. Finally the cumulative mass flux is plotted for the 0.2032 m chord NACA 0012 in figure 4-74.

Lastly a similar set of plots was generated for the 0.6096 m chord NACA 0015. Using the measured wall deflection profile for the model at 8 degrees effective angle of attack, and the same porosity coefficient that was determined for the larger NACA 0012 the theoretical pressure distribution is compared to that measured (figure 4-75). This figure shows a measured pressure distribution that matches the theoretical for a panel method angle of attack of 9 degrees. This corresponds to a lift interference correction of approximately -11.2%. The overall magnitude of the wall deflection for this case was significantly larger than for the other models. The NACA 0015 model was the final model tested after almost 3 months of running the tunnel in excess of 18 hours a day. This resulted in lower Kevlar window tension for the final model which is most likely the cause of the larger window deflections. Furthermore, uncertainty in the angle of attack setting is also believed to have contributed to the experimental interference correction. Observations made during the 2006 testing showed that pressure variations along the window were larger when the windows were unable to be fully tensioned. Comparison with the 2007 data confirmed the smaller variations in static pressure coefficient when the window tension was increased. The larger static pressure coefficient magnitude of the 2007 NACA 0015 data is presumably due in part to this decrease in window tension. Finally the cumulative mass flux is plotted for the 0.6096 m chord NACA 0015 in figure 4-76.

Overall this prediction method serves to validate the experimental data for the 0.914 m chord NACA 0012 model. In addition two separate data sets of models of varying chord and thickness were shown using the same porosity assumptions. Lift interference correction values were able to be determined using the information about the wall shape and mean pressure data for each model. Future modifications to this prediction method would allow

The experimentally determined interference correction is plotted against several other values for lift interference corrections for a model of this size in a free jet, of -50%

(computed from the method of Brooks et al.) or -73% (computed using the method of Barlow et al.). This is shown graphically in figure 4-77. Free Flight is plotted with a line at a 45 degree angle, or the geometric angle equal to the effective angle of attack. These models that are used to show the interference correction for this tunnel are of varying degrees of thickness and camber, and data was taken over a wide range of geometric and effective angles of attack. The slope of each of these lines represents the lift interference, and as can be seen from this figure, the Kevlar windows serve to reduce the aerodynamic losses that are generally present in a free jet, with an interference correction that is half of that determined for an open jet wind tunnel.

Virginia Tech Anechoic Facility

Stability Tunnel

Description	the tunnel is a continuous, closed jet, single return subsonic wind tunnel with a 7.32 m long interchangeable test section
Power	600 H.P DC Electric Motor driving a 4.27 m propeller
Test Section	1.83 m square test solid wall aerodynamic removeable test section
Speed Range	0-80 m/s with Reynolds numbers to 5 million per meter
Turbulence Levels	0.024% and 0.031% at 30 and 57 m/s respectively
Acoustic Treatment	223 square meters of Urethane and Melamine Foam around the circuit, in addition to a hand cut Melamine fan liner and turning vane treatment

Acoustic Test Section

Description	The anechoic test section features a tensioned Kevlar side wall that is acoustically open and aerodynamically closed. This configuration allows for efficient aerodynamic measurements as well as far field acoustic measurements in a low background noise environment
Dimensions	7.32 m long and 1.83 m square removeable test section. Pure Kevlar window length is 5.13 m
Speed Range	0-80 m/s with Reynolds numbers to 5 million per meter
Acoustic Treatment	steel panel cutouts padded with fiberglass and melamine foam were covered with tensioned Kevlar. These form acoustic absorbers on each side of the test section, on upstream and downstream ends (4 total)
Window Material	Kevlar 120 tensioned to 0.5 tonne per linear meter
Window Frames	ENCO Large Roller Chase Frames, with 4.950 x 2.489 m outer dimensions
Floor and Ceiling	steel perforate covered in tensioned Kevlar 120 cloth. Acoustic treatment under the panels are 0.457 m acoustic wedges with frequency attenuation to 100 Hz
Window Restraint	1 in x 1 in x 0.25 in Neodymium Magnets
Model Mount	aluminum mounting panel with exterior mounted rotation system to secure full test section span, 0.089 m diameter spar models vertically.

Acoustic Chambers

Description	Two anechoic chambers were designed to enclose the modified test section. Each chamber consists of a steel and MDF exterior structure enclosing an arrangement of acoustic wedges, and is assembled in two parts.
Dimensions	the full width and height of the assembled facility measure 8.255 m and 6.096 m respectively, and is mounted on two 2 m steel platforms
Acoustic Treatment	0.46-m high acoustic foam wedges measuring 0.31×0.62m at the base, were arranged in a checkerboard pattern. These wedges have a low frequency attenuation to140 Hz
Background Noise Levels	Measured Sound Pressure Levels are some 25 dB below those in the hard wall configuration

Table 4-1. List of the 2007 Anechoic Facility Characteristics, including modifications made during the final calibration in 2007

Test Point	Flow Speed	Tunnel Conditions
1	11.577	Anechoic 2007, Completed circuit treatment
2	22.099	Anechoic 2007, Completed circuit treatment
3	31.253	Anechoic 2007, Completed circuit treatment
4	42.335	Anechoic 2007, Completed circuit treatment
5	51.584	Anechoic 2007, Completed circuit treatment
6	58.434	Anechoic 2007, Completed circuit treatment
7	11.504	Anechoic 2006, no circuit treatment
8	22.028	Anechoic 2006, no circuit treatment
9	31.232	Anechoic 2006, no circuit treatment
10	42.452	Anechoic 2006, no circuit treatment
11	51.458	Anechoic 2006, no circuit treatment
12	10.681	Hard Wall- treatment on walls of settling chamber and fan liner
13	20.486	Hard Wall- treatment on walls of settling chamber and fan liner
14	31.125	Hard Wall- treatment on walls of settling chamber and fan liner
15	41.421	Hard Wall- treatment on walls of settling chamber and fan liner
16	52.096	Hard Wall- treatment on walls of settling chamber and fan liner
17	61.844	Hard Wall- treatment on walls of settling chamber and fan liner
18	72.362	Hard Wall- treatment on walls of settling chamber and fan liner
19	10.708	Hard Wall - diffuser baseline
20	20.419	Hard Wall - diffuser baseline
21	30.166	Hard Wall - diffuser baseline
22	40.302	Hard Wall - diffuser baseline
23	50.795	Hard Wall - diffuser baseline
24	60.191	Hard Wall - diffuser baseline
25	70.196	Hard Wall - diffuser baseline
26	10.833	Hard Wall-complete fan liner, settling chamber and Large Wall
27	20.672	Hard Wall-complete fan liner, settling chamber and Large Wall
28	31.272	Hard Wall-complete fan liner, settling chamber and Large Wall
29	41.436	Hard Wall-complete fan liner, settling chamber and Large Wall
30	51.447	Hard Wall-complete fan liner, settling chamber and Large Wall
31	61.706	Hard Wall-complete fan liner, settling chamber and Large Wall
32	72.033	Hard Wall-complete fan liner, settling chamber and Large Wall

Table 4-2. Complete list of all microphone measurements made during the final calibration in 2007

Location	*X* Location (m)	Velocity (m/s)	δ (mm)	δ* (mm)	θ (mm)
Inlet Floor	0.813	27.301	54.10	6.70	4.53
Inlet Ceiling	0.813	29.395	49.02	6.82	4.52
Inlet Starboard Wall	0.813	28.096	49.02	5.27	3.66
Inlet Port Wall	0.813	28.725	52.00	5.25	3.43
Downstream Floor	6.121	30.499	110.00	12.35	8.36
Downstream Floor	6.121	49.452	118.00	19.19	12.34
Downstream Ceiling	6.121	30.003	107.00	13.06	9.19
Downstream Ceiling	6.121	48.696	122.90	16.92	12.82
Downstream Starboard Wall	6.121	29.551	102.10	12.63	8.87
Downstream Starboard Wall	6.121	49.372	106.20	15.45	9.95
Downstream Port Wall	6.121	29.832	112.00	12.34	8.46
Downstream Port Wall	6.121	49.256	123.00	16.45	11.50
NACA 0012 at 0 AOA Port Wall	6.121	28.987	133.60	30.24	14.54
NACA 0012 at 8 AOA Port Wall	6.121	28.106	210.80	21.28	13.58
NACA 0012 at 0 AOA Starboard Wall	6.121	29.295	130.20	23.55	14.53
NACA 0012 at 8 AOA Starboard Wall	6.121	28.068	212.25	58.63	44.11

Table 4-3. Boundary layer measurements that were made during the 2007 calibration along with the measured thickness, displacement thickness and momentum thickness. *X* Location is referenced to the test section entrance at the contraction.

Figure 4-1. Melamine Foam (51 mm thick) lining the port side wall of the diffuser section of the wind tunnel circuit.

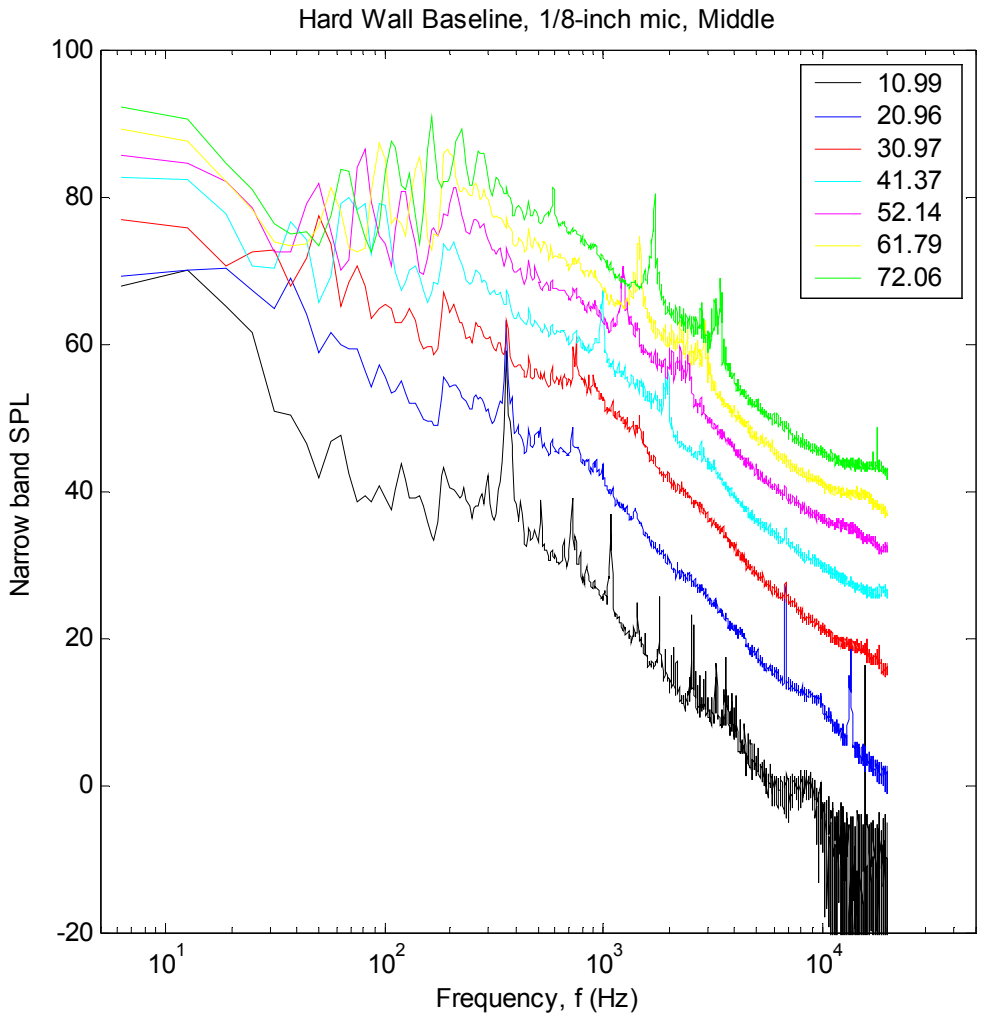

Figure 4-2. Diagram of the spectra plots for the hard wall configuration at the start of the treatment process. Hard Wall Baseline is also denoted by diffuser treatment since a test case in the diffuser was covered at this time

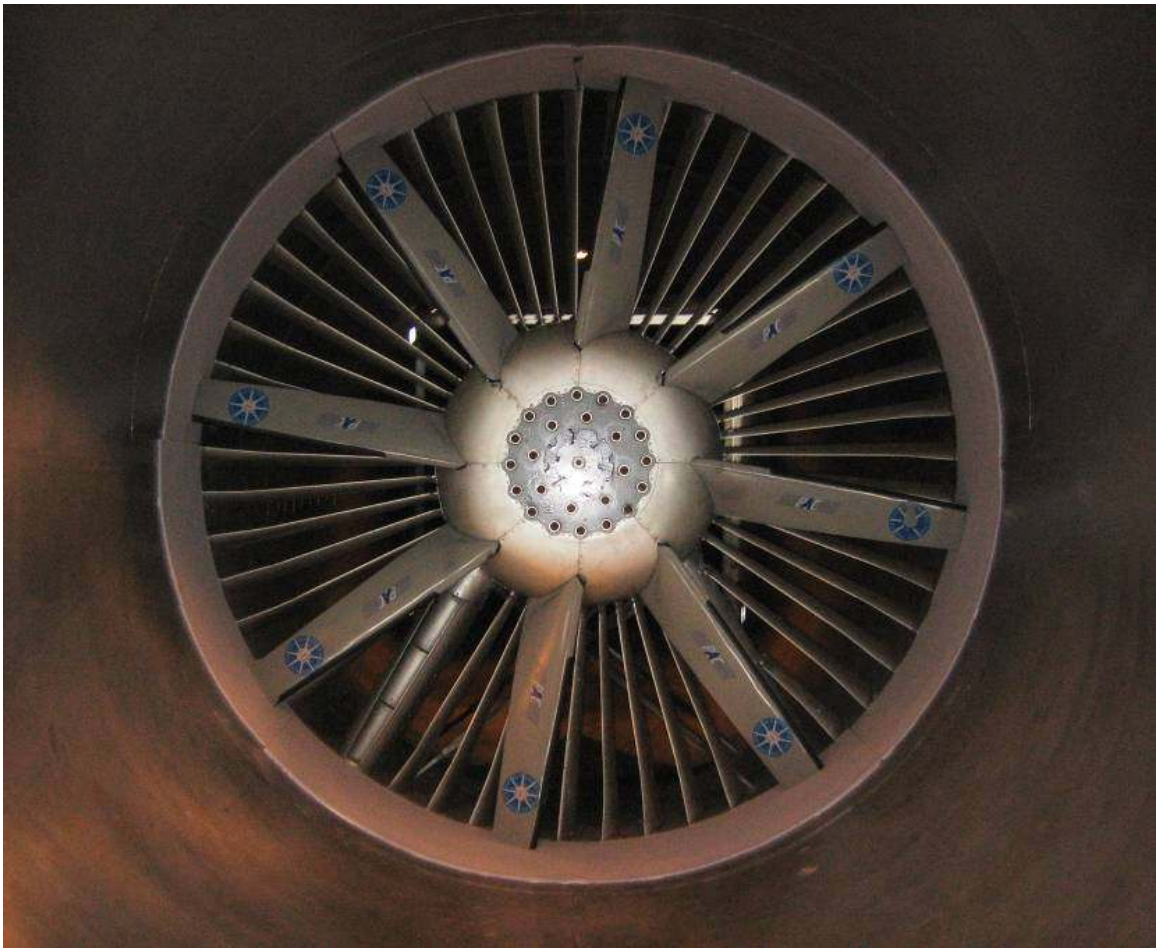

Figure 4-3. Melamine Foam (~19 mm) lining the 0.762 m width around the circumference of the fan blades.

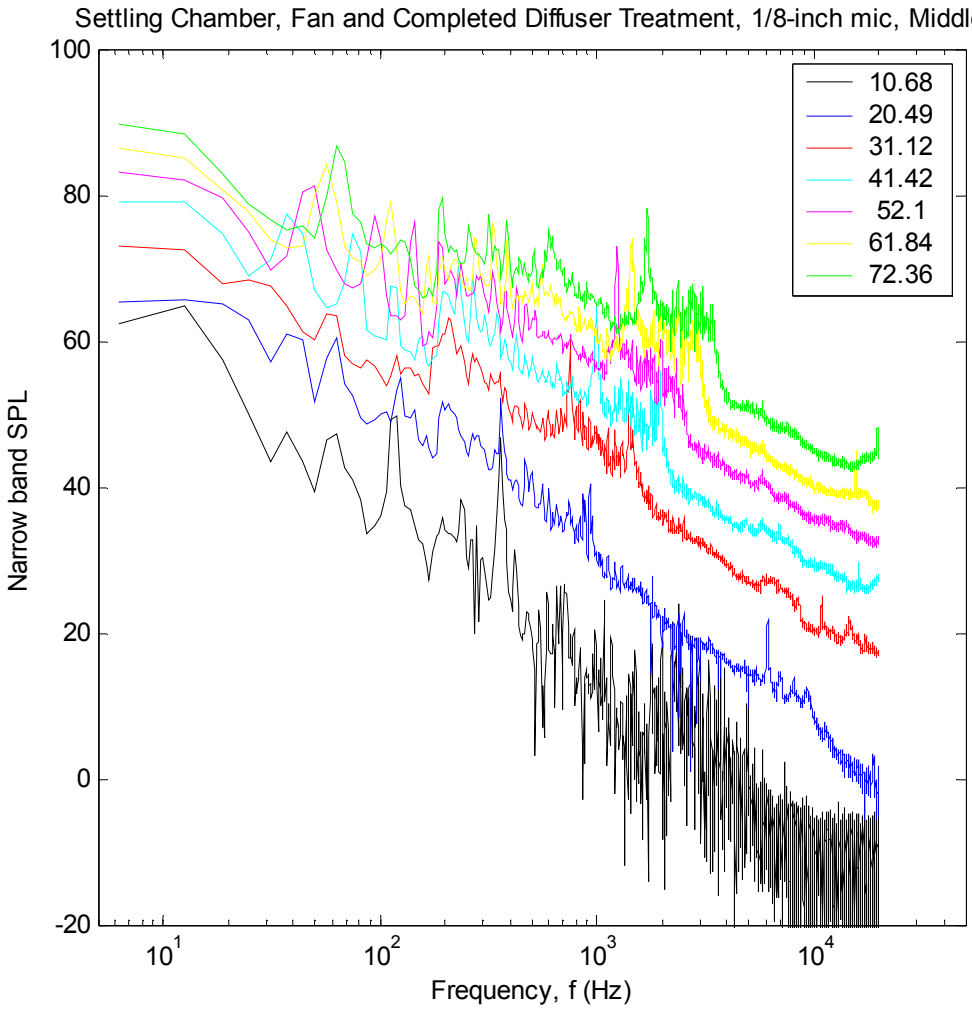

Figure 4-4. Diagram of the spectra plots for the hard wall configuration after the fan liner was added and the settling chamber was complete.

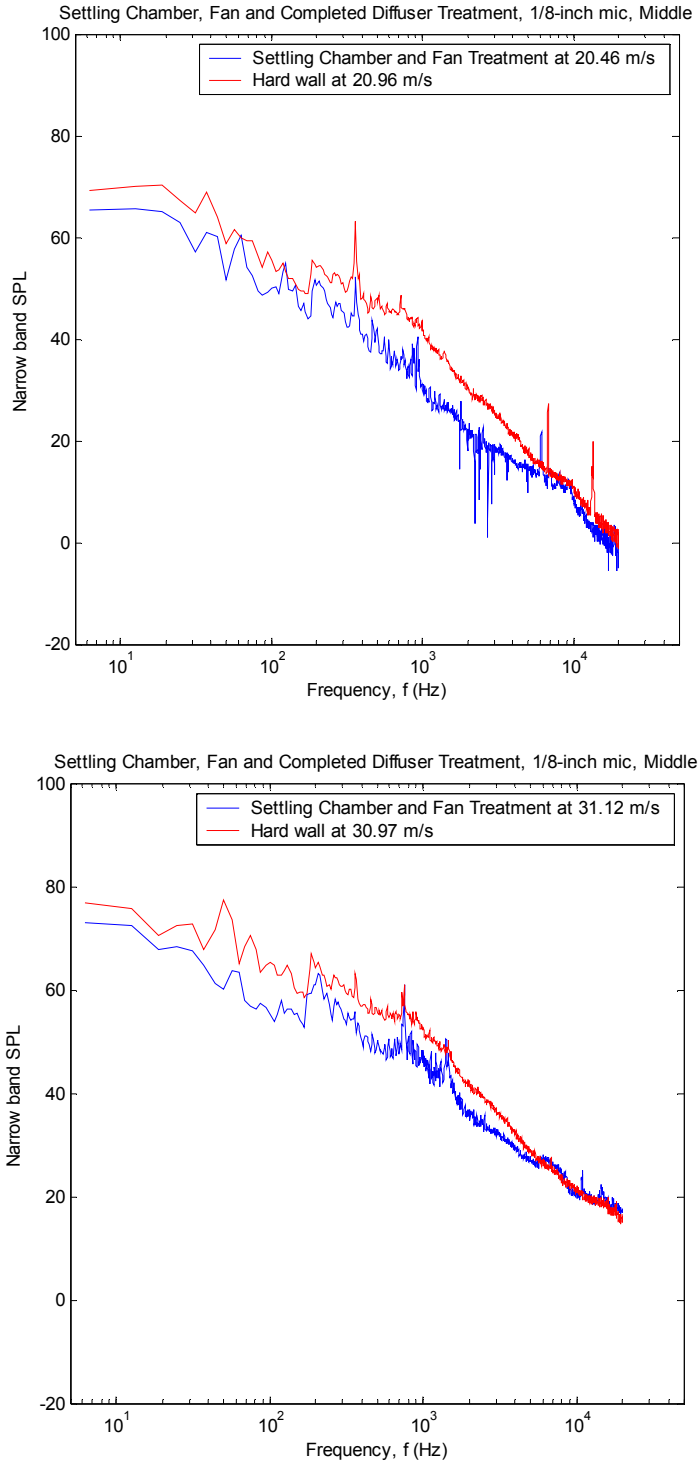

Figure 4-5. Diagram of the spectra plots after the fan liner was added and the settling chamber was complete, compared to the original hard wall configuration. Comparison speed is 20.48 m/s (top) and 30.12 m/s (bottom)

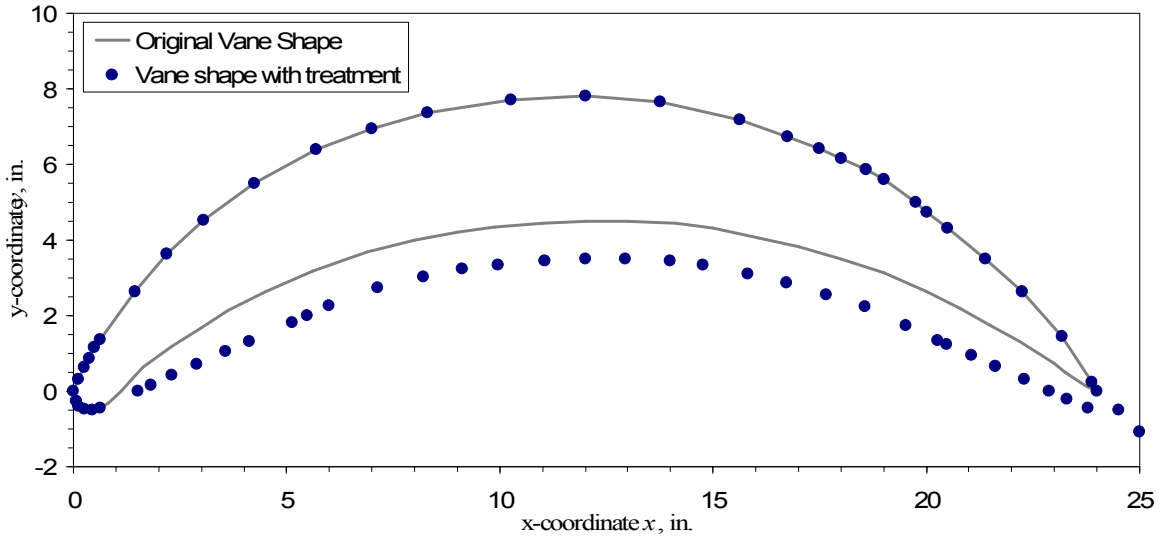

Figure 4-6. Comparison of vane shape with and without treatment (Top). Melamine Foam (1 inch thick) lining the Northeast turning vanes (Bottom).

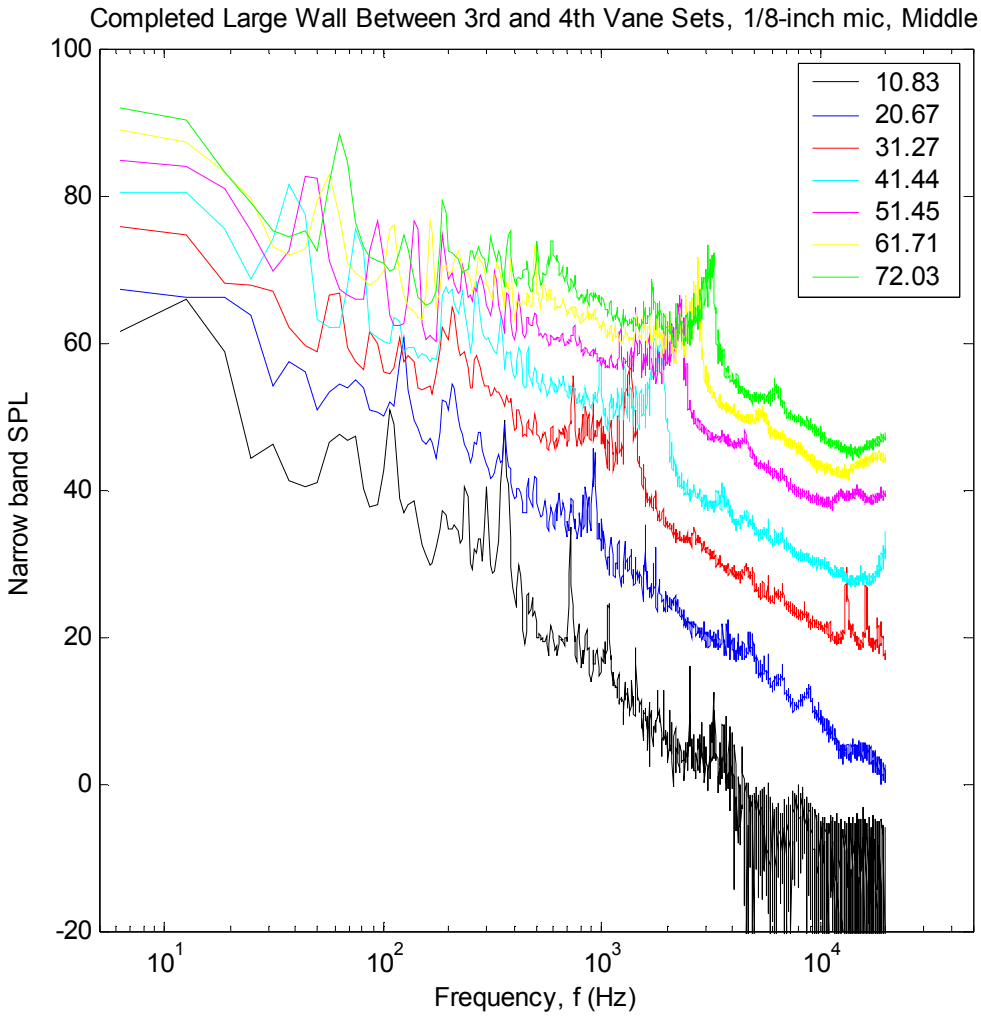

Figure 4-7. Diagram of the spectra plots for the hard wall configuration after the wall area between the 3rd and 4th vanes sets was completed.

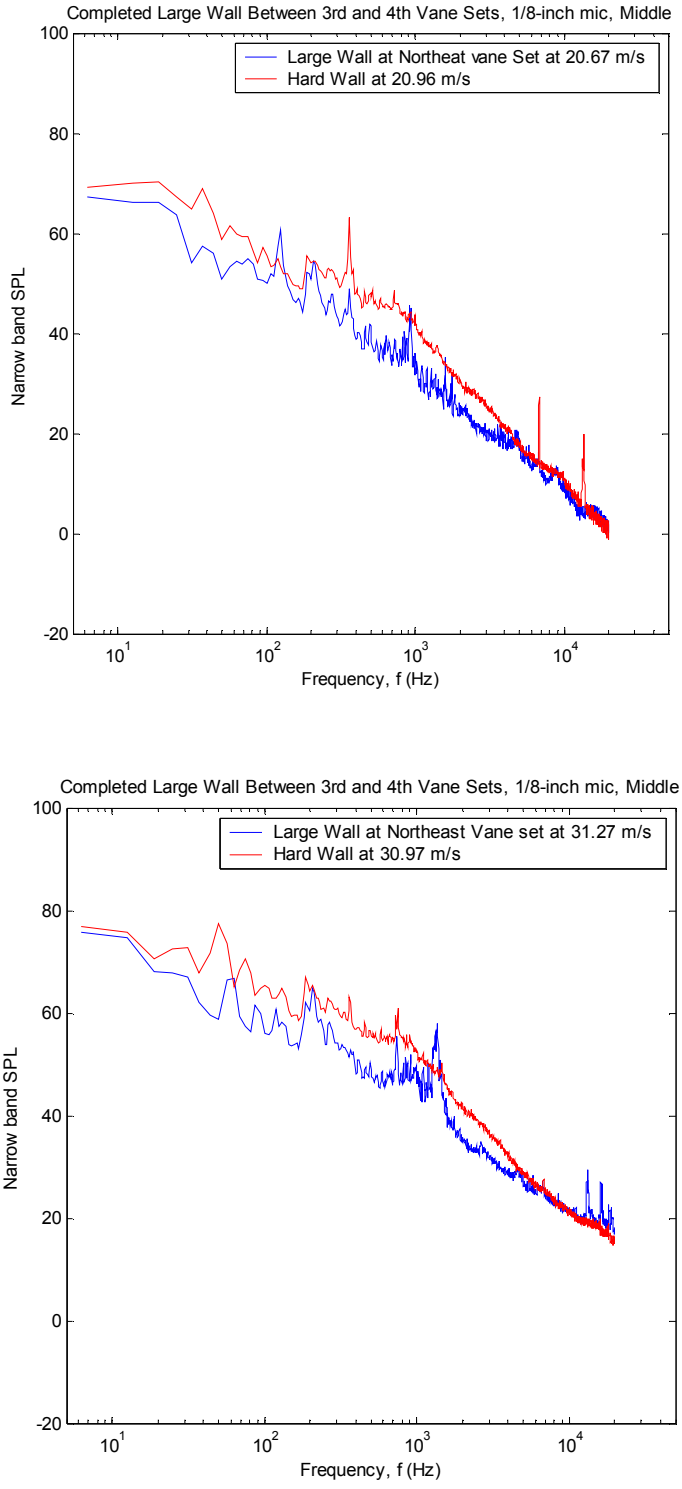

Figure 4-8. Diagram of the spectra plots after area between the 3rd and 4th vane sets was completed, compared to the original hard wall configuration. Comparison speed is 20.67 m/s (top) and 30.27 m/s (bottom)

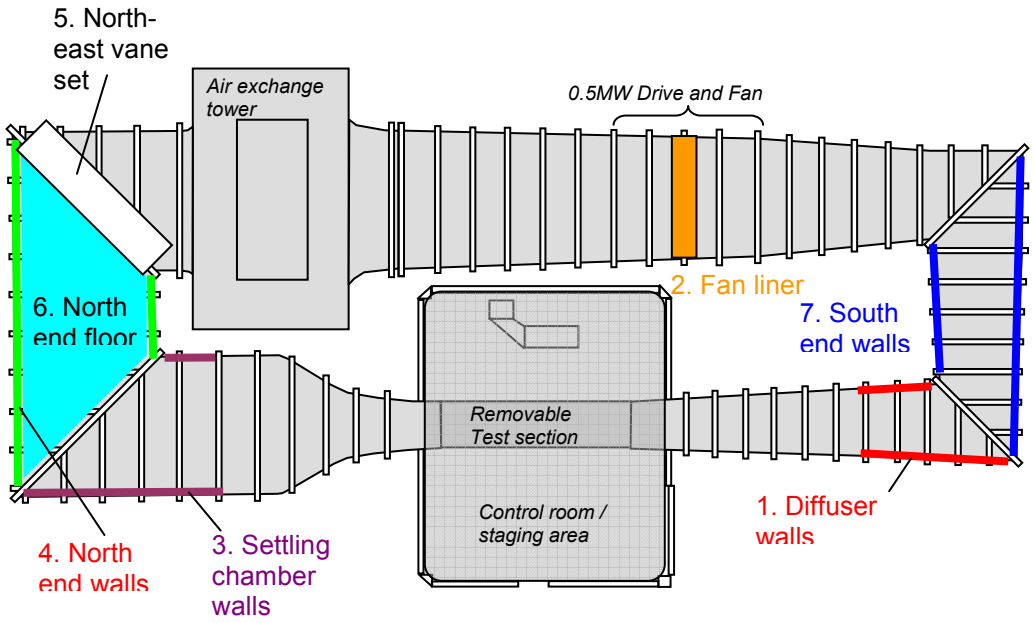

1. 28m^2 of 50.8mm Melamine foam
2. Variable thickness Melamine fan liner
3. 56m^2 of 50.8mm Urethane foam
4. 74m^2 of 50.8mm Urethane foam
5. Aerodynamic contoured turning vane treatment (Melamine)
6. 37m^2 of 50.8 mm Urethane foam
7. 28m^2 of 50.8mm Urethane foam

Figure 4-9. Complete diagram of all of the acoustic treatment stages for the wind tunnel.

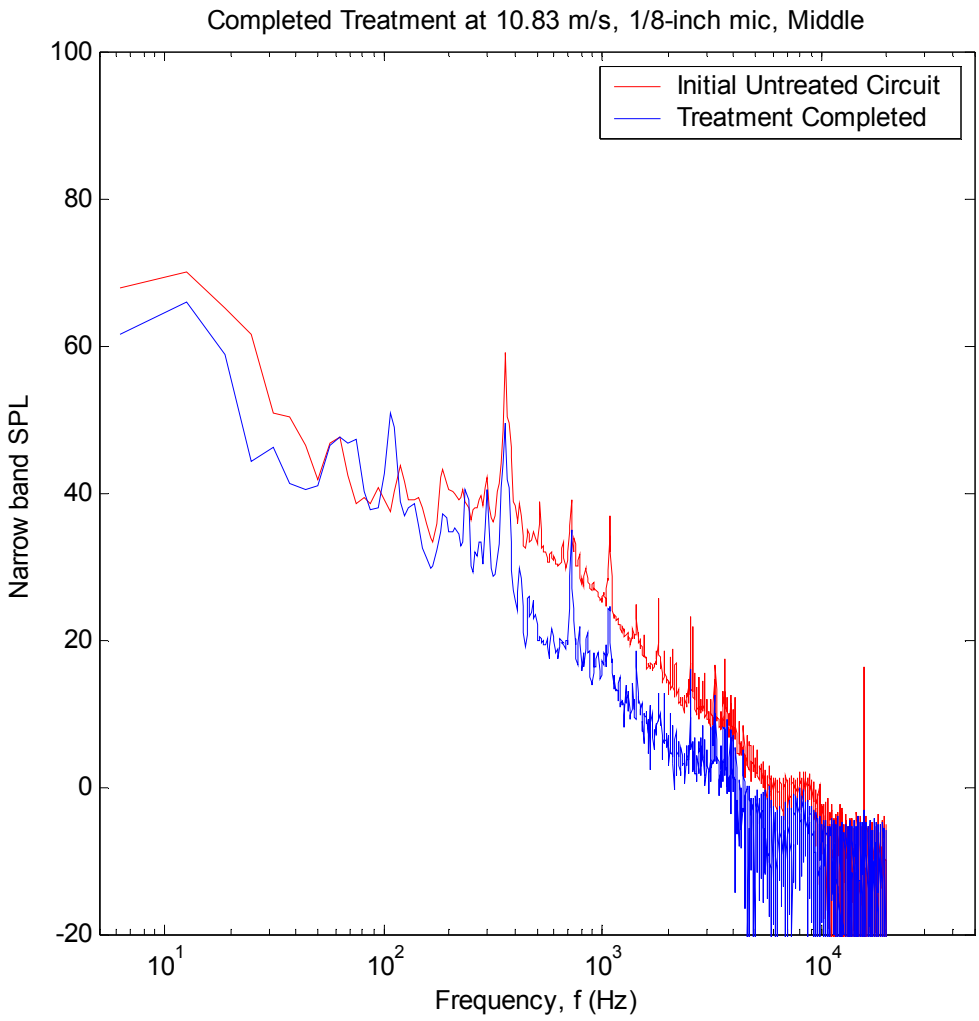

Figure 4-10. Comparison of the final treatment against the original untreated circuit at a nominal speed of 10 m/s

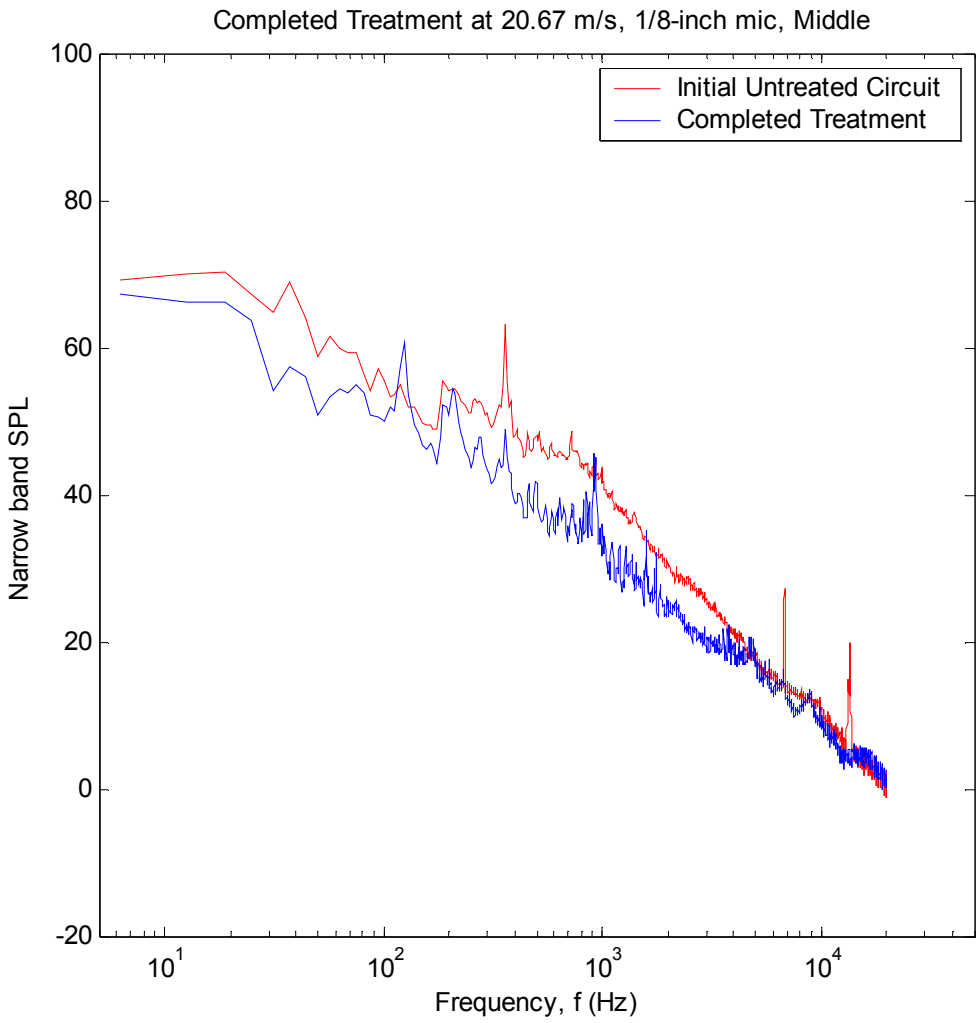

Figure 4-11. Comparison of the final treatment against the original untreated circuit at a nominal speed of 20 m/s

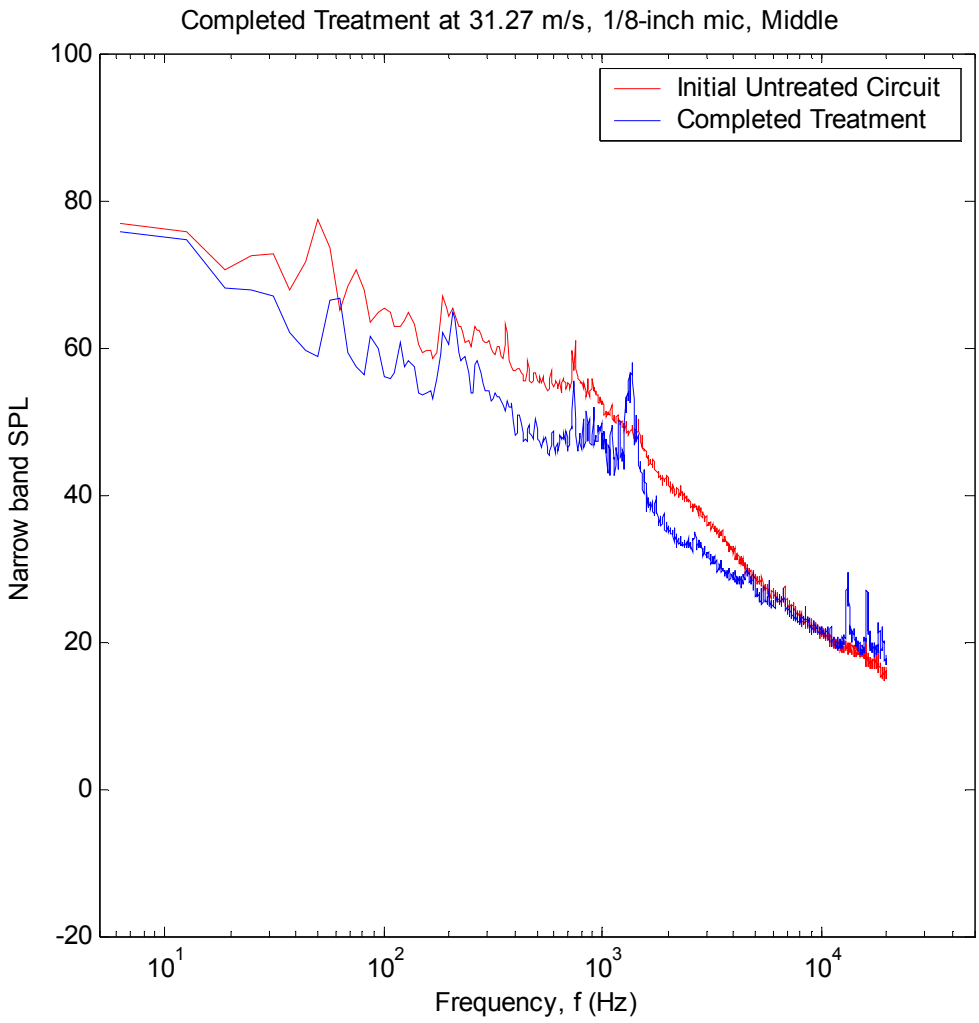

Figure 4-12. Comparison of the final treatment against the original untreated circuit at a nominal speed of 31 m/s

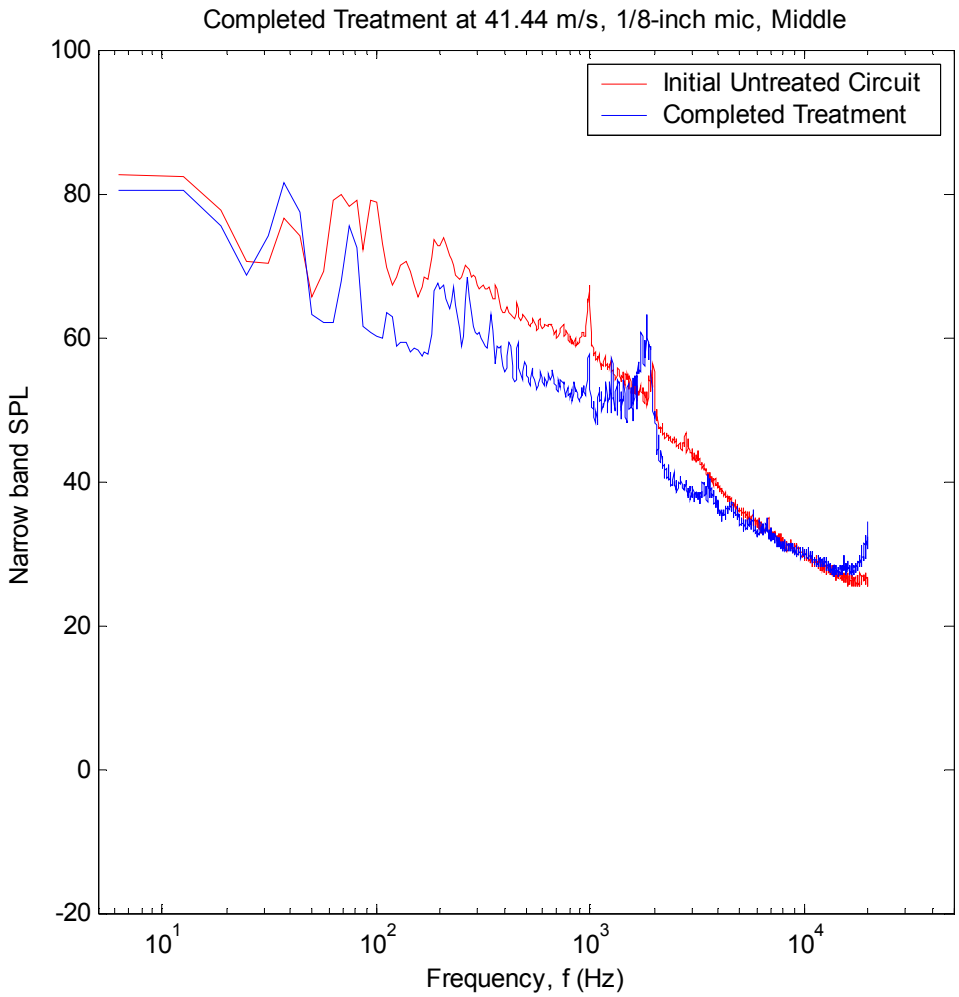

Figure 4-13. Comparison of the final treatment against the original untreated circuit at a nominal speed of 41 m/s

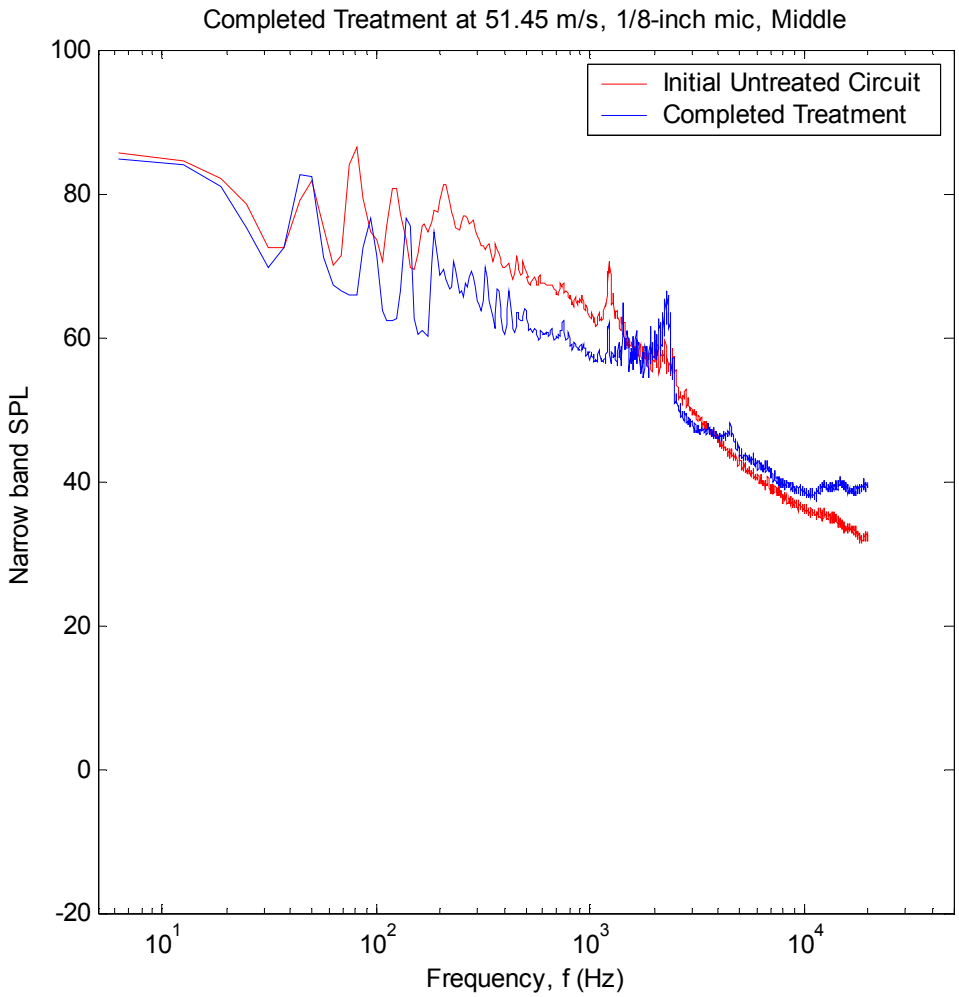

Figure 4-14. Comparison of the final treatment against the original untreated circuit at a nominal speed of 51 m/s

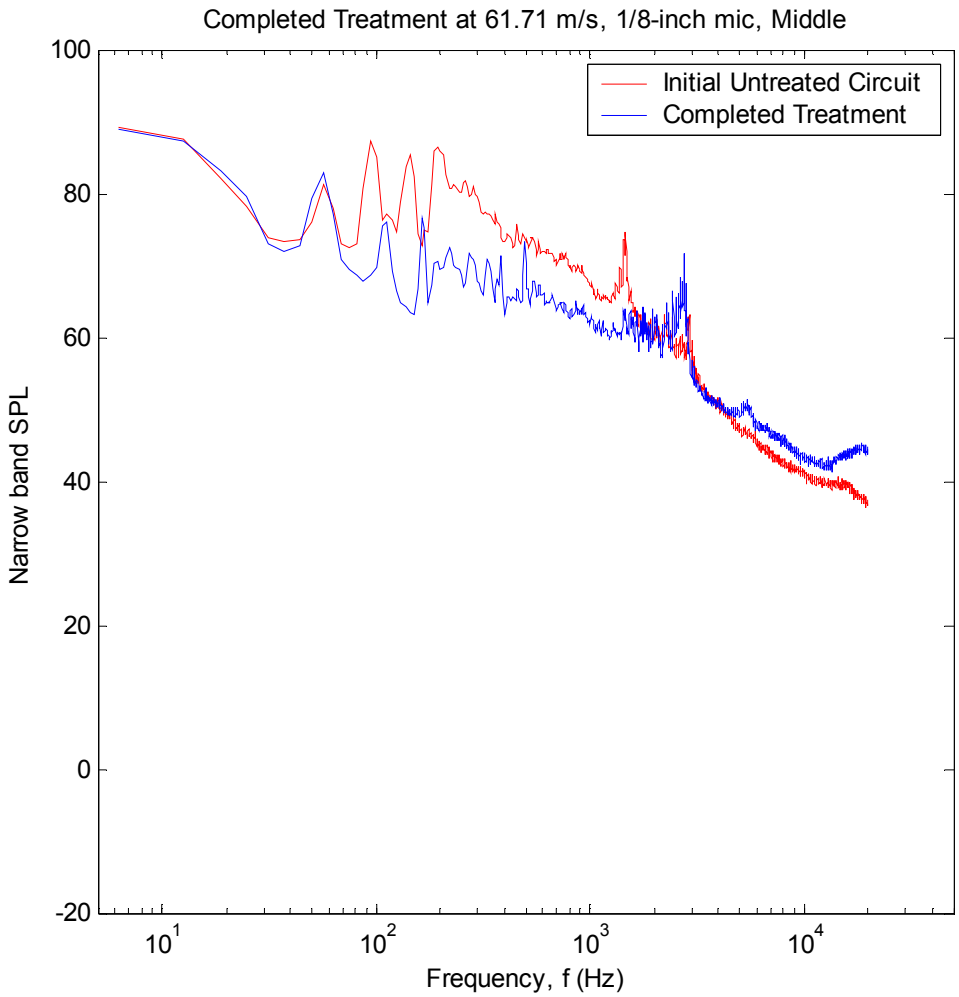

Figure 4-15. Comparison of the final treatment against the original untreated circuit at a nominal speed of 61 m/s

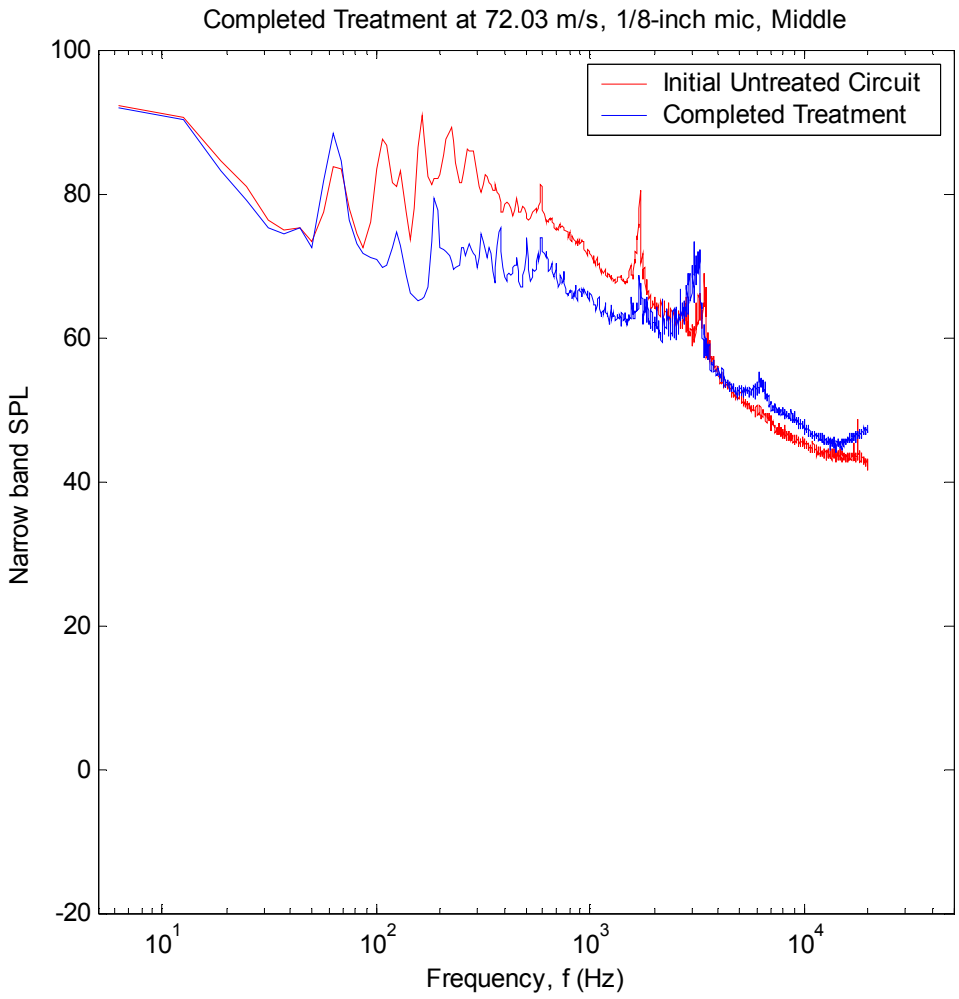

Figure 4-16. Comparison of the final treatment against the original untreated circuit at a nominal speed of 72 m/s

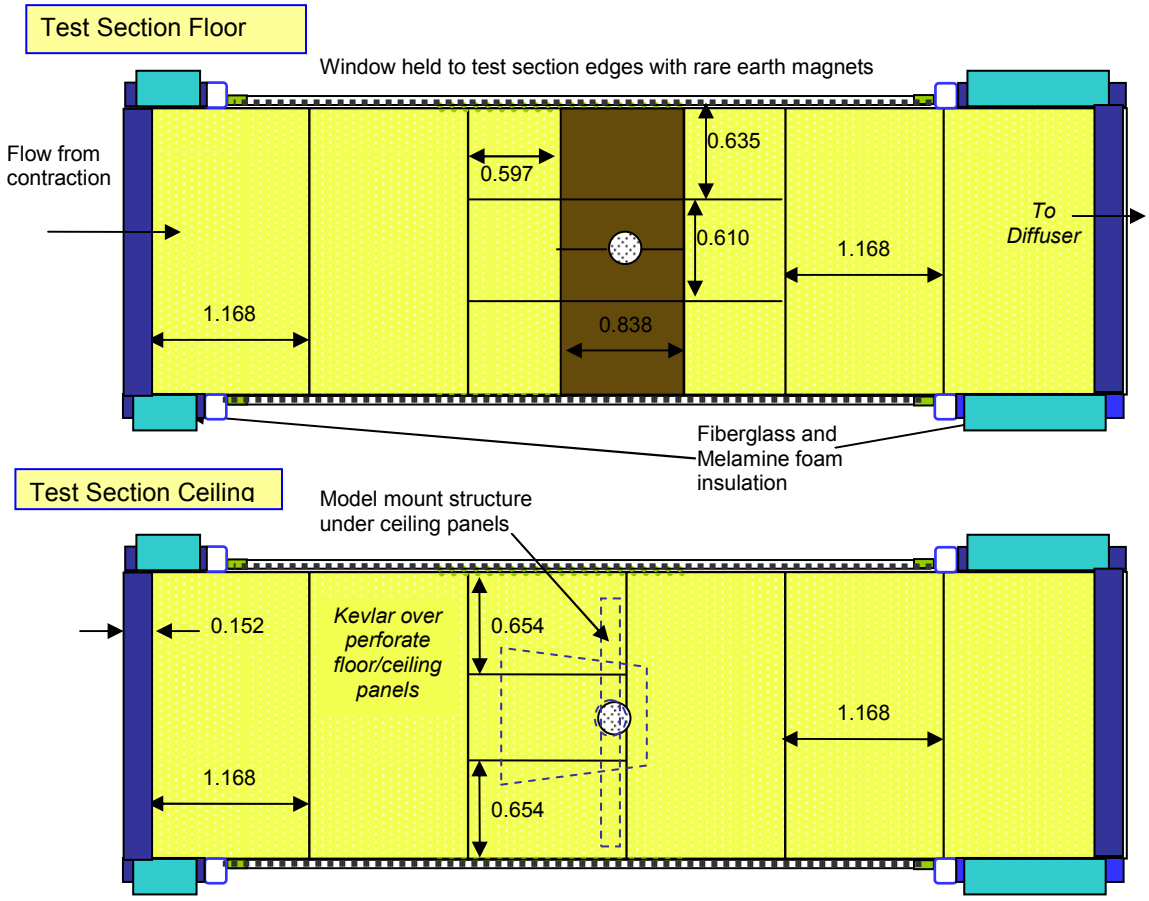

Figure 4-17. Diagram of the completed anechoic test section with all of the modifications made during the 2007 entry

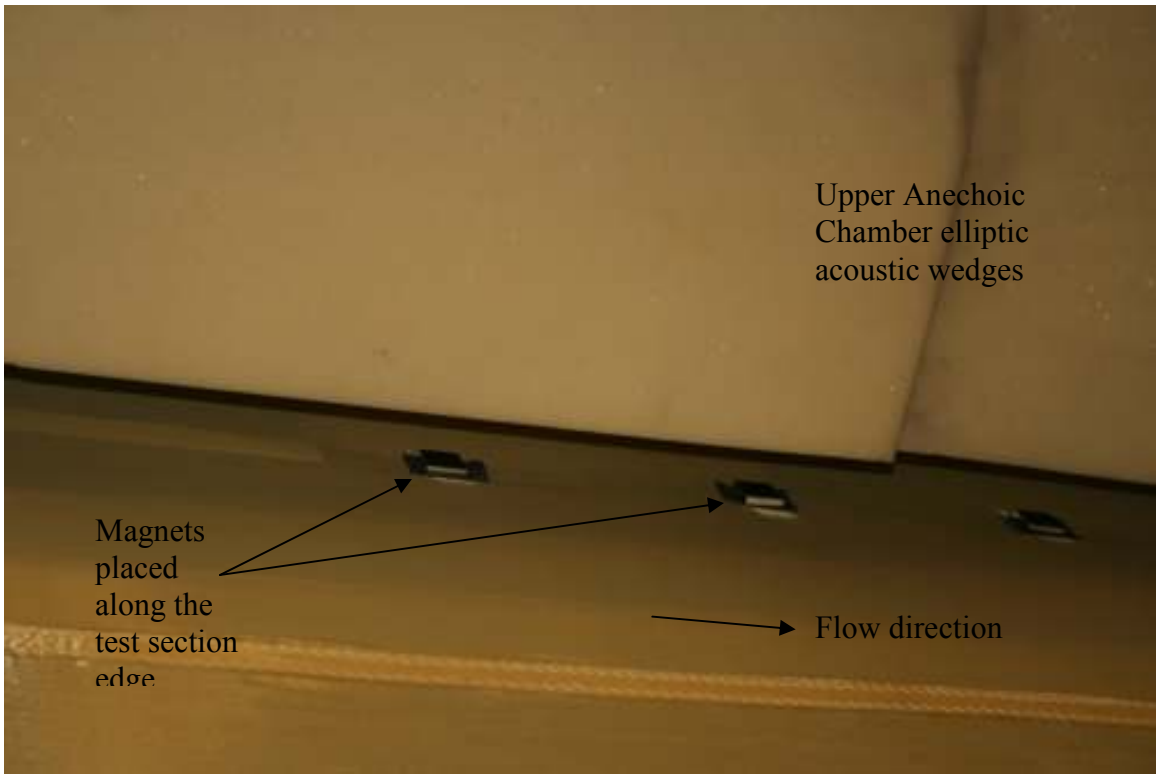

Figure 4-18. 1” x 1” x ¼” Neodymium magnets were used to attach the Kevlar window to the edge of the test section. These magnets placed every 3 inches or so, helped to reduce the load felt by the windows at high speeds or with a model at a high angle of attack.

Figure 4-19. Airfoil Model mounted on the rotation endplates used to generate angle of attack changes.

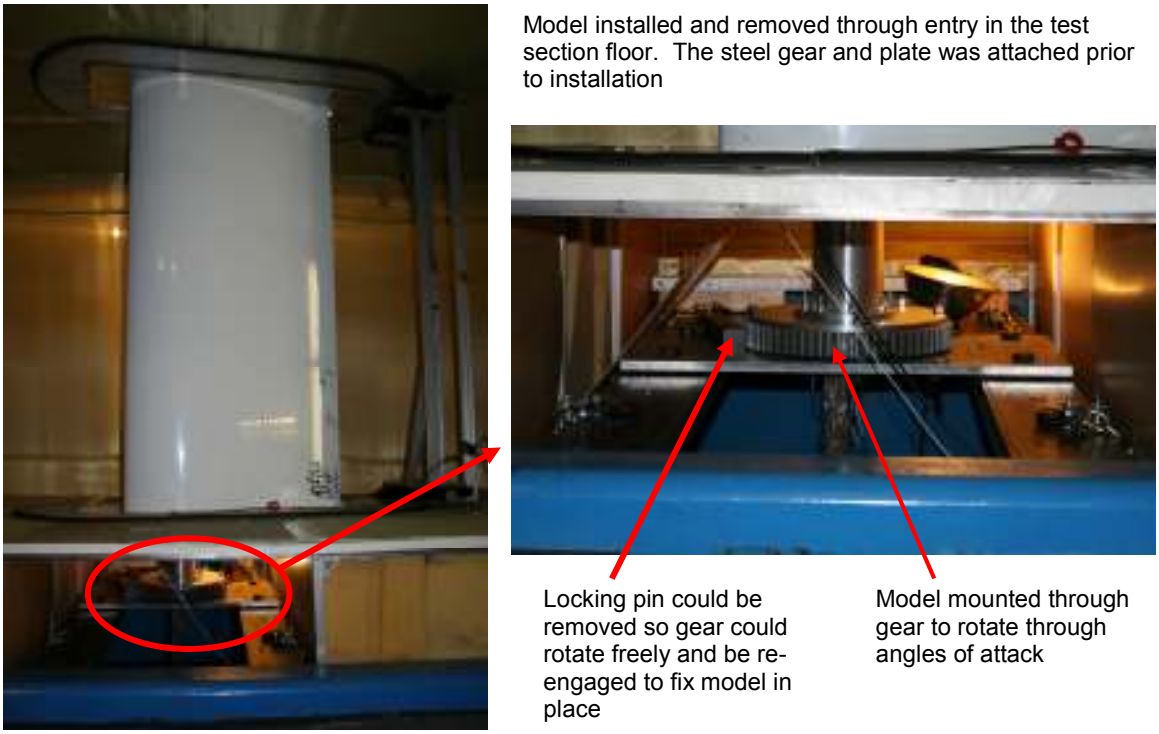

Figure 4-20. Angle of attack rotation system.

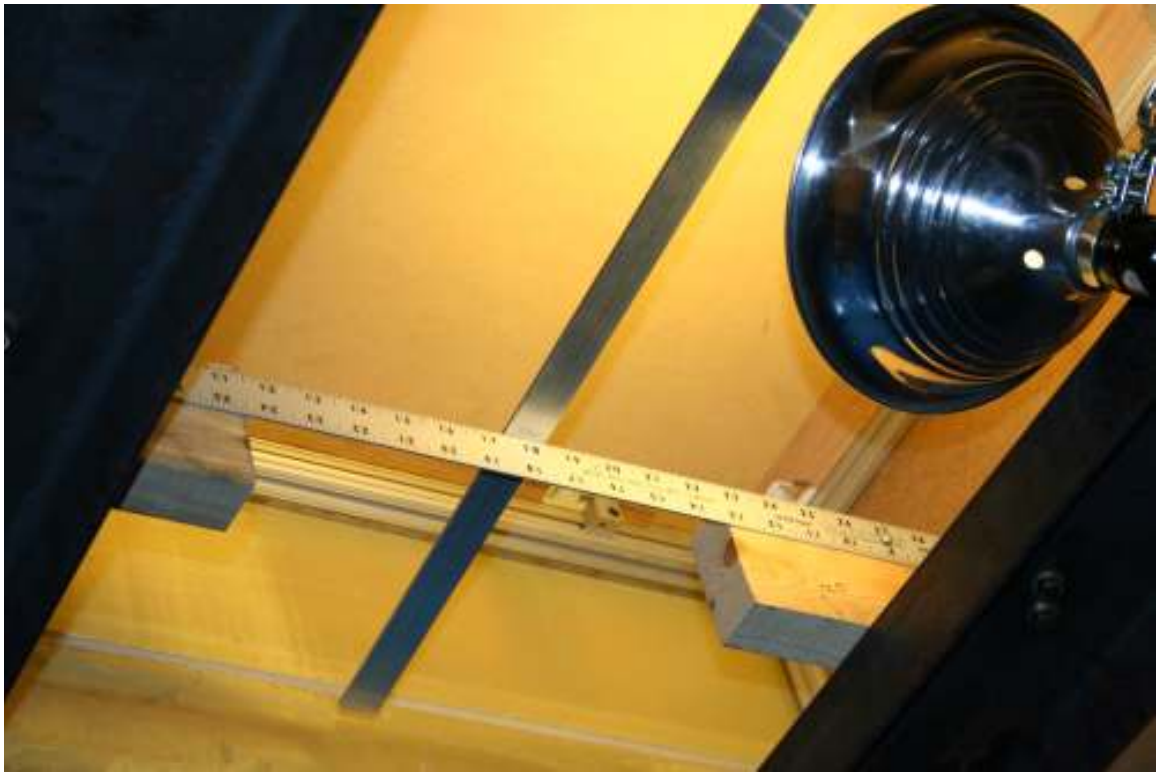

Figure 4-21. Sting used to read model rotation angle. This was used to determine the model angle of attack.

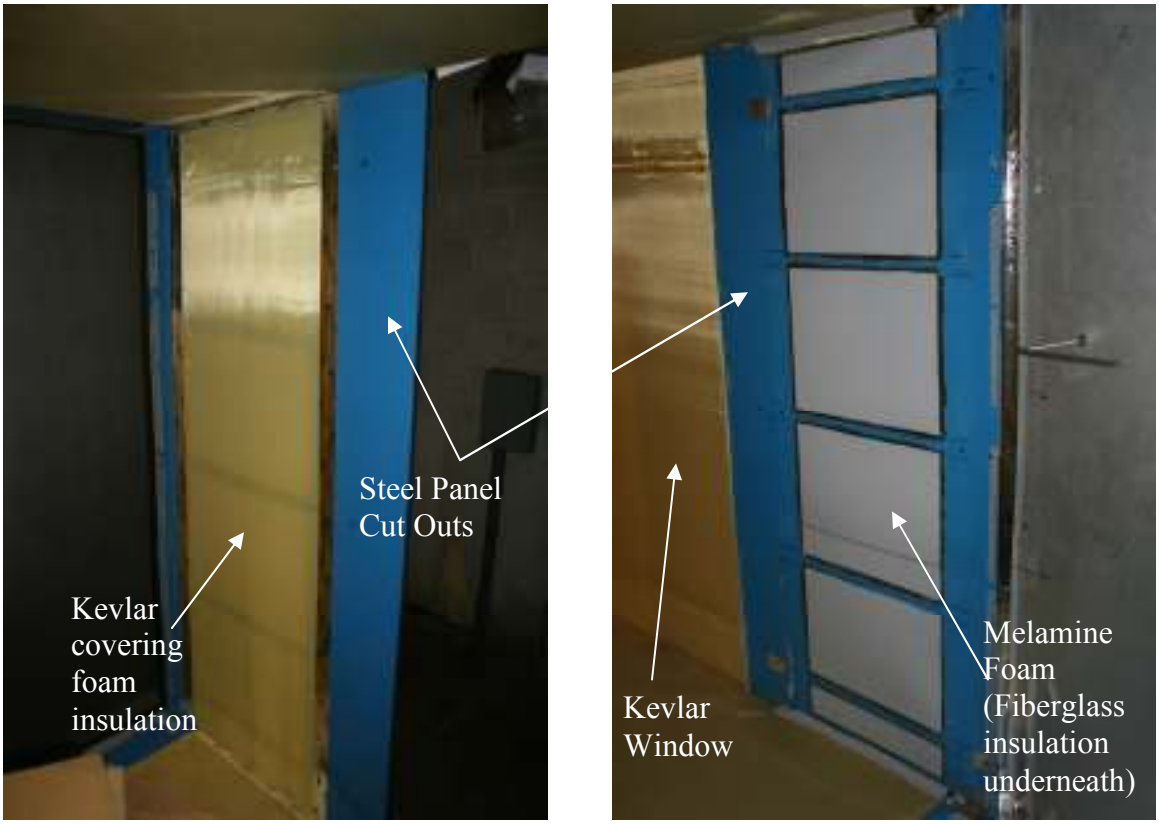

Figure 4-22. The photograph (left) shows the newly installed acoustic absorbers with the Kevlar covering. The photograph (right) shows the original steel panel with the acoustic liner.

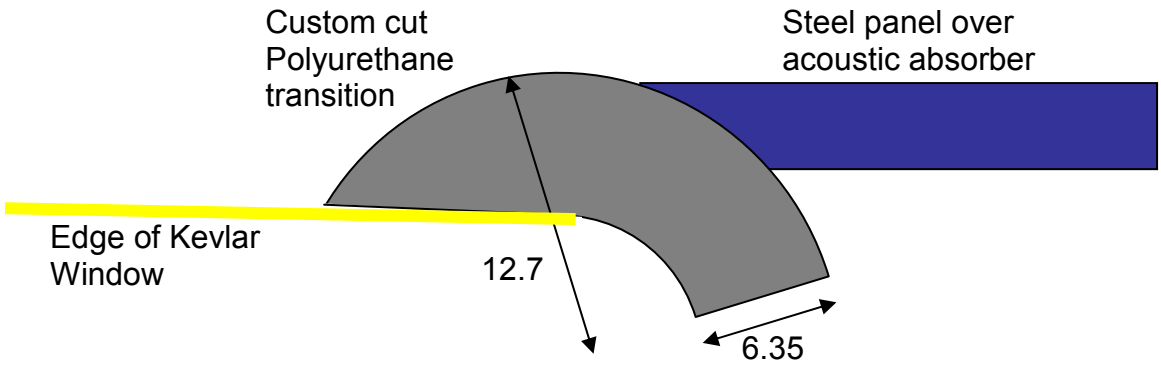

Figure 4-23. Diagram of the window transition used to prevent any sound radiation from the step between the acoustic absorber and the Kevlar window.

Figure 4-24. Photograph showing the redesigned model catcher.

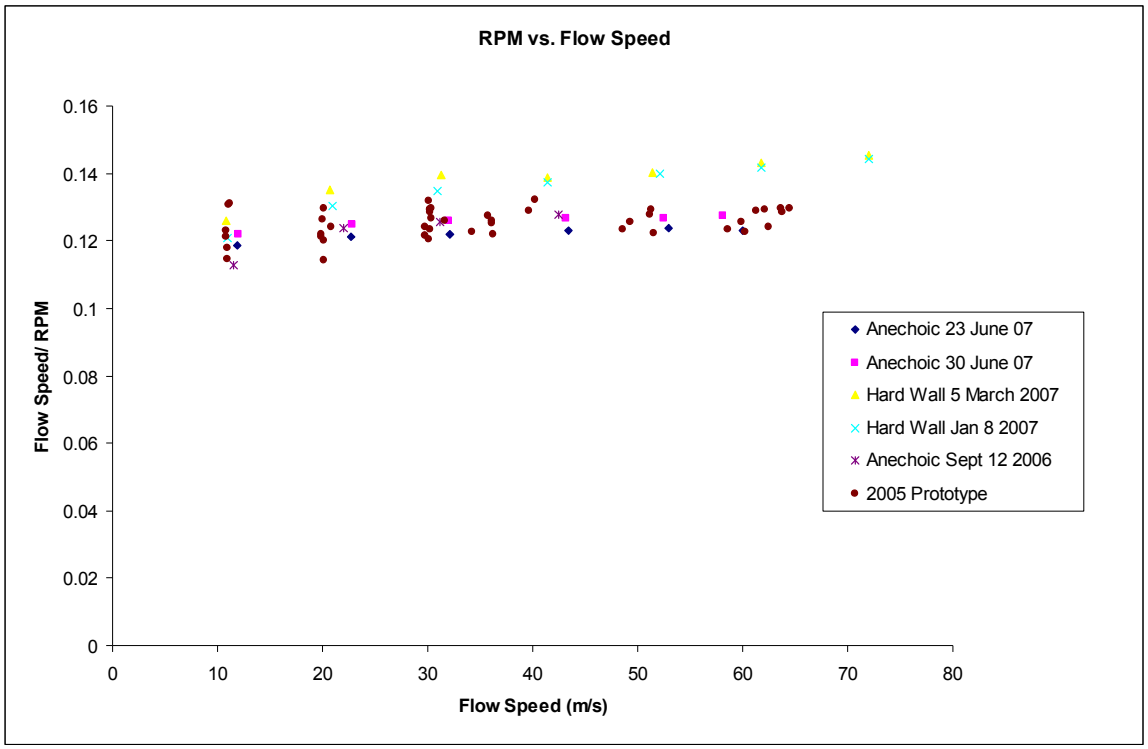

Figure 4-25. Comparison of the Fan revolutions per minute with the flow speed in the test section

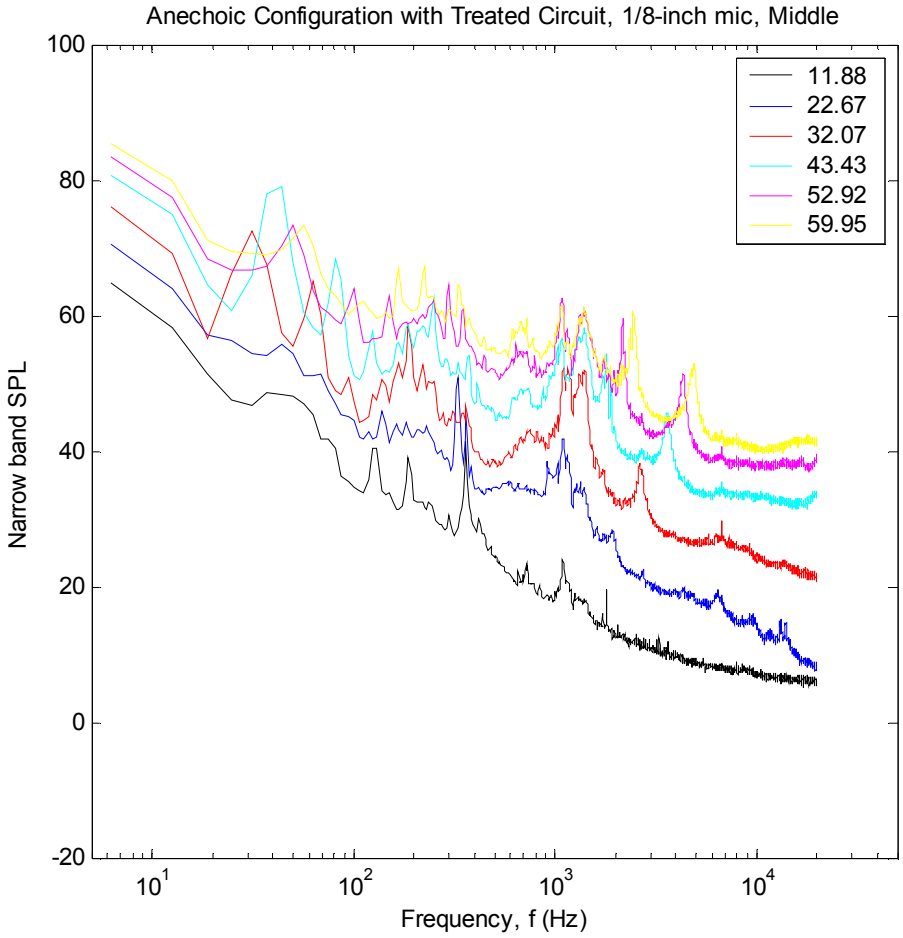

Figure 4-26. In Flow Noise Levels for the Anechoic Test section with treated circuit, measured during the final calibration in 2007

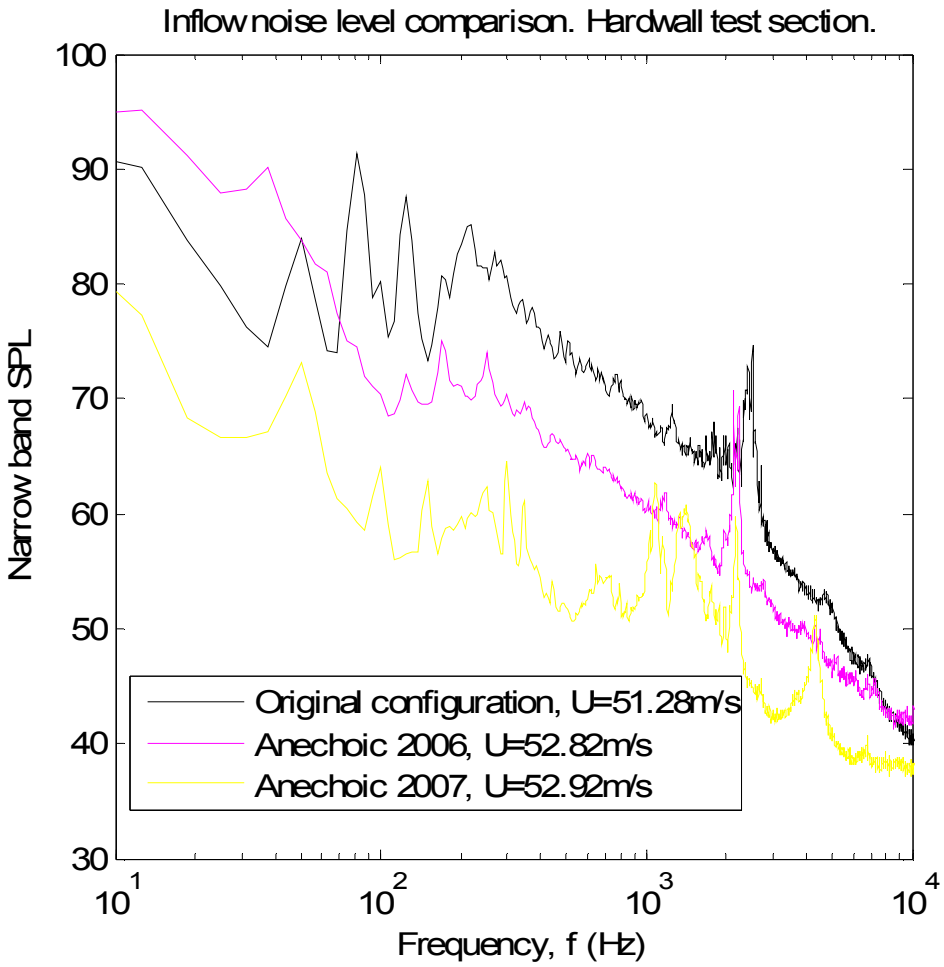

Figure 4-27. Overall reductions for a nominal flow speed of 52 m/s for the hard wall, and two anechoic configurations

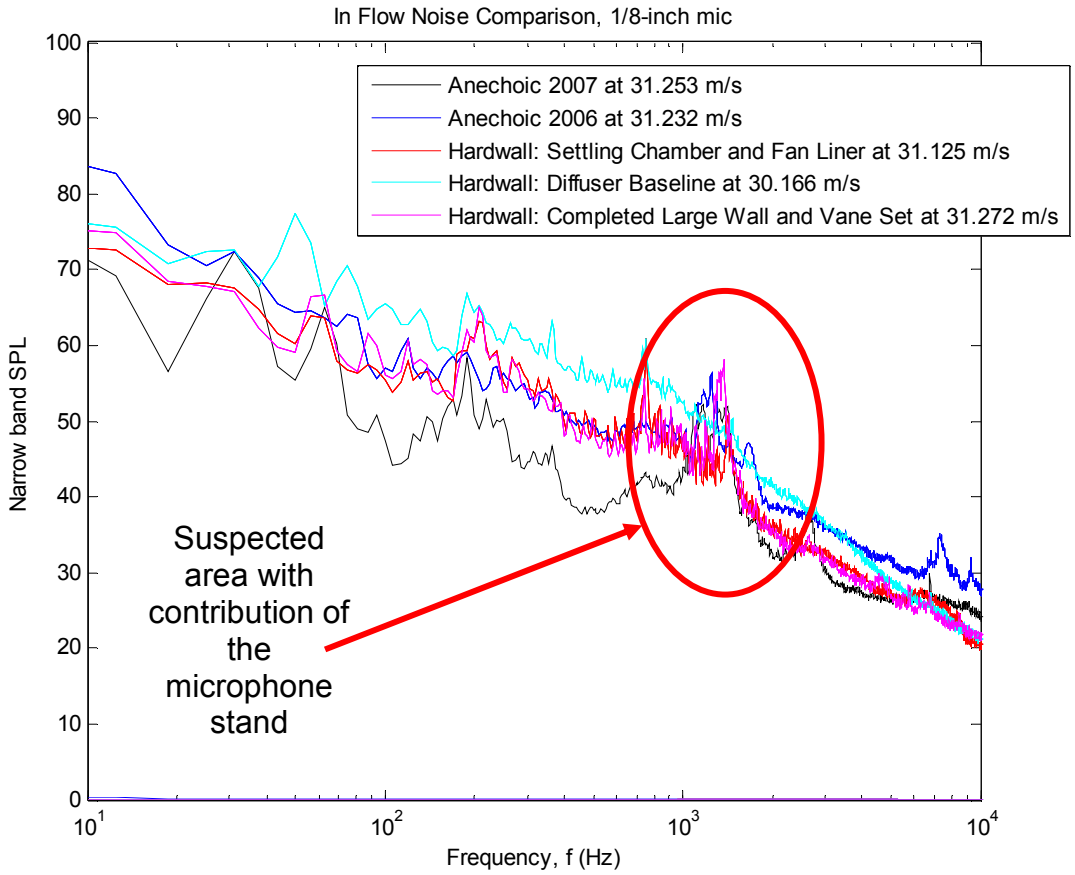

Figure 4-28. Comparison of all of the tunnel treatment stages and configurations for a nominal tunnel velocity of 30 m/s. This data does not have the contribution of the microphone stand subtracted out

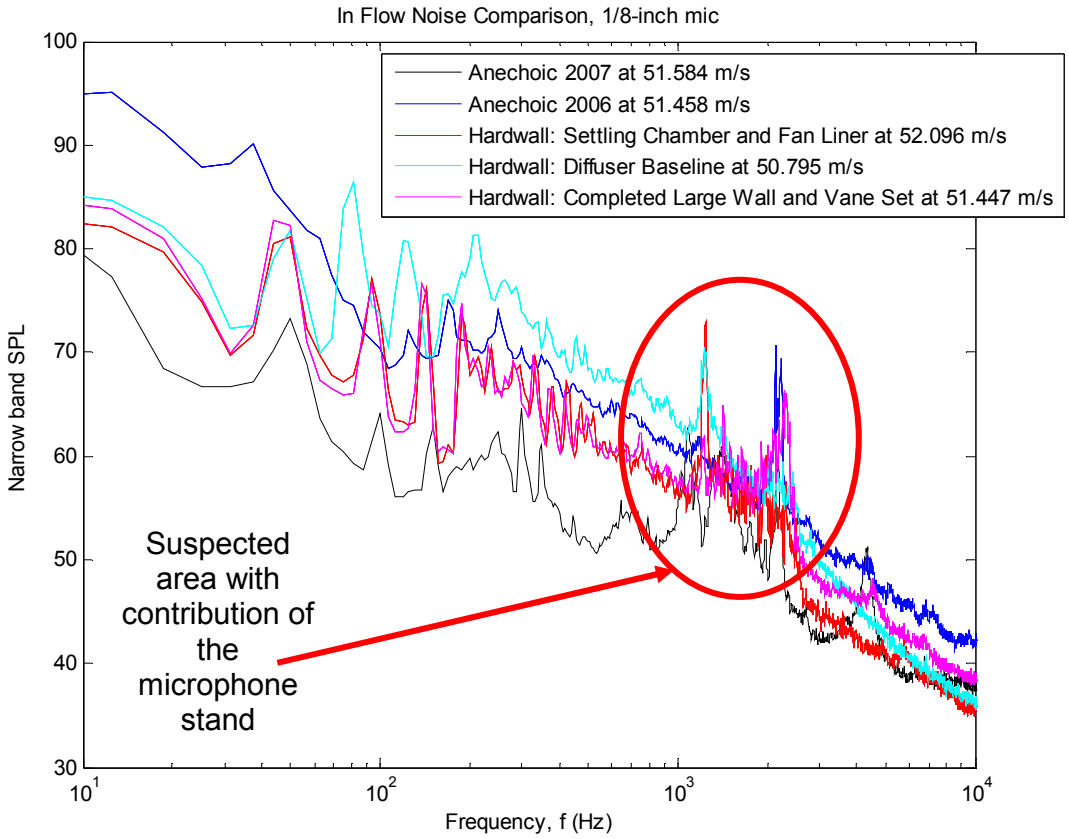

Figure 4-29. Comparison of all of the tunnel treatment stages and configurations for a nominal tunnel velocity of 50 m/s. This data does not have the contribution of the microphone stand subtracted out

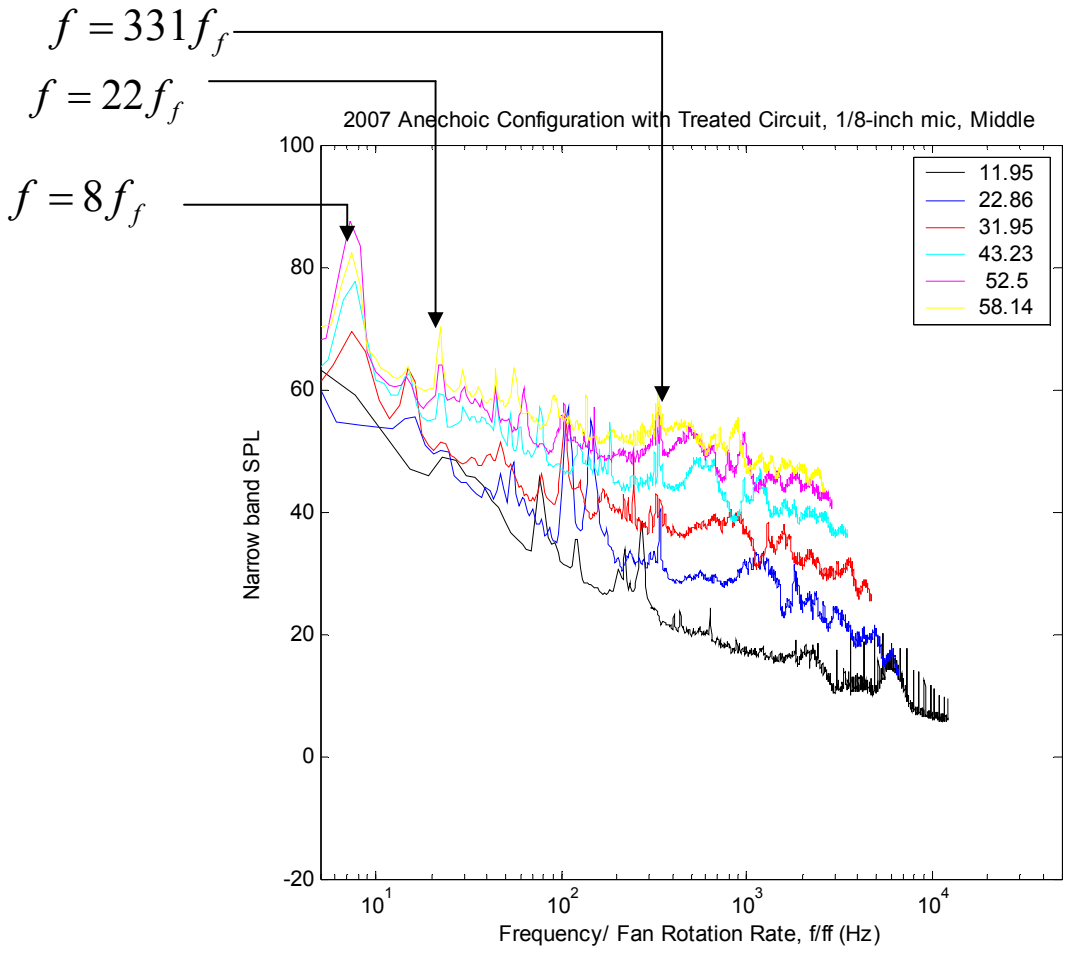

Figure 4-30. Acoustic spectra plotted against frequency normalized on the fan rotation rate *ff* = RPM/60.

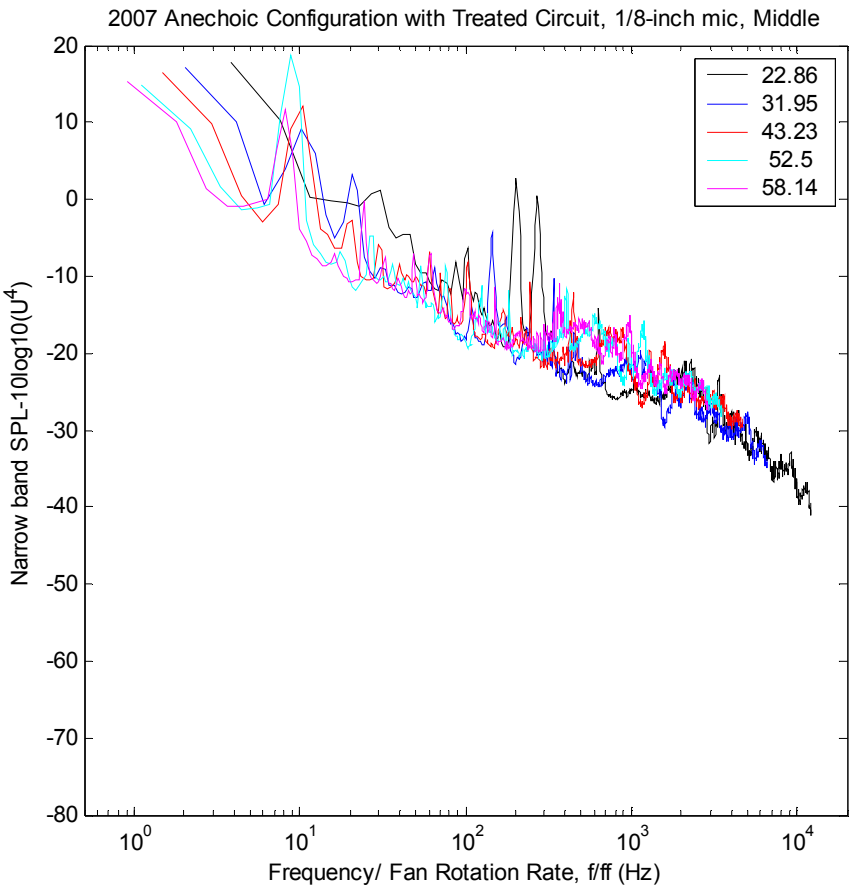

Figure 4-31. In-flow noise spectra measured at mid-section location with the 1/8th-inch microphone in the 2007 anechoic configuration with frequency scaled on fan rotation rate ff and spectral level scaled on the 4th power of the velocity. The 10 m/s case left out due to plot distortion

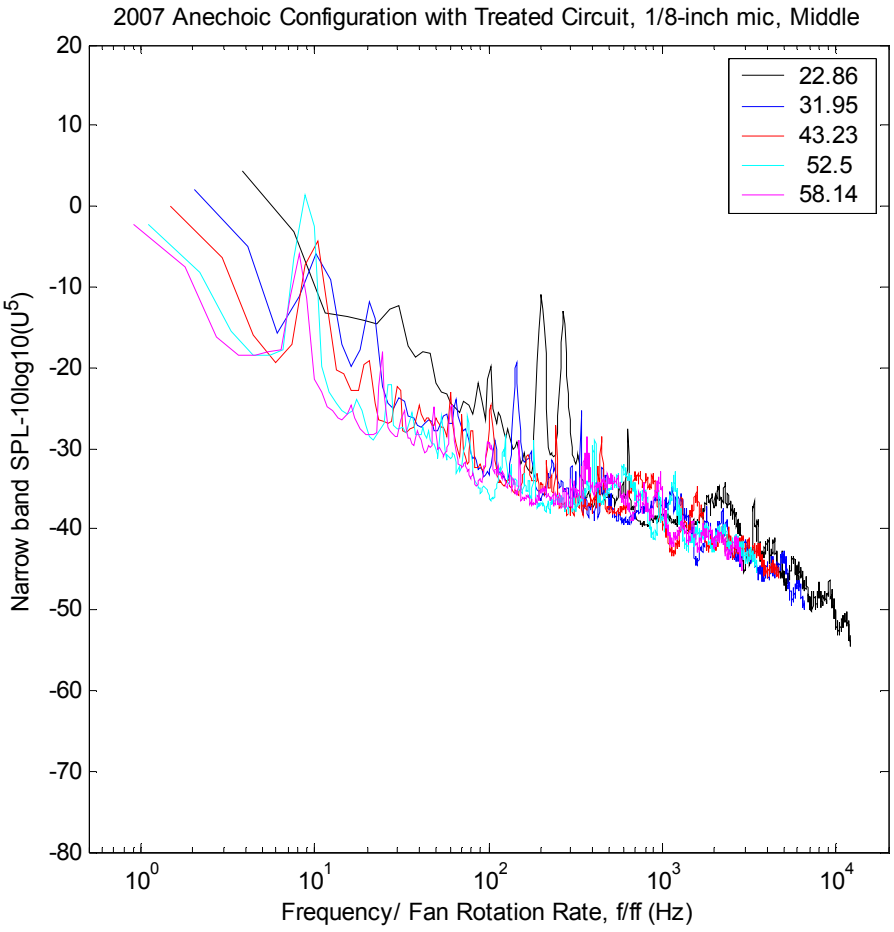

Figure 4-32. In-flow noise spectra measured at mid-section location with the 1/8th-inch microphone in the 2007 anechoic configuration with frequency scaled on fan rotation rate ff and spectral level scaled on the 5th power of the velocity. The 10 m/s case left out due to plot distortion

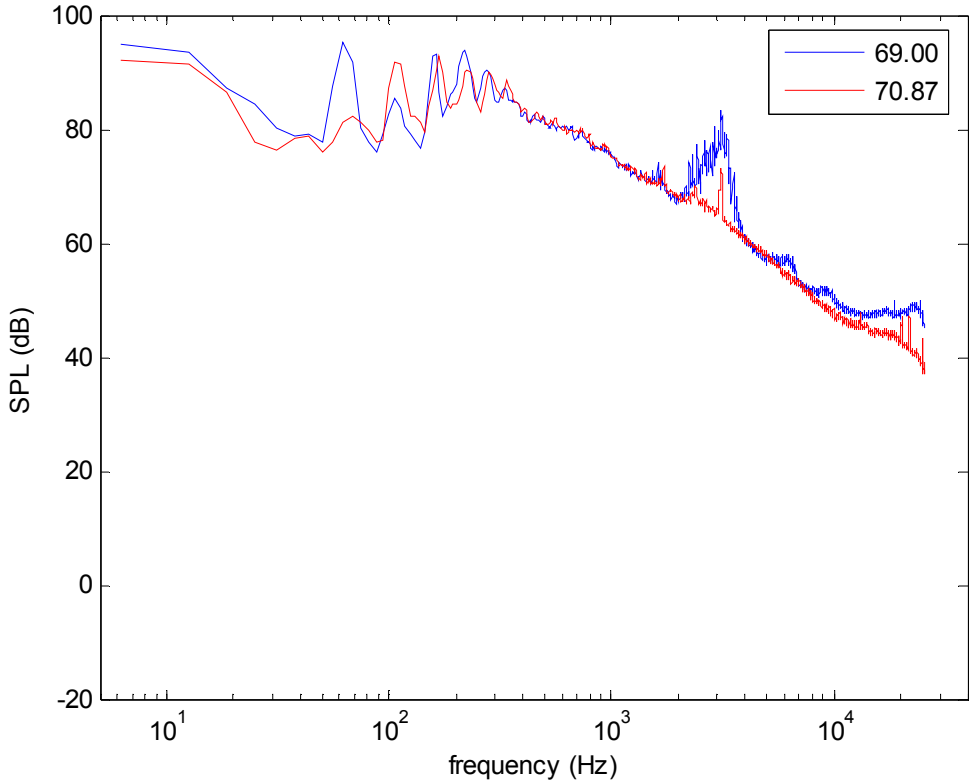

Figure 4-33. Comparison of the Inflow microphone data to that taken out of flow at the same stream wise position for a nominal flow speed of 70 m/s

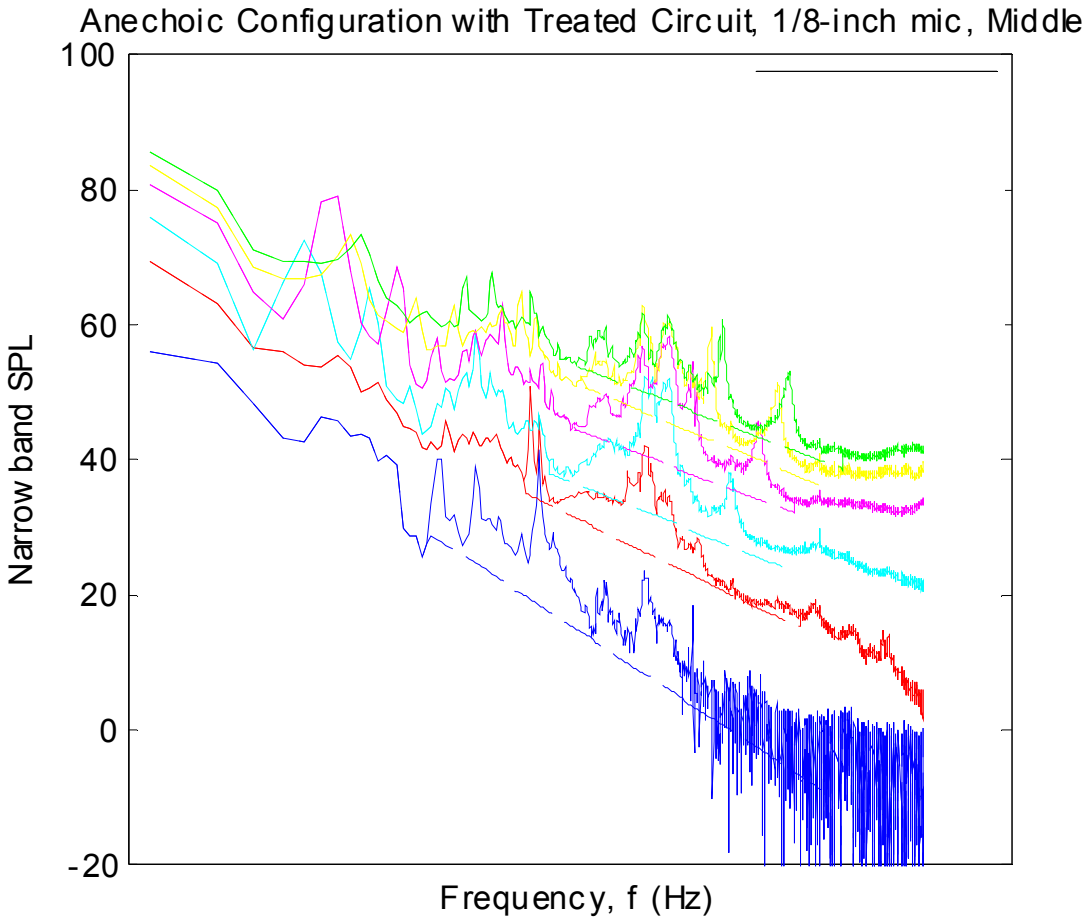

Figure 4-34. Approximation (dashed lines) of the acoustic spectra with the microphone stand removed compared to the original anechoic data

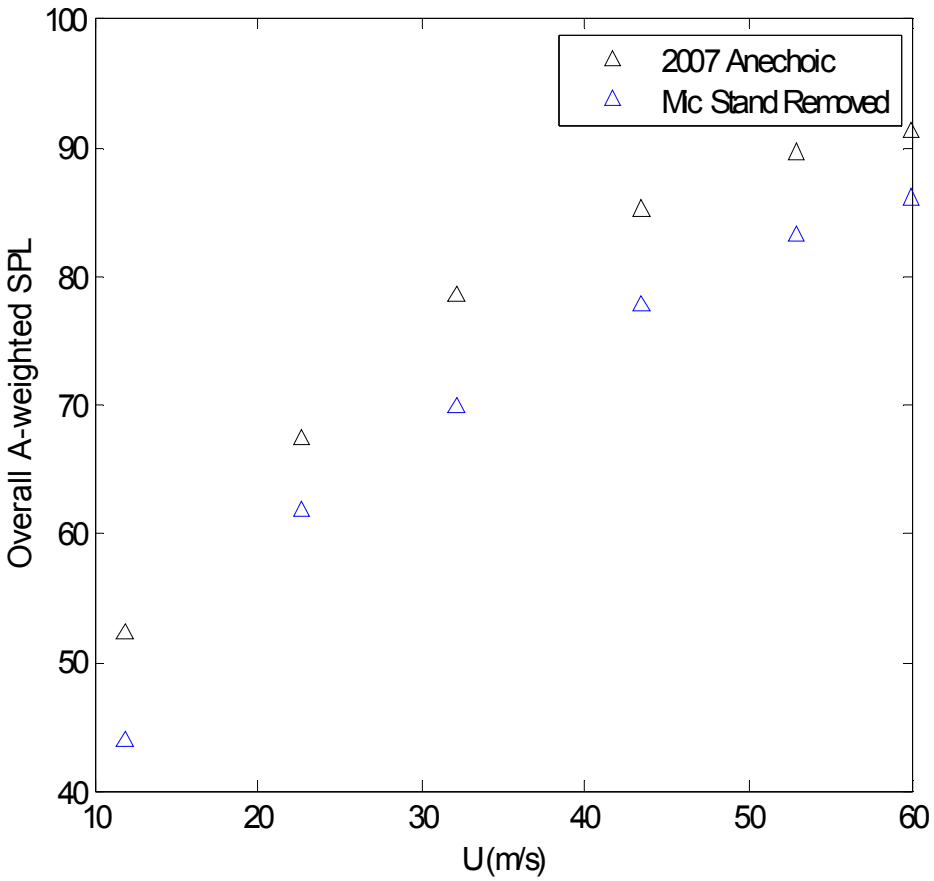

Figure 4-35. Comparison of the A-weighted SPL as a function of flow speed for the microphone stand present and removed.

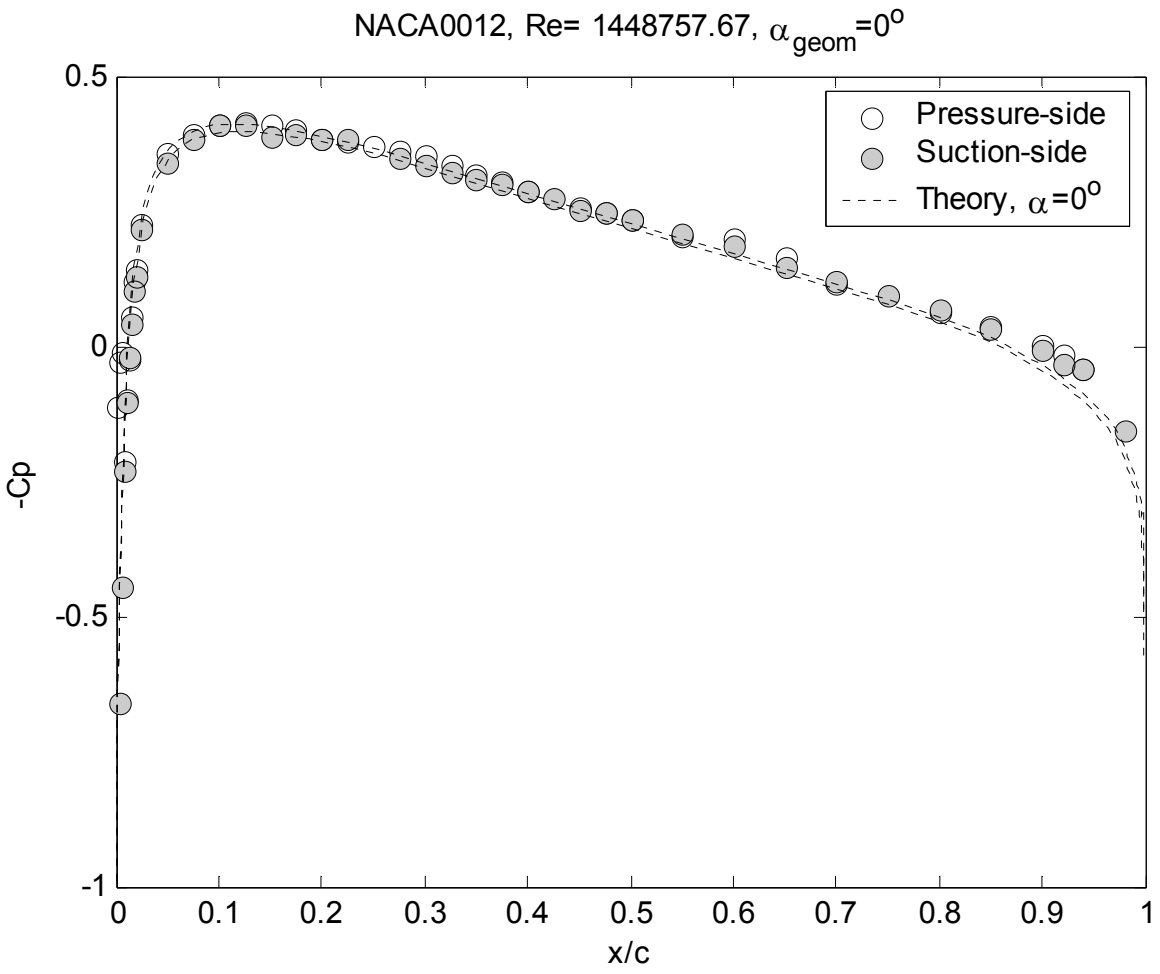

Figure 4-36. NACA 0012 at nominal 28 m/s and 0 deg. Effective AOA

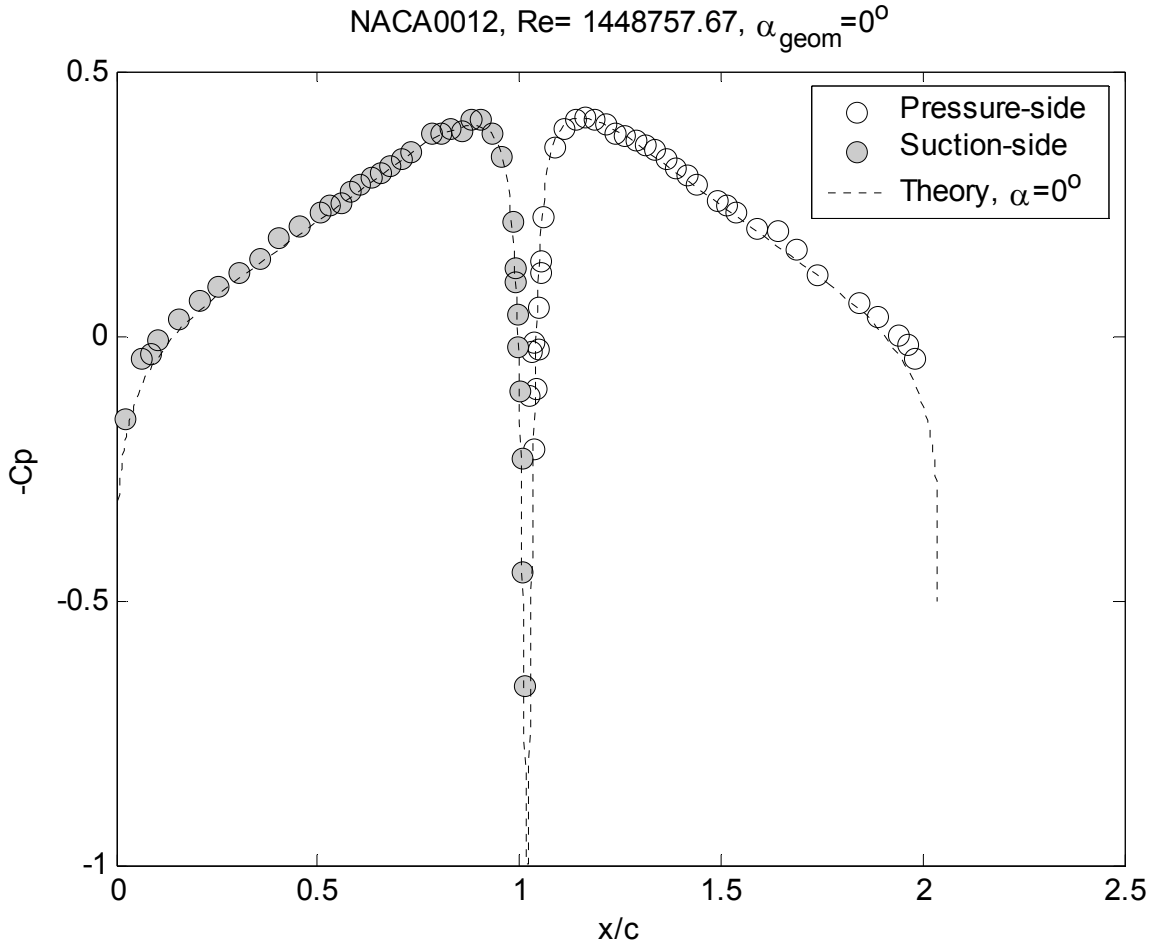

Figure 4-37. Edge length pressure distribution for the NACA 0012 at 0 deg. effective AOA at 28 m/s

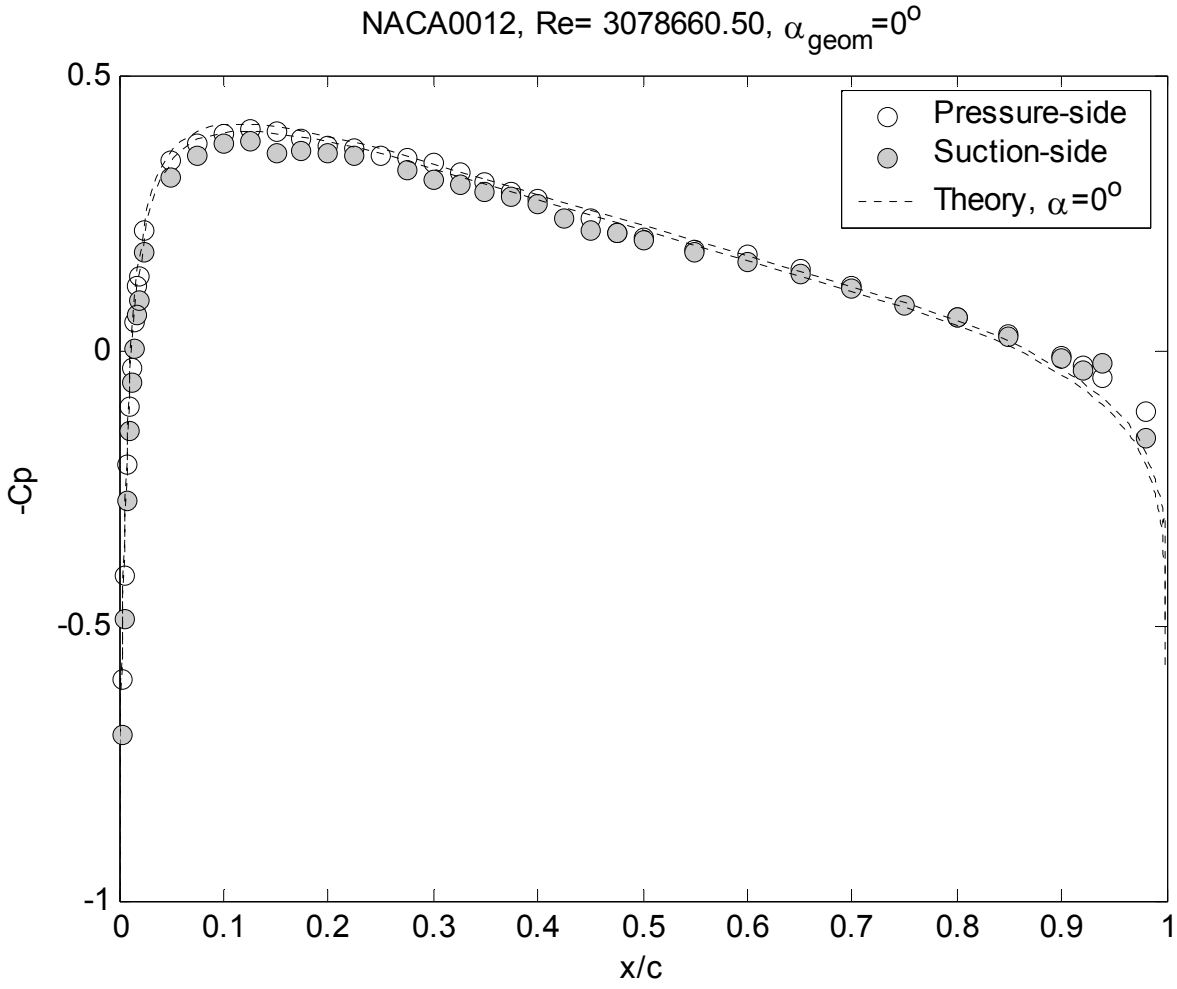

Figure 4-38. NACA 0012 at nominal 56 m/s and 0 deg. Effective AOA

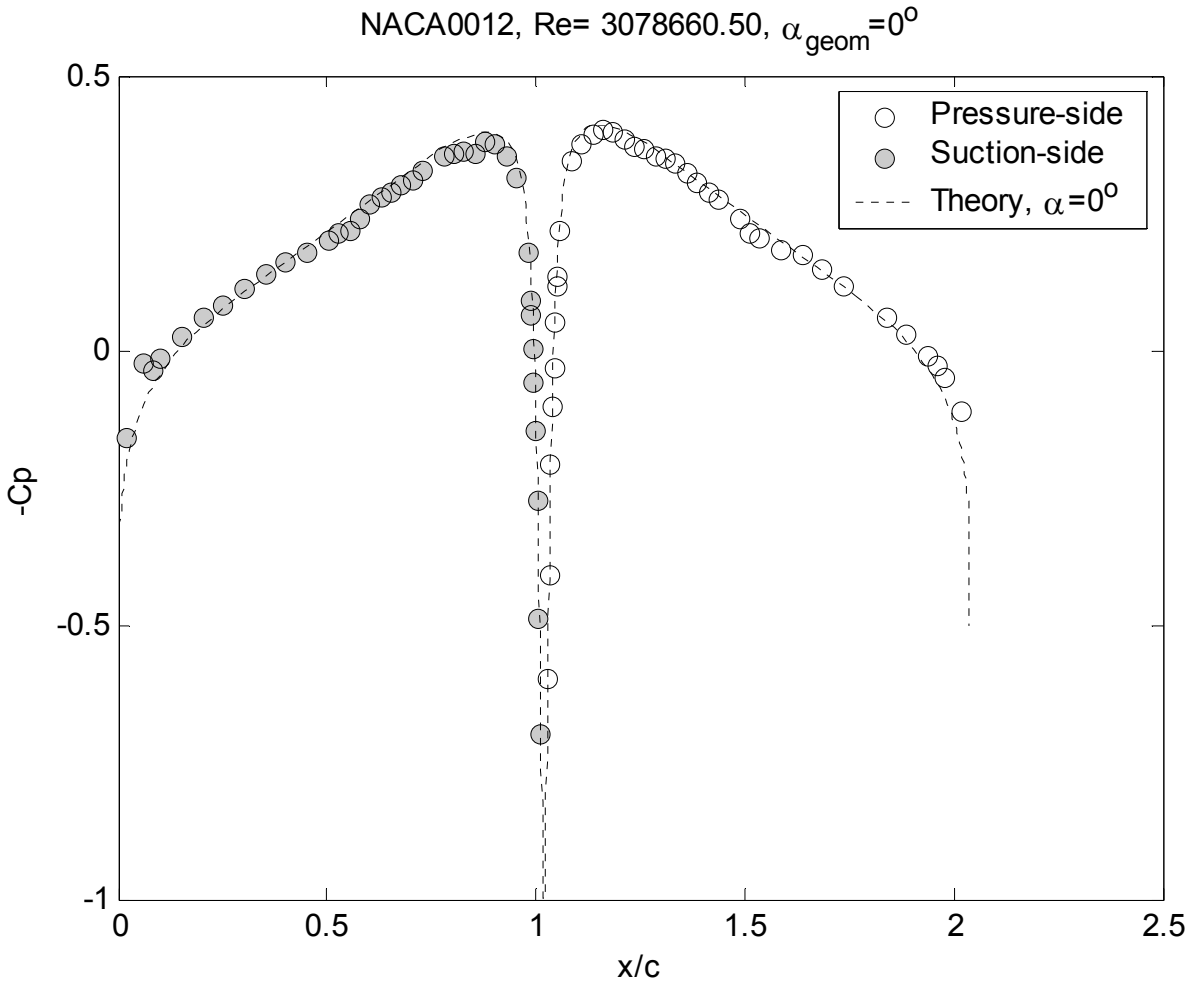

Figure 4-39. NACA 0012 at 0-degrees effective AOA at 56 m/s

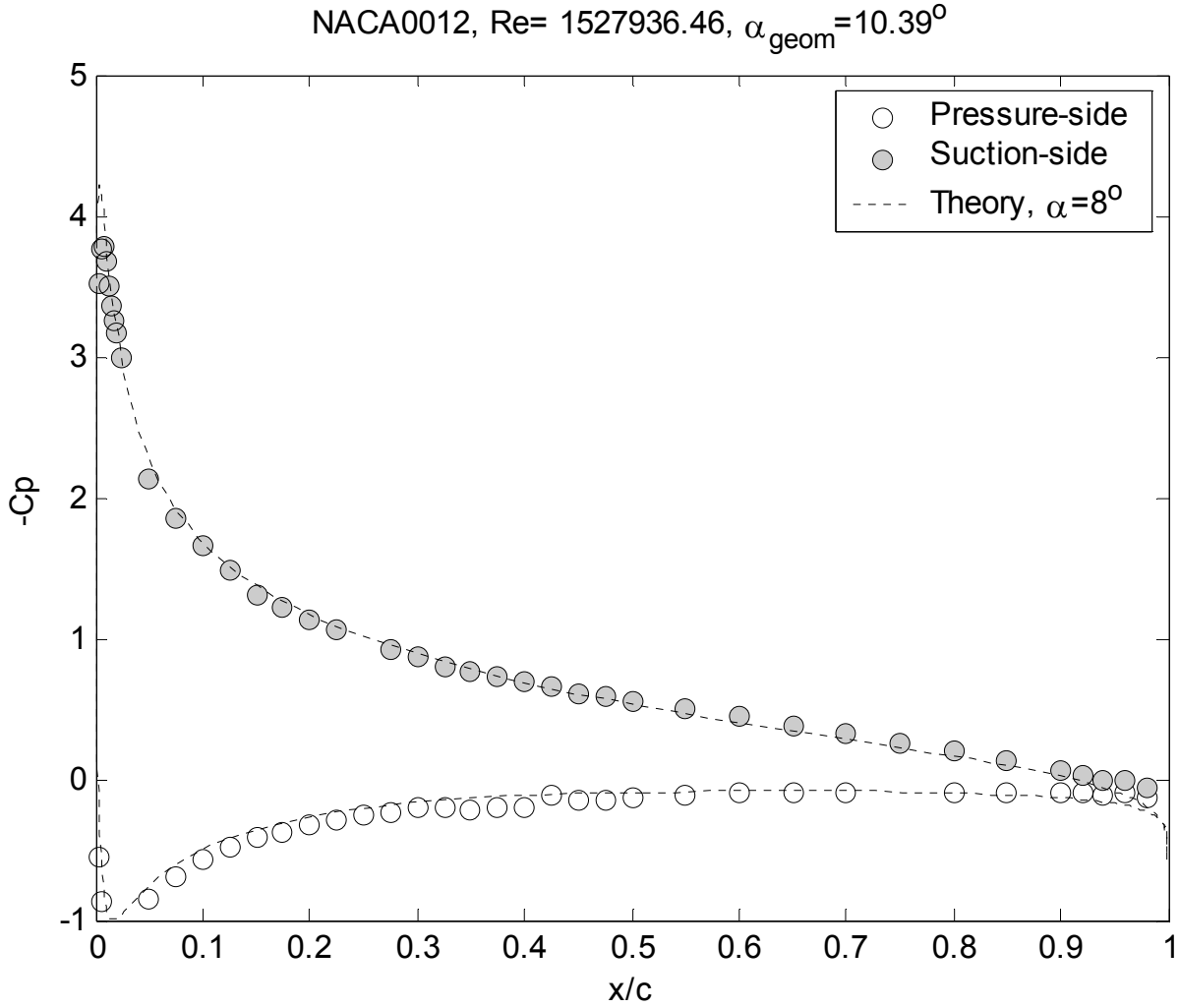

Figure 4-40. NACA 0012 at nominal 30 m/s and 8 deg. Effective AOA

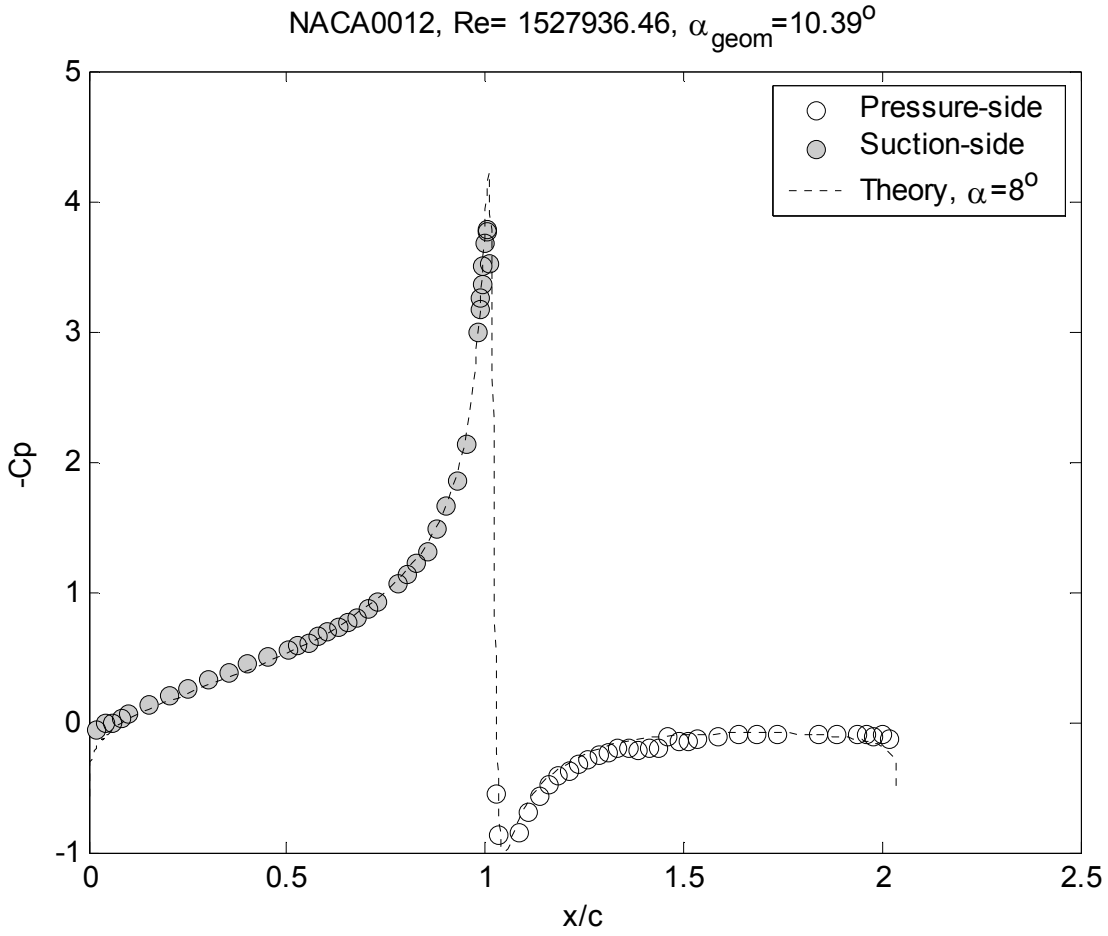

Figure 4-41. NACA 0012 at 8-degrees effective AOA and 30 m/s

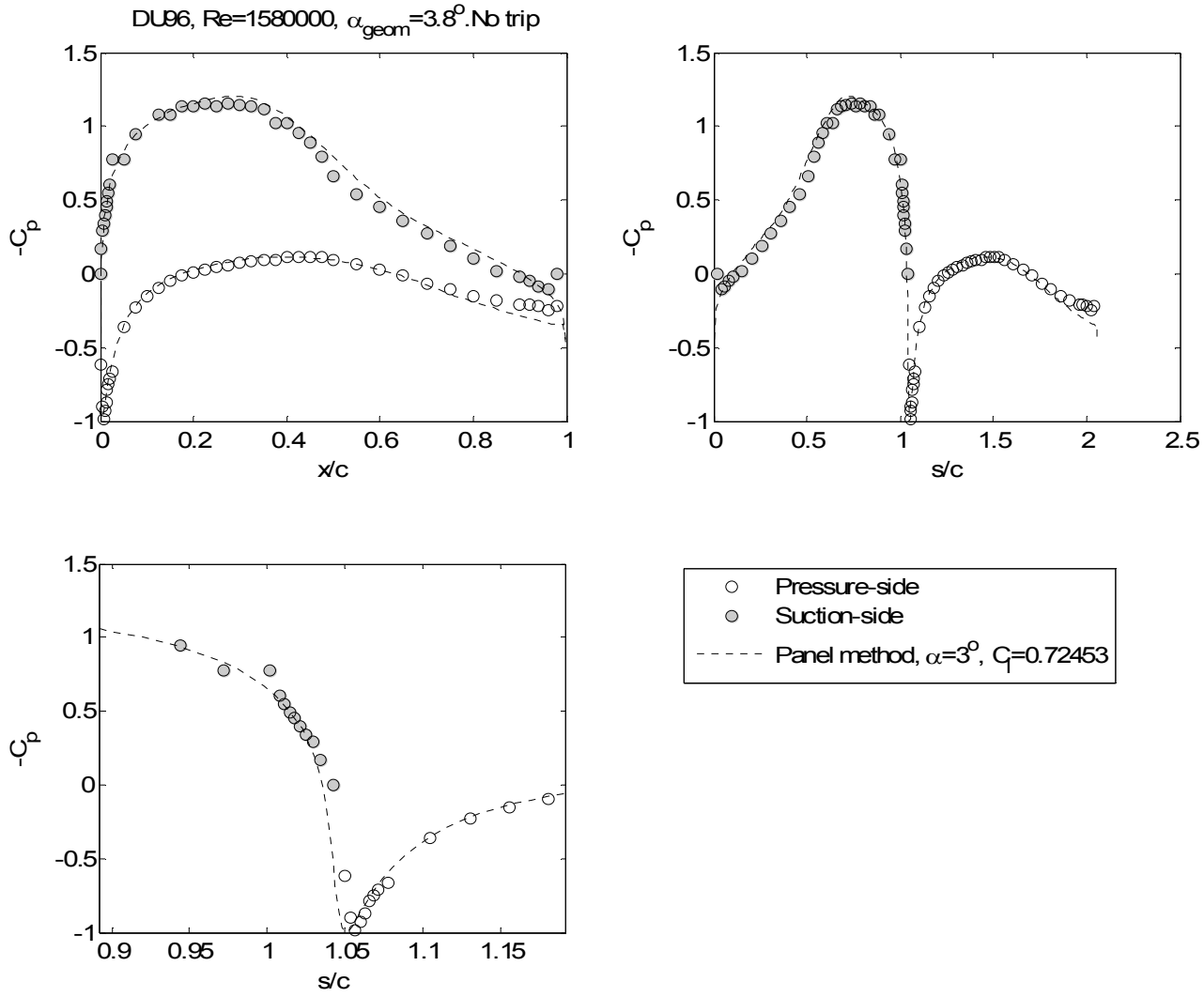

Figure 4-42. Comparison of the measured to the experimental model pressure distributions for the DU96 at a 3.8 geometric angle of attack

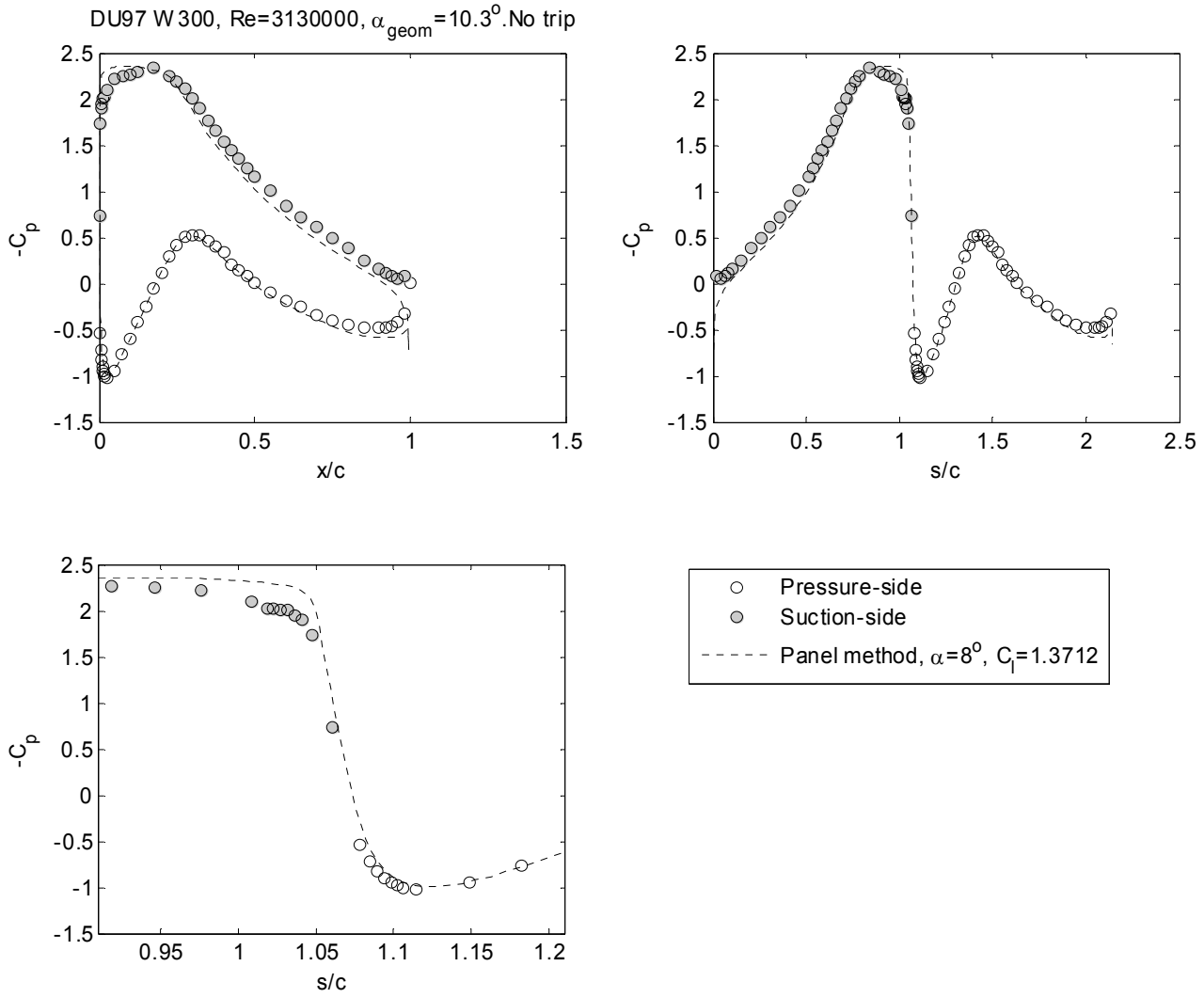

Figure 4-43. Comparison of the measured to the experimental model pressure distributions for the DU97-W300 at a 10.3 geometric angle of attack

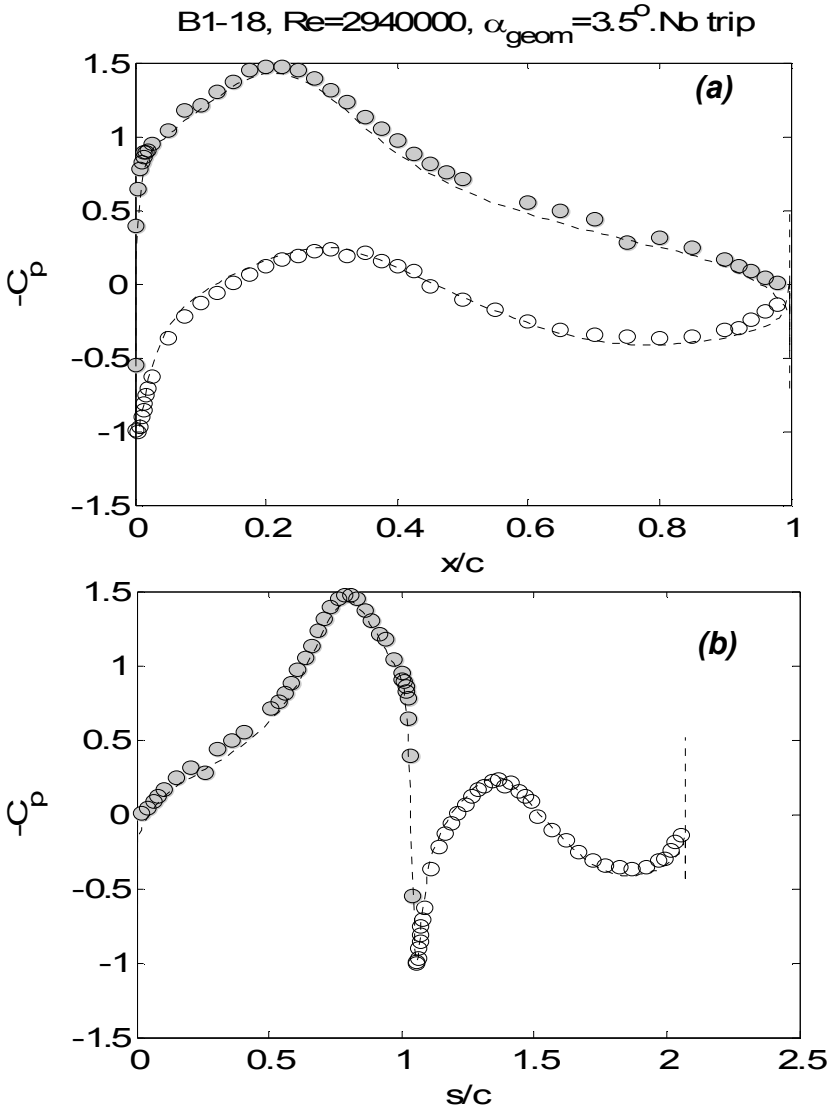

Figure 4-44. Mean pressure distribution on the B1-18 airfoil at 2.7 degrees effective angle of attack and a Reynolds number of 2940000 without trip. Filled symbols – suction side, open symbols, pressure side, dashed line – panel method result. (a) Pressure plotted vs. chord wise distance x/c, and (b) vs. edge length s/c.

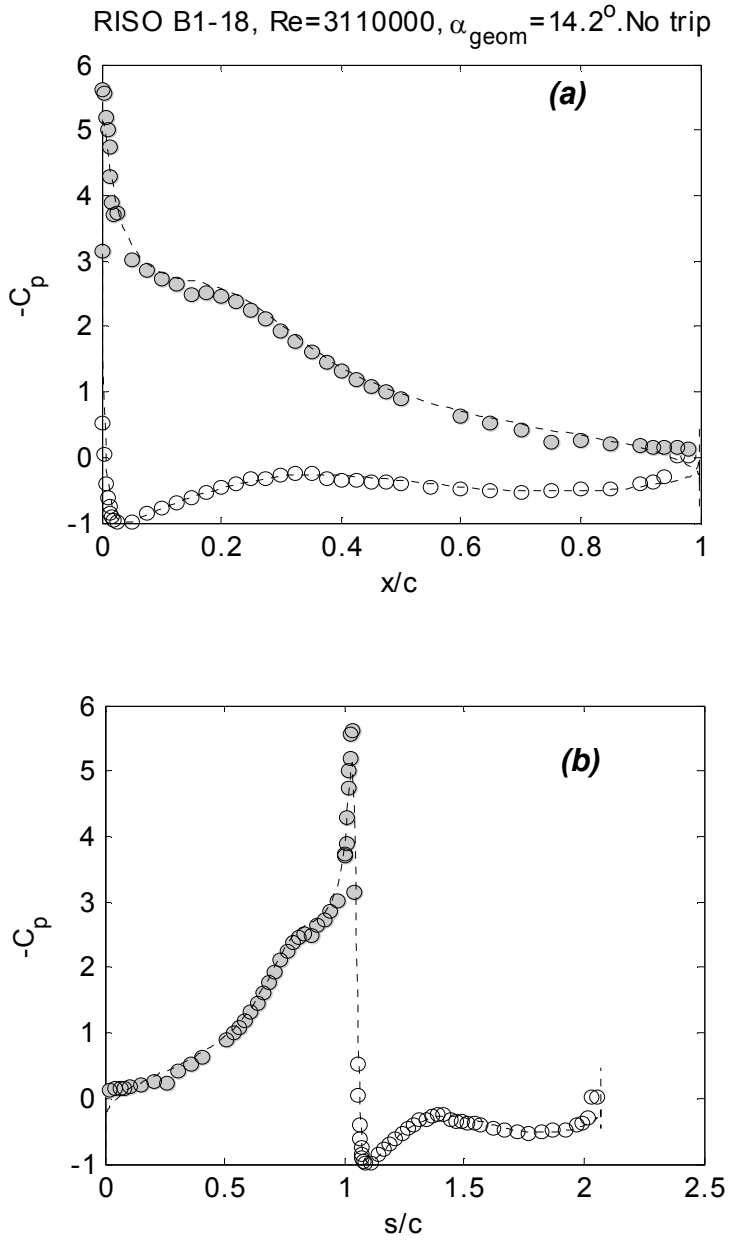

Figure 4-45. Mean pressure distribution on the B1-18 airfoil at 11 degrees effective angle of attack and a Reynolds number of 3110000 without trip. Filled symbols – suction side, open symbols, pressure side, dashed line – panel method result. (a) Pressure plotted vs. chord wise distance x/c, and (b) vs. edge length s/c.

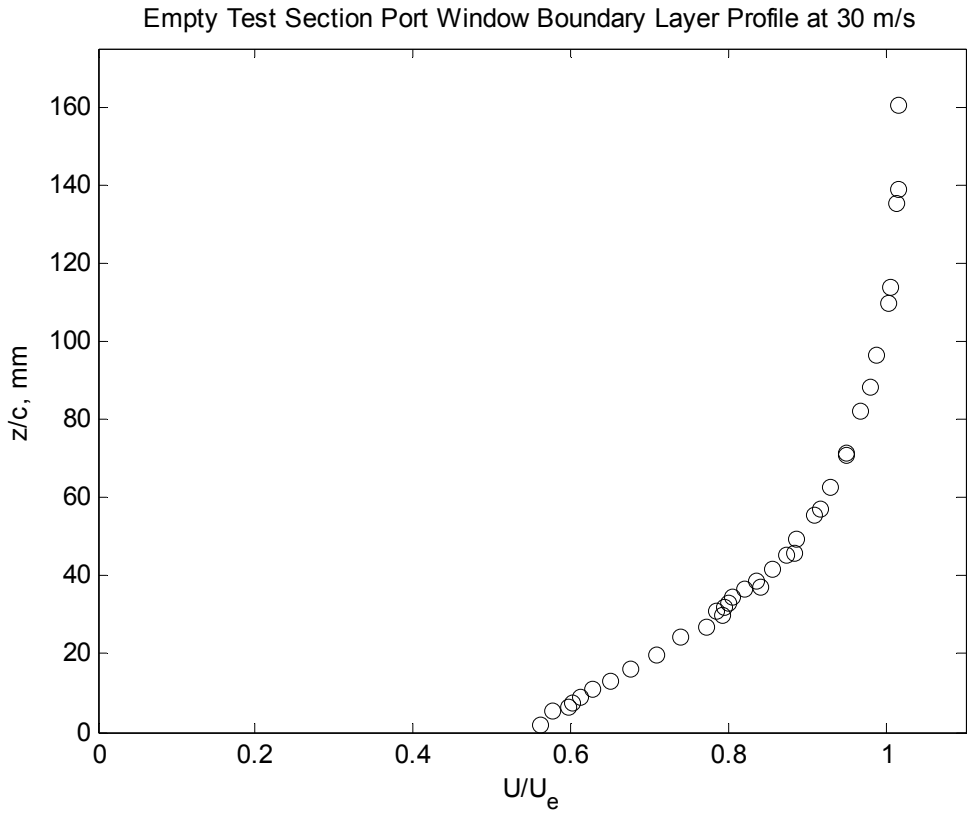

Figure 4-46. Empty test Section Port window boundary layer profile at the downstream location.

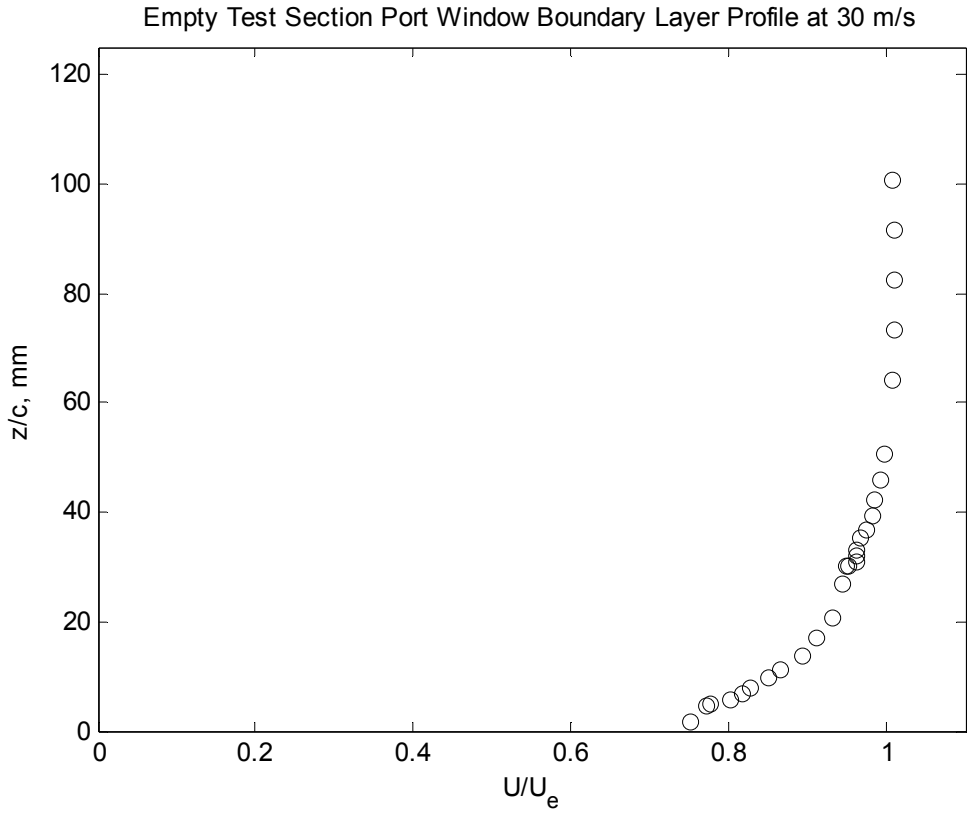

Figure 4-47. Boundary Layer profile for the empty test section pressure window at the inlet for 30 m/s.

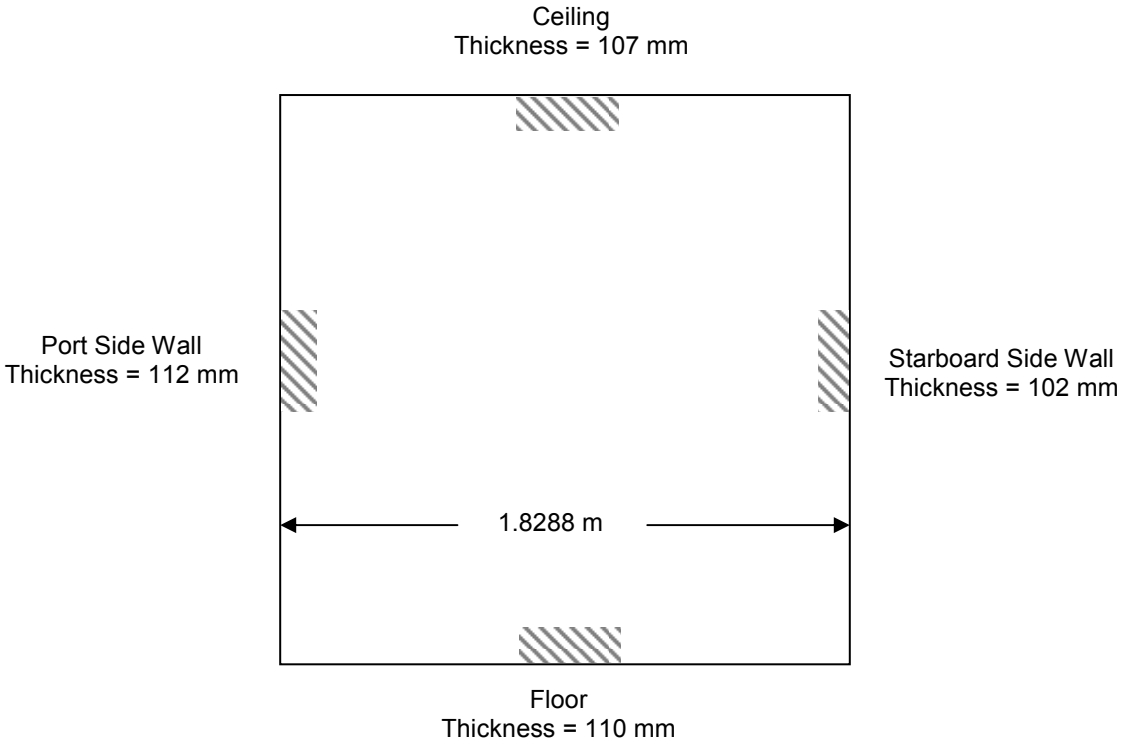

Figure 4-48. Boundary Layer Thickness Distribution on Downstream End of Test Section for 30 m/s

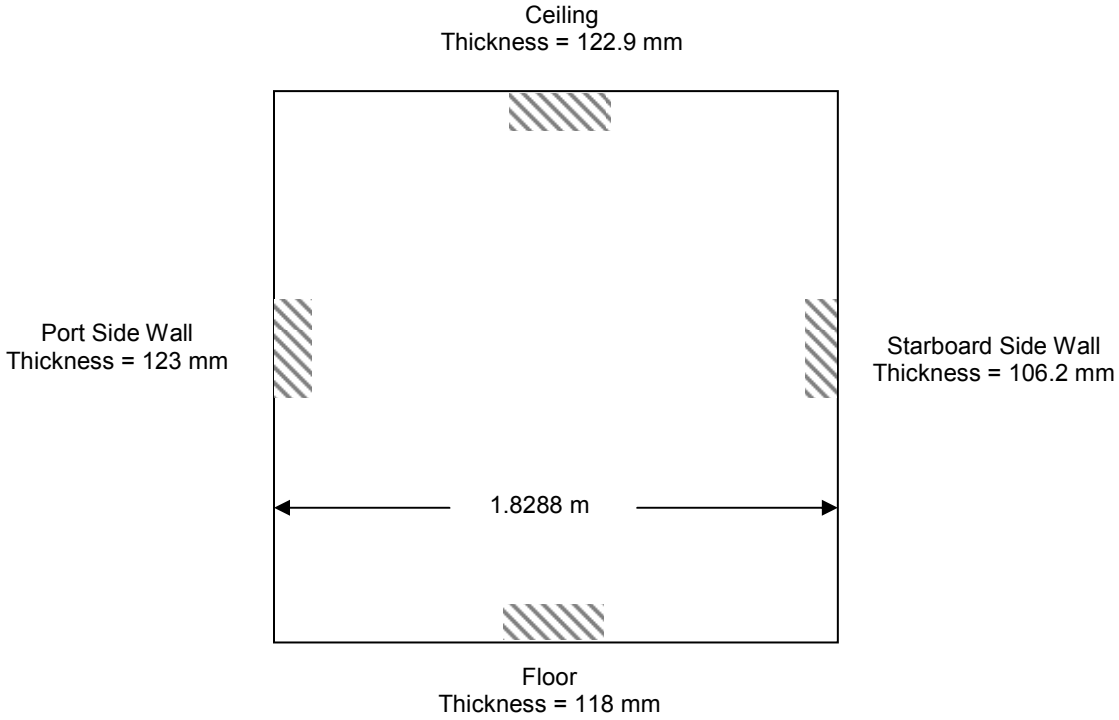

Figure 4-49. Boundary Layer Thickness Distribution on Downstream End of Test Section for 50 m/s

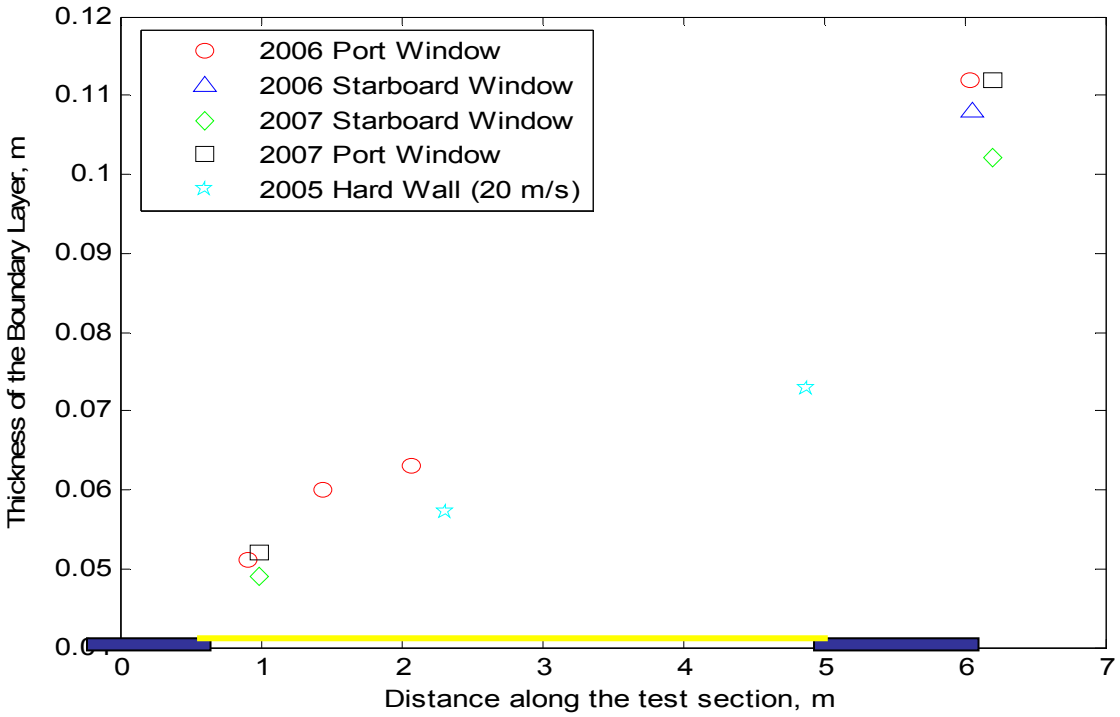

Figure 4-50. Comparison of the Boundary Layer Thickness values for various calibration stages

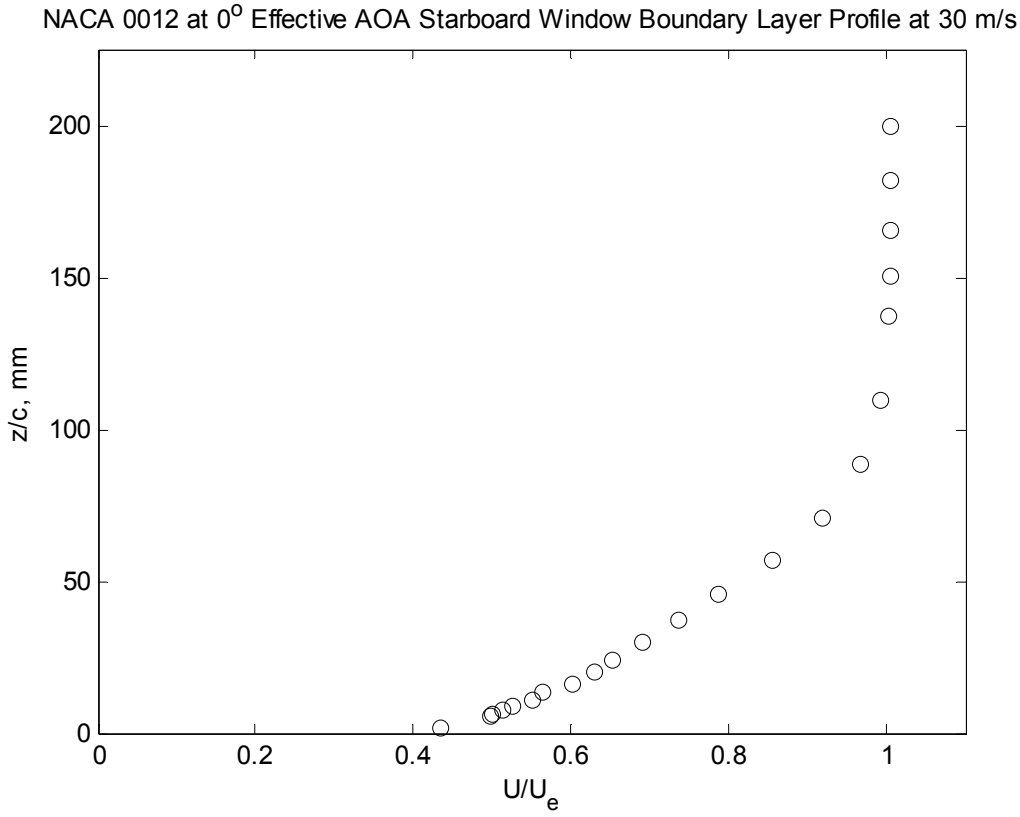

Figure 4-51. Boundary Layer profile with the NACA 0012 model at 0 degrees effective AOA on the starboard side window.

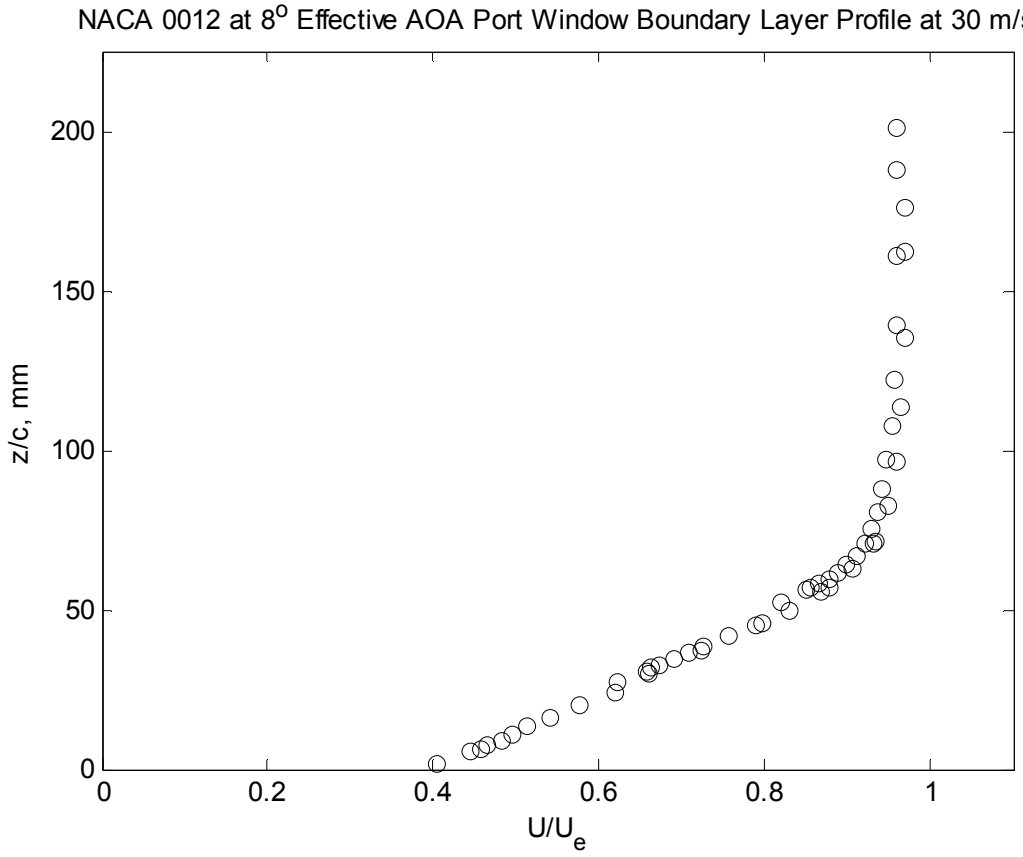

Figure 4-52. Boundary Layer profile with the NACA 0012 model at 8 degrees effective AOA on the port side window.

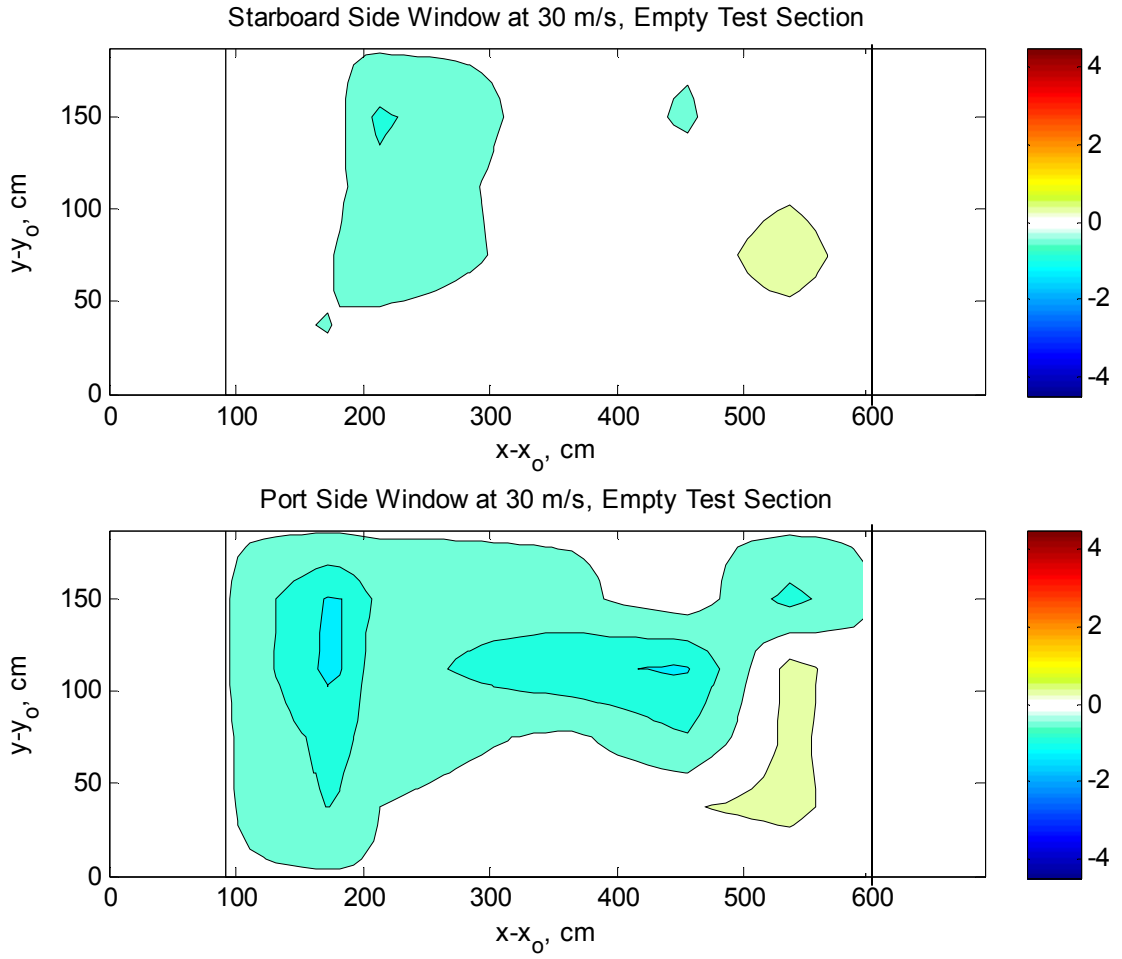

Figure 4-53. Window Deflection Profile for the empty test section at a nominal flow speed of 30 m/s

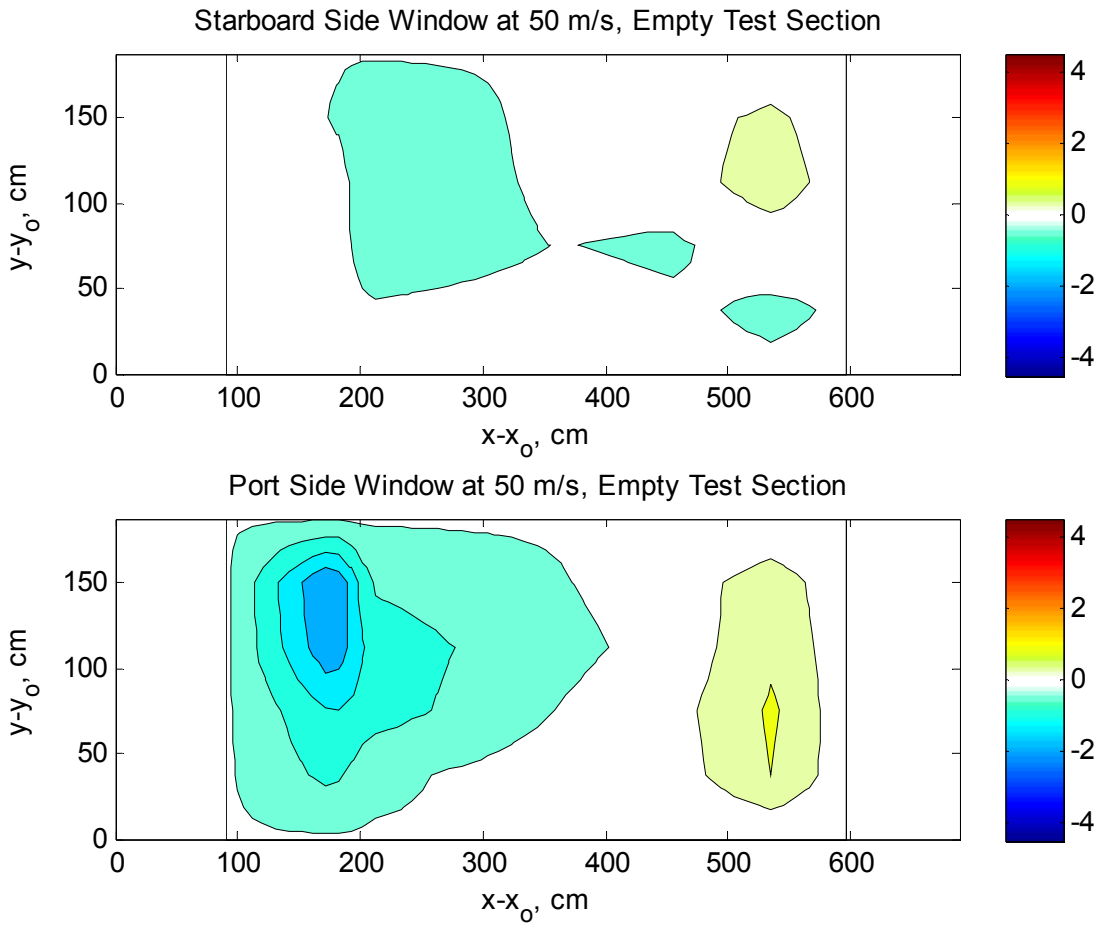

Figure 4-54. Window Deflection Profile for the empty test section at a nominal flow speed of 50 m/s

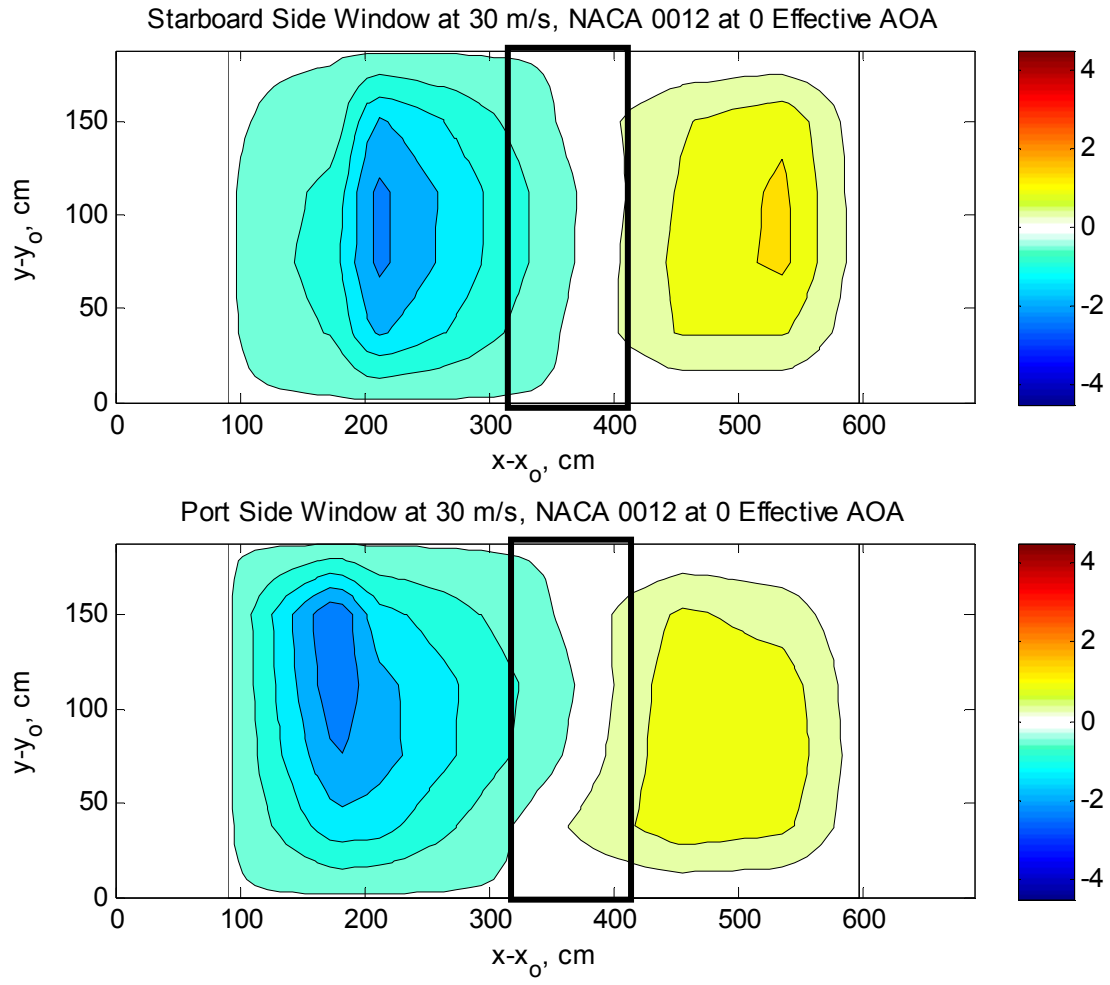

Figure 4-55. Window Deflection Profile with the NACA 0012 model at 0 degrees effective angle of attack at 30 m/s

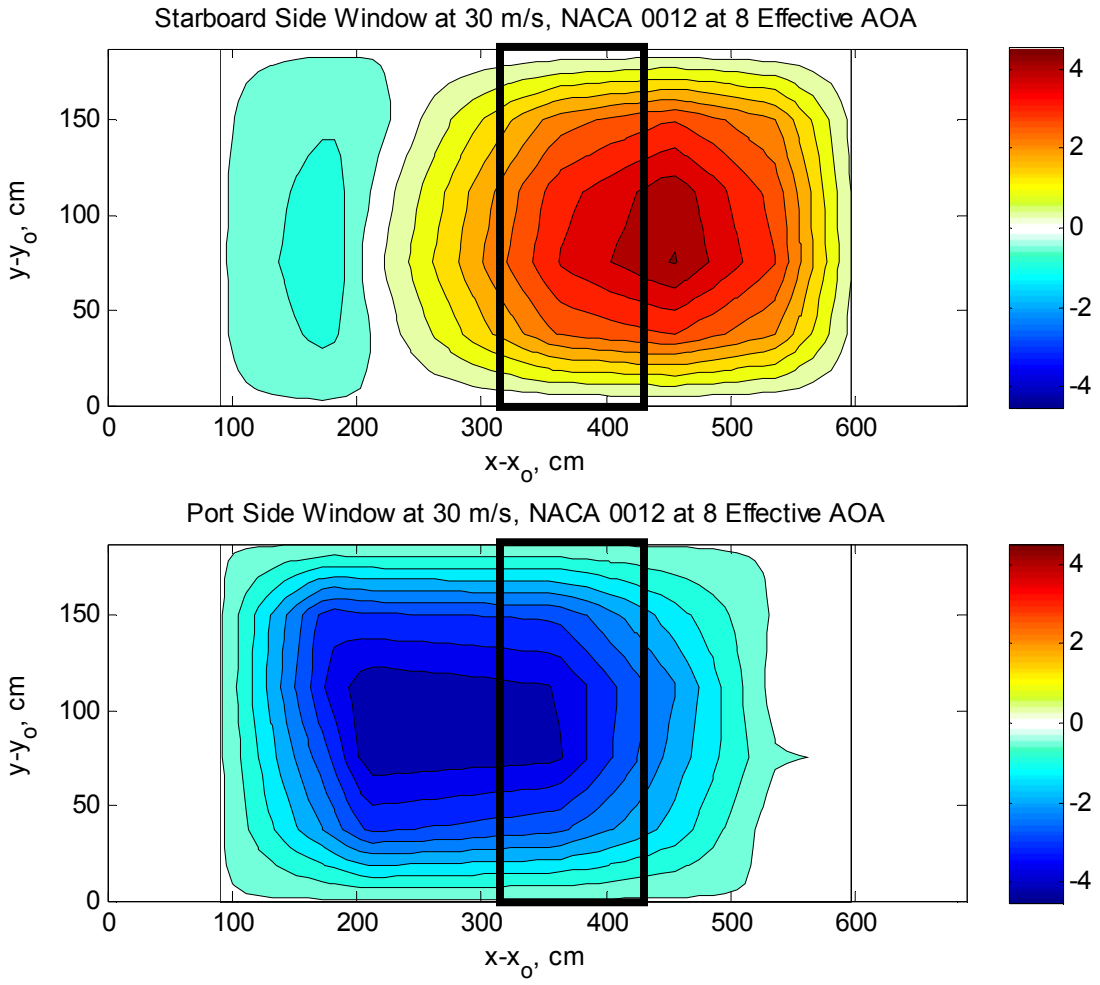

Figure 4-56. Window Deflection Profile with the NACA 0012 model at 8 degrees effective angle of attack at 30 m/s.

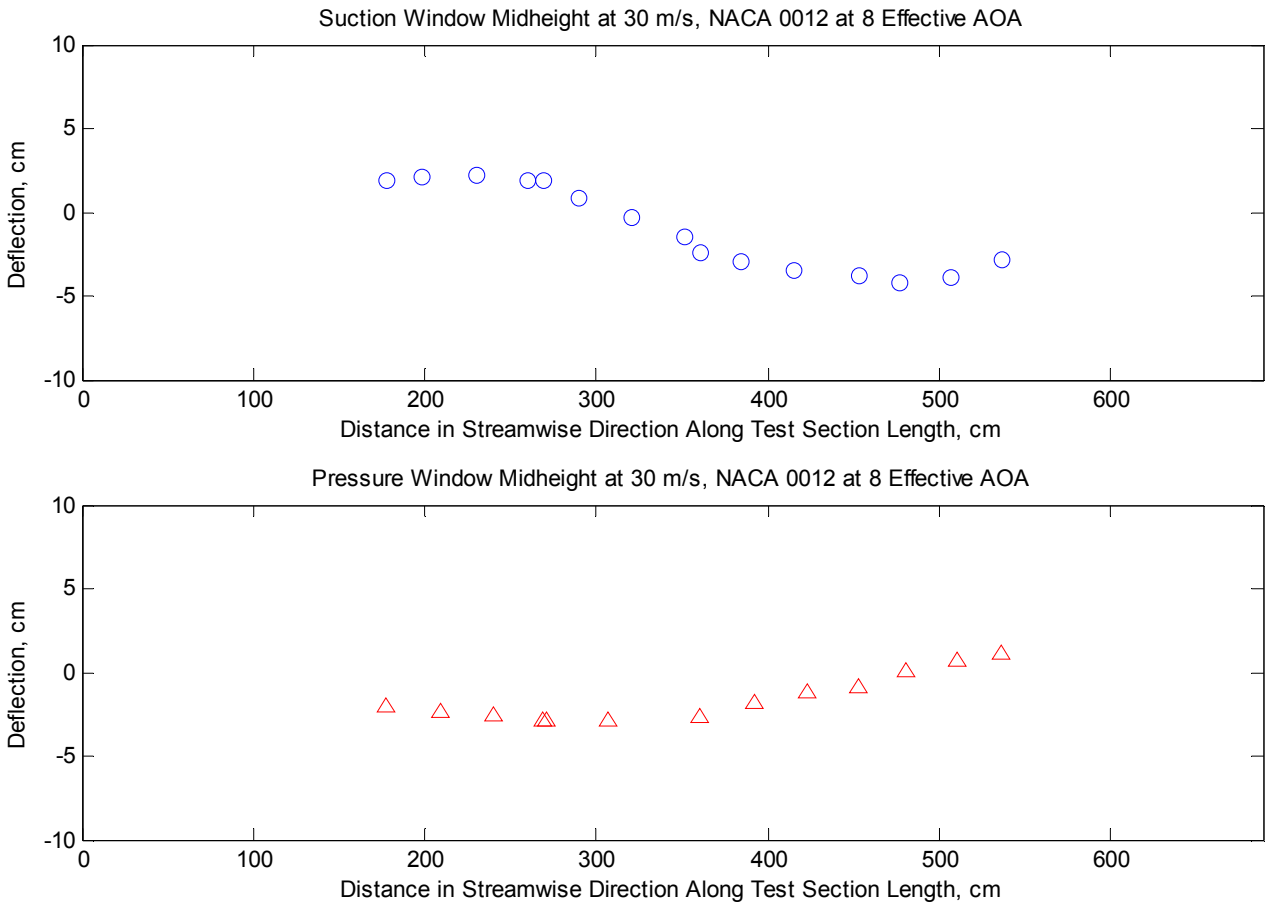

Figure 4-57. Displacement for each window along the midline for the airfoil at 8 degrees effective angle of attack

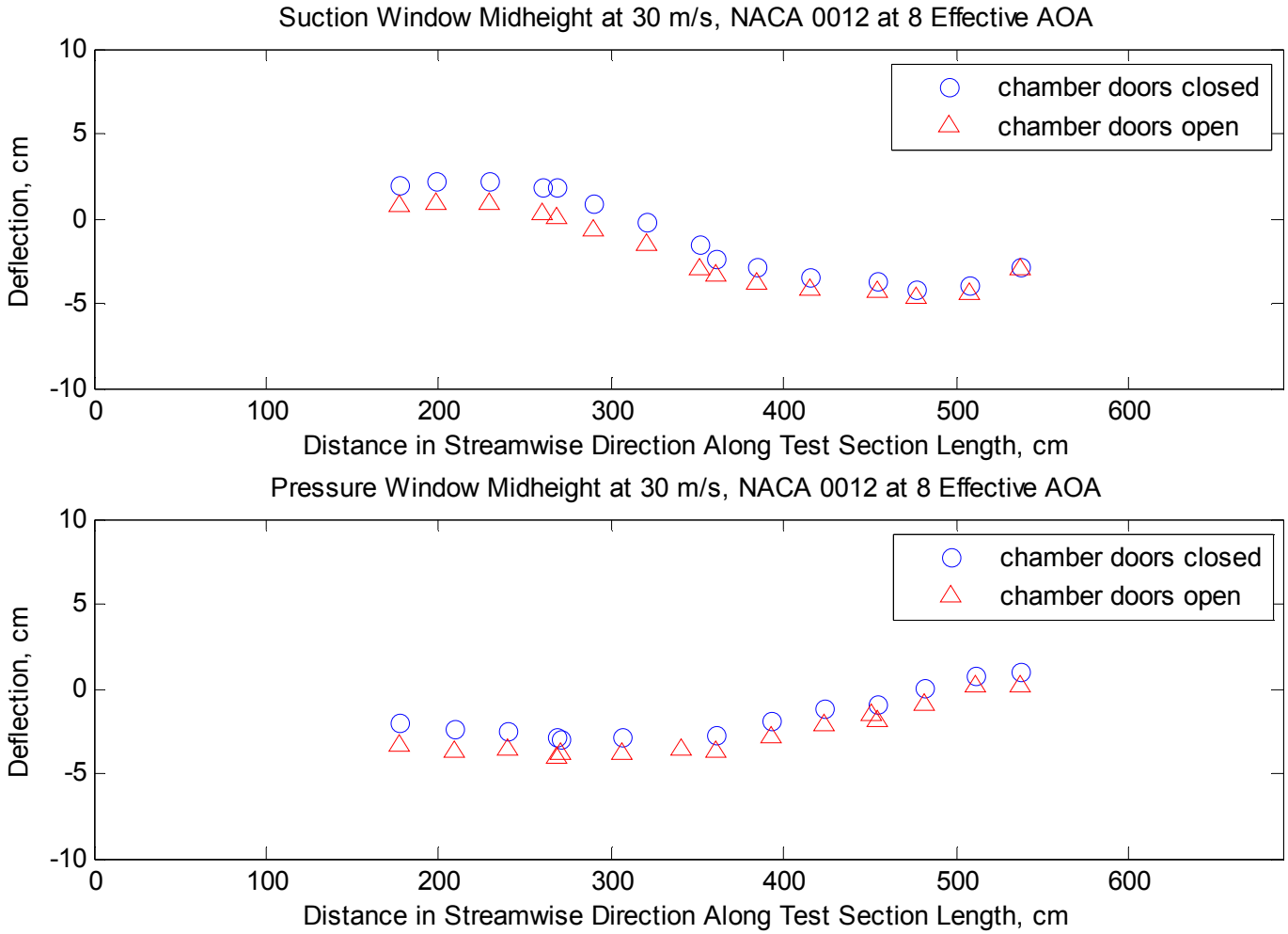

Figure 4-58. Displacement for each window along the midline for the airfoil at 8 degrees effective angle of attack with the chamber doors open and then closed

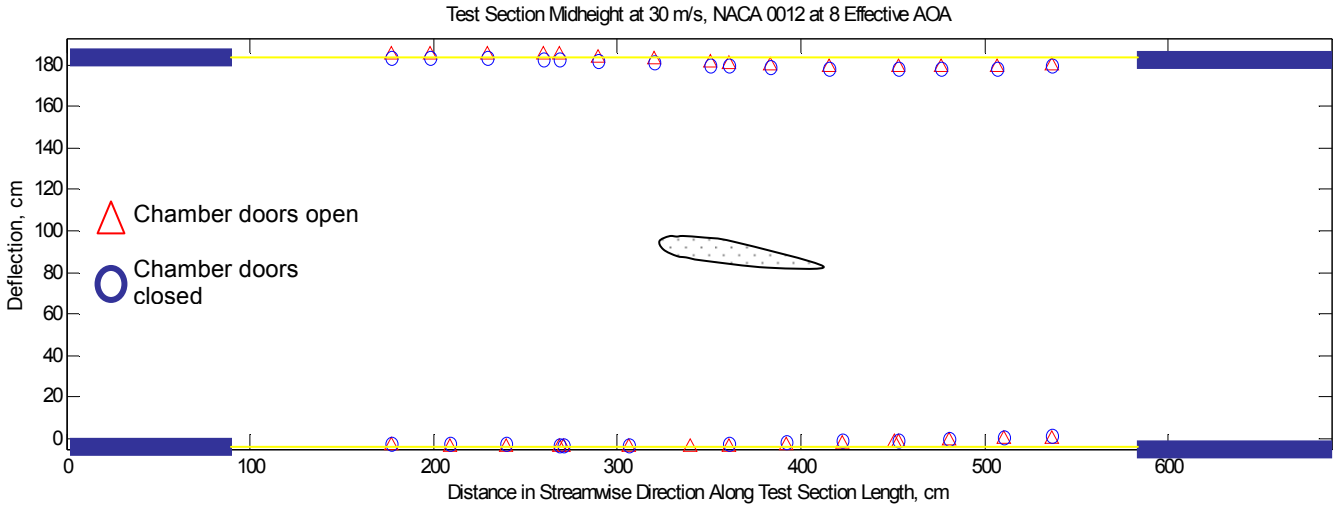

Figure 4-59. Displacement for each window along the midline for the airfoil at 8 degrees effective angle of attack, shown on the scale of the tunnel

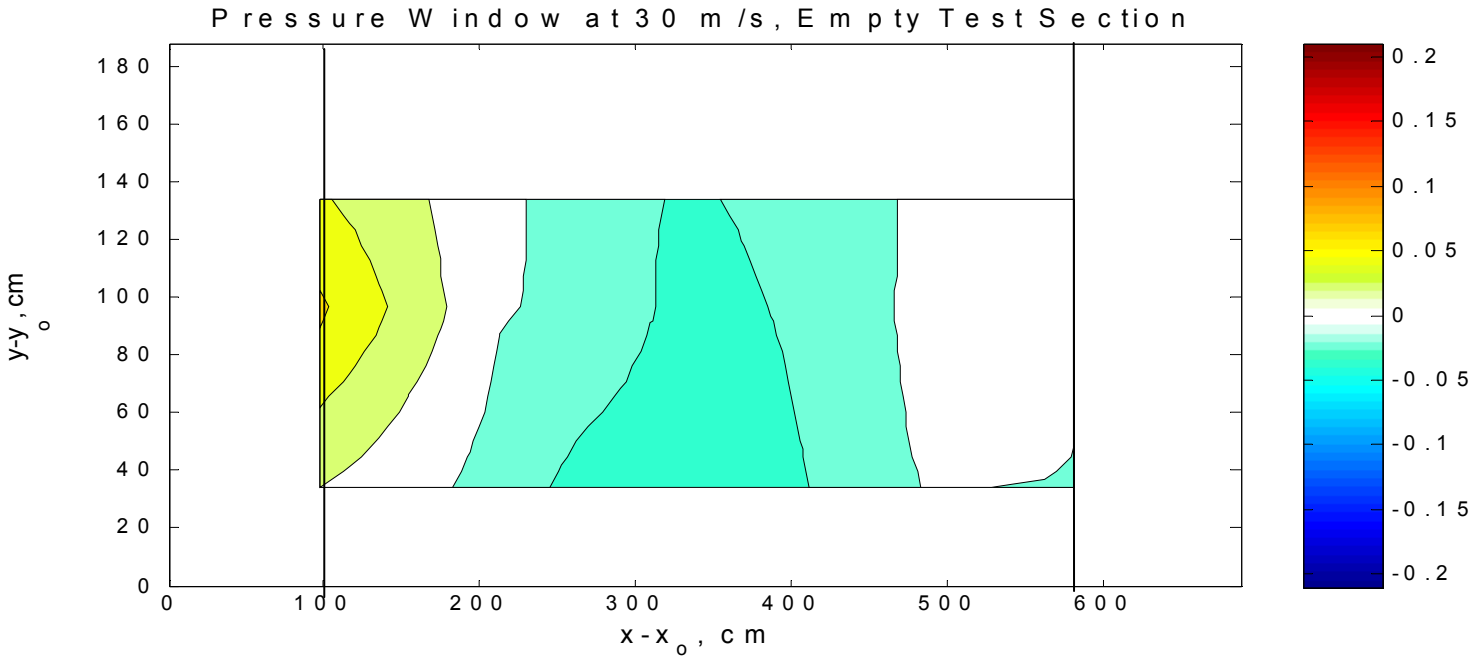

Figure 4-60. Variation of the static pressure coefficient along the window for the empty test section at a nominal flow speed of 30 m/s

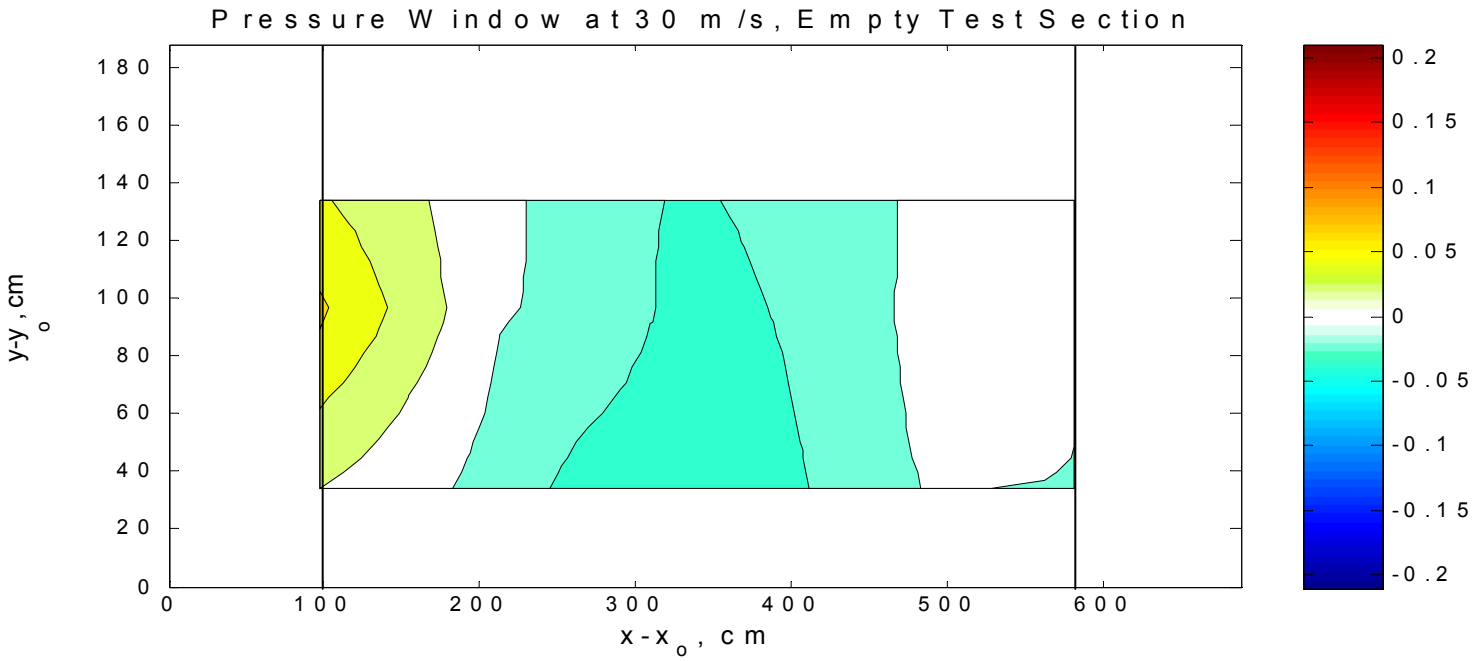

Figure 4-61. Variation of the static pressure coefficient along the window for the empty test section at a nominal flow speed of 50 m/s

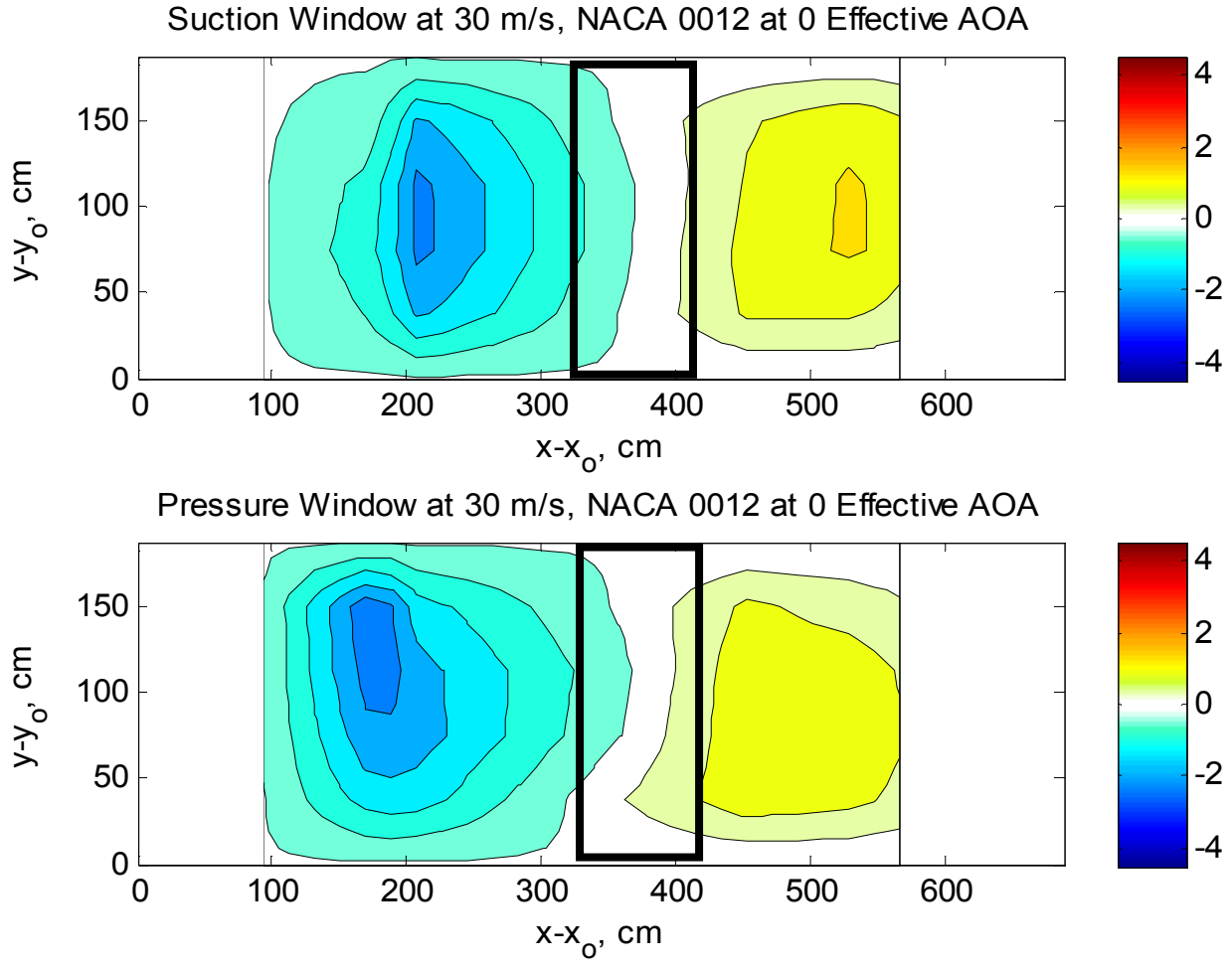

Figure 4-62. Variation of the static pressure coefficient along the window for the NACA 0012 model at 0 degrees effective angle of attack and a nominal flow speed of 30 m/s

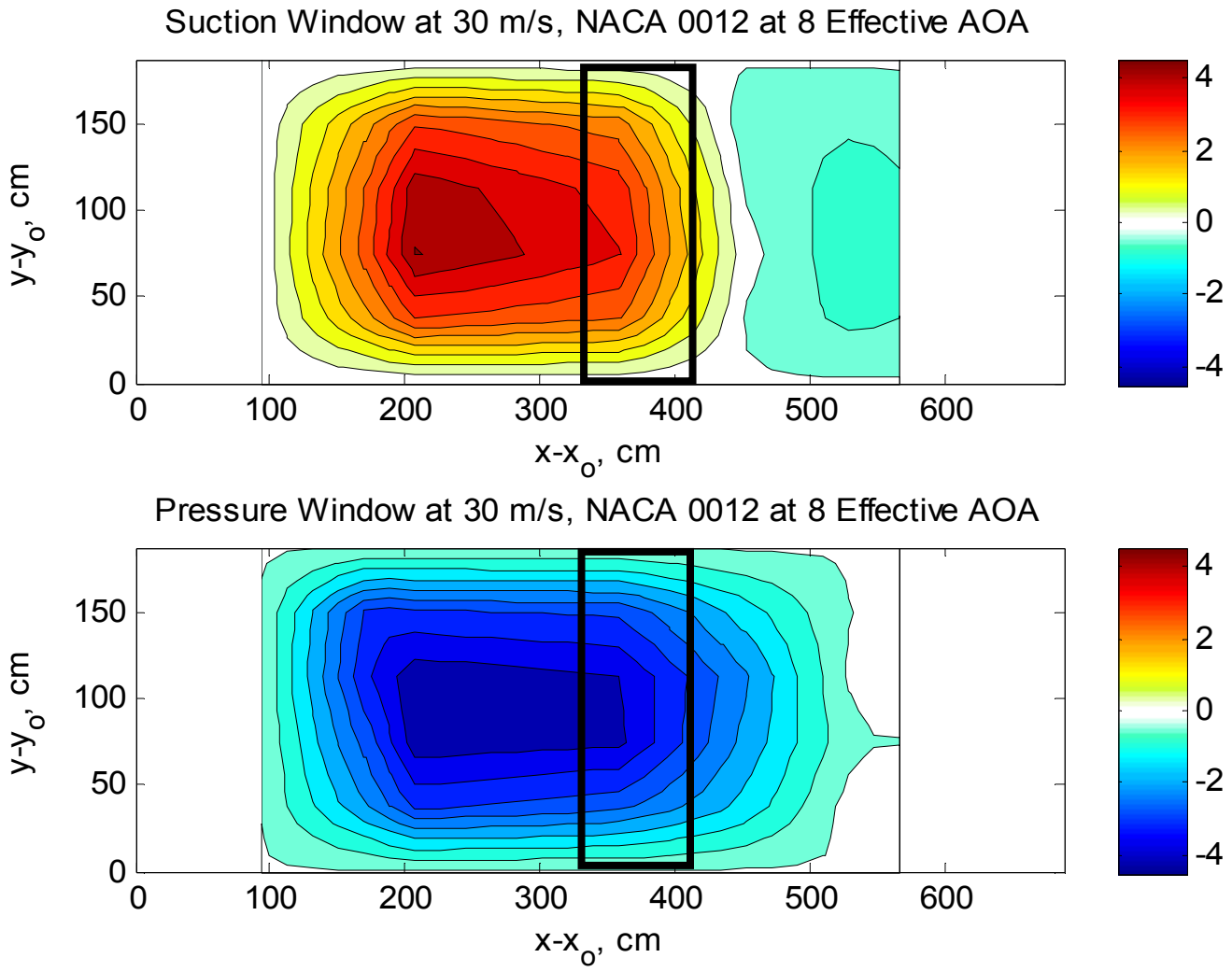

Figure 4-63. Variation of the static pressure coefficient along the window for the NACA 0012 model at 8 degrees effective angle of attack and a nominal flow speed of 30 m/s

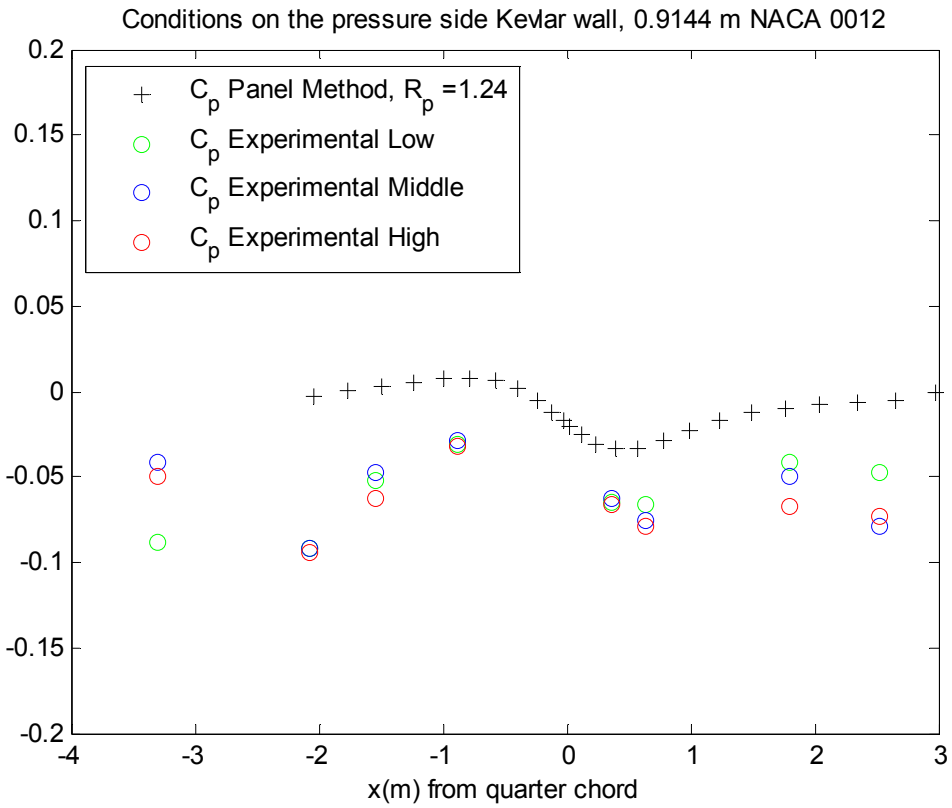

Figure 4-64. Comparison of the prediction method to the experimental window pressure measurements for the NACA 0012 model at a 0 degree effective angle of attack.

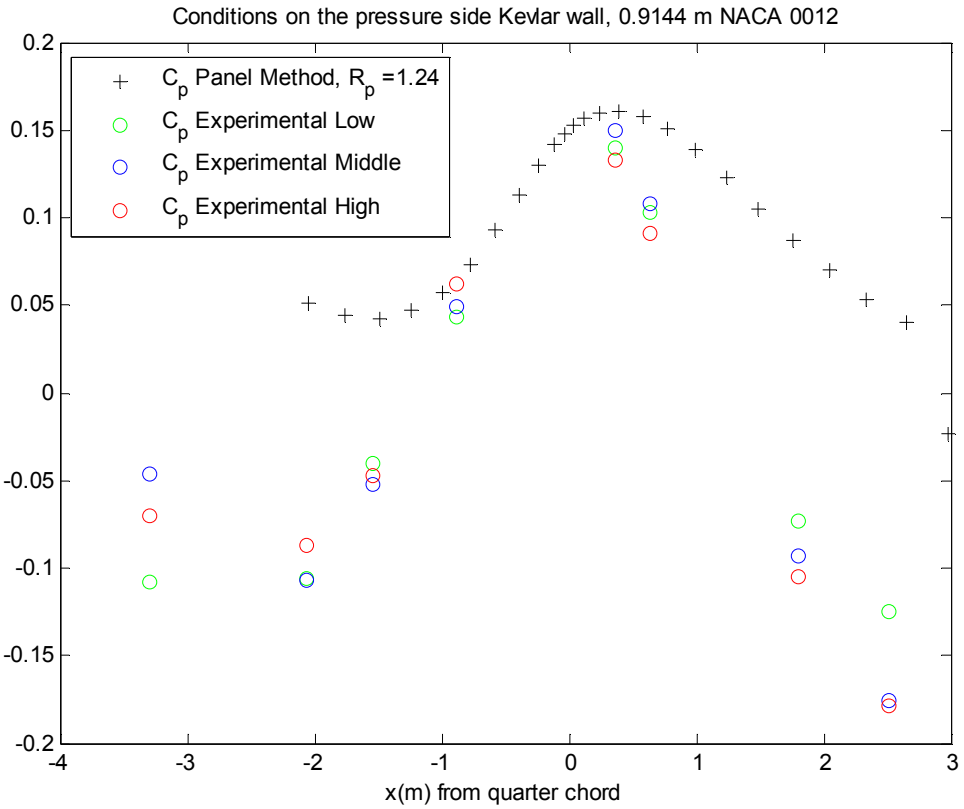

Figure 4-65. Comparison of the prediction method to the experimental window pressure measurements for the NACA 0012 model at a 8 degree effective angle of attack.

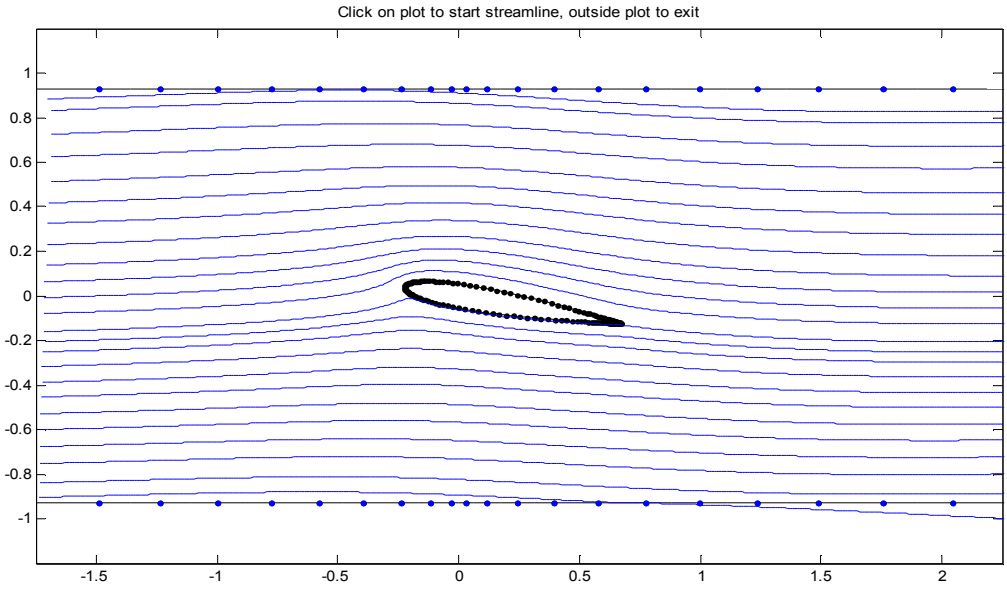

Figure 4-66. Streamlines for the prediction method with the porosity coefficient calibrated.

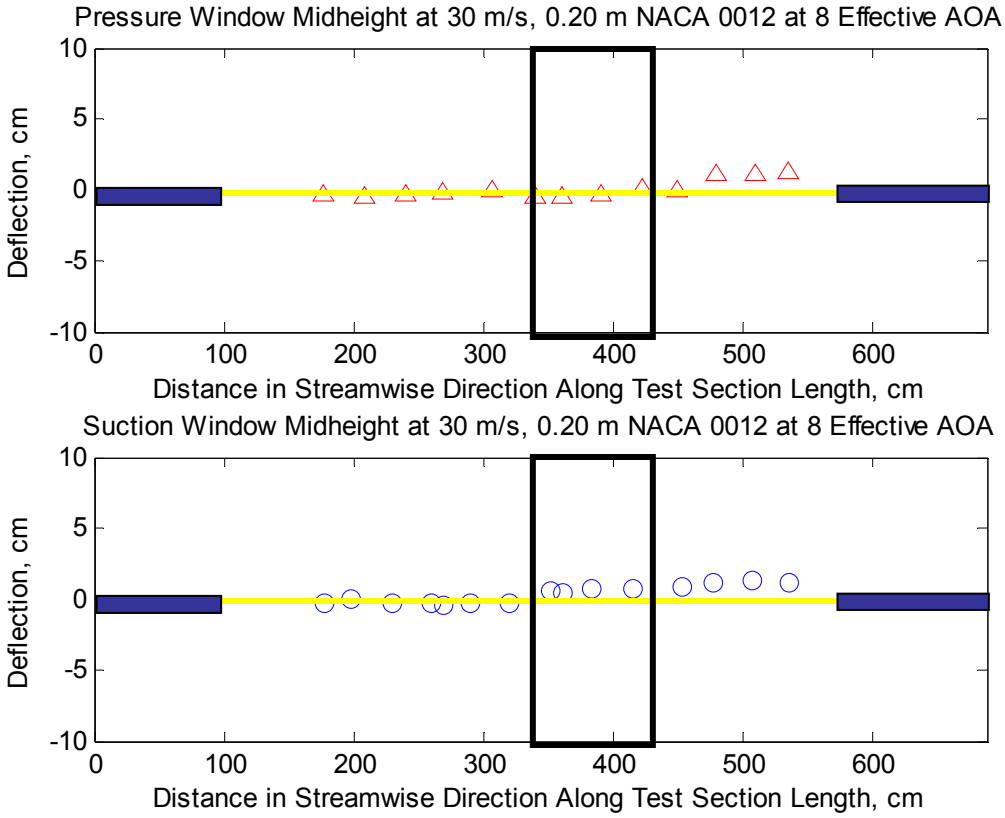

Figure 4-67. Displacement for each window along the midline for the 0.20 m NACA 0012 airfoil at 8 degrees effective angle of attack

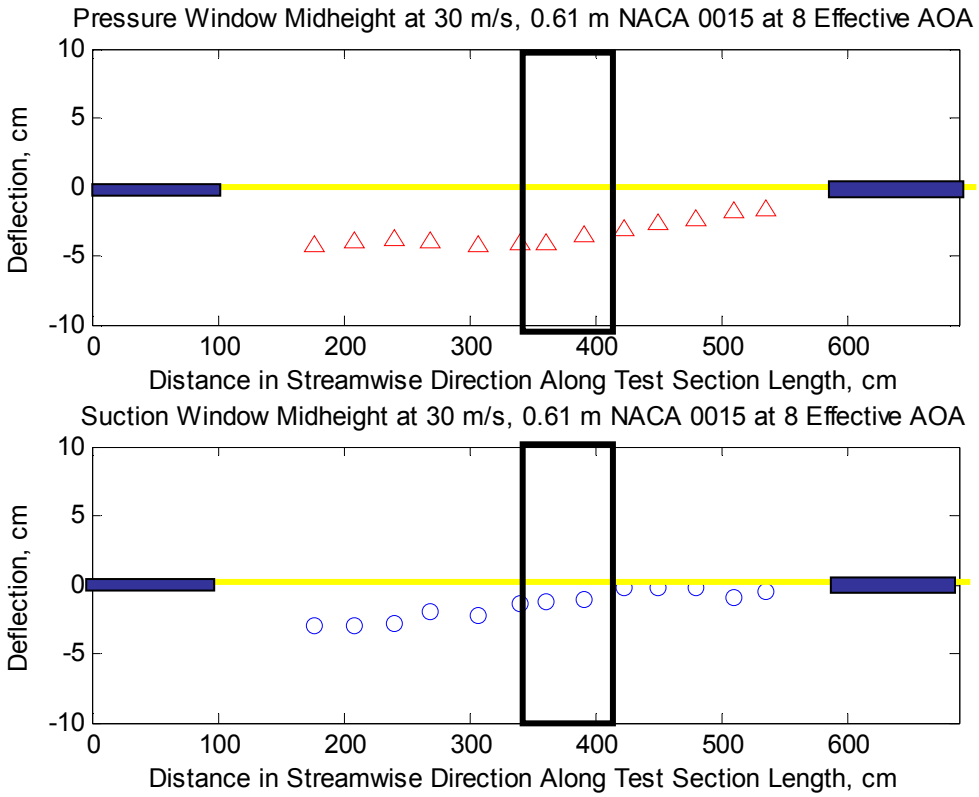

Figure 4-68. Displacement for each window along the midline for the 0.61 m NACA 0015 airfoil at 8 degrees effective angle of attack

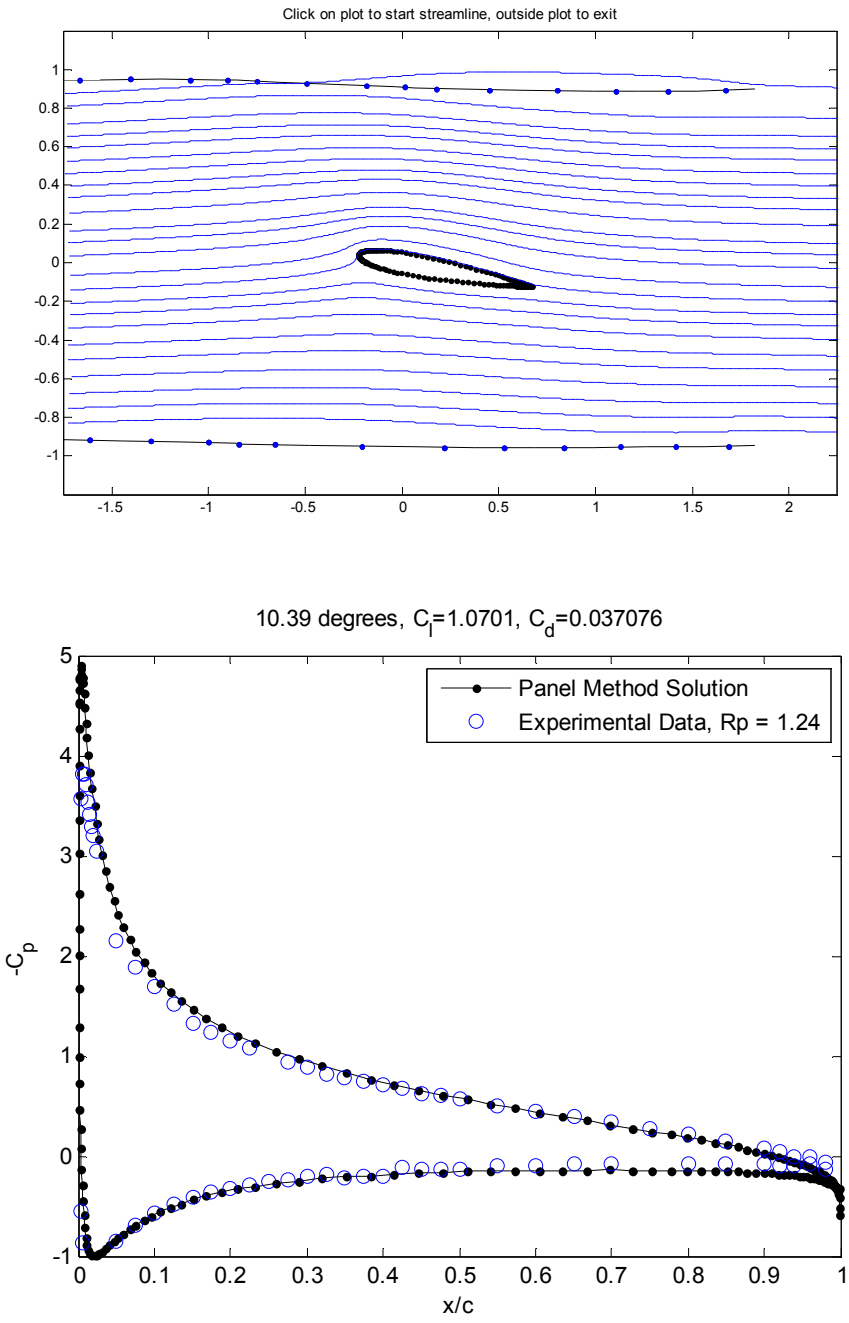

Figure 4-69. Streamline pattern for the prediction method modified to account for the deflection of the windows for the NACA 0012 (0.91 m) at 8 degrees effective angle of attack (top) and comparison of the measured to predicted pressure distribution (bottom)

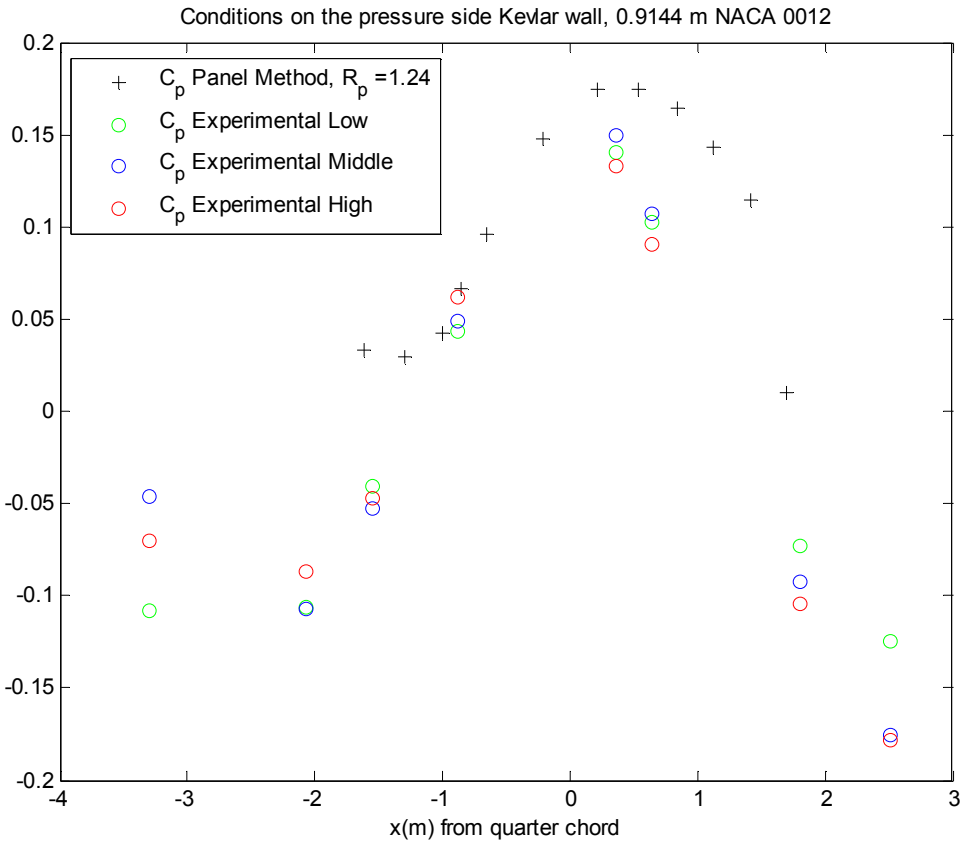

Figure 4-70. Comparison of the prediction method modified for the window deflection to the experimental window pressure measurements for the NACA 0012 model at an 8 degree effective angle of attack.

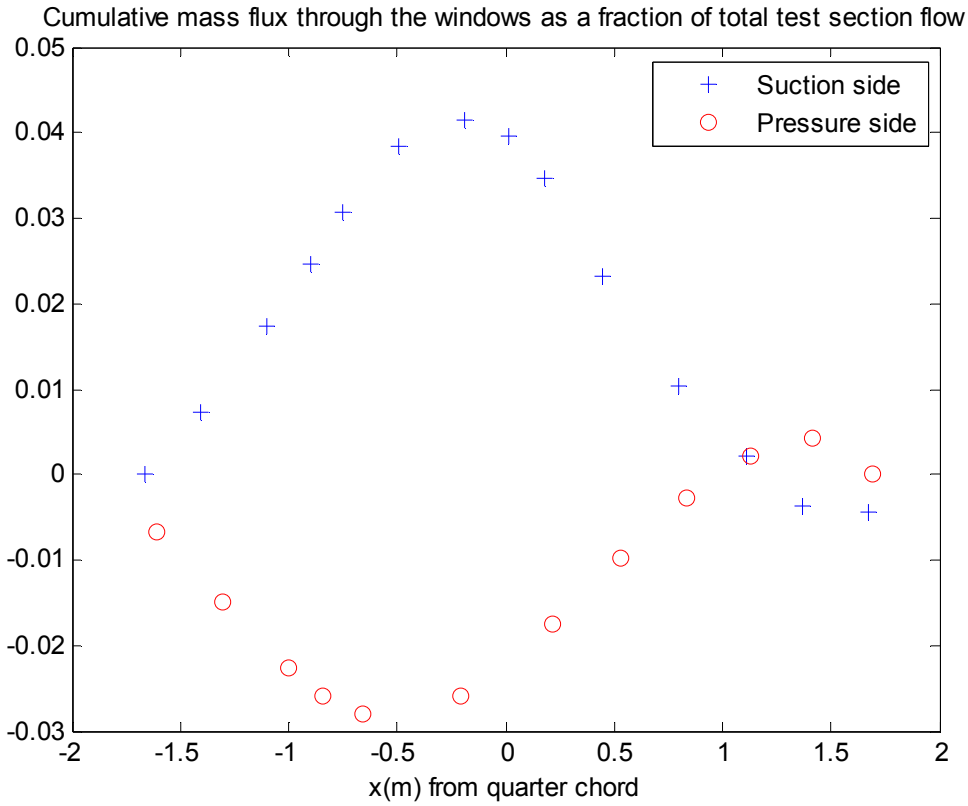

Figure 4-71. Prediction method calculation of the cumulative mass flow for the NACA 0012 model at an 8 degree effective angle of attack

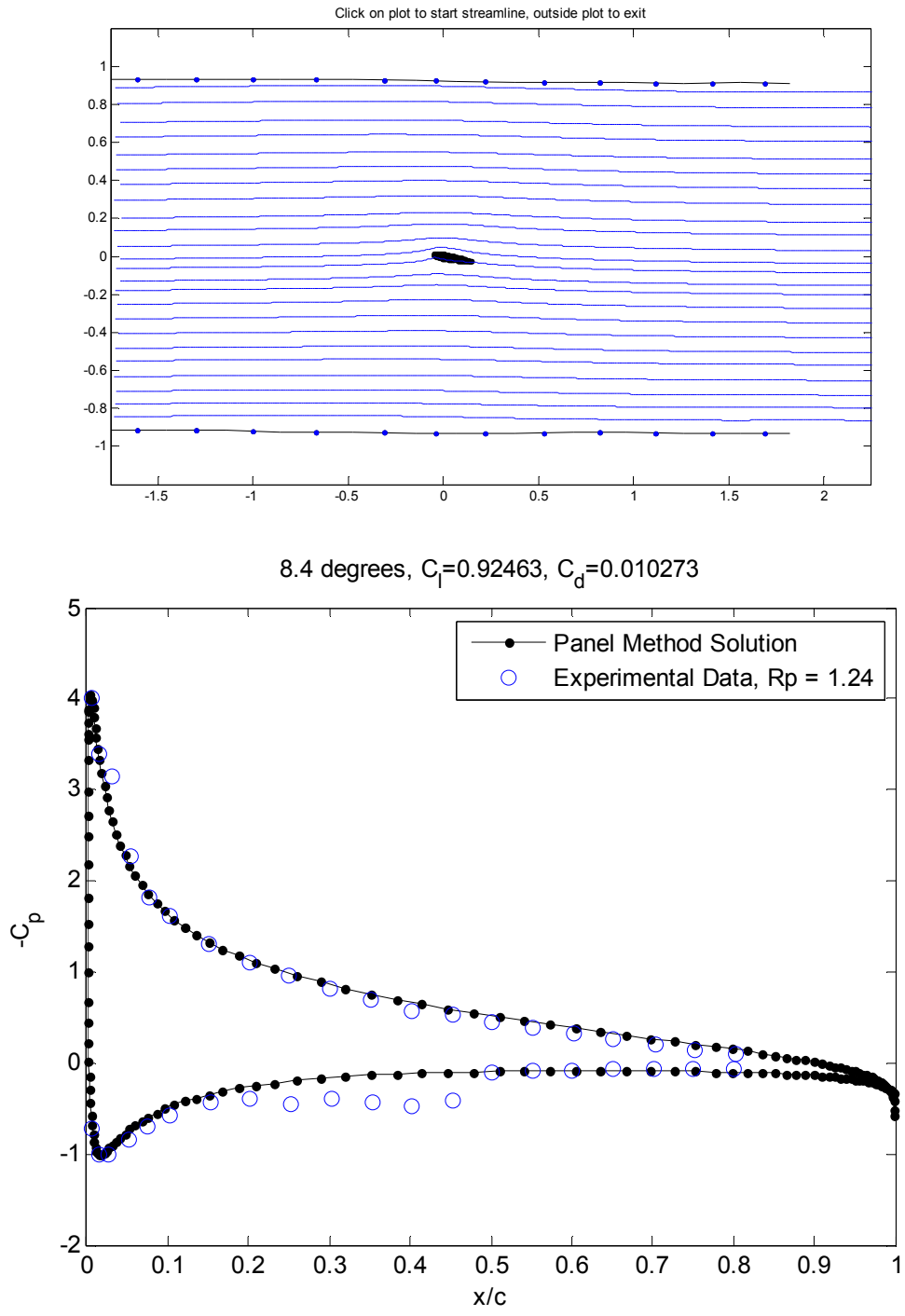

Figure 4-72. Streamline pattern for the prediction method modified to account for the deflection of the windows for the NACA 0012 (0.21 m) at 8 degrees effective angle of attack (top) and comparison of the measured to predicted pressure distribution (bottom)

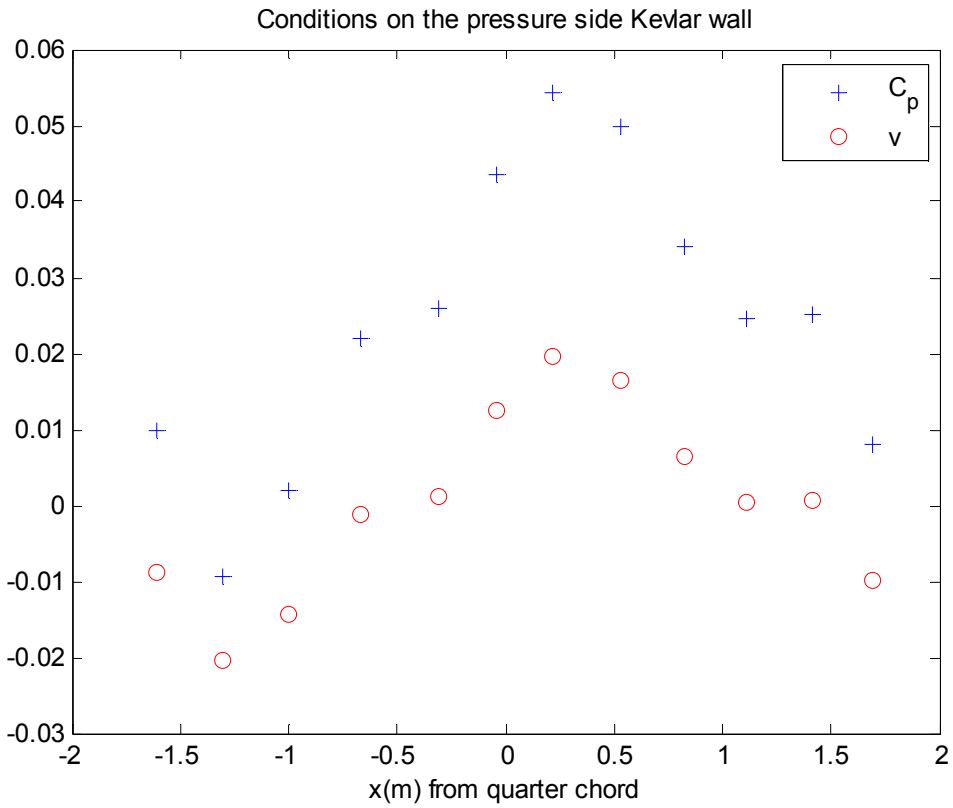

Figure 4-73. Prediction method calculation the static pressure coefficient variation along the pressure side widow for the NACA 0012 (0.20 m) model at an 8 degree effective angle of attack.

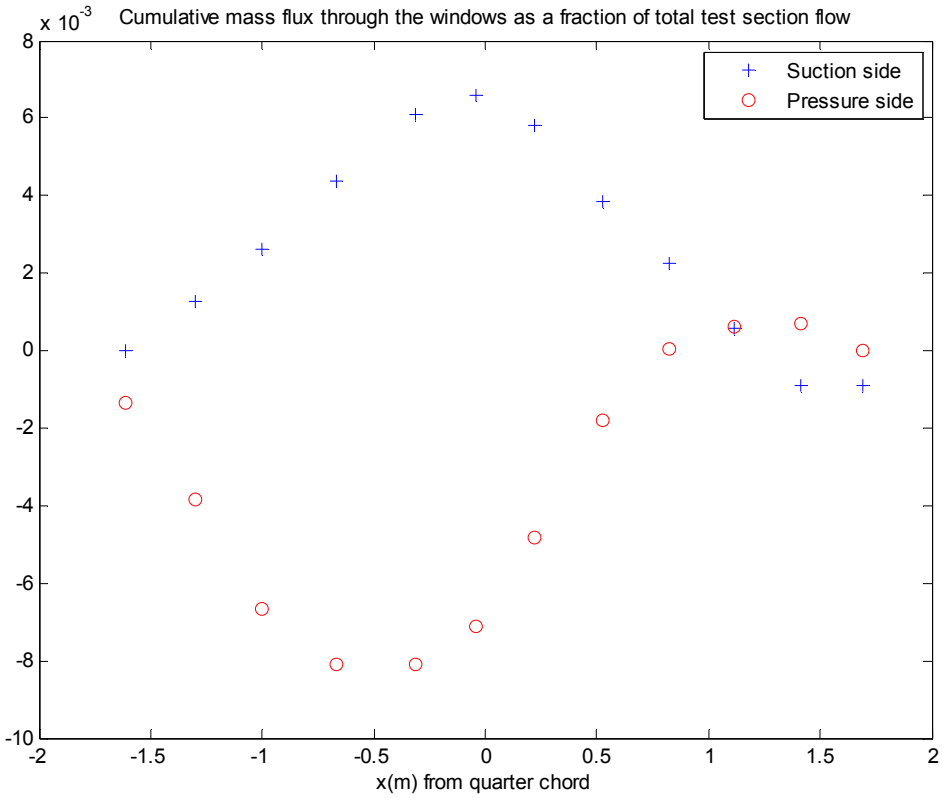

Figure 4-74. Prediction method calculation of the cumulative mass flow for the NACA 0012 (0.20 m) model at an 8 degree effective angle of attack.

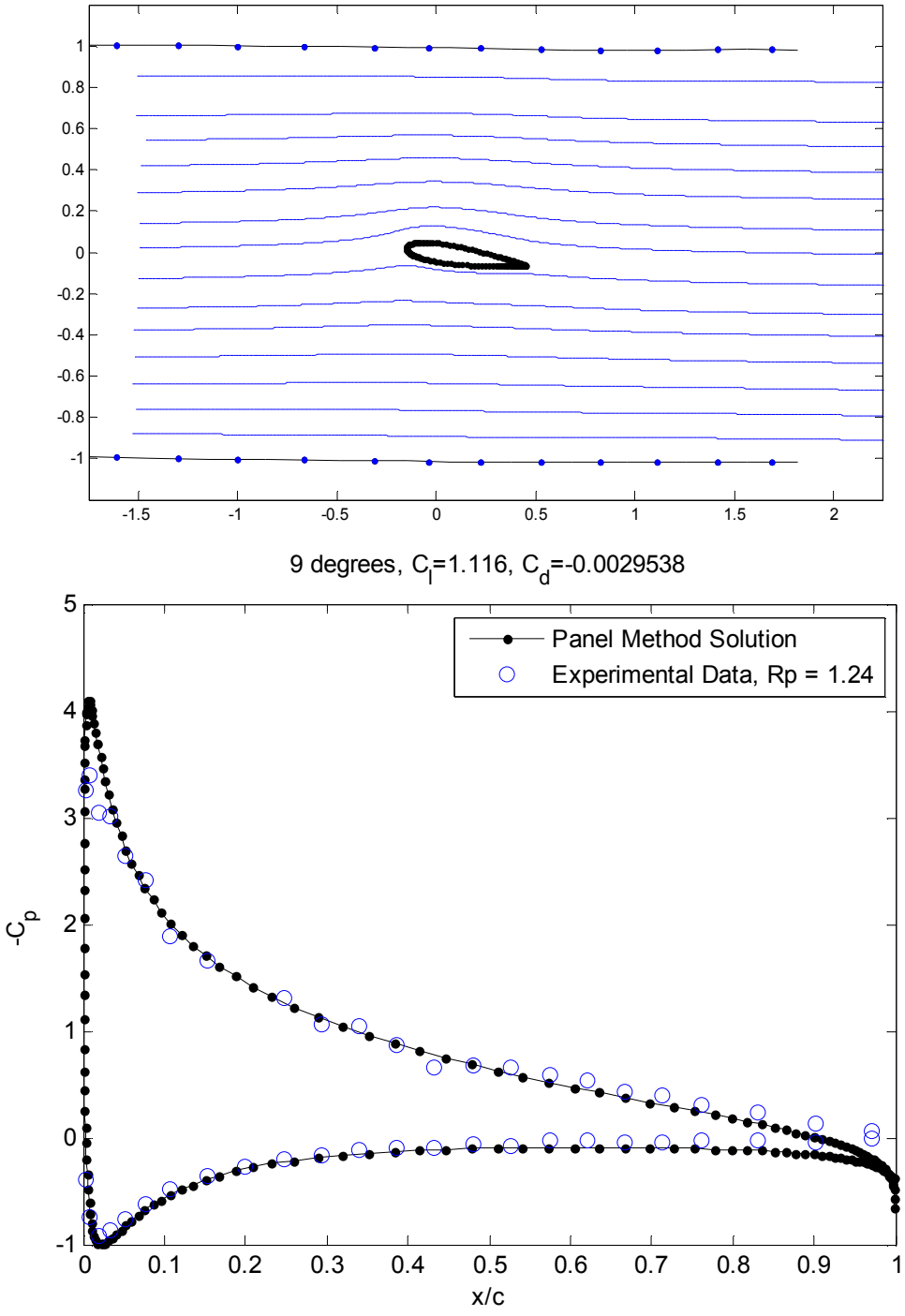

Figure 4-75. Streamline pattern for the prediction method modified to account for the deflection of the windows for the NACA 0015 (0.61 m) at 8 degrees effective angle of attack (top) and comparison of the measured to predicted pressure distribution (bottom)

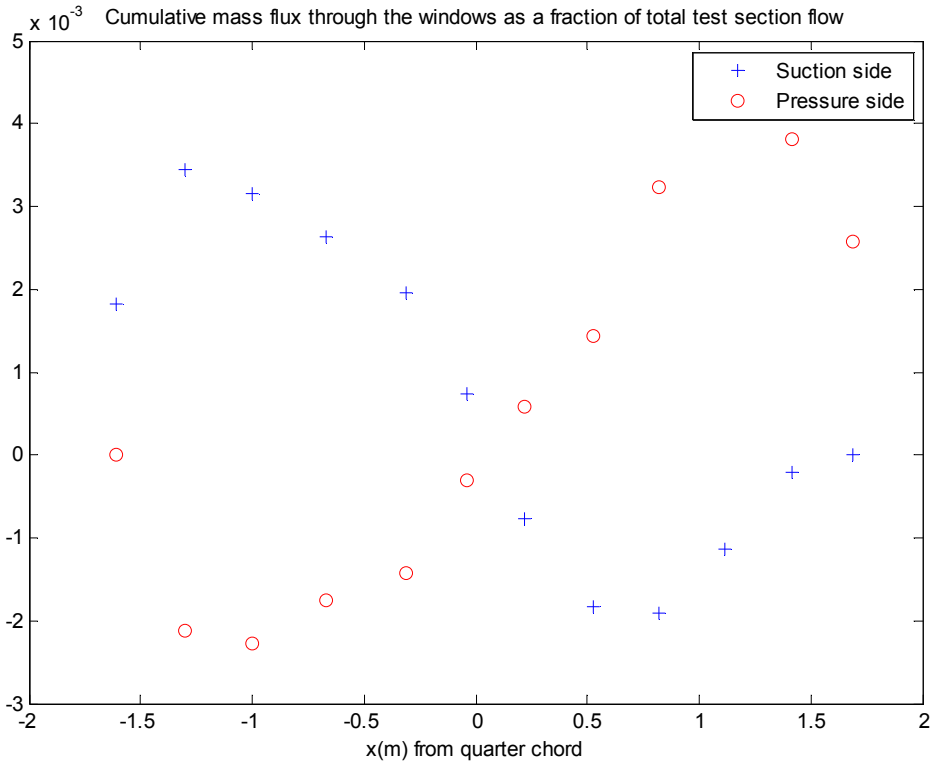

Figure 4-76. Prediction method calculation of the cumulative mass flow for the NACA 0015 (0.61 m) model at an 8 degree effective angle of attack.

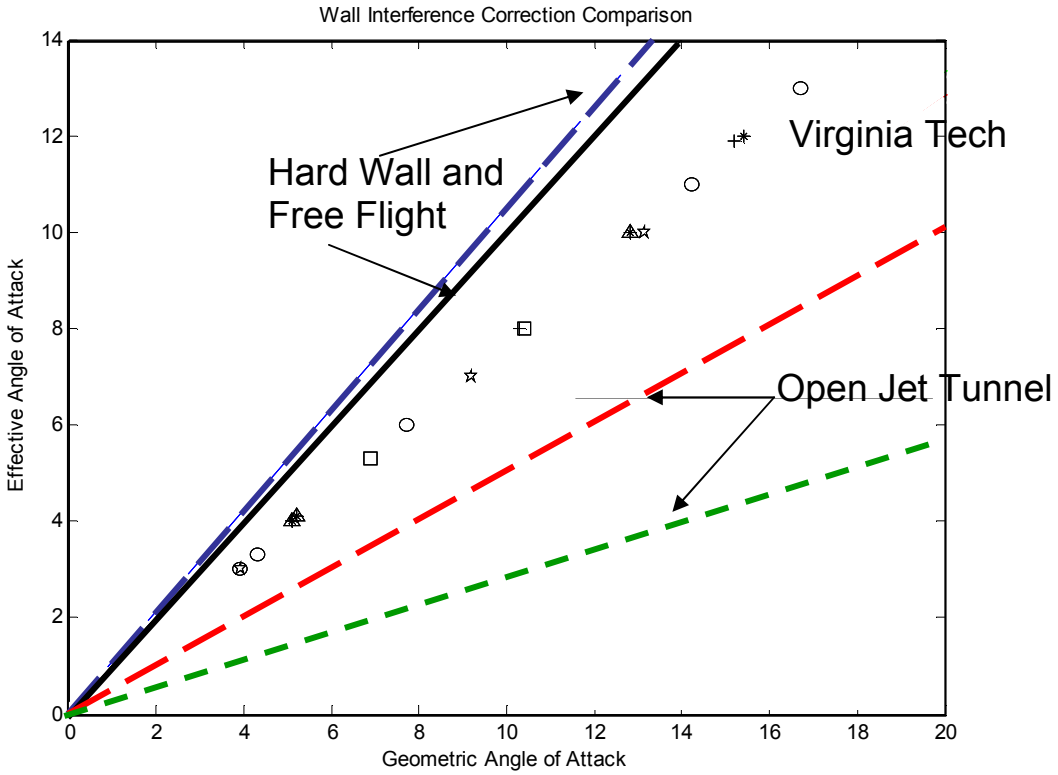

Figure 4-77. Comparison of several other values for lift interference corrections; for free flight, hard wall tunnel condition and two open jet configurations.

5. CONCLUSIONS

The acoustic treatment and calibration of a new anechoic system for the Virginia Tech Stability Wind Tunnel has been performed. This novel design utilizes tensioned Kevlar cloth to provide a stable flow boundary, which eliminates the need for a free jet and jet catcher. As part of the validation process a series of measurements were performed both to confirm the reduction in overall test section noise levels and to ascertain the effect of these modifications on the test section aerodynamics under a range of conditions.

With the completed facility installed in 2006 several preliminary measurements were taken to compare with the prototype configuration. Measurements were taken of the background noise levels in the test section as well as a full test matrix covering the performance of the Kevlar windows. Both the deflection of the windows, and the potential for air flow through the windows was considered for a variety of flow speeds in the empty tunnel. Additionally preliminary measurements of the boundary layer thickness for the inlet and exit of the test section, as well as at various locations along the Kevlar windows was computed. The Kevlar window performance tests, as well as the boundary layer profiles were repeated with the 0.6096 m chord NACA 0015 model installed for a variety of flow speeds and angles of attack. A preliminary interference correction was determined as well.

Following the preliminary facility installation and calibration in 2006, the treatment of the hard wall tunnel circuit was accomplished. A total of 223 square meters of the circuit was treated with a combination of 5 cm thick Urethane and Melamine foam. Additionally a custom designed treatment was installed around the fan blades as well as the northeast turning vane set. These included baseline experiments that reveal the aerodynamic and aeroacoustic performance of the tunnel in its original solid wall configuration, including measurements of the hard wall flow quality and back ground noise levels. Following the treatment of the test section circuit, several acoustic measurements were taken to determine the effect on the overall background noise levels. Additionally the fan RPM as a function of flow speed was considered to ensure there were no adverse aerodynamic effects.

Following the completion of the circuit treatment, several modifications were made to the anechoic test section before reinstallation for the facility validation in 2007. These modifications include the design of a new quiet model catcher installed upstream of the fan and the installation of acoustic absorbers into the walls of the test section at the inlet and exit. Several new pieces of equipment were also designed to increase the accuracy and reduce the uncertainty for the aerodynamic measurements that would be repeated for the 2007 validation. This equipment included a boundary layer and wake probe rake as well as a window pressure measurement rail.

With the 2007 facility installed a wide range of measurements were taken to compare with the prototype and 2006 configurations. Measurements were taken of the background noise levels in the test section, both in and out of the flow, as well as a full test matrix covering the performance of the Kevlar windows. Both the deflection of the windows, and the potential for air flow through the windows was considered for a variety of flow speeds in the empty tunnel. Additionally measurements of the boundary layer thickness as well as displacement and momentum thickness were measured and computed for the inlet and exit of the test section. The Kevlar window performance tests, as well as the boundary layer profiles were repeated with the 0.9144 m chord NACA 0012 model installed for a variety of flow speeds and angles of attack. Finally the interference correction was determined experimentally for several models of varying thickness and camber. These results were compared to a panel method prediction that accounts for the porosity and the displacement of the windows.

The following conclusions were drawn:

1. **The acoustic treatment reduces background noise levels to a value comparable with other facilities**. Fan tones dominate the noise levels in the original hard wall configuration at low frequencies and broadband noise dominates at high frequencies. Overall A-weighted sound pressure levels increase as the sixth power of the flow velocity, reaching 109dB at 64 m/s (Camargo *et al*). The addition of the acoustic treatment to the wind tunnel circuit and around the fan housing reduces the background noise levels by as much as 10 dB across the frequency range. With the addition of the modified anechoic facility, the back ground noise levels are reduced even further, to give

overall levels with the completed facility that are as much as 25 dB below the original solid wall configuration. In this configuration the Virginia Tech Stability Wind Tunnel has noise levels comparable, and in many cases much lower, than a large number of other aeroacoustic facilities.

2. **The Kevlar walls can replace a free jet and jet catcher**. Measurements taken both within the test section and in the adjacent chambers also show that large Kevlar windows can be used to quietly and stably contain the flow, eliminating the need for an open-jet and jet catcher system. Measurements of the window deflection over a range of flow speeds in the empty test section and with the model installed show window displacement values at 30 m/s of less than 1 cm (empty test section) and less than 4 cm (NACA 0012 at 8 degrees effective angle of attack). Boundary layer growth for the anechoic test section was approximately 30% larger than for the hard wall section, presumably due to the porosity of the Kevlar windows. Additionally no vibration of the window was observed and phased array measurements made with and without the airfoil demonstrated their acoustic transparency.

3. **The aerodynamic characteristics of an airfoil model mounted in the Kevlar walled test section are consistent with theoretical expectations.** Mean pressure distributions were measured for a NACA 0012 airfoil section at various angles of attack and Reynolds numbers. The measured pressure distributions agreed well with a 2-D inviscid solution at the computed effective angles of attack. Additional mean pressure distributions of several other models of varying thickness and camber were compared to a panel method approximation. These distributions showed good agreement over a wide range of the model edge length at effective angles of attack computed in the same manner as the NACA 0012.

4. **The Kevlar windows reduce the lift interference compared to an open jet tunnel**. Interference effects with the Kevlar side walls can accurately be accounted for using an effective angle of attack. The effective angle correction is a constant fraction of the geometric angle, -22% in the present case, this was reduced from the -28% value

determined during the prototype testing. The correction is significantly less than that expected for free jet correction of -50 to -73%. The observed transpiration through the Kevlar windows is thought to be responsible for most of the residual correction. Panel method comparison of the NACA 0012 model at 8 degrees effective angle of attack shows a predicted window pressure distribution that is comparable to that measured at the same conditions. Further reduction of the interference correction may be possible with increased tensioning of the window and ensuring a true air tight seal between the chambers and the test section boundary.

REFERENCES

1. Brooks, T. F., Pope, D. S., and Marcolini, M. A., "Airfoil Self Noise and Prediction," NASA-RP-1218, 1989.
2. Barlow, J., Rae, A., and Pope, A., Low Speed Wind Tunnel Testing, 3rd edition, Wiley, New York, 1999.
3. Theodorsen, T., "The Theory of Wind Tunnel Wall Interference," NACA-RP-410, Langley Field, Va, 1931.
4. Baldwin Jr., B., Turner, J., and Knechtel, E., "Wall Interference in Wind Tunnels with Slotted and Porous Boundaries," NACA-TN-3176, 1954.
5. Woods, L.C, "On the Theory of Two Dimensional Wind Tunnels with Porous Walls," *Royal Society -- Proceedings*, v 233, n 1192, Dec 6, 1955, p 74-90
6. Mokry, M. "Residual Interference and Wind Tunnel Wall Adaptation," *27th Aerospace Sciences Meeting*, Reno, NV, Jan 9-12, 1989. AIAA-89-0147
7. Bottin, B., Carbonaro, M., and Schroeder, W., "First Runs of the Adaptive Wall Wind Tunnel T'3 at VKI: Calibration and Application of a Flexible Wall Adaptation Technique on a NACA 0012 Airfoil", *4th Belgian Congress on Theoretical and Applied Mechanics*, Leuven, Belgium, May 22-23, 1997
8. Crites, R., "Wall Interference Reduction Methods for Subsonic Wind Tunnels," *3rd Aerospace Sciences Meeting and Exhibit*, Reno, NV, January 9-12, 1995. AIAA-1995-0107
9. Dietrich, D.,Heidmann, F., and Abbott, J., "Fan Acoustic Signatures in an Anechoic Wind Tunnel*," Journal of Aircraft*, v 14, n 11, Nov, 1977, p 1109-1116.
10. Jansson, D., Methew J., and Hubner, J., "Design and Validation of an Aeroacoustic Anechoic Test Facility," *8th AIAA/CEAS Aeroacoustics Conference*, Breckinridge, CO, June 17-19, 2002. AIAA-2002-2466
11. Mathew, J., Bahr, C., Carroll, B., Sheplak, M., Cattafesta, L., "Design, Fabrication and Characterization of an Anechoic Wind Tunnel Facility," *11th AIAA/CEAS Aeroacoustics Conference*, Monterey, CA, May 23-25, 2002. AIAA-2005-3052

12. Jaeger, S. M., Horne, W. C., and Allen, C. S., "Effect of Surface Treatment on Array Microphone Self-Noise," *6th AIAA/CEAS Aeroacoustics Conference*, Lahaina, HI, June 12-14, 2000. AIAA-2000-1937
13. Ravetta, P. A., Burdisso, R. A., and Ng, W. F., "Wind Tunnel Aeroacoustic Measurements of a 26%-scale 777 Main Landing Gear," *10th AIAA/CEAS Aeroacoustics Conference*, Manchester, Great Britain, May 10-12, 2004. AIAA-2004-2885
14. Camargo, H. E., Smith, B. S., Devenport, W. J., and Burdisso, R. A., "Evaluation and Calibration of a Prototype Acoustic Test Section for the Virginia Tech Stability Wind Tunnel," Departments of Aerospace and Ocean Engineering and of Mechanical Engineering, Virginia Polytechnic Institute and State University, Report VPI-AOE-294, Blacksburg, VA, 2005, URL: http://www.aoe.vt.edu/research/facilities/stab/tunnel_acoustics.php.
15. Smith, B. S., Camargo, H. E., Burdisso, R. A., Devenport, W. J., "Development and Testing of a Novel Acoustic Wind Tunnel Concept," *11th AIAA/CEAS Aeroacoustics Conference*, Monterey, CA, May 23-25, 2005. AIAA-2005-3053
16. Choi, K., and Simpson, R.L., "Some Mean Velocity, Turbulence and Unsteadiness Characteristics of the VPI & SU Stability Wind Tunnel," Department of Aerospace and Ocean Engineering, Virginia Polytechnic Institute and State University, Blacksburg, Virginia 24061, Report VPI-Aero-161, 1987
17. Zsoldos, J. S. and Devenport, W. J., "An experimental investigation of interacting trailing vortex pairs", Proceedings of the 19th Symposium on Naval Hydrodynamics, Seoul, South Korea, August, 1992
18. Staubs, J., "Real Airfoil Effects on Leading Edge Noise," PhD Dissertation, Virginia Polytechnic Institute and State University, Blacksburg, Virginia 24061, June 2008
19. Duell, E., Walter, J., Arnette, S., Yen, J., "Recent Advances in Large Scale Aeroacoustic Wind Tunnels," *8th AIAA/CEAS Aeroacoustics Conference*, Breckinridge, CO, June 17-19, 2002. AIAA-2002-2466
20. Glegg, S., Devenport, W., Staubs, J. "Leading Edge Noise" *12th AIAA/CEAS Aeroacoustics Conference*, Boston, MA, May 23-25, 2005. AIAA-2006-2424.

21. Taylor, G., “Fluid Flow in Regions Bounded by Porous Surfaces,” *Royal Society Proceedings*, Vol. 234, n 1199, Mar 6, 1956. pp. 456-475
22. Ulbrich, N., “Description of Panel Method Code ANTARES,” NASA/CR-2000-209592, May 2000
23. Keller, J., “Numerical Calculation of Boundary Induced Interference in Slotted of Perforates Wind Tunnels Including Viscous Effects in Slots,” NASA Technical Note D-6871, Langley Research Center, August 1972